Université catholique de Louvain
École Polytechnique de Louvain
Institute of Condensed Matter and Nanosciences
Bio- and Soft Matter

Temperature Dependence of Volume and Surface Properties of Thermo- and Photo-responsive Polymer Brushes

Pengyu Zhuang

Thesis submitted to obtain the degree of
Doctor in Materials Science Engineering

Member of Jury:

Prof. **Alain M. Jonas**, Supervisor (UCL, Belgium)
Prof. **Karine Glinel**, Supervisor (UCL, Belgium)
Prof. **Jean-François Gohy**, President (UCL, Belgium)
Prof. **Christine Dupont-Gillain** (UCL, Belgium)
Prof. **Dominique Hourdet (**P & M Curie University, France**)**
Dr. **Ali Dirani (**Datwyler Sealing Solutions, Belgium**)**

Louvain-La-Neuve, October 2016

Summary

This work focuses on the temperature dependent volume and surface hydrophilicity of dense polymer brushes, which are assemblies of macromolecules densely grafted on a surface. Hydrophilicity refers to the affinity of water for polymer molecules, measured by the degree of swelling of the brush by water (volume hydrophilicity) or by a contact angle of water on the brush surface (surface hydrophilicity). A finer understanding of volume and surface hydrophilicity of polymer brushes is still needed as a function of environmental parameters, especially for temperature- and photo-responsive brushes, in order to put them into practical applications in biological and biomedical fields.

In this work, several representative homopolymer brushes of various volume properties, including temperature-responsive polymer brushes with a collapse transition temperature close to physiological conditions, are synthesized by surface initiated atom transfer radical polymerization (SI-ATRP). Then, their volume and surface hydrophilicities depending on temperature are studied in water, leading to an elucidation of the relationship between volume and surface hydrophilicities. The results reveals that the swelling degree of a temperature-responsive polymer brush shows a gradual but strong decrease with temperature before the brush totally collapses, whereas its surface hydrophilicity changes marginally with temperature across the collapse transition. In contrast, both the surface and volume hydrophilicities of hydrophilic homopolymer brushes vary little with temperature; however, they are not correlated together.

Copolymerization between highly hydrophilic monomers and monomers comprising functional groups affords a range of brushes with continuously-varying properties; by grafting photochromic azobenzene molecules onto the functional monomer units, photo-responsiveness ensues. Temperature-dependent measurements of the volume and surface hydrophilicity of these copolymer brushes, grafted or not with azobenzene, are then measured in water. The results show that the volume hydrophilicity can be tuned by changing the composition in a copolymer brush or by grafting its component chains with hydrophobic photochromic molecules; however, the effect of photo-irradiation affects only marginally their volume and surface hydrophilicity. We discuss these results based on the dynamical reorganization of chain segments at the brush/water interface, and based on the reorganization of water structure in the volume of the brush.

Acknowledgement

First of all, I would like to express my very special thanks to my supervisor: Prof. Alain M. Jonas for the opportunity given to me to do a Ph.D on polymer brushes in his research group. During my 4-year Ph.D studies, he provided me with excellent supervision and patient guidance. Without his endless support and help, I would not have been able to finish this dissertation. During the frequent discussions we had together, I learnt a lot about the how to analyze the data thoroughly and think about problems appeared during experiments deeper. I believe I will benefit a lot from his serious and rigorous attitude to research in my later career. In addition, I also want to thank him for the help he provided in my daily life. Only with the help, could my wife and I live much happier and easier, and finally graduate on time.

I would also like to thank my another supervisor: Prof. Karine Glinel for her continuous guidance and support for my research. She helps me improve a lot in many detailed aspects such as how to write my PowerPoint slides of a lecture more clearly and finely, how to improve the abstracts to be submitted for a conference and polish this thesis. Besides, she also put a lot energy into our usual discussions and provided many useful suggestions. Without her help, support and patient guidance, I would not also graduate successfully.

My warmest thanks goes to Prof. Jean-François Gohy who kindly accepted to be a member of the jury committee during my Ph.D studies and the president of the jury committee of my thesis. I thank him for his concern on my thesis writing, the useful suggestions on improving this thesis, and the helpful support from him during my dissertation.

I sincerely thank Prof. Christine Dupont for her kind acceptation to be a member of the jury committee during my Ph.D studies and the secretary of the jury committee of my thesis. I thank Christine for allowing me to use the QCM-D machine to do experiments and her detailed comments on this manuscript and many useful suggestions on improving the quality of this thesis.

I also faithfully thank Prof. Dominique Hourdet for being a member of the jury committee of this thesis and his attending my dissertation far from Paris. Prof. Hourdet gave me many detailed comments on the manuscript, some useful ideas of doing further experiments and many suggestions on polishing this thesis.

My sincere thanks must go on to Dr. Ali Dirani for his much help during my Ph.D research ranging from guiding me to do experiments at the beginning to ordering products for my experiments. Cooperation with him for the work is a happy experience. I also thank him for his sparing time from his busy work to be a member of the jury committee and attending my dissertation. His useful questions and comments about my experiments and manuscript helps me a lot in enriching this work.

Many thanks to Dr. Antony Fernandes, Dr. Qian Ye and Dr. Xiaofeng Ma for the help they provided such as the training of operating X-ray reflectometer, distilling monomers and synthesizing the ATRP silane. Without their help, I could not do my experiments progressively.

I thank Prof. Bernard Nysten and Cécile D'Haese for their assistance with AFM training and experiments. Many thanks to Sabine Bebelman for the training in operating the FTIR machine and the help she provided in measuring some samples. Many thanks to Pascal Lipnik

for the help provided in operating the optical spectrometer. Thank Delphine Magnin for the help in operating the X-ray reflectometer and solving the problems happened to this machine. Thanks to Pascal Van Velthem for the help supported in solving some technical problems of computer and software.

My sincere thank goes to the secretary, Aurore Becquevort. She was very helpful to order some urgent products and order the room for my public defense. Besides, she also helped me a lot when I need to find something. Her help in time spared me a lot of time. I am very grateful for that. Many thanks to Colette Douchamps for the help she provided in purchasing chemical products and some special instruments for my experiments. She also saved me much time for my experiments. Thank Piraux Luc for the help gave to me during my Ph.D study.

I want to thank Prof. Sophie Demoustier-Champagne for the help and warmness she provided during my study in BSMA.

I also would like to thank my Chinese friends and colleagues. Jun Yin, Ronggang Cai and Yang Li provided me lots of help ranging from doing experiments to my daily life. Yun Yin and Ronggang Cai also helps my wife and me a lot. Without their help and friendness, we could not live so easier and happier in Louvain-la-Neuve. I also thank Shouwei Zhang, with whom I came together and shared the room for the first year, for the help given during my studying here and mutual communications in daily life.

Many thanks to Diana Ramirez-Wong and Catherine Philippart, who shared me with the same office. They are very helpful when I need to find something or ordering some products for my experiments and friendly in daily life. I thank Dr. Sabrine Belbekhouche, Dr. Hailu G.

Kassa, Dr. Annie Zhe Cheng, Dr. Naïma Sallem, Dr. Saghi Saghazadeh, Quentin Voleppe, Amir Bahrami, Dr. Hadi Goldansaz, Claire Chattaway, and all other members of BSMA who I have not mentioned. Many thanks to some Chinese friends: Meijie Li, Wei Cao, Weifeng Cui, Peng Li, Prof. Guoyong Gu, Dr. Zhengang Wang, Dr. Yongchao Jia, Dr. Pengyu Yan, Yuan Zhang, Zimin Li, Zhijian Wang, Ran Ye and Shashuang Xu. I will always revember the happy time we spent together.

I am very grateful to my parents and my sister for their understanding and emotional support far from Belgium. Thanks for not giving me any pressure in my life and allowing me to live my life in the way I want. May you three always be happy and healthy.

I thank my wife Cuimin Tang. Thanks to god for letting me meet you in your early life and marry you just after your graduation from college. I thank you for your endless support, patience and tolerance in our daily life. The 3-year living and studying together in Louvain-la-Neuve is the happiest time I ever have had. Without any doubt, you have been the most precious person in my life.

Contents

Summary ····· **I**

Acknowledgement ····· **III**

Abbreviations ····· **XIII**

1 Introduction ····· **1**

References ····· 7

2 Litterature review ····· **11**

2.1 Definition of polymer brush and description of stimuli-responsive brushes ····· 11

2.1.1 Thermo-responsive polymers ····· 12

2.1.2 Thermo-responsive polymer brush ····· 18

2.1.3 Definition of volume and surface hydrophilicities for a polymer brush ····· 20

2.1.3.1 The swelling coefficient of a polymer brush mirrors its volume hydrophilicity ····· 20

2.1.3.2 The cosine of the contact angle of water on a water equilibrated polymer brush defines its surface hydrophilicity 22

2.1.4 Photo-responsive polymer brushes ····· 25

2.1.5 Thermo-/photo-responsive free polymer chains and brushes ····· 27

2.1.6 Other stimuli-responsive polymer brushes ····· 31

2.2 Preparation of polymer brushes ····· 35

2.2.1 General description of the different approaches ····· 35

2.2.2 Description of controlled/"living" radical polymerization (CRP) techniques ····· 38

2.2.2.1 Preparation of polymer brushes by physical adsorption ····· 42

2.2.2.2 Preparation of polymer brushes by “grafting to” approach ····· 43
2.2.2.3 Preparation of polymer brushes by “grafting from” approach ····· 48
2.3 Characterization techniques ····· 51
2.3.1 Quartz crystal microbalance with dissipation monitoring (QCM-D) ····· 51
2.3.2 Ellipsometry ····· 55
2.3.3 Equilibrium contact angle measurement ····· 58
2.4 Applications of stimuli-responsive polymer brushes ····· 61
2.4.1 Surfaces tuning cell/surface interactions 61
2.4.2 Antifouling surfaces ····· 63
2.4.3 Surfaces controlling drug release ····· 66
References ····· 69
3 Temperature Dependence of the Surface and Volume Hydrophilicity of Hydrophilic Polymer Brushes ····· 91
3.1 Abstract ····· 91
3.2 Introduction ····· 93
3.3 Experimental section ····· 96
3.3.1 Materials ····· 96
3.3.2 Brush synthesis. ····· 97
3.3.3 QCM-D ····· 97
3.3.4 Ellipsometry ····· 98
3.3.5 Equilibrium contact angle measurement ····· 99
3.4 Results and discussion ····· 100
3.4.1 Brush surface hydrophilicity by equilibrium contact angle measurements ····· 100

3.4.2 Determination of brush swelling by ellipsometry ····· 109
3.4.3 Determination of the brush swelling by QCM-D ····· 112
3.4.4 Comparison between ellipsometric and acoustic swelling coefficients ····· 117
3.4.5 Brush volume hydrophilicity from swelling measurements ····· 125
3.4.6 Surface versus volume hydrophilicity of a brush ····· 126
3.5 Conclusions ····· 131
3.6 Supporting information ····· 132
3.6.1 Detailed synthesis protocols of the brushes ····· 132
3.6.2 Effect of measurement conditions on the water contact angle measured in the captive bubble configuration ····· 135
3.6.3 Different possible fits of the QCM-D data of a $PMEO_2MA$ and a POEGMA brush ····· 140
3.6.4 Generalized acoustic swelling coefficients of all brushes ····· 142
3.7 Acknowledgments ····· 143
References ····· 144
4 Temperature-Dependence of the Swelling and Surface Wettability of Dense Polymer Brushes ····· 153
4.1 Abstract ····· 153
4.2 Introduction ····· 155
4.3 Surface and volume hydrophilicity of dense polymer brushes ····· 157
4.3.1 Temperature-dependent surface hydrophilicity of dense PNIPAM brushes ····· 158

4.3.2 Temperature-dependent swelling and volume hydrophilicity of dense PNIPAM brushes ····· 161
4.3.3 Thermo-responsive poly(oligo(ethylene oxide)methacrylate) copolymer brushes – versatile functional alternatives to PNIPAM ····· 167
4.3.4 Surface and volume hydrophilicity of non-thermo-responsive poly(oligo(ethylene oxide)methacrylate) copolymer brushes 170
4.4 Conclusions ····· 175
4.5 Acknowledgments ····· 176
References ····· 177
5 Synthesis of Hydrophilic P(DMA-*co*-HEMA) Copolymer Brushes by Surface-initiated ATRP ····· 185
5.1 Abstract ····· 185
5.2 Introduction ····· 186
5.3 Materials and methods ····· 192
5.3.1 Materials ····· 192
5.3.2 Preparation of the initiator monolayer ····· 193
5.3.3 Polymer brush synthesis ····· 193
5.3.4 FTIR measurement ····· 197
5.4 Results and discussion ····· 200
5.4.1 Polymer brush synthesis under different reaction conditions ····· 200
5.4.2. Thickness and HEMA content of P(DMA-*co*-HEMA) brushes ····· 210
5.4.3. Mayo-Lewis Analysis and Distribution of Sequence Lengths ····· 214

5.5 Conclusions ····· 217
5.6 Supporting information of brush thickness measured by ellipsometry and FTIR and P(DMA-co-HEMA) brush composition ····· 218
References ····· 219
6 Temperature Dependence of the Surface and Volume Hydrophilicity of DMA-based Photochromic Copolymer Brushes ····· 225
6.1 Abstract ····· 225
6.2 Introduction ····· 226
6.3 Materials and Experiments ····· 235
6.3.1 Materials ····· 235
6.3.2 Azobenzene synthesis ····· 236
6.3.3 Determination of the extinction coefficient by Ultraviolet-visible (UV) spectroscopy ····· 237
6.3.4 Grafting azobenzene groups onto P(DMA-*co*-HEMA) brushes ····· 237
6.3.5 Yields of AZO grafted onto P(DMA-*co*-HEMA) brushes ····· 239
6.3.6 Photo-isomerization ····· 241
6.3.7 Volume swelling measurement by ellipsometry ····· 241
6.3.8 Equilibrium contact angle measurement ····· 241
6.4 Results and discussion ····· 242
6.4.1 Extinction coefficient determination ····· 242
6.4.2 Yield of AZO grafted onto P(DMA-*co*-HEMA) brushes ····· 243

6.4.3 Photo-isomerization of AZO groups in P(DMA-*co*-HEMA)-CONH-AZO brush ····· 245
6.4.4 Swelling coefficients of P(DMA-*co*-HEMA) brushes 246
6.4.5 Swelling coefficients of P(DMA-*co*-HEMA)-CONH-AZO brushes ····· 247
6.4.6 Swelling coefficients of P(DMA-*co*-HEMA)-OOC-AZO brushes ····· 249
6.4.7 Surface hydrophilicity of P(DMA-*co*-HEMA) brushes ·· ····· 257
6.4.8 Surface hydrophilicity of P(DMA-*co*-HEMA)-CONH-AZO brushes ····· 258
6.4.9 Surface hydrophilicity of P(DMA-*co*-HEMA)-OOC-AZO brushes ····· 260
6.5. Conclusions ····· 262
References ····· 263
7 Conclusions and Perspectives ····· 271

Abbreviations

CRP: controlling/“living” radical polymerization

SI-ATRP: surface initiated atom transfer radical polymerization

RAFT: reversible addition-fragmentation transfer

NMP: nitroxide-mediated polymerization

Bpy: 2, 2'-bipyridine

PMDETA: *N,N,N’,N’,N’’*-pentamethyldiethylenetriamine

HMTETA: 1,1,4,7,10,10,10-hexamethyltriethylenetetraamine

Me_6TREN: tris(2-dimethylaminoethyl)amine

QCM-D: quartz crystal microbalance-with dissipation monitoring

FTIR: fourier transform infrared spectrometer

LCST: lower critical solution temperature

UCST: upper critical solution temperature

PNIPAM: poly(N-isopropyl acrylamide)

POEGMA: poly(oligo(ethylene glycol) methacrylate)

PDMA: poly(*N*,*N*-dimethyl acrylamide)

PEG: poly(ethylene glycol)

$PMEO_2MA$: poly(diethylene glycol methyl ether methacrylate)

$PMEO_3MA$: poly(2(2-(2-methoxyethoxy)ethoxy)ethyl methacrylate)

PHEMA: poly(2-hydroxyethyl methacrylate)

PDEMA: poly(*N*,*N*-diethyl acrylamide)

PDMAEMA: poly(dimethylaminoethyl methacrylate)

PMMA: poly(methyl methacrylate)

ONB: O-nitrobenzyl

SP: spiropyran

AZO: azobenzene

DSC: *N*,*N*'-disuccinimidyl carbonate

DCC: *N*,*N*'-dicyclohexylcarbodiimide

DMAP: 4-(dimethylamino)pyridine

NHS: *N*-hydroxysuccinimide

1 Introduction

Hydrophilic polymer brushes are of critical importance for biological and biomedical applications ranging from antifouling and antibacterial coatings,[1-4] lubrication,[5] cell culturing,[6, 7] to drug delivery.[8, 9] The performance of polymer brushes not only relies on their bulk properties, but also heavily depends on their surface properties.[10] However, the importance of the volume and surface properties is different depending on a specific application. For instance, when a hydrophilic polymer brush is used as coating on the surface of a marine equipment, a surface property (persistent antifouling) is seeked for non-specific protein adsorption.[3, 4] When it is coated on an implantable medical device, it is better for the surface to have non-fouling[3, 4], antibacterial[3, 4] and low friction[5] properties at the same time, which combine surface and volume properties.[11] Whereas the volume swelling degree of a hydrophilic polymer brush in water should be considered when the polymer brush is used as a reservoir for the progressive release of drugs. An example is killing bacteria with some bactericides loaded or anchored into hydrophilic polymer brushes.[1]

Nowadays, stimuli-responsive polymer brushes are becoming increasingly popular for biological and biomedical applications; these brushes have volume and surface properties that can be tuned by an external stimulus, such as temperature, pH or light, *etc*.[12] For instance, a poly(N-isopropyl acrylamide) (PNIPAM) brush is temperature-responsive, with a LCST of ~32°C in water. At a temperature lower than the LCST, the free polymer chains are soluble in water, and the brush is highly swollen; while it starts to collapse when the temperature

increases above the LCST, causing a large change of swelling of the volume which passes from hydrophilic to hydrophobic. However, as shown in this thesis, this transition is marked by only a small change of the surface wettability.[13] Thus, studying the change of volume and surface hydrophilicities of trigger-responsive polymer brushes upon external stimuli including temperature, pH and light, may benefit us for designing and applying stimuli-responsive polymer brushes for real applications. It is one of the objectives of this thesis to progress further in this issue of volume vs surface properties of hydrophilic and stimuli-responsive polymer brushes.

In order to impart the polymer brushes with extra properties such as photo-responsiveness, post-modification is usually used, which requires that the polymer brushes should bear functional groups. In that case, copolymerization between two or more different monomers is usually desired. One of them can bear functional groups for post-modification.[14] To synthesize the polymer brushes including copolymer brushes, the "grafting from" approach is preferred due to the advent of controlling/"living" radical polymerization (CRP) techniques including atom transfer radical polymerization (ATRP),[15-18] which can control the brush thickness, composition and functionality of the brushes, in turn leading to controlled volume and surface properties.[4, 19]

Consistent with the previous background, the aims of this thesis include synthesizing hydrophilic polymer brushes consisting of homopolymer and copolymer chains by surface initiated atom transfer radical polymerization (SI-ATRP) to control the brush thickness, composition and chain architecture; monomers bearing functional groups are used to introduce photo-responsiveness or anchor

biomacromolecules for later use. Here, photochromic molecules of the azobenzene family will be grafted onto copolymer brushes by post-modification, imparting the copolymer brushes with photo-responsiveness; finally, the temperature-dependent volume and surface hydrophilicity properties of the synthesized polymer brushes including hydrophilic polymer brushes without LCSTs, polymer brushes with LCSTs and photo-responsive copolymer brushes will be studied by in-situ ellipsometry, quartz crystal microbalance-with dissipation monitoring (QCM-D) and equilibrium water contact angle measurement in the captive bubble configuration, respectively, in an attempt to clarify the correlation between the volume and surface hydrophilicities. The structure of the thesis is as follows:

(1) in chapter 2, the definition of polymer brushes, several important categories of responsive-polymer brushes, the brush growth methods such as "grafting to" and "grafting from" approaches are first introduced; then characterization techniques for studying the volume and surface hydrophilicity properties (important concepts also defined there) are described, such as in-situ ellipsometry, QCM-D and equilibrium water contact angle measurement; finally, several important potential applications of polymer brushes are given.

(2) in chapter 3, several representative polymer brushes including highly hydrophilic polymer brushes of poly(oligo(ethylene oxide) methacrylate) (POEGMA) and poly(*N*, *N*-dimethyl acrylamide) (PDMA) without LCSTs in the probed temperature range, temperature-responsive polymer brushes consisting of PNIPAM and poly(diethylene glycol methyl ether methacrylate) ($PMEO_2MA$) with LCSTs close to the physiological temperature, and non-temperature

responsive but functional poly(2-hydroxyethyl methacrylate) (PHEMA) brushes, are synthesized by SI-ATRP. Two different methods to quantitatively measure the swelling coefficients of the above homopolymer brushes in water are discussed in details (in situ-ellipsometry and QCM-D) and the results obtained by these two techniques are compared. A protocol of measuring the equilibrium water contact angle in the captive bubble configuration is introduced to obtain reproducible results of surface wettability. Thereby, the temperature dependent volume and surface hydrophilicities are studied, and their correlation is clarified.

(3) in chapter 4, different techniques such as scanning probe microscopy (AFM), in-situ ellipsometry and QCM-D for measuring the swelling degrees of PNIPAM brushes are compared based on literature data and our own work, and the surface wettability of PNIPAM is studied by measuring the equilibrated water contact angle on the surface. The temperature-dependence of volume and surface hydrophilicities of PNIPAM brushes is thereby further studied. Then OEGMA-based copolymer brushes are synthesized by copolymerizing hydrophilic OEGMA with MEO_2MA or HEMA to obtain thermo-responsive polymer brushes or introduce functional hydroxyl groups for further grafting biomacromolecules or photochromic moieties such as azobenzene groups. The volume and surface hydrophilicities of thermo-responsive P(OEGMA-*co*-MEO_2MA) brushes dependent on temperature are studied by in-situ ellipsometry and equilibrated water contact angle measurement, and their behavior is shown to be similar to PNIPAM's. Finally, the temperature-dependence of volume and surface hydrophilicity of non-responsive hydrophilic copolymer

brushes of P(OEGMA-*co*-HEMA) grafted or not with azobenzene groups are studied by in-situ ellipsometry and equilibrated water contact angle measurement and compared.

(4) in chapter 5, homopolymer brushes of PDMA and PHEMA, and hydrophilic P(DMA-*co*-HEMA) brushes are synthesized by SI-ATRP in aqueous solution. Different reaction conditions including changing the monomer concentrations, ligands, activators/deactivators, or water/methanol ratios are tried to synthesize the polymer brushes in a controlled way. After optimizing the reaction conditions for synthesizing P(DMA-*co*-HEMA) brushes, their compositions are determined by FTIR spectroscopy to obtain the reactivity ratios of the monomers, from which the architecture of the copolymer chains in brushes of different compositions are simulated. It is indeed important to know the degree of blockiness of the chains, as this can have an impact on the way the chains interact with water.

(5) in chapter 6, a series of P(DMA-*co*-HEMA) brushes are synthesized by SI-ATRP with the reaction conditions optimized in chapter 5, and azobenzene groups are grafted onto the HEMA units via either DSC-activated esterification or amination reactions. The compositions of the terpolymer brushes are determined by FTIR and UV spectroscopies. After grafting, the reversible photo-isomerization of the azobenzene groups upon photo-irradiation is proved by UV spectroscopy and in-situ ellipsometry. The volume and surface hydrophilicities of PDMA-based copolymer brushes grafted or not with azobenzene groups are finally studied by in-situ ellipsometry and equilibrium contact angle measurements in water, as a function of temperature.

(6) in chapter 7, a brief summary of the mains results is introduced for this thesis and some perspectives are suggested at the end for further research and potential applications.

References

1. Gao, G. et al. Antibacterial surfaces based on polymer brushes: investigation on the influence of brush properties on antimicrobial peptide immobilization and antimicrobial activity. *Biomacromolecules* **12**, 3715-3727 (2011).
2. Gao, G. et al. The biocompatibility and biofilm resistance of implant coatings based on hydrophilic polymer brushes conjugated with antimicrobial peptides. *Biomaterials* **32**, 3899-3909 (2011).
3. Banerjee, I., Pangule, R.C. & Kane, R.S. Antifouling coatings: recent developments in the design of surfaces that prevent fouling by proteins, bacteria, and marine organisms. *Adv. Mater.* **23**, 690-718 (2011).
4. Krishnamoorthy, M., Hakobyan, S., Ramstedt, M. & Gautrot, J.E. Surface-initiated polymer brushes in the biomedical field: applications in membrane science, biosensing, cell culture, regenerative medicine and antibacterial coatings. *Chem. Rev.* **114**, 10976-11026 (2014).
5. Kobayashi, M. & Takahara, A. Tribological properties of hydrophilic polymer brushes under wet conditions. *Chem. Rec.* **10**, 208-216 (2010).
6. Cole, M.A., Voelcker, N.H., Thissen, H. & Griesser, H.J. Stimuli-responsive interfaces and systems for the control of protein–surface and cell–surface interactions. *Biomaterials* **30**, 1827-1850 (2009).

7. Loschonsky, S. et al. Surface-Attached PDMAA−GRGDSP Hybrid Polymer Monolayers that Promote the Adhesion of Living Cells. *Biomacromolecules* **9**, 543-552 (2008).
8. Wu, L., Glebe, U. & Böker, A. Surface-initiated controlled radical polymerizations from silica nanoparticles, gold nanocrystals, and bionanoparticles. *Polym. Chem.* **6**, 5143-5184 (2015).
9. Stuart, M.A. et al. Emerging applications of stimuli-responsive polymer materials. *Nat. Mater.* **9**, 101-113 (2010).
10. Luzinov, I., Minko, S. & Tsukruk, V.V. Adaptive and responsive surfaces through controlled reorganization of interfacial polymer layers. *Prog. Polym. Sci.* **29**, 635-698 (2004).
11. Bhat, R.R., Chaney, B.N., Rowley, J., Liebmann-Vinson, A. & Genzer, J. Tailoring Cell Adhesion Using Surface-Grafted Polymer Gradient Assemblies. *Adv. Mater.* **17**, 2802-2807 (2005).
12. Chen, T., Ferris, R., Zhang, J., Ducker, R. & Zauscher, S. Stimulus-responsive polymer brushes on surfaces: Transduction mechanisms and applications. *Prog. Polym. Sci.* **35**, 94-112 (2010).
13. Zhuang, P., Dirani, A., Glinel, K. & Jonas, A.M. Temperature Dependence of the Surface and Volume Hydrophilicity of Hydrophilic Polymer Brushes. *Langmuir* **32**, 3433–3444 (2016).
14. Dirani, A. et al. Reversible Photomodulation of the Swelling of Poly(oligo(ethylene glycol) methacrylate) Thermoresponsive Polymer Brushes. *Macromolecules* **45**, 9400-9408 (2012).

15. Pyun, J., Kowalewski, T. & Matyjaszewski, K. Synthesis of Polymer Brushes Using Atom Transfer Radical Polymerization. *Macromol.Rapid Commun.* **24**, 1043-1059 (2003).
16. Edmondson, S., Osborne, V.L. & Huck, W.T. Polymer brushes via surface-initiated polymerizations. *Chem. Soc. Rev.* **33**, 14-22 (2004).
17. Barbey, R. et al. Polymer Brushes via Surface-Initiated Controlled Radical Polymerization Synthesis, Characterization, Properties, and Applications. *Chem. Rev.* **109**, 5437-5527 (2009).
18. Olivier, A., Meyer, F., Raquez, J.-M., Damman, P. & Dubois, P. Surface-initiated controlled polymerization as a convenient method for designing functional polymer brushes: From self-assembled monolayers to patterned surfaces. *Prog. Polym. Sci.* **37**, 157-181 (2012).
19. Wagner, N. & Theato, P. Light-induced wettability changes on polymer surfaces. *Polymer* **55**, 3436–3453 (2014).

Chapter 1: Introduction

2 Literature review

2.1 Definition of polymer brush and description of stimuli-responsive brushes

Polymer brushes are made of dense polymer chains which are tethered by one end to solid substrate surfaces or interfaces.[1, 2] Due to the high grafting density, the polymer chains are forced to stretch perpendicularly away from the surface or interface to avoid overlapping as much as possible and minimize strong segment-segment interactions (Scheme 2.1.A).[1] At lower grafting densities, the segments of individual chains do not "feel" each other, and behave more or less like free chains except for one end tethered on the surface. If the interactions between the polymer segments and surface are weak, these polymer chains adopt a "mushroom" conformation with the coil dimension similar to that of free chains (Scheme 2.1.B). However, if the polymer segments strongly adsorb to the underlying surface, the tethered polymer chain looks like a flat "pancake" (Scheme 2.1.C).[3, 4]

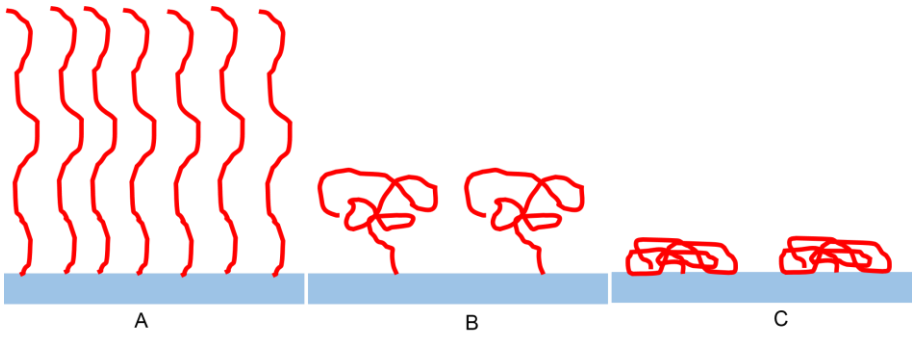

Scheme 2.1. Representation of the polymer chain conformation as a function of the grafting density.

Compared to traditional polymer brushes, stimuli-responsive polymer brushes are polymer layers whose properties like the degree of swelling, the surface wettability, the net charge or the bioactivity are dramatically altered when exposed to an external stimulus.[1, 4-6] Depending on the stimulus, three categories of stimuli-responsive brushes can be distinguished: brushes responding to chemical changes like pH or ionic strength variations or the presence of chemical agents; brushes responding to a physical parameter like temperature, light or voltage; and brushes whose properties vary in presence of specific biochemical agents such as antigens, enzymes or ligands.[7-9] Different stimuli-responsive polymer brushes can be synthesized according to the targeted application. Thereafter temperature-responsive (also called thermo-responsive), pH-responsive and light-responsive (also called photo-responsive) polymer brushes will be described in detail due to their extensive applications, notably in the biochemical field, to control the adhesion of biological entities or the delivery of drugs.

2.1.1 Thermo-responsive polymers

Thermo-responsive polymers are largely exploited among all the stimuli-responsive polymers since the temperature can be easily varied. Two kinds of thermo-responsive polymers are distinguished: polymers showing a lower critical solution temperature (LCST) and an upper critical solution temperature (UCST) (Figure 2.1.). For a polymer displaying a LCST, the macromolecular chains adopt an expanded random coil conformation in the solvent at low temperature, but start to collapse and aggregate when the temperature increases above LCST. In contrast, for a polymer exhibiting an UCST, the macromolecular chains

are insoluble in the solvent at the temperature below UCST and become soluble when the temperature is higher than UCST. The nature of the solvent, the molar mass and the composition of macromolecular chains and the temperature might affect the solubility of the macromolecular chains.[10-12]

From a thermodynamical point of view, the phase separation in solution can be described according to a phase diagram based on a bimodal curve. The bimodal curve is the boundary that separates one miscible phase of a polymer solution from two immiscible phases. For each solution composition, the bimodal curve describes the temperature from which a phase separation is observed. When the bimodal curve shows a minimum with the solution composition, this minimum corresponds to LCST (Figure 2.1 left). In contrast, when the bimodal curve shows a maximum with the solution composition, this maximum corresponds to UCST (Figure 2.1 right). The other points of the bimodal curve correspond to "cloud point" or "turbidity point". For example, a solution of LCST polymer with X_B concentration (Figure 2.1, left) shows a phase separation for temperatures higher than T_C. In contrast, a solution of UCST polymer with $X_{B'}$ concentration (Figure 2.1, right) shows a phase separation for temperatures lower than $T_{C'}$. However, T_C and $T_{C'}$ are not LCST and UCST since they do not correspond to the minimum and the maximum of the bimodal curve, respectively.

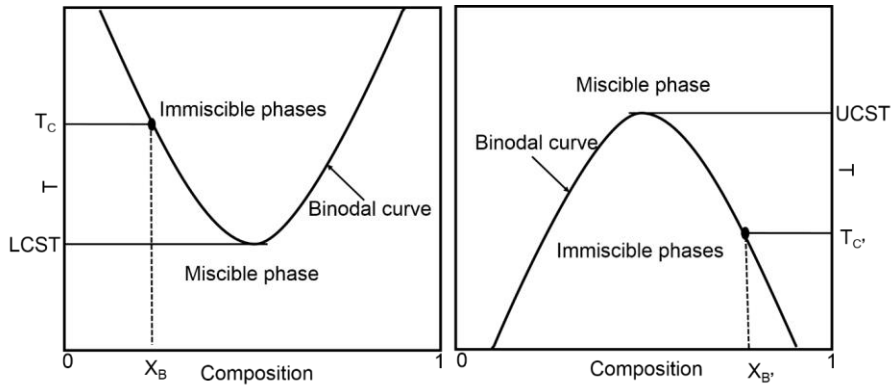

Figure 2.1. Phase diagrams of polymer solutions exhibiting a LCST (left) or an UCST (right).

The solubility of a polymer in a given solvent can be first estimated by the basic thermodynamic relationship established by Gibbs[13]:

$$\Delta G_m = \Delta H_m - T\Delta S_m \quad (1)$$

where ΔG_m is the free energy of mixing, ΔH_m the enthalpy of mixing, ΔS_m the entropy of mixing and T the temperature. For a complete solubilization of the polymer to occur,

$$\Delta G_m < 0 \quad (2).$$

However, the negativity of ΔG_m is only a necessary condition, but not sufficient for complete solubility of a polymer in a solvent, since phase separation also occurs due to thermal fluctuations when the solution composition lies in a range where the second derivative of ΔG_m versus polymer concentration is negative. Flory and Huggins developed a theory allowing to assess the variation of the free energy of mixing with polymer concentration, which is described by the following equation[14-17]:

$$\Delta G_m = RT\,[n_1 ln\varphi_1 + n_2 ln\,\varphi_2 + \chi_{12} n_1 \varphi_2] \quad (3)$$

where R is gas constant, n_i is the number of moles of component i, φ_i is the volume fraction of component i, and χ_{12} is the Flory-Huggins interaction parameter. Polymer chains are considered in a good solvent when χ_{12} is lower than 0.5.

The phase separation of a polymer solution is determined by the competition between the polymer-solvent, polymer-polymer and solvent-solvent interactions. In a good solvent, the interactions between polymer chains and solvent molecules are much stronger than intramacromolecular and intermacromolecular interactions between polymer chains.[18] However the value of χ_{12} depends also on temperature. The standard theory of Flory-Huggins predicts that χ_{12} decreases with increasing temperature, corresponding to a better solubility and the possible existence of an upper critical solution temperature (UCST). More elaborate treatments, which take into account entropic effects linked to the difference of size of the monomer segments and solvent molecules, the existence of free volume in the solution, or specific effects associated to H-bonding, predict the possibility to have χ_{12} increasing with increasing temperature, thereby leading to a lower critical solution temperature (LCST).

The polymers showing an UCST in aqueous solution are certainly relevant for biological applications.[10] However there are only a few number of polymers showing such a behavior. Therefore, only thermo-responsive polymers with a LCST in aqueous solution are described here. The LCST value is an important parameter to be taken into account for the applications of thermo-responsive polymers. For instance, biomedical and biological applications require LCST in the range of 20-40°C. The most representative thermo-responsive polymer

showing a LCST close to the physiological temperature in water are poly(*N*-isopropyl acrylamide) (PNIPAM) with a transition temperature of 32°C,[19-24] poly(*N*,*N*-diethyl acrylamide) (PDEMA) with a transition temperature of 33°C,[25] poly(dimethylaminoethyl methacrylate) (PDMAEMA) with a cloud point ranging from 14 to 50°C, depending on pH,[26] poly(2-(2-methoxyethoxy)ethyl methacrylate) ($PMEO_2MA$) with a transition temperature of ~26°C[27-29] and poly(2(2-(2-methoxyethoxy)ethoxy)ethyl methacrylate) ($PMEO_3MA$) with a transition temperature of 52°C (Scheme 2.2).[30]. However the LCSTs of some of them such as PDEMA[25] and PDMAEMA,[26, 31] are strongly affected by the ionic strength and pH of the solution. Therefore PNIPAM with a LCST of 32°C became the most popular thermo-responsive polymer studied.[22, 23] As a result, a lot of PNIPAM derivatives have been synthesized for different applications ranging from the control of cell adhesion to drug delivery.[7, 32, 33,34, 35] However, PNIPAM and its derivatives have some inherent disadvantages such as questionable biocompatibility, phase transition hysteresis, and variation of the responsiveness as a function of the ionic strength. Moreover the nature of end groups and molar mass of PNIPAM chains influence their thermal behavior.[23, 36, 37] For the above reasons, $PMEO_2MA$ which shows a LCST of about 26°C insensitive to ionic strength and molar mass of the chains, recently emerged as a potential more interesting thermo-responsive polymer than PNIPAM.[38] Moreover $PMEO_2MA$ can be considered like a poly(ethylene glycol) (PEG) analog with a good biocompatibility. If the side chains consist of 2 or 3 ethylene glycol (EO) units, the corresponding polymer is called $PMEO_2MA$ or $PMEO_3MA$. When the side chains are made of longer EO units, the

monomer is named oligo(ethylene glycol) methacrylate (OEGMA) and the corresponding polymer is called POEGMA. The LCST of POEGMA increases with the length of the oligo(ethylene glycol) side chains.[27, 29, 38] For instance, POEGMA with oligo(ethylene glycol) side chains varying from 4 to 9 EO units and ended by methoxy groups, show LCST ranging from 64 to 90°C in water. [27, 29, 38] Moreover, the LCST of P(MEO_2MA-*stat*-OEGMA) copolymers can be finely tuned between the LCST of pure P(MEO_2MA) (i.e. 26°C and the LCST of POEGMA as a function of the composition of the copolymer.[27] In addition, the LCST of these copolymers is almost independent of their molar mass and their concentration of the solution,[27] although the ionic strength affects the LCST of thermo-responsive polymers slightly such as the LCST of PNIPAM or copolymers of MEO_2MA and OEGMA.[38] Normally, adding salts such as NaCl, NaBr and KCl into the aqueous solution will decrease the LCST of thermo-responsive polymers by up to a few degrees due to interactions between the cations and the polymer such as the direct interaction between cations and oxygen atoms of amide groups in PNIPAM. The cations of salts have stronger affinity with the oxygen atoms of amide groups than with any other atoms. The cation interaction strength with the polymer is inversely correlated with the cation-anion contact pair association constant, which means that the weaker the cation-anion interaction is, the stronger the cation binds to the polymer, whereas anions have little association with the polymer.[39]

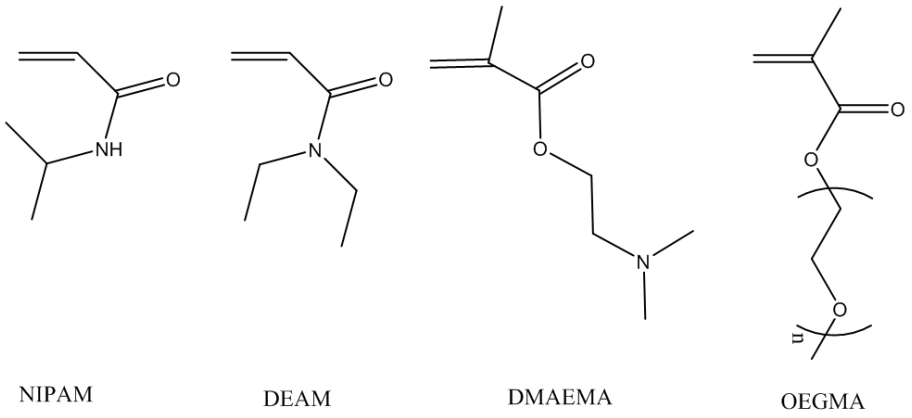

Scheme 2.2. Schematic structures of the monomers used to produce water-soluble thermo-responsive polymers.

2.1.2 Thermo-responsive polymer brush

A polymer brush is made of macromolecules with one extremity anchored on the solid surface. Therefore the substrate restricts the degree of freedom of the chains compared to free polymer chains in solution. Thermo-responsive polymer brushes are typically based on thermo-responsive polymers described in the section 2.1.1. These brushes show a collapse transition which is similar to the collapse transition observed for free polymer chains in solution. However it has been shown that thermo-responsive polymer brushes display a gradual collapse behavior with the temperature, starting from bottom to top surface. Accompanying the surface collapse transition, the surface wettability of the polymer brush also changes. For instance, the PNIPAM brush was synthesized by ATRP from polystyrene (PS) surface by Mizutani *et al.*[40] It was observed that the brush thickness decreases with temperature. Moreover, when the temperature is lower than the LCST of PNIPAM, the brush adopts a swollen state with a

hydrophilic surface. However, for temperatures higher than the LCST of PNIPAM, the macromolecular chains collapse by repelling the surrounded water, creating a less hydrophilic surface.[40] Sun *et al.* synthesized PNIPAM polymer brushes from flat silicon substrates by surface initiated atom transfer radical polymerization (Si-ATRP). They showed that the surface wettability of these polymer brushes can be reversibly switched with the temperature. Indeed when the temperature increased from 25°C to 40°C, the water contact angle measured in static condition, increased from ~63.5°C to ~93.2°. Moreover the water contact angle returned to 63.5°C when the temperature was subsequently decreased to 25°C. This effect can be explained by the competition between intermolecular and intramolecular hydrogen bonds, below and above the collapse temperature. At temperatures below the collapse temperature, the interactions between the PNIPAM chains and water molecules through hydrogen bonding are predominant leading to the hydrophilicity of the surface. At temperatures higher than the collapse temperature, the intramolecular hydrogen bonds between C=O and N-H groups in PNIPAM chains cause a compact and collapsed conformation of PNIPAM chains, reducing the interactions of C=O and N-H groups with water molecules. Thus the surface of the PNIPAM brush exhibits hydrophobicity at high temperatures.[41] Using the change of the surface wettability accompanying the collapse of the polymer chains is of great importance to control cell adhesion or to switch the antibacterial or antifouling properties of surface.[28, 42] More details about these applications are provided in the section 2.4 of this chapter.

2.1.3 Definition of volume and surface hydrophilicities for a polymer brush

It is often seen in the literature that a thermo-responsive polymer brush switches from hydrophilic to hydrophobic across its LCST. This is a statement which requires caution, and a significant part of this thesis will discuss this issue. In particular, in this document, we will be using repeatedly the notions of *surface and volume hydrophilicities* of polymer brushes; these notions are generally ambiguous, and are taken here as proxies for a specific meaning which is described in this section.

2.1.3.1 The swelling coefficient of a polymer brush mirrors its volume hydrophilicity

As the volume and surface hydrophilicities are the main properties studied in this thesis, here we first define rigorously the notions of volume and surface hydrophilicity, and remind a few theoretical notions on the swelling and surface properties of polymer brushes. The hydrophilicity of a polymer can be defined by the adimensional second virial coefficient of the segment interactions in water, *v*, which is also the excluded volume of a segment normalized by its sterically-excluded volume. Positive excluded volumes correspond to good solvents; negative excluded volumes are for poor solvents in which the chain segments experience a strong attraction.[43] The normalized excluded volume is related to the Flory-Huggins polymer/water interaction parameter, χ_{12}, by :

$$\nu \propto \frac{1}{2} - \chi_{12} \qquad (1);$$

lower χ_{12} values correspond to a higher affinity of the repeat units for water.[43]

The second virial coefficient of the polymer segments in water directly controls the degree of swelling of the brush in water, which is measured by the brush swelling coefficient :

$$\alpha \triangleq \frac{h}{h_d} \qquad (2),$$

with h the thickness of the swollen brush and h_d its dry thickness. Within the mean field treatment of planar polymer brushes in a solvent,[44, 45] the swollen thickness h of a brush in a strong solvent reads :

$$h \simeq \left(\frac{8}{\pi^2}\right)^{1/3} v^{1/3}(a^2\sigma)^{1/3} Na \qquad (3)$$

with N the number of Kuhn segments per chain, each segment being of size a (which is the cubic root of its Van der Waals volume), and σ the number of chains grafted per unit surface. Since the dry brush thickness is $h_d = Na^3\sigma$, the swelling coefficient is, in the strong solvent limit :

$$\alpha \simeq \left(\frac{8}{\pi^2}\right)^{1/3} s_{op}^{2/3} v^{1/3} \propto s_{op}^{2/3}\left(\frac{1}{2} - \chi_{12}\right)^{1/3} \qquad (4),$$

in which $s_{op} = (\sigma a^2)^{-1}$ is the openness of the brush, *i.e.*, the ratio between the average cross-section of the chains and the cross-section of a Kuhn segment. Therefore, the swelling coefficient of a strongly hydrophilic brush in water depends not only on the affinity of the volume of the brush for water, as expressed by the second virial coefficient ($v >> 0$ in a good solvent) or the interaction parameter ($\chi_{12} << 0.5$ in a good solvent), but also on the volume available for water penetration between the grafted chains, as expressed by s_{op}. For brushes of similar openness, the swelling coefficient thus provides a scale of hydrophilicity, higher values of v (lower χ_{12}) corresponding to water being a better solvent and to a larger swelling coefficient. This expression also shows that

brushes of lower grafting density (higher s_{op}) are more swollen for a given polymer/solvent pair (hence, at constant χ_{12}).

If water is a really poor solvent ($v << 0$ and $\chi_{12} >> 0.5$), equation (4) does not apply and must be replaced by:[45]

$$\alpha \simeq \frac{2w}{|v|} = \frac{2w}{\chi_{12} - \frac{1}{2}} \qquad (5)$$

in which w is the dimensionless third virial coefficient of segment interactions. Here again, the swelling coefficient provides a measure of hydrophilicity, with lower values of α obtained for brushes of more negative excluded volume v (hence, less hydrophilic brushes). However, the swelling coefficient is not dependent anymore on the openness of the brush : brushes of different grafting densities thus swell similarly in this collapsed regime. Finally, a responsive polymer brush passing from the good to bad solvent case transits by its Θ-state (at v = 0 and $\chi_{12} = 0.5$), at which point :

$$\alpha_{\Theta} = \frac{4}{\pi}\left(\frac{w}{2}\right)^{1/4} s_{op}^{1/2} \qquad (6);$$

less densely grafted brushes of higher openness s_{op} are thus also more swollen at the Θ point, as would be expected.

2.1.3.2 The cosine of the contact angle of water on a water equilibrated polymer brush defines its surface hydrophilicity

The surface hydrophilicity of a brush in contact with water is defined by the difference of free energy of the surface when in contact with water vapor, $\gamma_{br/v}$, and with liquid water, $\gamma_{br/w}$, normalized by the

surface tension of liquid water, $\gamma_{w/v}$. According to the Young-Dupré's equation,[46] this normalized difference is equal to the cosine of the contact angle θ_w of a droplet of water lying on the brush placed *in water vapor* :

$$\cos\theta_w = \frac{\gamma_{br/v} - \gamma_{br/w}}{\gamma_{w/v}} \qquad (7).$$

A swollen brush having the same surface hydrophilicity as liquid water would have $\gamma_{br/v} = \gamma_{w/v}$ and $\gamma_{br/w} = 0$, with consequently a spreading water droplet and $\cos\theta_w = 1$; conversely, a surface having the same affinity for the hydrophobic dilute vapor phase and the hydrophilic liquid water would mark the beginning of the range of hydrophobic samples with $\cos\theta_w = 0$ and $\theta_w = 90°$.

Equation (7) only rigorously applies to a brush at equilibrium with both water vapor and a droplet of liquid water; in these circumstances, the chemical potential of water is identical everyplace, with consequently the brush being swollen to the same degree below the water vapor and the droplet of liquid water. The surface of the brush however differs below liquid water and water vapor : a different surface excess of monomer units or water molecules may exist at both interfaces (a phenomenon called *adsorption*); the statistical configuration and conformational energy of the chain segments exposed at each interface may differ; and, for copolymer brushes, the surface composition in monomer units may be different at the two interfaces. Therefore, the thermodynamic functions describing the brush surface differ below water vapor and liquid water, even though the volume of the brush is swollen to the same extent in both regions.

The corresponding differences in excess surface entropy and free enthalpy can be obtained from experiments performed on brushes placed in equilibrium conditions, at constant pressure and constant brush area. Then, the difference of excess surface free enthalpy of the brush below water vapor and liquid water is :

$$\Delta g_s = \gamma_{br/v} - \gamma_{br/w} = \gamma_{w/v} \cdot \cos\theta_w \qquad (8).$$

If experiments are performed at different temperatures, and with a proper selection of the Gibbs dividing interface, it is also possible to obtain the difference of excess surface entropy Δs_s of the brush in water vapor and in liquid water, corrected for the contribution Δs_{ads} arising from adsorbed water molecules:[28]

$$\Delta s_s - \Delta s_{ads} = s_{br/v} - s_{br/w} - (\Gamma_v \overline{S}_v - \Gamma_w \overline{S}_w) = -\frac{\partial(\gamma_{w/v} \cdot \cos\theta_w)}{\partial T} \qquad (9),$$

in which $\overline{S}_\beta$ is the molar entropy of water vapor (β = v) or liquid water (β = w), and Γ_β is the surface excess of water molecules adsorbed on the brush interface with vapor or liquid water.

It is important to stress that these equations consider a brush at equilibrium with both the liquid and vapor phases of the probe solvent, and are thus relevant for the properties of a brush fully immersed in water as is the case for many applications of hydrophilic brushes; the equations are however not applicable to the case of a partially and heterogeneously-swollen brush, such as obtained when placing a droplet of water onto a brush in an atmosphere non-saturated by water vapor.

2.1.4 Photo-responsive polymer brushes

Light is another important parameter used to stimulate polymer brushes. By comparison with the temperature, the pH or other stimuli, the light stimulus offers the advantage to be clean, rapid and quick. Moreover, such a stimulus does not request any direct contact with the materials.[47] Photo-responsive polymer brushes usually bear photochromic molecules on side chains[48, 49] or backbone including ends,[8, 26] which are able to respond to light. The response of such responsive brushes with light involves changes of physical properties like degree of swelling and surface wettability.[31, 50-52] These property changes can be advantageously exploited to control drugs release, tune cell adhesion or switch easily the biomacromolecular activity with the light.[53, 54]

The photochromic molecules grafted on polymer brushes can be divided into irreversible groups and reversible groups. The irreversible photochromic groups are linked to polymer chains via photocleavable bonds, which undergo cleavage upon UV irradiation. O-nitrobenzyl (ONB) derivatives (Scheme 2.3. a) are the most popular ones. Upon UV irradiation (λ ~365 nm), the ONB groups are cleaved which results in the formation of a carboxylic acid groups. The presence of these carboxylic groups into the brush induces a brush swelling due to the electrostatic interactions and a higher surface wettability. Therefore the surface and volume properties of the brush can be tuned by photo-irradiation and pH variation.[51, 52, 55] Reversible photochromic groups grafted on polymer brushes are usually azobenzene (AZO) moieties(Scheme 2.3 b) or spiropyran (SP) derivatives (Scheme 2.3 c). Indeed AZO group can be reversibly isomerized by photo-irradiation (λ

~330 nm for visible light, λ ~450 nm for UV light) between a hydrophobic trans-isomer with 0D dipole moment and a less hydrophobic cis-isomer of 3D dipole moment.[56] By changing the polarity of grafted AZO groups upon photo-irradiation, the properties of the polymer brush such as the swelling and surface wettability, can be reversibly changed.[56]

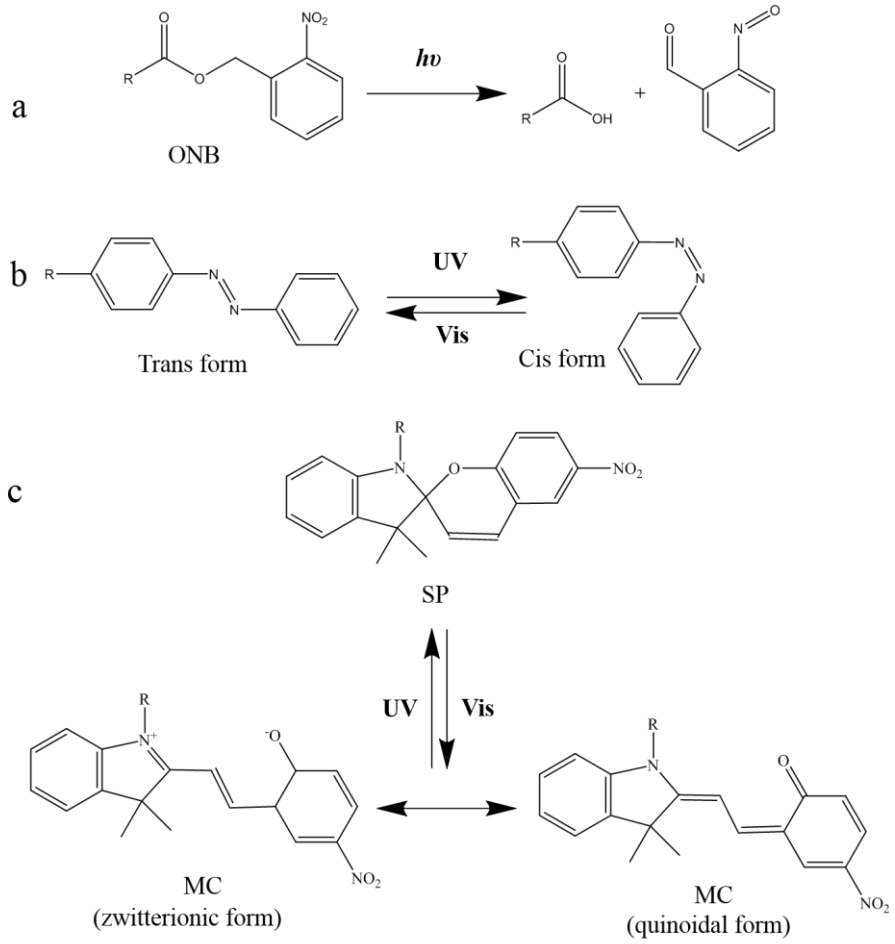

Scheme 2.3. Schematic structures of ONB (a),[44,45] AZO (b)[56] and SP (c)[57, 58] photo-responsive groups and the transfer processes upon photo-irradiation.

The photo-irradiation (λ ~250 - 380 nm) of colorless SP groups involves the breakage of C-O binding leading to the formation of the colored merocyanine (MC) form. Two MC isomers exist: the zwitterionic and quinoidal forms. The ratio between both isomers depends on solvent polarity. The zwitterionic MC form is dominant in polar media, whereas the quinoidal MC form exists mainly in less polar media.[57, 58] This feature contributes to the complexity of photo-responsive polymers bearing SP groups, but also provides more possibilities to change the properties of the polymers as a function of the pH and light.

As the photochromic groups are hydrophobic and bulky, they are usually incorporated into free polymer chains by direct polymerization or or copolymerization of monomers bearing photochromic groups or by post-modification of polymer chains. Photo-responsive polymer brushes are however usually synthesized by post-modification. This means that polymer brushes are fabricated first, then photochromophores such as AZO or SP groups are incorporated onto the formed polymer brushes.

2.1.5 Thermo-/photo-responsive free polymer chains and brushes

By incorporating photochromic groups onto thermo-responsive macromolecular chains, polymers showing both temperature- and photo-responsiveness are produced. The LCST of these polymers can be tuned by photo-irradiation. Shimoboji *et al*. synthesized thermo- and photo-responsive copolymers consisting of *N*,*N*-dimethyl acrylamide (DMA) and *N*-4-phenylazophenyl acrylamide or 4-phenylazophenyl

acrylate units via radical copolymerization in the presence of an end functional hydroxyl group, which can be converted to vinylsulfone (VS) group. The thermo- and photo-responsive polymer can conjugate enzyme of endoglucanase 12A by reacting the terminal vinyl sulfone group of the polymer with the sulfhydryl group of the enzyme forming an enzyme-polymer conjugation (see Scheme 2.4).[59] As the LCST of this copolymer can be tuned by photo-irradiation with UV or visible light, thus tuning the dissolution or precipitation of the polymer without changing temperature. By tuning the dissolution or precipitation of the polymer upon photo-irradiation, can the activity of the enzyme be switched on or off.[59] The same authors also grafted similar copolymers on streptavidin. It was shown that the complexation between the modified streptavidin and biotin was activated only upon UV irradiation due to the swelling of copolymer chains and consequently the exposure of specific binding sites of the enzyme.[60]

Many studies dealing with the tuning of the LCST of thermo-responsive polymers incorporating AZO groups were reported in the literature. The responsive behavior of these derivatives have been systematically investigated as a function of the molar mass and the structure of polymer chains, the polarity and the amount of AZO groups grafted as well as the nature of the surrounding solvent.[8, 61-63]

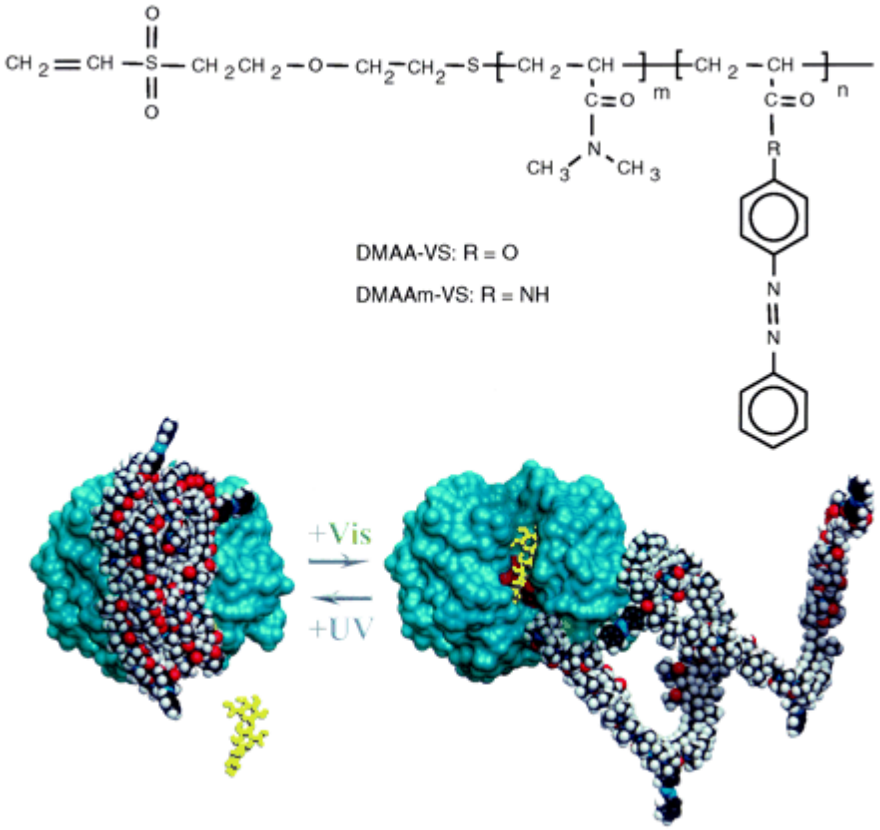

Scheme 2.4. Description of a photo-responsive enzyme switch grafted by temperature- and photo-responsive copolymer chains: (top) structure of the copolymer chains; (bottom) schematic model of the structure of the grafted enzyme with and without light exposure.[59]

Temperature-/photo-responsive polymer brushes are usually synthesized according to a 2 step process. First, thermo-responsive polymer brushes with functional groups on side chains or end chains are synthesized. Then photochromic groups are grafted onto functional groups via reactions like active esterification or amination to impart the polymer brushes with photo-responsiveness. Otherwise, the thickness of photo-responsive polymer brushes synthesized directly by free

radical polymerization from the surface or by grafting preformed photo-responsive macromolecules onto the substrate is very thin due to the crowded polymer chains and bulky photo-chromophores. Dirani *et al*. synthesized poly(HOEGMA-*co*-MEO_2MA) brushes grown from silicon substrates then coupled with azobenzene groups. (Scheme 2.5).[48] They systematically studied the influence of the grafting density of the brush, the composition of the copolymer chain in MEO_2MA and HOEGMA and the brush thickness on the yield of AZO grafting. They showed that the yield of AZO groups grafted on the brushes decreased with the brush grafting density but increased with polymer brush thickness if it is lower than 100 nm. In addition, the swelling of the polymer brushes was successfully reversibly switched upon UV irradiation but remains limited. This suggests that the change of the dipole moment of AZO groups does not affect significantly the swelling of polymer brush.

Photo-sensitive polymer brushes bearing photochromic molecules like ONB[58] or SP[64, 65] have also been synthesized. However, the photo-response of polymer brushes incorporating ONB groups is not reversible. Moreover, the photo-responsive behavior of polymer brushes bearing SP groups is complex due to their pH and solvent sensitiveness.

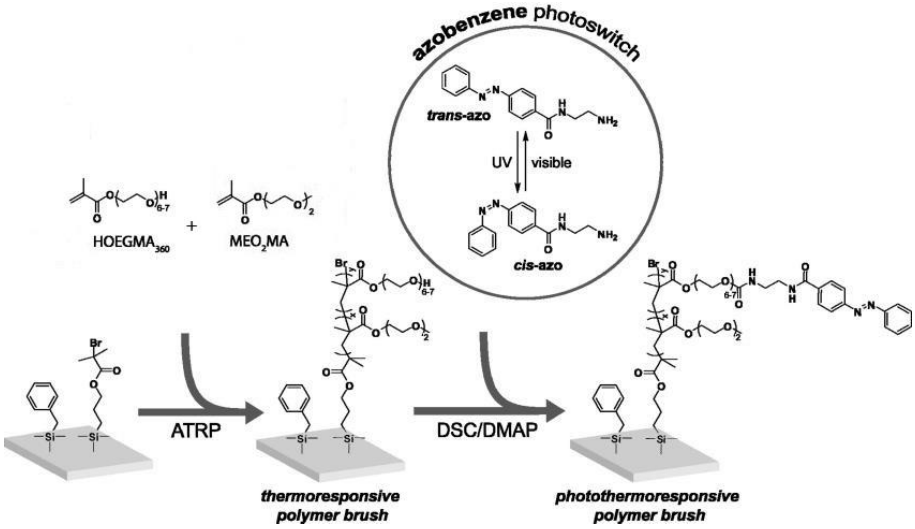

Scheme 2.5. Schematic illustration of the synthesis of OEGMA-based thermo-/photo-responsive copolymer brushes grown on silicon surfaces. Adapted from ref.[48]

2.1.6 Other stimuli-responsive polymer brushes

Polymer brushes containing ionizable groups in their repeat units respond to pH or ionic strength. Depending on the nature of the ionizable groups, the pH-responsive polyelectrolyte brushes can be divided into two types: weak polyacid brushes and polybase brushes, which both undergo an ionization/deionization transition at a specific pH named pKa. Weak polyacid brushes accept protons at low pH and donate them at natural or high pH, while polybase brushes are deprotonated at high pH and become positively ionized at neutral and low pH.[9] A large number of reports have been published on pH-responsive polymer brushes. However, the most frequently used pH-responsive polyacid brushes are based on polyacrylic (PAA) or poly(methacrylic acid) (PMAA) and pH-responsive polybase brushes are based on poly(*N*, *N*-dimethylamidenoethyl methacrylate)

(PDMAEMA). The volume swelling degree and surface wettability of these brushes depend on pH, ionic strength and grafting densitity.[5, 6, 9]

Excepted for the well-known stimuli-responsive polymer brushes mentioned above, there are some other special stimuli-responsive polymer brushes such as redox-responsive or glucose-responsive polymer brushes for the applications in biomedical fields.[66, 67] When initiators containing disulfide bonds are used to synthesize polymer brushes or when macromolecular chains contain disulfide bonds, the brushes can exhibit redox-responsive properties. Indeed the disulfide bonds can be cleaved and convert to thiols in the presence of reducing agents like glutathione (GSH). Redox-responsive brushes are usually grafted onto nanoparticles for drug delivery.[66, 67] Another type of stimuli-responsive brush is related to glucose-responsive brush that are used as biosensors for detecting the blood glucose level in treating diabetes. This disease is caused by insulin deficiency and hyperglycemia, reflected by high blood glucose concentration in blood.[68] Traditionally, the monitoring of glucose concentration in blood by using glucose-responsive polymer is based on grafting glucose oxidase (GOx) onto polymer brushes. At the presence of oxygen, the GOx on the polymer brush catalyzes the oxidation of glucose into gluconic acid via redox reactions.[68] Another approach to detect the blood glucose is based on glucose-responsive brushes bearing phenylborate acid and its derivatives. Indeed these chemical groups show glucose-responsiveness due to their ability to form reversible complexation with diols such as glucose through the formation of boronate ester.[69-71] According to this approach, Chen *et al*. grafted glucose-responsive polymer brushes consisting of poly(*N*-isopropyl

acrylamide)-*co*-poly(acrylic acid)-(3-aminophenyl-boronic acid) (PNIPAM-*co*-PAA-PBA) on gold surfaces and microcantilever arrays to detect glucose at physiologically relevant concentrations. The swelling of polymer brushes bearing boronic acid groups is much higher than the swelling of PNIPAM-*co*-PAA brushes without boronic acid groups. In the same way, the stress variation measured for microcantilevers is much higher when they are grafted with polymer brushes bearing boronic acid groups compared to PNIPAM-*co*-PAA brushes. For a given glucose concentration, the swelling ratio of glucose-responsive brushes increases with the amount of boronic acid groups grafted on the brush. . Moreover the swelling ratio of polymer brushes bearing a certain amount of boronic acid groups increases with the glucose concentration, for a given range. The microcantilevers grafted with the polymer brush bearing boronic acid groups sensitively bend with the glucose concentration increasing. Thus these cantilevers can be used to estimate the glucose concentration in complex physiological mixtures.[72]

In several cases, dual-responsive polymer brushes or multi-responsive polymer brushes have been synthesized to broaden the applications of these smart polymer materials. As it was mentioned above, photochromic groups like AZO are usually incorporated into thermo-responsive polymer brushes to tune their collapse temperature upon photo-irradiation in aqueous solution. Therefore the collapse temperature of these AZO-grafted thermo-responsive polymer brushes changes as a function of the wavelength used during the light irradiation.[48] Brushes responding to both pH and temperature were also synthesized. The collapse temperature of these dual brushes is tuned as

a function of pH values, causing the change of the swelling degree and surface wettability of polymer brushes with pH and temperature.[73]

Polymer brushes responding to both pH and glucose were also successfully synthesized by Liu *et al*.[54] For this, phenylboronic acid-containing polymer brushes were grafted on an array of aligned silicon nanowires. The resulting layers were shown to respond reversibly to pH and glucose. These layers were successfully used to capture then release cancer cells in presence of glucose (Scheme 2.6).[54] Indeed phenylboronic acid (PBA) group does not only form a complex with diols, but also with sialic acid in a given pH condition. However sialic acid is overexpressed in the membrane of certain cells like cancer cells. Therefore polymer brushes incorporating PBA were used to reversibly capture then release cancer cells by changing pH and glucose concentration.

Although some research on dual-responsive polymer brushes have been conducted, the research on multi-responsive polymer brushes is still rare. For instance, spherical copolymer brushes showing thermo-, pH- and photo-responsive behavior were synthesized from DMAEMA and 7-(2-methacryloyloxyethoxy)-4-methylcoumarin (CMA) on silica nanoparticles.[31] Indeed while DMAEMA units provide pH and temperature responsiveness, CMA units are cross-linked via the formation of dimers upon UV irradiation at $\lambda > 300$ nm. Moreover these CMA dimers are cleaved upon UV irradiation at $\lambda < 300$ nm.[74] The cross-linking density can be easily controlled by alternating irradiation of the copolymer brushes at wavelengths of 365 and 254 nm. As a consequence, the volume phase separation and diameter of spherical

brushes grafted onto silica nanoparticles is tuned as a function of the pH and the photo-irradiation.[31]

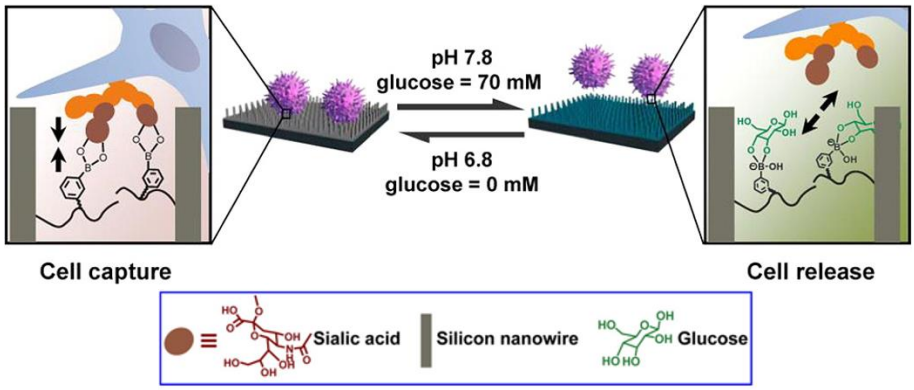

Scheme 2.6. Schematic process of the pH- and glucose-responsive polymer brush grafted on silicon nanowire surface to proceed cancer cell capture and release. Adapted from ref. [54]

2.2 Preparation of polymer brushes

2.2.1 General description of the different approaches

Generally, there are two methods to synthesize polymer brushes on solid surfaces: physical adsorption (also called physisorption) and chemical grafting. (Scheme. 2.7) For physical adsorption, block copolymers physically adsorb onto a suitable substrate surface by strongly attracting one block compared with the other one (Scheme 2.7 a). Chemical grafting refers to polymer chains connected with a substrate surface via covalent bonds, which can be accomplished by either "grafting to" or grafting from" approaches. For the "grafting to" approach, preformed polymer chains are attached directly on suitable substrate via reactions between the end-functional groups of the macromolecular chains and appropriate groups on pretreated surfaces

(Scheme 2.7 b). This brush growth method is quite simple and the structures of the macromolecules to be grafted can be predesigned. However, it is difficulty to achieve high grafting densities due to steric crowding of the surface reactive sites by the already adsorbed polymer chains.[5, 9] As to "grafting from" approach, an initiator monolayer is first introduced onto the surface of the substrate then initiate polymerization of monomers to produce long polymer chains (Scheme 2.7 c).[5, 9] This brush grafting method is very efficient to fabricate brushes with high grafting densities and thus thick brushes, and even control the compositions, structures and functionalities of the grafted macromolecules due to the development of controlled/"living" radical polymerization (CRP) techniques such as atom transfer radical polymerization (ATRP), reversible addition-fragmentation transfer (RAFT) polymerization and nitroxide-mediated polymerization (NMP).[5, 9] The grafting density and polymer chain length might affect significantly the properties of thermo-responsive polymer brushes such as the swelling of brushes in aqueous solution. Generally, low grafting densities correspond to low brush thicknesses. When the grafting density decreases, the swelling coefficient of a thermo-responsive polymer brush increases, and its temperature sensitivity (the slope of swelling versus temperature) decreases with increasing grafting density.[75, 76] The collapse transition of thermo-responsive polymers in brushes occurs gradually and thus broadly with temperature, not like a sharp coil-globule transition observed for isolated polymer chains in water.[76, 77] Although grafting density has strong effects on the swelling degree of thermo-responsive polymer brushes, it influences little the surface wettability of the brush since, as we will show, the surface

wetting is mainly sensitive to specific details of the conformations and atomic composition of the outermost region of the brush.[78]

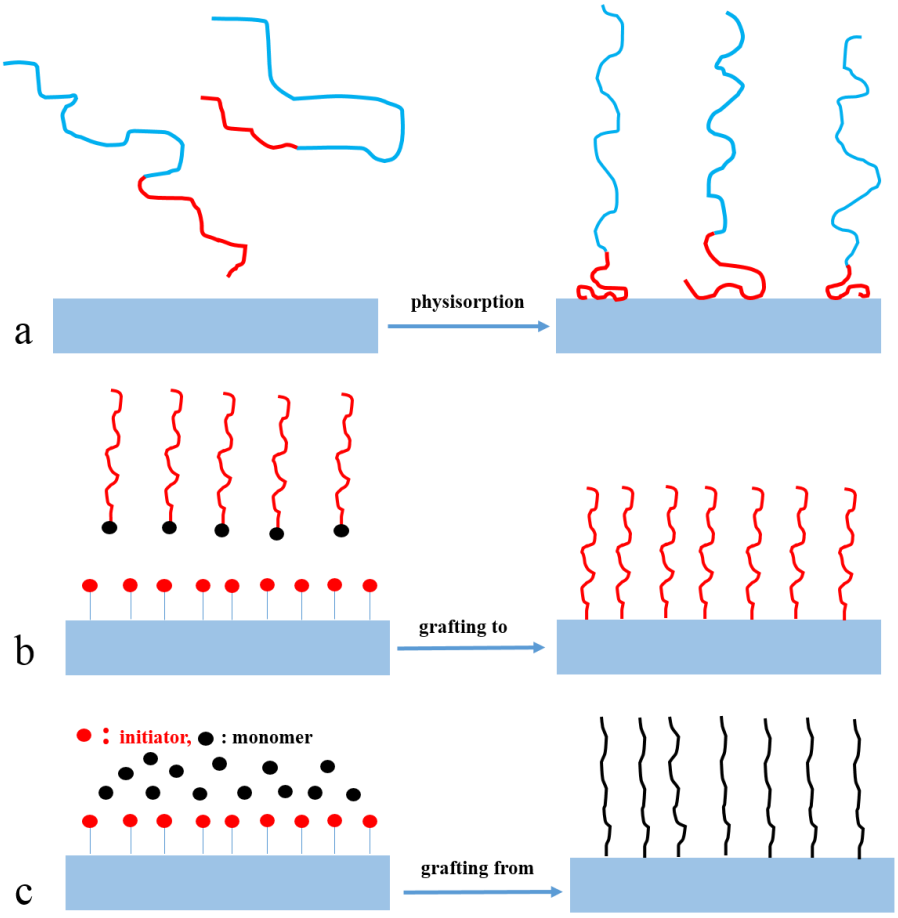

Scheme 2.7. Schematic illustration of the different approaches used to synthesize polymer brushes: (a) physical adsorption of block copolymer; (b) chemical grafting according to "grafting to" approach; (c) chemical grafting according to "grafting from" approach.

2.2.2 Description of controlled/"living" radical polymerization (CRP) techniques

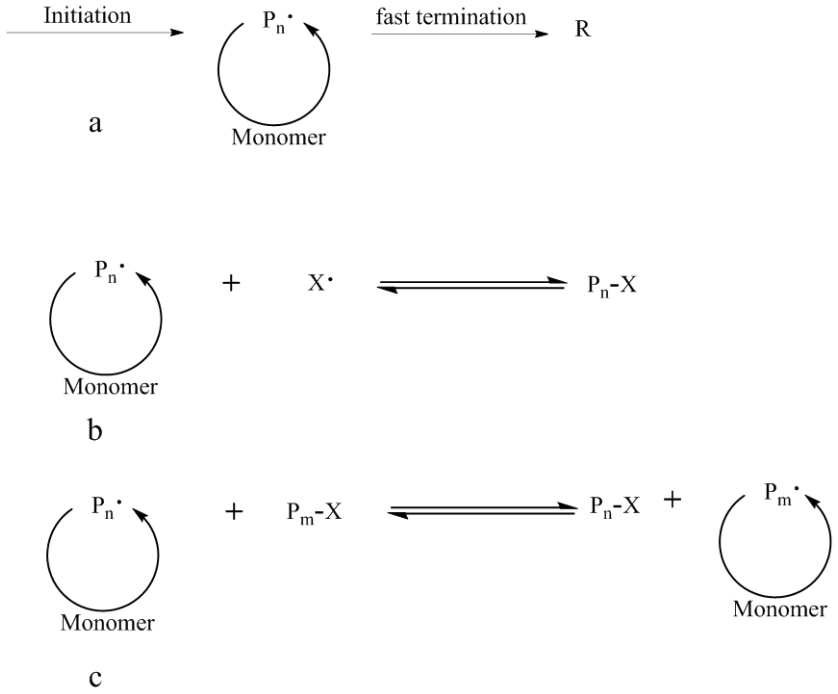

Scheme 2.8. Schematics of propagating processes of living radical polymerization, (a) conventional radical polymerization with fast termination, (b) living radical polymerization via radical deactivated, and (b) living radical polymerization via radical transfer.

Before describing the preparation of polymer brushes, it is necessary to firstly elucidate the mechanisms of CRP techniques due to their importance for the synthesis of well-defined polymers. Compared with the fast termination of propagating radicals or initial radicals coming from initiators in conventional polymerization (Scheme 2.8 a), in CRP, the initial radicals almost form at the same time and initiate monomers producing propagating radicals (Pn·**)**. These ones can be

reversibly deactivated (Scheme 2.8 b) or reversibly transferred (Scheme 2.8 c) to dormant from (P_n-X) in the presence of reagents. This rapid equilibration between the active and dormant forms ensures that all the chains possess an equal chance for growth and that all chains grow, albeit intermittently.[79, 80]

Among the CRP techniques, ATRP is the most popular one due to the large amount of monomers suitable for ATRP. The mechanism of ATRP is shown in Scheme 2.9. It involves the use of an alkyl halide initiator and a catalyst based on a transition metal halide coupled with a suitable nitrogen-based ligand. The initiator molecules become instantaneously active radicals that initiate monomers to produce growing chains. Then growth of the chains is constantly generated at a low concentration through a reversible redox process catalyzed by a transition metal complex which undergoes a one-electron oxidation with concomitant abstraction of a halogen atom (X) from dormant species (R-X). Thus the growing radicals continue to initiate monomers leading to the formation of longer chains with a very small percentage of termination (< 5%). The reversible process between the dormant species (Pn-X) and the metal complex rapidly establishes an equilibrium that is predominately shifted to the side with very low radical concentration. Because each growing chain has the same probability to react with free monomers to form living/dormant polymer chains, very similar molecular weights and narrow molecular weight distribution are obtained.[9, 80, 81]

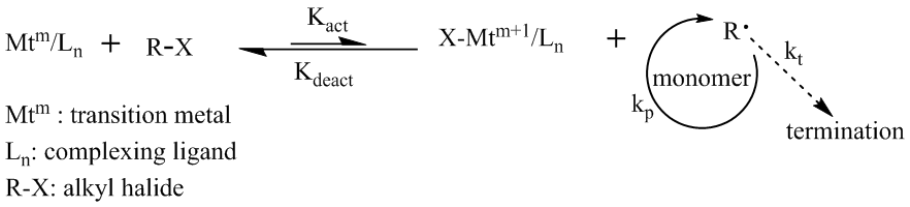

Scheme 2.9. Description of the ATRP process.

A large variety of monomers can be polymerized by ATRP technique such as styrenes, (meth)acrylates, and (meth)acrylamides. However, until now, well-controlled polymerization of acrylamides is still difficult to reach, mainly due to the complexation between the amide groups and ligands.[82-86] In addition initiator, catalyst system and solvent have to be carefully selected to control the polymerization.[24, 83, 86, 87] The initiators are usually alkyl chloride or alkyl bromide. The common used transition metal is copper chloride or copper bromide. The widespreadly used ligands are 2, 2'-bipyridine (Bpy), *N*,*N*,*N'*,*N'*,*N''*-pentamethyldiethylenetriamine (PMDETA), 1,1,4,7,10,10,10-hexamethyltriethylenetetraamine (HMTETA) and tris(2-dimethylaminoethyl)amine (Me_6-TREN). The structures of the above ligands are shown in Scheme 2.10. There are a great number of solvents that can be used for ATRP such as benzene, toluene, anisole, diphenyl ether, ethyl acetate, dimethyl formamide (DMF), ethylene, alcohols, carbon dioxide and water. Depending of the nature of the monomer and catalyst used, a suitable solvent has to be selected. Moreover the solvent can play a role in side chain transfer reactions and catalyst poisoning.[81] Sometimes, in order to change the kinetics of polymerization, deactivators can be added in the reaction mixture or mixed copper halides can be used.

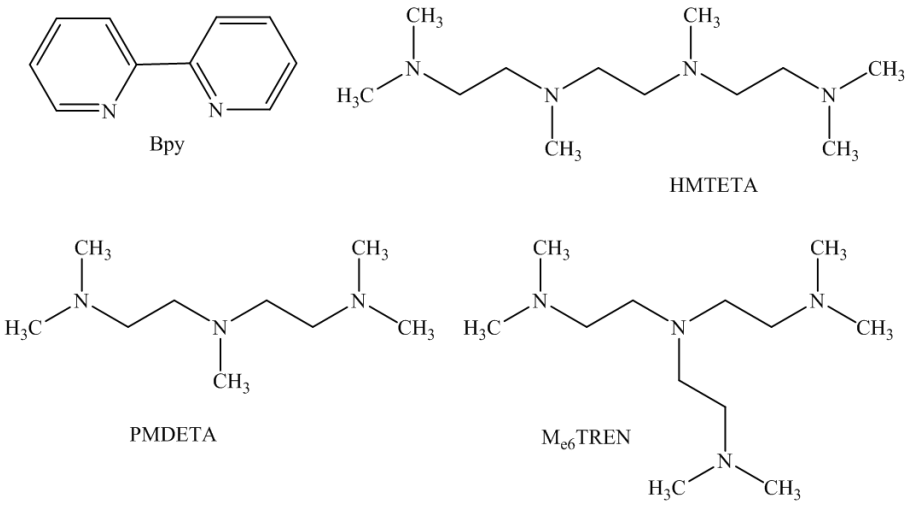

Scheme 2.10. Structures of common nitrogen ligands used for ATRP.

RAFT polymerization is similar to conventional radical polymerization, only differing in the addition of a RAFT agent, also called chain transfer agent (CTA), which is usually a thiocarbonylthiol derivative with a stabilizing Z-group and a reinitiating R-group (see the CTA structure in Scheme 2.11) The key process determining the controlled polymerization is the formation of a rapid deactivation-activation equilibrium between the propagating radicals and RAFT agents established through chain-transfer reactions (Scheme 2.11).[67, 79, 88] So, the selection of the RAFT is critically important due to its major role in the chain-transfer reactions.[79] In contrast with ATRP, the monomers such as acrylamides like DMA or NIPAM and monomers bearing ionic groups or hydroxyl-groups such as substituted (meth)acrylamides, can be polymerized in a controlled way by RAFT even in aqueous solution.[89-94]

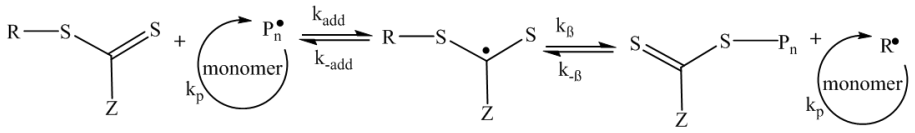

Scheme 2.11. Description of the deactivation-activation process involved between the propagating radical and RAFT agent during the RAFT polymerization.

Compared to ATRP and RAFT polymerization techniques, NMR is less exploited due to the limited monomers that can be used with this technique or due to the strict reaction conditions required.[67, 95]. For this reason, NMR is not described here.

2.2.2.1 Preparation of polymer brushes by physical adsorption

Physical adsorption of copolymer chains on a solid surface is a reversible process, achieved by the assembly of block copolymers or end-functional polymers on a solid substrate surface. Solvents and substrate surfaces have to be specially selected or treated to obtain the selective adsorption of one block of the copolymer. Typically an ideal solvent must precipitate one block forming an "anchor" layer on the surface and dissolve the other block forming the polymer brush in solution. Parsonage *et al.* studied a series of polymer brushes fabricated by physisorption of poly(styrene-*b*-4-vinylpyridine) (PS-*b*-PVP) of various molar masses. As toluene is a good solvent for PS but a bad solvent for PVP, PVP blocks precipitate on the surface while PS blocks swell in toluene forming a brush.[96]

Fytas *et al.* fabricated PS-*b*-PEO brushes on a glass surface consisting a PEO anchor and a PS brush in toluene. Although toluene is a good solvent for both PS and PEO, there is a stronger attraction

between the surface and polar PEO blocks compared to PS block. Therefore PS blocks formed the brush while PEO blocks form the anchor part.[97]

Although the adsorption of copolymer chains on the solid surface is performed easily, the structure of the resulting polymer brushes is difficult to maintain notably when the interactions between the substrate and the block copolymer are achieved through weak forces like van de Waals forces and hydrogen bonding. Moreover the surface grafting density and other characteristic dimensions like chain contour length, geometry of the brush structures are in a thermodynamic equilibrium condition so that they can be easily changed by variation of the surrounding conditions. For instance, heating the sample or adding another solvent can cause dewetting or desorption of the adsorbed copolymer chains.[1, 98] For these reasons, the preparation of polymer brushes chemically grafted on the surfaces has been developed.

2.2.2.2 Preparation of polymer brushes by "grafting to" approach

"Grafting to" approach refers to preformed and end-functionalized polymer chains reacting with a suitable surface functional groups under appropriate conditions to form a tethered polymer brush. It means that the free polymer chains should bear functional groups which can react with the surface functional groups through chemical reactions. But this requirement limits the number of polymers that can be used to prepare polymer brushes. In addition, it is difficult to achieve high grafting density and high thickness of polymer brush due to the steric hindrance between the grafted polymer chains.[1, 5, 99] However, the main advantage for this approach is that the composition and structure of polymer chains

can be predesigned by CRP techniques or other controlled polymerization techniques, which is very useful to synthesize specific polymer brushes like Y-shaped polymer brushes or brush with specific surface properties.

Minko *et al*. synthesized binary polymer brushes showing adaptable surface wettability as a function of the nature of the solvent.[100] For this, they first grafted a monolayer of 3-glycidoxypropyl-trimethoxysilane with an end-functional epoxy group onto a silicon substrate; then they performed a step-by-step grafting of carboxyl-terminated polystyrene (PS) and poly(2-vinylpyridine) (PVP) on the modified surface (Scheme 2.12). By changing the time or/and temperature grafting of the first polymer, it was possible to tune the composition of the binary brushes. It was shown that the film undergoes a phase segregation at the nanoscopic scale. Moreover upon exposure to different solvents, the surface morphology reversibly switches from "ripple" to "dimple" structures which results in a surface energetic state that switches from hydrophobic to hydrophilic.[100]

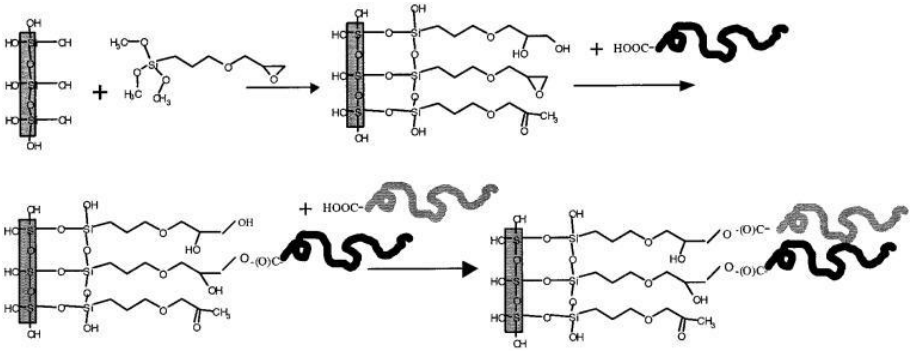

Scheme 2.12. Schematic representation of the "grafting to" synthesis of binary brushes responding to solvent: black chain represents PS and gray chain represents PVP.[100]

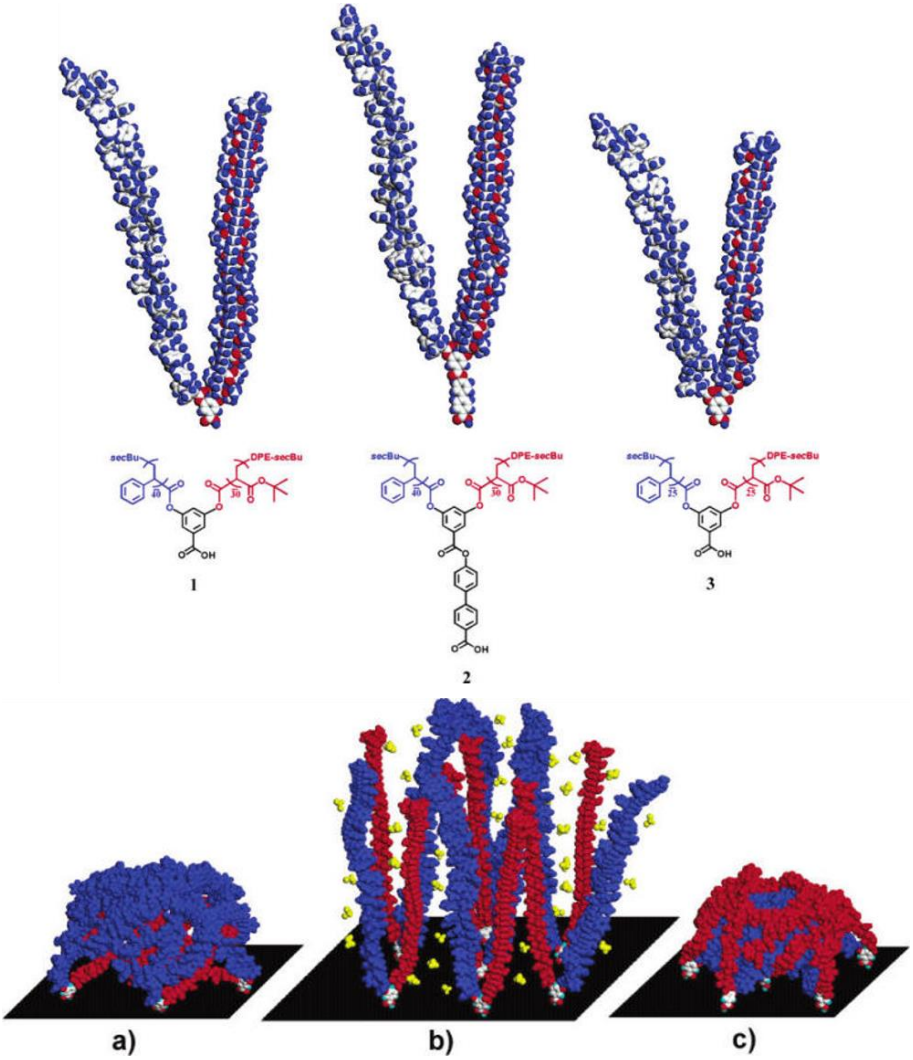

Scheme 2.13. (Top) Schematics of chemical structure and molecular graphics of Y-shaped block copolymers consisting of PS and PAA with a short (1 and 3) and a long (2) aromatic functional stem. (Bottom) molecular models showing conformational rearrangements of polymer arms of Y-shaped brushes in selective solvents: (a) segregated pinned micelle, (b) Y-shaped polymer brush of (1) in a nonselective solvent and (c) top-open craterlike structure in a selective solvent showing collapsed PS arms partially covered by PAA chains. Adapted from ref. [101]

Julthongpiput *et al*. synthesized Y-shaped amphiphilic polymer brushes consisting of polystyrene (PS) and poly(acrylic acid) arms connected onto a hydrolyzed poly(tert-butyl acrylate) segment (Scheme 2.13). The surface wettability of these brushes can be switched by changing the nature of the surrounding solvent due to the conformational rearrangement of PS and PAA arms.[101]

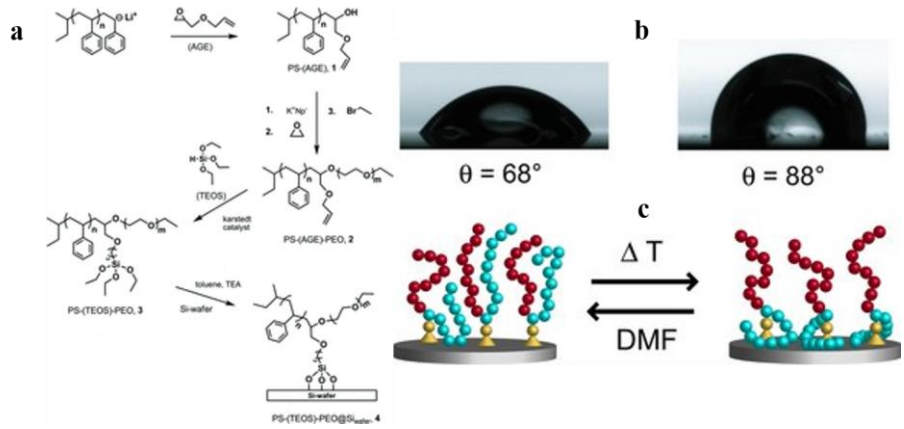

Scheme 2.14 Schematics of synthesis of the Y-shaped polymer brush incorporating PS and PEO arms and its surface wettability change, (a) the pre-synthesis Y-shaped polymer and the synthesis of Y-shaped polymer brush, (b) the surface wettability change of the polymer brush, (c) schematic of the conformational re-arrangement of the arm of PEO causing the change of surface wettability upon heating or DMF treatment. Red chains: PS, blue chains: PEO. Adapted from ref [102]

According to a similar approach, Tonhauser *et al*. synthesized Y-shaped polymer brushes based on PS and PEO arms of different lengths. (Scheme 2.14). The surface wettability of these brushes can be reversibly varied by increasing the temperature or by adding organic

solvent such as DMF due to the conformational change of PEO chains in these conditions.[102]

In order to overcome the drawbacks of the "grafting to" approach, Rauch combined the "grafting to" approach with clicking reaction (thermo azide-alkyne cycloaddition) to extend the polymer chains (Scheme 2.15). Briefly, surfaces treated with poly(glycidyl methacrylate) (PGMA) were first grafted with PNIPAM chains bearing trimethylsilyl (TMS)-protected alkyne end-groups. The cleavage of these TMS moieties generates active alkyne groups that subsequently react with azide-functionalized PNIPAM chains spin-coated on the surface.[103] This procedure allows to produce thick and dense PNIPAM brushes whose thickness in water is highly sensitive to temperature. The enhanced sensitivity of such thermo-responsive brushes is useful to tune protein adsorption and cell adhesion.[103]

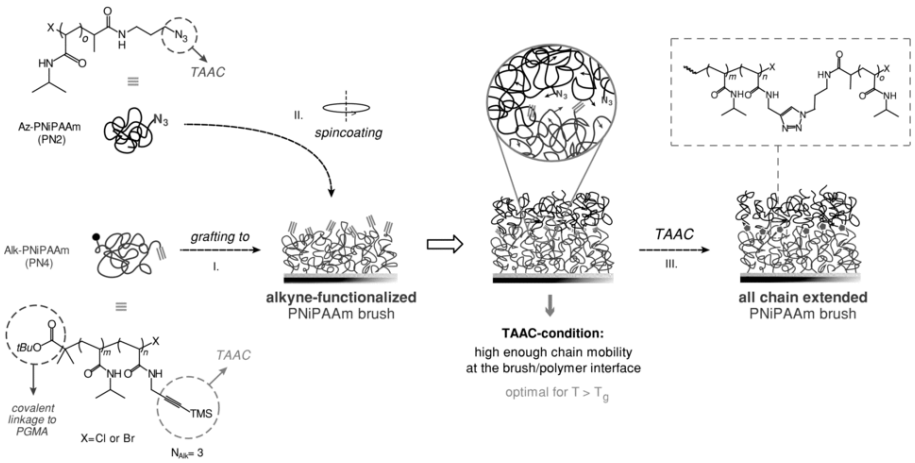

Scheme 2.15. Schematic procedure of the synthesis of PNIPAM brushes based on a "grafting to" approach combined with click chemistry.[103]

2.2.2.3 Preparation of polymer brushes by "grafting from" approach

With the fast development of CRP techniques, especially the development of ATRP in recent decades, the "grafting from" approach has been extensively used for the preparation of polymer brushes. Surface initiated ARTP (SI-ATRP) is the most efficient and robust method to synthesize polymer brushes with a given thickness, narrow molar mass distribution and well-defined composition and architecture. Experimentally, a surface grafted by an ATRP initiator is introduced in the reaction mixture containing the monomers. The ATRP initiators can be easily anchored onto various solid surfaces of different nature and geometry, such as flat or curved surfaces or even on side chains of pre-anchored macromolecules, which allows to synthesize flat, spherical or molecular brushes that are composed of a flexible backbone with densely grafted side chains.[2]

The nature of the solid substrate chosen for the fabrication of the polymer brush is very important since it determines the process to immobilize the initiator. The silicon oxide-based planar surfaces or nanoparticles are commonly used to synthesize planar and spherical brushes, respectively. For this, these surfaces are grafted with a monolayer of chlorosilane or alkoxysilane end-functionalized with an ATRP initiator group.[104, 105]

In order to control the length and the structure of macromolecular chains grown from the surface, different parameters have to be optimized such as the composition of the solvent or the catalyst system. Moreover deactivators or free initiators are usually added in the reaction mixture to better control the reaction.

For instance Ejaz *et al.* synthesized poly(methyl methacrylate) (PMMA) brushes by SI-ATRP from a self-assembled monolayer (SAM) of 2-(4-chlorosulfonylphenyl)ethyl trimethoxysilane.[106] The authors found that free initiator has to be added in the reaction mixture to control the molar mass and the polydispersity of polymer chains. Indeed when sacrificial initiator of *p*-toluenesulfonyl chloride is added in the reaction mixture, the growth of PMAA brushes is well-controlled. Besides, they also found that the brush thickness is proportional to the molar mass of free polymer chain produced in solution and suggested that the molar mass of tethered chains is almost equal or at least proportional to that of the free polymer. As the molar mass of the chains of the brush cannot be measured, adding free initiator in the reaction mixture during the brush growth allows to estimate the molar mass of tethered polymer chains by measuring the molar mass of free polymer chains in a conventional way. However, the method to estimate the molar mass of tethered chains by measuring the molar mass of free chain in solution is still under debate. Recently, Turgman-Cohen *et al* turned to Monte Carlo computer simulations to investigate the simultaneous controlled radical polymerization in solution and from a flat surface. They found that the polymer chains grafted on the surface possess a lower molar mass and a higher polydispersity index compared to free polymer chains.[107] It was simulated that the molar mass and polydispersity of tethered chains depend on their grafting density (σ) and the fraction of tethered macromolecular chains (η) relative to the free macromolecular chains formed in solution. The difference between the molar masses of the two populations of polymers decreases with decreasing σ and increasing η.[108]

Instead of adding sacrificial initiators, Matyjaszewski *et al.* added deactivators based on Cu^{2+} species such as $CuCl_2$ or $CuBr_2$, to perform SI-ARTP. By this way, they successfully controlled the growth of PS brush as well as poly(styrene-*co*-acrylate) brushes.[109] Sometimes, a mixture of activators/deactivators is also added in the reaction solution to control brush growth. For instance, Huang *et al.* showed that the growth of poly(2-hydroxyethyl methacrylate) (PHEMA) brushes by SI-ATRP rapidly stopped when only CuCl catalyst was added in the reaction mixture. However the thickness of the polymer brush increased almost linearly up to 700 nm after a reaction time of 12 h if $CuBr_2$ deactivator was added in the medium.[110] Matyjaszewski *et al.* pointed out that using such halide activator/deactivator systems improves the control of SI-ATRP due to the lower free energy of dissociation of the C-Br bond compared to the C-Cl. This supports the shift of the equilibrium between dormant and propagating radical species to the side of dormant species.[111] Brown *et al.* synthesized oligo(ethylene glycol) methacrylate-based polymer brushes in a controlled way by using such a catalyst system via SI-ARTP.[112]

Polar solvents, especially water, significantly increase the polymerization rate of SI-ARTP.[110, 113-115] Huang *et al.* fabricated well-defined PHEMA brush with 700 nm-thickness after 7 h in pure aqueous solution using water-accelerated SI-ATRP.[110] Although water accelerates the rate of polymerization, it also increases the rate of termination. Therefore, it is sometimes useful to add less polar solvent in the reaction mixture to better control the polymerization.[24, 116] For instance, Robinson *et al.* controlled the polymerization of HEMA in

pure methanol or 50/50 methanol/water mixed solvent without adding deactivator such as $CuBr_2$.[115]

When growing polymer brushes from nanoparticle surface, the size of nanoparticles as well as the presence of free initiator in the mixture have a great influence on the control of the polymerization. Werne *et al*. have systematically studied the influence of the size of silica nanoparticles coated with a monolayer of ATRP initiator, on the growth of PSS and PMMA brushes.[117] They found that the control of the polymerization is not only related to the termination mechanism but also to the diameter of nanoparticles and the presence of free initiator in the mixed solution. Indeed, the grafting density of initiator layer formed on the surface of smaller nanoparticles is higher than the grafting density of initiator layer formed on the surface of larger nanoparticles due to the higher surface area-to-volume ratio of the smaller nanoparticles. As a consequence the initial initiator/monomer ratio is higher for smaller particles. Moreover, adding a small amount of free initiators in the medium increases the initial initiator/monomer ratio and improves the control of the polymerization. Moreover a slower rate of polymerization was observed when deactivators were added in the medium. However such an approach did not improve the control of the polymerization.[117].[109]

2.3 Characterization techniques

2.3.1 Quartz crystal microbalance with dissipation monitoring (QCM-D)

The quartz crystal microbalance (QCM) technique was developed from the discovery of the piezoelectric effect of quartz crystal by Curie

brothers. This technique consists in measuring the resonance frequency of a quartz sensor connected to an external driving oscillator circuit. The sensor, commonly called thickness shear mode resonator (TSM resonator) is composed of a thin disk of a single crystal quartz covered by metal electrodes deposited on both sides. It is usually produced from the so called "AT-cut" (cut with an angle of 35° 10′ with respect to the optical z-axis) that provides good thermal stability in the range of 0-50°C and pure shear mode of oscillation.[118, 119]

The specific AT-cut crystal operates in the TSM. Shear waves of opposite polarity are generated from the electrodes on each side of the crystal so that the shear displacement is in plane with the crystal surface (Scheme 2.16).[119] Both shear waves go through the quartz thickness then are reflected on the opposite crystal surface to return to their origin. A constructive interference between the incident and return waves occurs when the acoustic wavelength is an odd multiple of twice the crystal thickness (i.e. $2d_q$ with d_q the crystal thickness) and standing wave conditions are established. Particle displacement of the standing acoustic wave is maximum at the crystal surface ($z = \pm d_q/2$) and a displacement node exists in the center of the resonator ($z = 0$). The eigenfrequency f_n of the n^{th} overtone can be expressed by

$$f_n = \frac{\upsilon_p n}{2dq} \qquad (4),$$

where υ_p is the propagation velocity of acoustic wave in quartz crystal and n the harmonic number. The resonance frequency is mainly determined by the crystal thickness dq. This equation reveals that the surface electrodes can excite only odd harmonics, *i.e* n =1, 3, 5…. When an additional layer is deposited uniformly on the crystal surface, the additional mass resulting from the presence of this layer increases the

thickness of the resonator. As a consequence the eigenfrequency of the crystal decreases. The mass deposited on the crystal surface can be estimated from the measurement of the variation of the eigenfrequency of the crystal and the device operates like a microbalance. The most used quartz crystal has an intrinsic resonance frequency f_0 of about 5 MHz with a thickness of 300 μm and a diameter in the range of 10-25 mm.[120]

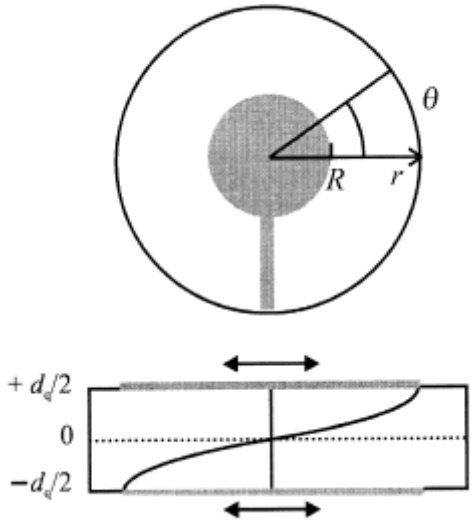

Scheme 2.16. Schematic illustration of the quartz sensor used in quartz crystal microbalance (QCM) technique. The gray area depicts the metal electrodes.[119]

In 1959, Sauerbrey found for a thin, rigid and uniform film deposited on a sensor surface that the oscillating frequency of the quartz crystal decreases with the bound elastic mass deposited when the resonator is operated in air or vacuum.[121] The linear relationship between the frequency change (Δf) and the deposited mass (Δm) is given by:

$\Delta f = -2\Delta m f_0^2/(A\sqrt{\mu_q \rho_q})$ (5),

where A is the electrode area, f_0 is the intrinsic crystal frequency and μ_q and ρ_q are the shear modulus and density of quartz crystal, respectively.[121]

However for most applications, the resonator is operated in liquid. In that case, the deposited layer is not considered like elastic but usually viscoelastic. Therefore the Sauerbrey equation does not apply anymore in this condition. Indeed the viscoelasticity and density of the layer cause the energy dissipation due to the oscillatory motion excited at the interfacial solid-liquid region and the resonant frequency shift. This energy dissipation can be obtained by measuring the dissipation factor *D*, which is inversely proportionally to the decay time constant:

$D = (\pi f \tau)^{-1}$ (6),

where τ is the time constant for the amplitude decay measured from the switch off the power source and f is the resonant frequency.[122]

For a very thin viscoelastic polymer film deposited on quartz crystal surface and immersed in a fluid, the frequency (Δf_n) and dissipation shifts (ΔD_n) (compared to the bare reference crystal) can be obtained from the Voigt model consisting of a spring and a dashpot arranged in parallel:

$$\Delta f_n \approx -\frac{1}{2\pi\rho_q t_q}\left\{\frac{\eta_l}{\delta_l} + h_f \rho_f \omega_n\right) - 2h_f \left(\frac{\eta_l}{\delta_l}\right)^2 \frac{\eta_f \omega_n^2}{\mu_f^2 + \omega_n^2 \eta_f^2}\} + \alpha_f(\omega_n) \quad (7),$$

$$\Delta D_n \approx \frac{1}{\omega_n \rho_q t_q}\left\{\frac{\eta_l}{\delta_l} + 2h_f \left(\frac{\eta_l}{\delta_l}\right)^2 \frac{\mu_f {\omega_n}^2}{\mu_f^2 + \omega_n^2 \eta_f^2}\right\} + \alpha_D(\omega_n) \quad (8),$$

where ρ_q, t_q and ω are the density, thickness and resonance angular frequency of the quartz crystal, respectively; η(*l* or *f*) and μ(*l* or *f*) are the shear viscosity and modulus of the fluid (index l) or film (index, f),

respectively; $\delta_l = (2\eta_l\rho_l^{-1}\omega^{-1})^{1/2}$ is the viscous penetration depth, with ρ_l the density of the fluid; and h_f and ρ_f the thickness and density of the film, respectively.[122]

Therefore the quartz crystal microbalance with dissipation monitoring (QCM-D) technique allows to measure the viscoelastic and swelling properties of adsorbed thin films in liquid.[123-125] It is notably used to study complex interactions such as the adsorption of DNA, proteins and cells on modified sensor surfaces.[118-120, 126]

2.3.2 Ellipsometry

Ellisometry consists in measuring the polarization change of light before and after its interaction with a sample. The setup consists of a light source, a polarizer, an analyzer, optional phase-shifting compensators as well as a photo-sensitive detector (Scheme 2.17). The light source is preselected by the polarizer generating linearly polarized light with an incidence angle of φ before irradiating the sample, while the reflective light is treated by the analyzer and monitored by the detector. The principle of ellipsometry measurement is illustrated in Scheme 2.18. The electric field of the incident light can be decomposed into two components E_{is} and E_{ip}, which are parallel and orthogonal to the plane of incidence, respectively. The plane of incidence refers to the plane spanned by the propagation direction of the light and the normal to the surface. The electric field of the reflected light is decomposed into two component E_{rs} and $E_{rp,}$ which are parallel and orthogonal to the plane of incidence, respectively. The complex reflection coefficients γ_s and γ_p which defined how much the electric field is reflected in the parallel and orthogonal incidence planes are defined as E_{rs}/E_{is} and

E_{rp}/E_{ip}, respectively. E_{rp} and E_{rs} are usually different in amplitude and show phase shifts of δ_p and δ_s compared to E_{ip} and E_{is}. Although the absolute values of γ_s and γ_p can not be obtained, the ratio of complex reflection coefficients, γ_p/γ_s, and the phase difference ($\Delta = \delta_s - \delta_p$) between parallel and perpendicular components can be calculated. The absolute value of γ_p/γ_s is called the amplitude ratio, $\tan\Psi$, where Ψ is the angle between the direction of the reflected light and the direction of its decomposed part. The complex reflection ratio, ρ is defined as below:

$$\rho = \frac{\gamma_p}{\gamma_s} = \frac{E_{rp}/E_{ip}}{E_{rs}/E_{is}} = tan(\Psi)\, e^{i\Delta} \qquad (9),$$

$$\text{with } tan(\Psi) = \frac{|\gamma_p|}{|\gamma_s|} \qquad (10).$$

Therefore the polarization change of light can be represented by the amplitude ratio $tan\Psi$, and the phase difference Δ.[127-129]

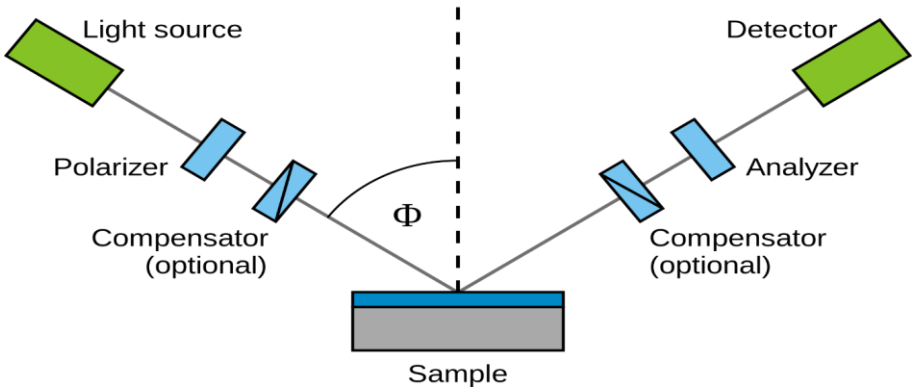

Scheme 2.17. Schematic setup of an ellipsometer equipped with optional phase-shifting compensators.

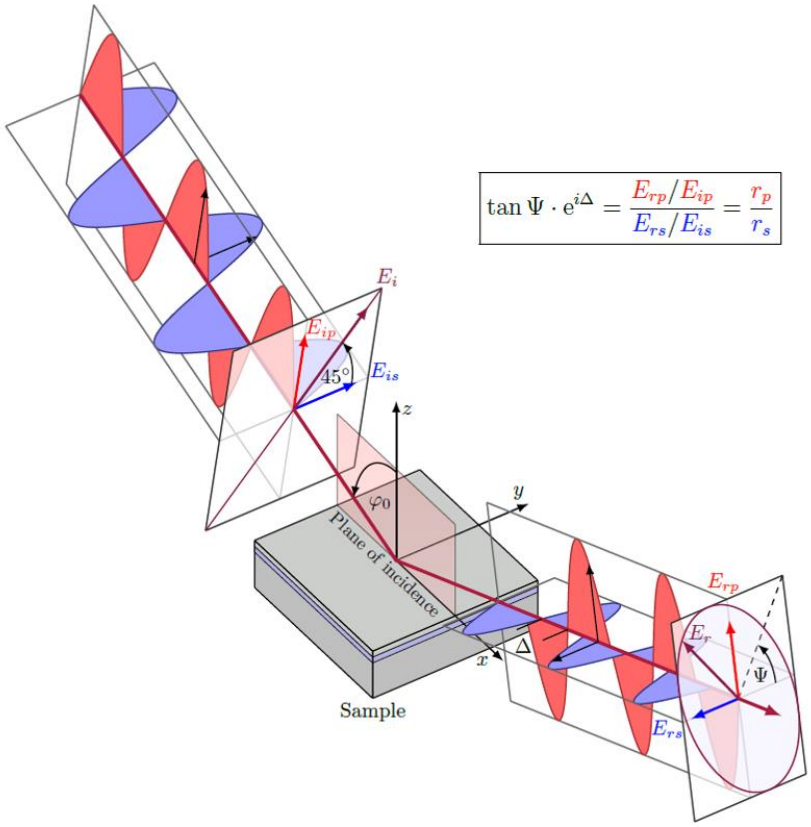

Scheme 2.18. Visualization of the polarization shift of light upon interaction with the sample.[129]

As a non-destructive optical technique, ellipsometry, is widely applied for the measurement of film thickness and optical constants such refractive index of polymer films. Due to its high sensitivity, ellipsometry is not only used to measure the thickness and optical properties of polymer films in dry state, but also to detect the extremely small differences in thickness and optical properties of polymer films immersed in fluid as a function of the temperature for instance. Therefore, ellipsometry can be used to monitor the swelling of polymer brushes in water versus temperature.[130] For example, Kooij *et al*. used

in-situ ellipsometry to probe the temperature-induced collapse of the PNIPAM brush in aqueous solution by measuring angles Ψ and Δ, the refractive index, and brush thickness with temperature.[131] When the PNIPAM brush collapses, the above measured parameters change significantly which is used to study the swelling behavior of the brush. The swelling behavior of polymer brushes can be even studied under different degrees of humidity.[132, 133]

2.3.3 Equilibrium contact angle measurement

The water contact angle measured between a water droplet and a solid surface is the most important parameter to evaluate the surface wettability. The determination of the value of the water contact angle can be done according to two different configurations: sessile drop or captive bubble.[28] In the sessile drop configuration, a liquid droplet is dropped on a solid surface and a picture of the liquid drop is captured. Then the contact angle which is formed at the three-phase boundary between the liquid, gas and solid is measured.

In the captive bubble configuration, the sample is immersed in a liquid such as water and an air bubble is deposited on the sample surface (Scheme 2.19). When the system reaches equilibrium, the contact angle at the liquid/substrate interface is measured. This angle is depicted by the Young-Dupré's equation,[134] by balancing the surface and interfacial energies acting in the horizontal plane:

$$\gamma_{gs} - \gamma_{sl} = \gamma_{gl} \cos\theta \qquad (11),$$

where θ is the contact angle and γ_{gs} , γ_{sl} and γ_{gl} are the interfacial tensions between gas-solid, solid-liquid and gas-liquid, respectively. As beautifully explained by Gray,[135] the definitions of surface tension and

surface free energy are perfectly possible under circumstances of non-equilibrium. However, interfacial tension and surface free energy are only identical when equilibrium is achieved, which is rare when working with solid surfaces which exhibit surface stresses, heterogeneities, roughness and variations in the amount of adsorbed compounds. In this context, it is important to note that equation (11) only strictly applies to equilibrium. The free energy of adhesion, which is also called the work of adhesion of the liquid to the solid (w_{sl}), due to the replacement of the unit area of solid-liquid interface by the gas-solid interface, can be given by Dupre's equation:

$$w_{sl} = \gamma_{gs} + \gamma_{gl} - \gamma_{sl} \qquad (12).$$

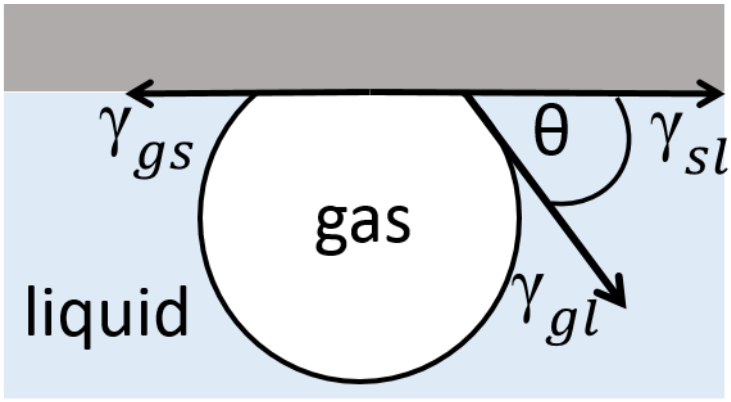

Scheme 2.19. Schematic illustration of an air bubble trapped on sample surface according to the captive bubble configuration.

The work of adhesion can be obtained by combining the above two equations:

$$w_{sl} = \gamma_{gl}(1 + cos\,\theta) \qquad (13),$$

where the work of adhesion refers to the work required to separate the air bubble from solid surface leaving a clean liquid-solid interface, which is always positive. This means that the contact of air bubble with

the solid surface decreases the free surface energy of the liquid-solid interface.[46]

The contact angle takes time to reach equilibrium. Moreover the contact angle measured in the sessile drop configuration varies with surface roughness and chemical heterogeneity of the surface. Besides, the penetration of the liquid into the solid, the swelling of the solid by the liquid or chemical reactions occurring on the sample surface can all affect the apparent contact angle values.[136] All the above factors contribute to the difficulty of measurement of the equilibrium contact angle.

The captive bubble configuration allows to measure the water contact angle at equilibrium and avoids the contact angle hysteresis and the penetration of the bubble through the sample surface.[27] It also allows the equilibrated diffusion of fluids in the solid and therefore helps to reach a condition closer to equilibrium, even though the captive bubble method also suffers from a series of drawbacks; for instance, it does not eliminate the contributions of roughness or heterogeneities to the surface tension. Because the brushes are thin, the mechanical deformation associated to the capillary forces remains limited; however, this would not be the case for hydrogels, for which the deformation of the surface at the triple line would be a supplementary factor to take into account.

2.4 Applications of stimuli-responsive polymer brushes

Stimuli-responsive polymer brushes are widely used in biomedical or biological fields to tune cell/surface interactions, to fabricate antifouling surfaces and to elaborate drug delivery systems.

The volume and surface properties such as volume swelling, chain collapse, surface wettability and surface phase separation of the stimuli-responsive brushes are of critical importance in the realization of the above mentioned systems.

2.4.1 Surfaces tuning cell/surface interactions

Tuning cell/polymer brush surface interactions is realized through tuning the adsorption or desorption of proteins playing a role in cell adhesion. This can be achieved by changing the surface wettability, hydration and dehydration of the outer surface of the brushes. Cellular responses such as adhesion, morphological changes, proliferation, and phenotypic changes are influenced by the concentration, composition and conformation of the layer of proteins that adsorbs rapidly on brush surfaces.[137-139]

Thermo-responsive PNIPAM films or brush have been extensively studied to control cell/surface interactions. PNIPAM brushes undergo a phase separation including volume and surface phase separations, while the temperature increases. When the temperature is lower than the LCST, PNIPAM brush adopts a swollen and hydrated state, which repels serum proteins and thus detaches cells. When the temperature increases beyond the LCST, PNIPAM brush starts to collapse and becomes dehydrated in surface, allowing adsorption of serum proteins. This results in cell attachment. The process of tuning cell attachment

and detachment by switching the swollen state of the PNIPAM brush with temperature is illustrated in Scheme.2.20.[139, 140]

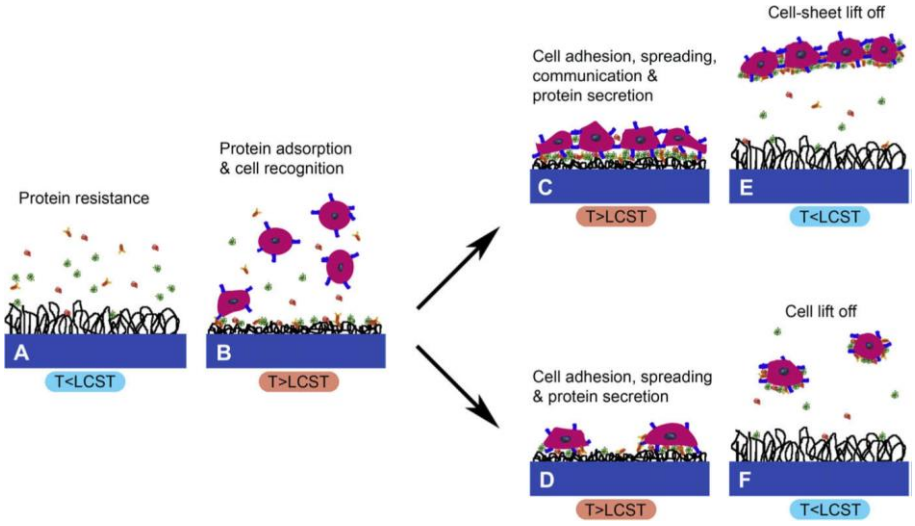

Scheme 2.20. PNIPAM-based thermo-responsive brush used to tune the attachment/detachment of cells. (A) Below the LCST, the surface repels protein adsorption which prevents the cell attachment. (B) Increasing the temperature above the LCST allows serum protein adsorption and cell attachment. (C) During extended cell culture, secretion of extracellular matrix (ECM) proteins along with cell proliferation and communication results in confluent cell sheets. (D) Low seeding density or short cell incubation time results in adherent cells without extensive cell-cell junction formation. (E and F) Cooling to below the LCST allows the release of intact cells (F) or cell sheets along with associated ECM proteins (E).[139]

Rare references report tuning cell/surface interaction by photo-responsive polymer brushes, although a few photo-responsive monolayers or very thin films based on photocleavable 2-nitrobenzyl (ONB) groups or spiropyran (SP) and AZO chromophores were developed to tune cell/surface interactions through photo-irradiation.[141,

[142] In general, the photo-isomerization of the photo chromophores has a limited ability to tune protein adsorption/desorption, mainly due to the little changes in physical properties that can be achieved.[139]

However, chromophores can be incorporated into thermo-responsive polymer brushes to produce dual thermo- and photo-responsive brushes. Tuning the LCST of thermo-responsive polymer brushes upon photo-irradiation allows to produce smart surfaces which can be used to tune cell/surface interactions.[143, 144] Dirani *et al*. synthesized dual thermo- and photo-responsive polymer brushes of P(MEO_2MA-*co*-HOEGMA) grafted with AZO groups by combining SI-ATRP and post-modification of polymer chains.[48] However the variation of the swelling degree of these brushes under UV irradiation was quite limited. Therefore the behavior of cells on these brushes was not studied.

2.4.2 Antifouling surfaces

Designing surfaces being able to prevent fouling by proteins and bacteria are very important for biomedical devices such as medical implants.[145-147] Indeed biocontamination of biological implants by proteins and bacteria induces infections and even causes death of patients.[148-151] The grafting of polymer brushes with antifouling properties on material surface is one of the strategies explored to overcome the problem of fouling coming from protein and bacterial attachment.[152] Immobilization of poly(ethylene glycol) (PEG) based brushes is one of the most common approach to impart antifouling properties to a surface.[151, 152] Indeed PEG is a well-known polymer resisting protein adsorption probably via steric repulsion coming from

the unfavorable elastic and osmotic stresses of the compressed polymer chains .[153] PEG layer form a "barrier" created by structured water associated with PEG.[153, 154] However, this polymer is not stimuli-responsive. In order to switch the antifouling properties of the surface by an external stimulus, some researchers have developed thermo-responsive brushes based on methacrylate monomer bearing PEG side chains. For instance, brushes prepared from oligo(ethylene glycol) methacrylate (OEGMA) monomers, with different lengths of side chains show a collapse transition at a given temperature which depends on the length of the oligo(ethylene glycol) side chain (see discussion in 2.1.1 section). Ma *et al*. synthesized pure P(OEGMA) brushes from silicon oxide surface by SI-ARTP. They evidenced that these brushes showed excellent protein resistance properties in serum.[155, 156] Jonas *et al.* further found that copolymer brushes based on MEO_2MA, OEGMA and HEMA are thermo-responsive and their transition temperature can be tuned as a function of the composition of the brushes.[27, 28] They notably produced thermo-responsive brushes showing collapse transition in the physiological range of temperature.[157]

Following this, Laloyaux *et al*.[42] synthesized thermo-responsive brushes switching from antibacterial to non-adhesive with the temperature (Scheme 2.21). For this, they prepared copolymer brushes made from MEO_2MA, HOEGMA and HEMA showing a collapse transition of about 35°C. Then, an antimicrobial magainin derivative was grafted onto the hydroxyl groups of the side chains of the brush. The authors showed that the copolymer brush adopted a swollen state at low temperature (i.e. 26°C) which exposed the peptide. Therefore

strong bactericidal behavior of these brushes was observed at room temperature. However when the incubation temperature was increased to 38°C, the copolymer brush collapsed while burying the peptide groups. As a consequence, copolymer brush shows a non-adhesive behavior at higher temperature due to the intrinsic non-adhesive nature of the copolymer chains.

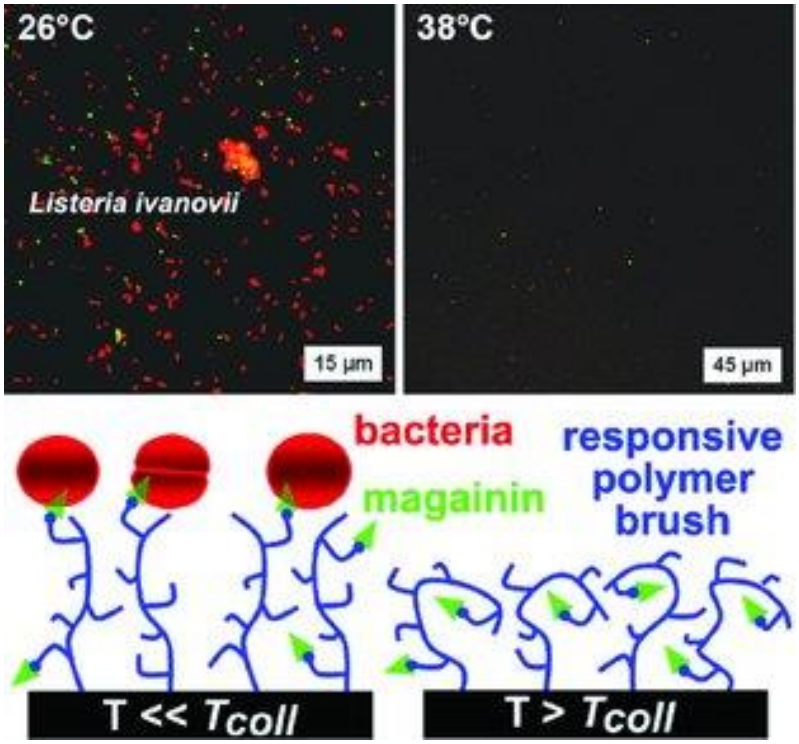

Scheme. 2.21. Thermo-responsive brush grafted with an antibacterial peptide (magainin) and showing a collapse temperature (T_{coll}) of about 35°C. (Top) Adhesion of *Listeria ivanovii* on this brush at a temperature below (26°C, left) and just above (36°C, right) the collapse temperature; bacterial cells were labeled with a Live/Dead kit in order to discriminate the alive (green) and dead cells (red). (Bottom) Variation of the structure of the peptide-grafted polymer brush as a function of the temperature.[42]

2.4.3 Surfaces controlling drug release

The drug delivery or control of the release of a drug from a material surface is another important application of stimuli-responsive polymer brushes. For this spherical polymer brushes are often synthesized by grafting polymers onto or from the surfaces of nanoparticles. This results in the formation of core-shell hybrid materials.[67, 158] The nanoparticles commonly used are silica,[159-161] gold [162-164] or polymeric nanoparticles.[165-167] Few studies report also on the synthesis of stimuli-responsive polymer brushes on planar surfaces for loading and releasing drugs.[168]

One representative example was reported by Kumar *et al.* who synthesized thermo-, photo- and pH- responsive block copolymer brushes by SI-ATRP in order to release a model organic substance using variation of pH, temperature or light irradiation (Scheme 2.22).[53] The authors synthesized copolymer brushes containing two thermo-responsive blocks based on poly(styrene-*b*-*N*-isopropyl acrylamide) (PS-*b*-PNIPAM) and poly(*N, N'*-dimethyl acrylamide)-b-poly(*N*-isopropyl acrylamide) (PDMA-*b*-PNIPAM). The swelling of PNIPAM block was tuned as a function of temperature, while the inner PS block was used to physically load the organic molecules such as Nile red used as a model drug. The swelling or collapse of PNIPAM blocks with temperature was used to open or close channels within the PNIPAM layer and consequently to control the release of the loaded Nile red molecules. Similarly, photo-responsive copolymer brushes based on polystyrene-*b*-poly(4,5-dimethoxy-2-nitrobenzyl methacrylate) (PS-*b*-PNBA) were synthesized. As the ONB groups are photo-sensitive and can be cleaved upon photo-irradiation, they impart the PS-*b*-PNBA

block copolymer brush with photo-responsiveness. Indeed after partial cleavage of ONB groups upon photo-irradiation, the hydrophilic methacrylic acid (MA) groups are formed into the brush. The degree of the cleavage of ONB groups can be controlled by controlling the light intensity and the photo-irradiation time, thus controlling the number of MA groups. As PNBA is hydrophobic, while MA is hydrophilic, the swelling of PNBA can be tuned by controlling the cleavage degree of ONB groups. Due to the irreversible photoinduced reaction, after complete cleavage of the ONB groups, the PS-b-PMA copolymer brush is formed. This resulting PS-*b*-PMA brush is pH-sensitive, with the reversible pH change, the swelling and collapse of PMA chains can be controlled by changing pH, thus controlling the release kinetics of Nile red loaded molecules.[53]

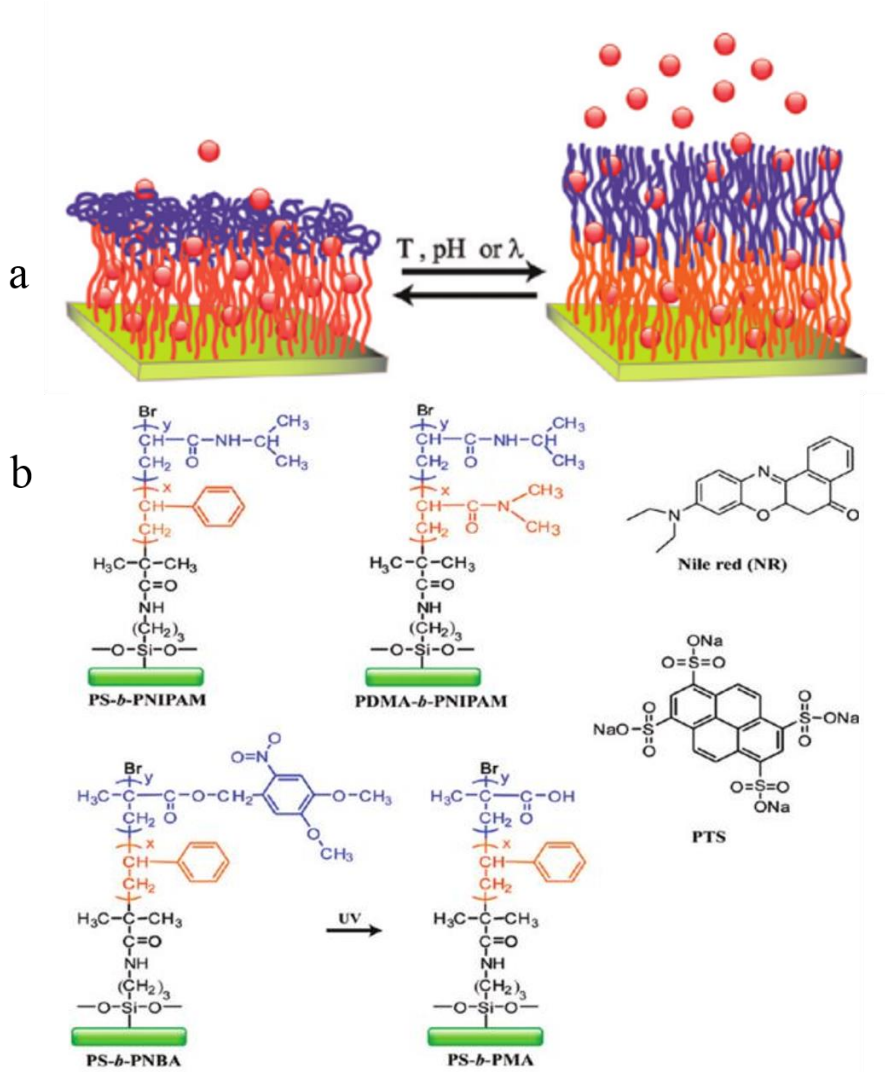

Scheme. 2.22. (a) Schematic illustration of surface-grafted diblock copolymer brushes with top layer being able to switch between collapsed and extended chains in response to temperature, pH or light. (b) chemical structures of the diblock copolymer brushes studied and the organic molecules used as model drug.[53]

References

1. Zhao, B. & Brittain, W.J. Polymer brushes: surface-immobilized macromolecules. *Prog. Polym. Sci.* **25**, 677-710 (2000).
2. Pyun, J., Kowalewski, T. & Matyjaszewski, K. Synthesis of Polymer Brushes Using Atom Transfer Radical Polymerization. *Macromol. rapid commun.* **24**, 1043-1059 (2003).
3. Tsujii, Y., Ohno, K., Yamamoto, S., Goto, A. & Fukuda, T. Structure and Properties of High-Density Polymer Brushes Prepared by Surface-Initiated Living Radical Polymerization. *Adv. Polym. Sci*. **197**, 1-45 (2006).
4. Minko, S. Responsive Polymer Brushes. *J. Macromol. Sci., Part C: Polym. Rev.* **46**, 397-420 (2006).
5. Barbey, R. et al. Polymer Brushes via Surface-Initiated Controlled Radical Polymerization Synthesis, Characterization, Properties, and Applications. *Chem. Rev.* **109**, 5437-5527 (2009).
6. Chen, T., Ferris, R., Zhang, J., Ducker, R. & Zauscher, S. Stimulus-responsive polymer brushes on surfaces: Transduction mechanisms and applications. *Prog. Polym. Sci.* **35**, 94-112 (2010).
7. Chan, A., Orme, R.P., Fricker, R.A. & Roach, P. Remote and local control of stimuli responsive materials for therapeutic applications. *Adv. Drug Deliv. Rev.* **65**, 497-514 (2013).
8. Jochum, F.D. & Theato, P. Temperature- and light-responsive smart polymer materials. *Chem. Soc. Rev.* **42**, 7468-7483 (2013).

9. Xu, F.J., Neoh, K.G. & Kang, E.T. Bioactive surfaces and biomaterials via atom transfer radical polymerization. *Prog. Polym. Sci.* **34**, 719-761 (2009).
10. Seuring, J. & Agarwal, S. Polymers with upper critical solution temperature in aqueous solution. *Macromol. rapid commun.* **33**, 1898-1920 (2012).
11. Zhang, Q. & Hoogenboom, R. Polymers with upper critical solution temperature behavior in alcohol/water solvent mixtures. *Prog. Polym. Sci.* **48**, 122-142 (2015).
12. Roth, P.J., Jochum, F.D. & Theato, P. UCST-type behavior of poly[oligo(ethylene glycol) methyl ether methacrylate] (POEGMA) in aliphatic alcohols: solvent, co-solvent, molecular weight, and end group dependences. *Soft Matter* **7**, 2484 (2011).
13. Arts, C.A.o., Sciences & University, Y. Transactions of the Connecticut Academy of Arts and Sciences, Vol. 5. (Connecticut Academy of Arts and Sciences, 1882).
14. Flory, P.J. Thermodynamics of high polymer solutions. *J. Chem. Phys.* **9**, 660-660 (1941).
15. Huggins, M.L. Solutions of long chain compounds. *J. chem. phys.* **9**, 440-440 (1941).
16. Flory, P.J. Thermodynamics of high polymer solutions. *J. Chem. Phys.* **10**, 51-61 (1942).
17. Huggins, M.L. Some Properties of Solutions of Long-chain Compounds. *J. Phys. Chem.* **46**, 151-158 (1942).

18. Roy, D., Brooks, W.L. & Sumerlin, B.S. New directions in thermo-responsive polymers. *Chem. Soc. Rev.* **42**, 7214-7243 (2013).
19. Eliassaf, J. AQUEOUS-SOLUTIONS OF POLY(N-ISOPROPYLACRYLAMIDE). *J. Appl. Polym. Sci.* **22**, 873-874 (1978).
20. Schild, H.G. Poly(N-isopropylacrylamide): experiment, theory and application. *Prog. Polym. Sci.* **17**, 163-249 (1992).
21. Boutris, C., Chatzi, E.G. & Kiparissides, C. Characterization of the LCST behaviour of aqueous poly(N-isopropylacrylamide) solutions by thermal and cloud point techniques. *Polymer* **38**, 2567-2570 (1997).
22. Wu, C. & Wang, X. Globule-to-Coil Transition of a Single Homopolymer Chain in Solution. *Phys. Rev. Lett.* **80**, 4092-4094 (1998).
23. Wang, X., Qiu, X. & Wu, C. Comparison of the Coil-to-Globule and the Globule-to-Coil Transitions of a Single Poly(N-isopropylacrylamide) Homopolymer Chain in Water. *Macromolecules* **31**, 2972-2976 (1998).
24. Xia, Y., Yin, X., Burke, N.A.D. & Stöver, H.D.H. thermal response of norrow-disperse poly(N-isopropylacrylamide) prepared by atom transfer radical polymerization. *Macromolecules* **38**, 5937-5943 (2005).
25. Idziak, I., Avoce, D., Lessard, D., Gravel, D. & Zhu, X.X. Thermosensitivity of Aqueous Solutions of Poly(N,N-diethylacrylamide). *Macromolecules* **32**, 1260-1263 (1999).

26. Tang, X., Liang, X., Gao, L., Fan, X. & Zhou, Q. Water-soluble triply-responsive homopolymers of N,N-dimethylaminoethyl methacrylate with a terminal azobenzene moiety. *J. Polym. Sci. A: Polym. Chem.* **48**, 2564-2570 (2010).
27. Jonas, A.M., Glinel, K., Oren, R., Nysten, B. & Huck, W.T.S. Thermo-Responsive Polymer Brushes with Tunable Collapse Temperatures in the Physiological Range. *Macromolecules* **40**, 4403-4405 (2007).
28. Laloyaux, X., Mathy, B., Nysten, B. & Jonas, A.M. Surface and Bulk Collapse Transitions of Thermo-responsive Polymer Brushes. *Langmuir* **26**, 838-847 (2009).
29. Lutz, J.-F. & Hoth, A. Preparation of Ideal PEG Analogues with a Tunable Thermosensitivity by Controlled Radical

Copolymerization of 2-(2-Methoxyethoxy)ethyl Methacrylate and Oligo(ethylene glycol) Methacrylate. *Macromolecules* **39**, 893-896 (2005).
30. Lutz, J.-F. Polymerization of oligo(ethylene glycol) (meth)acrylates: Toward new generations of smart biocompatible materials. *J. Polym. Sci. A: Polym. Chem.* **46**, 3459-3470 (2008).
31. Dong, Z., Mao, J., Wang, D., Yang, M. & Ji, X. Synthesis and Multi-Stimuli-Responsive Behavior of Poly(N,N-dimethylaminoethyl methacrylate) Spherical Brushes under Different Modes of Confinement in Solution. *Langmuir* **31**, 8930-8939 (2015).
32. Xue, C., Choi, B.-C., Choi, S., Braun, P.V. & Leckband, D.E. Protein Adsorption Modes Determine Reversible Cell

Attachment on Poly(N-isopropyl acrylamide) Brushes. *Adv. Funct. Mater.* **22**, 2394-2401 (2012).

33. Schmaljohann, D. Thermo- and pH-responsive polymers in drug delivery. *Adv. Drug Deliv. Rev.* **58**, 1655-1670 (2006).
34. Oikonomou, E.K., Bokias, G., Iliopoulos, I. & Kallitsis, J.K. Sequential Association of Anionic/Thermosensitive Diblock Copolymers with Cationic Surfactants. *Macromolecules* **46**, 1082-1092 (2013).
35. Zhou, D., Gao, X., Wang, W.-j. & Zhu, S. Termination of Surface Radicals and Kinetic Modeling of ATRP Grafting from Flat Surfaces by Addition of Deactivator. *Macromolecules* **45**, 1198-1207 (2012).
36. Kujawa, P. et al. Impact of End-Group Association and Main-Chain Hydration on the Thermosensitive Properties of Hydrophobically Modified Telechelic Poly(N-isopropylacrylamides) in Water. *Macromolecules* **39**, 341-348 (2005).
37. Xia, Y., Burke, N.A.D. & Stöver, H.D.H. End Group Effect on the Thermal Response of Narrow-Disperse Poly(N-isopropylacrylamide) Prepared by Atom Transfer Radical Polymerization. *Macromolecules* **39**, 2275-2283 (2006).
38. Lutz, J.-F., Akdemir, Ö. & Hoth, A. Point by Point Comparison of Two Thermosensitive Polymers Exhibiting a Similar LCST: Is the Age of Poly(NIPAM) Over? *J. Am. Chem. Soc.* **128**, 13046-13047 (2006).
39. Du, H., Wickramasinghe, R. & Qian, X. Effects of Salt on the Lower Critical Solution Temperature of Poly (N-

Isopropylacrylamide). *J. Phys. Chem. B* **114**, 16594-16604 (2010).

40. Mizutani, A., Kikuchi, A., Yamato, M., Kanazawa, H. & Okano, T. Preparation of thermo-responsive polymer brush surfaces and their interaction with cells. *Biomaterials* **29**, 2073-2081 (2008).
41. Sun, T. et al. Reversible Switching between Superhydrophilicity and Superhydrophobicity. *Angew. Chem. Int. Ed.* **43**, 357-360 (2004).
42. Laloyaux, X. et al. Temperature-Responsive Polymer Brushes Switching from Bactericidal to Cell-Repellent. *Adv. Mater.* **22**, 5024-5028 (2010).
43. Teraoka, I. in Polymer Solutions 69-166 (John Wiley & Sons, Inc., 2002).
44. Milner, S.T. Polymer Brushes. *Science* **251**, 905 (1991).
45. Zhulina, E.B., Borisov, O.V., Pryamitsyn, V.A. & Birshtein, T.M. Coil-globule type transitions in polymers. 1. Collapse of layers of grafted polymer chains. *Macromolecules* **24**, 140-149 (1991).
46. Schrader, M.E. Young-Dupre Revisited. *Langmuir* **11**, 3585-3589 (1995).
47. Mura, S., Nicolas, J. & Couvreur, P. Stimuli-responsive nanocarriers for drug delivery. *Nat. Mater.* **12**, 991-1003 (2013).
48. Dirani, A. et al. Reversible Photomodulation of the Swelling of Poly(oligo(ethylene glycol) methacrylate) Thermo-responsive Polymer Brushes. *Macromolecules* **45**, 9400-9408 (2012).
49. Wang, D., Ye, G., Wang, X. & Wang, X. Graphene functionalized with azo polymer brushes: surface-initiated

polymerization and photoresponsive properties. *Adv. Mater.* **23**, 1122-1125 (2011).

50. Florea, L., Diamond, D. & Benito-Lopez, F. Photo-Responsive Polymeric Structures Based on Spiropyran. *Macromol. Mater. Eng.* **297**, 1148-1159 (2012).
51. Wagner, N. & Theato, P. Light-induced wettability changes on polymer surfaces. *Polymer* **55**, 3436–3453 (2014).
52. Cui, J. et al. Phototunable Response in Caged Polymer Brushes. *Macromolecules* **45**, 3213-3220 (2012).
53. Kumar, S., Dory, Y.L., Lepage, M. & Zhao, Y. Surface-Grafted Stimuli-Responsive Block Copolymer Brushes for the Thermo-, Photo- and pH-Sensitive Release of Dye Molecules. *Macromolecules* **44**, 7385-7393 (2011).
54. Liu, H. et al. Dual-Responsive Surfaces Modified with Phenylboronic Acid-Containing Polymer Brush To Reversibly Capture and Release Cancer Cells. *J. Am. Chem. Soc.* **135**, 7603-7609 (2013).
55. Cui, J., Miguel, V.S. & del Campo, A. Light-triggered multifunctionality at surfaces mediated by photolabile protecting groups. *Macromol.Rapid Commun.* **34**, 310-329 (2013).
56. Kröger, R., Menzel, H. & Hallensleben, M.L. Light controlled solubility change of polymers: Copolymers of N,N-dimethylacrylamide and 4-phenylazophenyl acrylate. *Macromol. Chem. Phys.* **195**, 2291-2298 (1994).
57. Shiraishi, Y., Miyamoto, R. & Hirai, T. Spiropyran-Conjugated Thermo-responsive Copolymer as a Colorimetric Thermometer

with Linear and Reversible Color Change. *Org. Lett.* **11**, 1571-1574 (2009).

58. Klajn, R. Spiropyran-based dynamic materials. *Chem. Soc. Rev.* **43**, 148-184 (2014).
59. Shimoboji, T. et al. Photoresponsive polymer-enzyme switches. *Proc. Natl. Acad. Sci. U.S.A.* **99**, 16592-16596 (2002).
60. Shimoboji, T., Ding, Z.L., Stayton, P.S. & Hoffman, A.S. Photoswitching of Ligand Association with a Photoresponsive Polymer−Protein Conjugate. *Bioconjugate Chem.* **13**, 915-919 (2002).
61. Deshmukh, S., Bromberg, L., Smith, K.A. & Hatton, T.A. Photoresponsive Behavior of Amphiphilic Copolymers of Azobenzene and N,N-Dimethylacrylamide in Aqueous Solutions. *Langmuir* **25**, 3459-3466 (2009).
62. Zhao, Y. & He, J. Azobenzene-containing block copolymers: the interplay of light and morphology enables new functions. *Soft Matter* **5**, 2686 (2009).
63. Housni, A., Zhao, Y. & Zhao, Y. Using polymers to photoswitch the aggregation state of gold nanoparticles in aqueous solution. *Langmuir* **26**, 12366-12370 (2010).
64. Brown, A.A., Azzaroni, O. & Huck, W.T.S. Photoresponsive Polymer Brushes for Hydrophilic Patterning. *Langmuir* **25**, 1744-1749 (2009).
65. Dübner, M., Spencer, N.D. & Padeste, C. Light-Responsive Polymer Surfaces via Postpolymerization Modification of Grafted Polymer-Brush Structures. *Langmuir* **30**, 14971-14981 (2014).

66. Roy, D., Cambre, J.N. & Sumerlin, B.S. Future perspectives and recent advances in stimuli-responsive materials. *Prog. Polym. Sci.* **35**, 278-301 (2010).

67. Wu, L., Glebe, U. & Böker, A. Surface-initiated controlled radical polymerizations from silica nanoparticles, gold nanocrystals, and bionanoparticles. *Polym. Chem.* **6**, 5143-5184 (2015).

68. Wang, J. Electrochemical Glucose Biosensors. *Chem. Rev.* **108**, 814-825 (2008).

69. Matsumoto, A., Ikeda, S., Harada, A. & Kataoka, K. Glucose-Responsive Polymer Bearing a Novel Phenylborate Derivative as a Glucose-Sensing Moiety Operating at Physiological pH Conditions. *Biomacromolecules* **4**, 1410-1416 (2003).

70. Kataoka, K., Miyazaki, H., Bunya, M., Okano, T. & Sakurai, Y. Totally Synthetic Polymer Gels Responding to External Glucose Concentration: Their Preparation and Application to On−Off Regulation of Insulin Release. *J. Am. Chem. Soc.* **120**, 12694-12695 (1998).

71. Brooks, W.L.A. & Sumerlin, B.S. Synthesis and Applications of Boronic Acid-Containing Polymers: From Materials to Medicine. *Chem. Rev.* **116**, 1375-1397 (2016).

72. Chen, T. et al. Glucose-responsive polymer brushes for microcantilever sensing. *J. Mater. Chem.* **20**, 3391 (2010).

73. Laloyaux, X., Mathy, B., Nysten, B. & Jonas, A.M. Bidimensional Response Maps of Adaptive Thermo- and pH-Responsive Polymer Brushes. *Macromolecules* **43**, 7744-7751 (2010).

74. Kehrloesser, D., Baumann, R.-P., Kim, H.-C. & Hampp, N. Photochemistry of Coumarin-Functionalized SiO2 Nanoparticles. *Langmuir* **27**, 4149-4155 (2011).

75. Yim, H. et al. Effects of Grafting Density and Molecular Weight on the Temperature-Dependent Conformational Change of Poly(N-isopropylacrylamide) Grafted Chains in Water. *Macromolecules* **39**, 3420-3426 (2006).

76. Karim, A., Satija, S.K., Douglas, J.F., Ankner, J.F. & Fetters, L.J. Neutron Reflectivity Study of the Density Profile of a Model End-Grafted Polymer Brush: Influence of Solvent Quality. *Phys. Rev. Letters* **73**, 3407-3410 (1994).

77. Okano, T., Kikuchi, A., Sakurai, Y., Takei, Y. & Ogata, N. Temperature-responsive poly(N-isopropylacrylamide) as a modulator for alteration of hydrophilic/hydrophobic surface properties to control activation/inactivation of platelets. *J. Controlled Release* **36**, 125-133 (1995).

78. Bjoerling, M., Linse, P. & Karlstroem, G. Distribution of segments for terminally attached poly(ethylene oxide) chains. *J. Phys. Chem.* **94**, 471-481 (1990).

79. Moad, G., Rizzardo, E. & Thang, S.H. Living Radical Polymerization by the RAFT Process. *Aust. J. Chemi.* **58**, 379-410 (2005).

80. Braunecker, W.A. & Matyjaszewski, K. Controlled/living radical polymerization: Features, developments, and perspectives. *Prog. Polym. Sci.* **32**, 93-146 (2007).

81. Matyjaszewski, K. & Xia, J. Atom Transfer Radical Polymerization. *Chem. Rev.* **101**, 2921-2990 (2001).

82. Xiao, D. & Wirth, M.J. Kinetics of Surface-Initiated Atom Transfer Radical Polymerization of Acrylamide on Silica. *Macromolecules* **35**, 2919-2925 (2002).

83. Masci, G., Giacomelli, L. & Crescenzi, V. Atom Transfer Radical Polymerization ofN-Isopropylacrylamide. *Macromol.Rapid Commun.* **25**, 559-564 (2004).

84. Teodorescu, M. & Matyjaszewski, K. Atom Transfer Radical Polymerization of (Meth)acrylamides. *Macromolecules* **32**, 4826-4831 (1999).

85. Rademacher, J.T., Baum, M., Pallack, M.E., Brittain, W.J. & Simonsick, W.J. Atom Transfer Radical Polymerization of N,N-Dimethylacrylamide. *Macromolecules* **33**, 284-288 (2000).

86. Teodorescu, M. & Matyjaszewski*, K. Controlled polymerization of (meth)acrylamides by atom transfer radical polymerization. *Macromol.Rapid Commun.* **21**, 190-194 (2000).

87. Neugebauer, D. & Matyjaszewski, K. Copolymerization of N,N-Dimethylacrylamide with n-Butyl Acrylate via Atom Transfer Radical Polymerization. *Macromolecules* **36**, 2598-2603 (2003).

88. Beija, M., Marty, J.-D. & Destarac, M. RAFT/MADIX polymers for the preparation of polymer/inorganic nanohybrids. *Prog. Polym. Sci.* **36**, 845-886 (2011).

89. Convertine, A.J., Ayres, N., Scales, C.W., Lowe, A.B. & McCormick, C.L. Facile, Controlled, Room-Temperature RAFT Polymerization of N-Isopropylacrylamide. *Biomacromolecules* **5**, 1177-1180 (2004).

90. Thomas, D.B., Sumerlin, B.S., Lowe, A.B. & McCormick, C.L. Conditions for Facile, Controlled RAFT Polymerization of Acrylamide in Water. *Macromolecules* **36**, 1436-1439 (2003).

91. Thomas, D.B. et al. Kinetics and Molecular Weight Control of the Polymerization of Acrylamide via RAFT. *Macromolecules* **37**, 8941-8950 (2004).

92. Scales, C.W., Convertine, A.J. & McCormick, C.L. Fluorescent Labeling of RAFT-Generated Poly(N-isopropylacrylamide) via a Facile Maleimide−Thiol Coupling Reaction. *Biomacromolecules* **7**, 1389-1392 (2006).

93. Scales, C.W., Vasilieva, Y.A., Convertine, A.J., Lowe, A.B. & McCormick, C.L. Direct, Controlled Synthesis of the Nonimmunogenic, Hydrophilic Polymer, Poly(N-(2-hydroxypropyl)methacrylamide) via RAFT in Aqueous Media. *Biomacromolecules* **6**, 1846-1850 (2005).

94. Convertine, A.J. et al. Direct Synthesis of Thermally Responsive DMA/NIPAM Diblock and DMA/NIPAM/DMA Triblock Copolymers via Aqueous, Room Temperature RAFT Polymerization. *Macromolecules* **39**, 1724-1730 (2006).

95. Moad, G., Rizzardo, E. & Thang, S.H. Living Radical Polymerization by the RAFT Process—A First Update. *Aust. J. Chemi.* **59**, 669-692 (2006).

96. Parsonage, E., Tirrell, M., Watanabe, H. & Nuzzo, R.G. Adsorption of poly(2-vinylpyridine)-poly (styrene) block copolymers from toluene solutions. *Macromolecules* **24**, 1987-1995 (1991).

97. Fytas, G. et al. Probing Collective Motions of Terminally Anchored Polymers. *Science* **274**, 2041-2044 (1996).

98. Halperin, A., Tirrell, M. & Lodge, T. Tethered chains in polymer microstructures. *Macromolecules: Synthesis, Order and Advanced Properties, Adv. Polym. Sci.* 31-71 (1992).

99. Lee, H.-i., Pietrasik, J., Sheiko, S.S. & Matyjaszewski, K. Stimuli-responsive molecular brushes. *Prog. Polym. Sci.* **35**, 24-44 (2010).

100. Minko, S. et al. Synthesis of Adaptive Polymer Brushes via "Grafting To" Approach from Melt. *Langmuir* **18**, 289-296 (2002).

101. Julthongpiput, D., Lin, Y.-H., Teng, J., Zubarev, E.R. & Tsukruk, V.V. Y-Shaped Amphiphilic Brushes with Switchable Micellar Surface Structures. *J. Am. Chem. Soc.* **125**, 15912-15921 (2003).

102. Tonhauser, C. et al. Stimuli-responsive y-shaped polymer brushes based on junction-point-reactive block copolymers. *Adv. Mater.* **24**, 5559-5563 (2012).

103. Rauch, S., Eichhorn, K.-J., Kuckling, D., Stamm, M. & Uhlmann, P. Chain Extension of Stimuli-Responsive Polymer Brushes: A General Strategy to Overcome the Drawbacks of the "Grafting-To" Approach. *Adv. Funct. Mater.* **23**, 5675-5681 (2013).

104. Onclin, S., Ravoo, B.J. & Reinhoudt, D.N. Engineering Silicon Oxide Surfaces Using Self-Assembled Monolayers. *Angew. Chem. Int. Ed.* **44**, 6282-6304 (2005).

105. Ulman, A. Formation and Structure of Self-Assembled Monolayers. *Chem. Rev.* **96**, 1533-1554 (1996).

106. Ejaz, M., Yamamoto, S., Ohno, K., Tsujii, Y. & Fukuda, T. Controlled Graft Polymerization of Methyl Methacrylate on Silicon Substrate by the Combined Use of the Langmuir−Blodgett and Atom Transfer Radical Polymerization Techniques. *Macromolecules* **31**, 5934-5936 (1998).

107. Turgman-Cohen, S. & Genzer, J. Simultaneous bulk- and surface-initiated controlled radical polymerization from planar substrates. *J. Am. Chem. Soc.* **133**, 17567-17569 (2011).

108. Turgman-Cohen, S. & Genzer, J. Computer Simulation of Concurrent Bulk- and Surface-Initiated Living Polymerization. *Macromolecules* **45**, 2128-2137 (2012).

109. Matyjaszewski, K. et al. Polymers at Interfaces: Using Atom Transfer Radical Polymerization in the Controlled Growth of Homopolymers and Block Copolymers from Silicon Surfaces in the Absence of Untethered Sacrificial Initiator. *Macromolecules* **32**, 8716-8724 (1999).

110. Huang, W., Kim, J.-B., Bruening, M.L. & Baker, G.L. Functionalization of Surfaces by Water-Accelerated Atom-Transfer Radical Polymerization of Hydroxyethyl Methacrylate and Subsequent Derivatization. *Macromolecules* **35**, 1175-1179 (2002).

111. Matyjaszewski, K., Shipp, D.A., Wang, J.-L., Grimaud, T. & Patten, T.E. Utilizing Halide Exchange To Improve Control of Atom Transfer Radical Polymerization. *Macromolecules* **31**, 6836-6840 (1998).

112. Brown, A.A., Khan, N.S., Steinbock, L. & Huck, W.T.S. Synthesis of oligo(ethylene glycol) methacrylate polymer brushes. *European Polymer Journal* **41**, 1757-1765 (2005).

113. Wang, X.S., F. Lascelles, S., A. Jackson, R. & P. Armes, S. Facile synthesis of well-defined water-soluble polymers via atom transfer radical polymerization in aqueous media at ambient temperature. *Chem. commun.*, 1817-1818 (1999).

114. Wang, X.S. & Armes, S.P. Facile Atom Transfer Radical Polymerization of Methoxy-Capped Oligo(ethylene glycol) Methacrylate in Aqueous Media at Ambient Temperature. *Macromolecules* **33**, 6640-6647 (2000).

115. Robinson, K.L., Khan, M.A., de Paz Báñez, M.V., Wang, X.S. & Armes, S.P. Controlled Polymerization of 2-Hydroxyethyl Methacrylate by ATRP at Ambient Temperature. *Macromolecules* **34**, 3155-3158 (2001).

116. Ye, J. & Narain, R. Water-Assisted Atom Transfer Radical Polymerization of N-Isopropylacrylamide Nature of Solvent and Temperature. *J. Phys. Chem. B* **113**, 676-681 (2008).

117. von Werne, T. & Patten, T.E. Atom Transfer Radical Polymerization from Nanoparticles: A Tool for the Preparation of Well-Defined Hybrid Nanostructures and for Understanding the Chemistry of Controlled/"Living" Radical Polymerizations from Surfaces. *J. Am. Chem. Soc.* **123**, 7497-7505 (2001).

118. Marx, K.A. Quartz Crystal Microbalance: A Useful Tool for Studying Thin Polymer Films and Complex Biomolecular Systems at the Solution−Surface Interface. *Biomacromolecules* **4**, 1099-1120 (2003).

119. Janshoff, A., Galla, H.-J. & Steinem, C. Piezoelectric Mass-Sensing Devices as Biosensors—An Alternative to Optical Biosensors? *Angew. Chem. Int. Ed.* **39**, 4004-4032 (2000).

120. Janshoff, A. & Steinem, C. Quartz Crystal Microbalance for Bioanalytical Applications. *Sensors Update* **9**, 313-354 (2001).

121. Sauerbrey, G. Verwendung von Schwingquarzen zur Wägung dünner Schichten und zur Mikrowägung. *Zeitschrift für Physik* **155**, 206-222 (1959).

122. Voinova, M.V., Rodahl, M., Jonson, M. & Kasemo, B. Viscoelastic Acoustic Response of Layered Polymer Films at Fluid-Solid Interfaces: Continuum Mechanics Approach. *Phys. Scripta* **59**, 391 (1999).

123. Domack, A., Prucker, O., Rühe, J. & Johannsmann, D. Swelling of a polymer brush probed with a quartz crystal resonator. *Phys. Rev. E* **56**, 680-689 (1997).

124. Wiener, C.G., Weiss, R.A. & Vogt, B.D. Overcoming confinement limited swelling in hydrogel thin films using supramolecular interactions. *Soft Matter* **10**, 6705 (2014).

125. Höök, F. et al. Variations in Coupled Water, Viscoelastic Properties, and Film Thickness of a Mefp-1 Protein Film during Adsorption and Cross-Linking: A Quartz Crystal Microbalance with Dissipation Monitoring, Ellipsometry, and Surface Plasmon Resonance Study. *Anal. Chem.* **73**, 5796-5804 (2001).

126. Roach, P., Farrar, D. & Perry, C.C. Interpretation of Protein Adsorption: Surface-Induced Conformational Changes. *J. Am. Chem. Soc.* **127**, 8168-8173 (2005).

127. Fujiwara, H. in Spectroscopic Ellipsometry 81-146 (John Wiley & Sons, Ltd, 2007).
128. Cobet, C. in Ellipsometry of Functional Organic Surfaces and Films. (eds. K. Hinrichs & K.-J. Eichhorn) 1-26 (Springer Berlin Heidelberg, Berlin, Heidelberg; 2014).
129. Furchner, A. (Berlin, Technische Universität Berlin, Diss., 2014, 2014).
130. Bittrich, E. et al. in Ellipsometry of Functional Organic Surfaces and Films. (eds. K. Hinrichs & K.-J. Eichhorn) 79-105 (Springer Berlin Heidelberg, Berlin, Heidelberg; 2014).
131. Kooij, E.S., Sui, X., Hempenius, M.A., Zandvliet, H.J.W. & Vancso, G.J. Probing the Thermal Collapse of Poly(N-isopropylacrylamide) Grafts by Quantitative in Situ Ellipsometry. *J. Phys. Chem. B* **116**, 9261-9268 (2012).
132. Galvin, C.J., Dimitriou, M.D., Satija, S.K. & Genzer, J. Swelling of polyelectrolyte and polyzwitterion brushes by humid vapors. *J. Am. Chem. Soc.* **136**, 12737-12745 (2014).
133. Galvin, C.J. & Genzer, J. Swelling of Hydrophilic Polymer Brushes by Water and Alcohol Vapors. *Macromolecules* (2016).
134. Young, T. An Essay on the Cohesion of Fluids. *Philosophical Transactions of the Royal Society of London* **95**, 65-87 (1805).
135. Gray, V. Surface aspects of wetting and adhesion. *Chemistry and industry* **23**, 969-978 (1965).
136. Kwok, D.Y., Gietzelt, T., Grundke, K., Jacobasch, H.J. & Neumann, A.W. Contact Angle Measurements and Contact Angle Interpretation. 1. Contact Angle Measurements by

Axisymmetric Drop Shape Analysis and a Goniometer Sessile Drop Technique. *Langmuir* **13**, 2880-2894 (1997).

137. Nath, N., Hyun, J., Ma, H. & Chilkoti, A. Surface engineering strategies for control of protein and cell interactions. *Surf. Sci.* **570**, 98-110 (2004).
138. Keselowsky, B.G., Collard, D.M. & García, A.J. Surface chemistry modulates fibronectin conformation and directs integrin binding and specificity to control cell adhesion. *J. Biomed. Mater. Res. Part A* **66A**, 247-259 (2003).
139. Cole, M.A., Voelcker, N.H., Thissen, H. & Griesser, H.J. Stimuli-responsive interfaces and systems for the control of protein-surface and cell-surface interactions. *Biomaterials* **30**, 1827-1850 (2009).
140. Takezawa, T., Mori, Y. & Yoshizato, K. Cell Culture on a Thermo-Responsive Polymer Surface. *Nat. Biotech.* **8**, 854-856 (1990).
141. Nakanishi, J. et al. Photoactivation of a Substrate for Cell Adhesion under Standard Fluorescence Microscopes. *J. Am. Chem. Soc.* **126**, 16314-16315 (2004).
142. Rosario, R. et al. Photon-Modulated Wettability Changes on Spiropyran-Coated Surfaces. *Langmuir* **18**, 8062-8069 (2002).
143. Mendes, P.M. Stimuli-responsive surfaces for bio-applications. *Chem. Soc. Rev.* **37**, 2512-2529 (2008).
144. Edahiro, J.-i. et al. In Situ Control of Cell Adhesion Using Photoresponsive Culture Surface. *Biomacromolecules* **6**, 970-974 (2005).

145. Donlan, R.M. Biofilm Formation: A Clinically Relevant Microbiological Process. *Clinical Infectious Diseases* **33**, 1387-1392 (2001).

146. Pavithra, D. & Mukesh, D. Biofilm formation, bacterial adhesion and host response on polymeric implants—issues and prevention. *Biomedical Materials* **3**, 034003 (2008).

147. Vasilev, K., Cook, J. & Griesser, H.J. Antibacterial surfaces for biomedical devices. *Expert Rev. Med. Devic.* **6**, 553-567 (2009).

148. Amiji, M. & Park, K. Surface modification of polymeric biomaterials with poly(ethylene oxide), albumin, and heparin for reduced thrombogenicity. *J. Biomater. Sci., Polym. Ed.* **4**, 217-234 (1993).

149. Grundmann, H., Aires-de-Sousa, M., Boyce, J. & Tiemersma, E. Emergence and resurgence of meticillin-resistant Staphylococcus aureus as a public-health threat. *The Lancet* **368**, 874-885.

150. Eili, K., David, L.S. & Ramanan, L. Hospitalizations and Deaths Caused by Methicillin-Resistant Staphylococcus aureus, United States, 1999–2005. *Emerg. Infect. Disease.Emerg. Infect. Disease.* **13**, 1840 (2007).

151. Banerjee, I., Pangule, R.C. & Kane, R.S. Antifouling coatings: recent developments in the design of surfaces that prevent fouling by proteins, bacteria, and marine organisms. *Adv. Mater.* **23**, 690-718 (2011).

152. Yu, Q., Zhang, Y., Wang, H., Brash, J. & Chen, H. Anti-fouling bioactive surfaces. *Acta Biomater.* **7**, 1550-1557 (2011).

153. Jeon, S.I., Lee, J.H., Andrade, J.D. & De Gennes, P.G. Protein—surface interactions in the presence of polyethylene oxide. *J. Colloid Interface Sci.* **142**, 149-158 (1991).

154. Ostuni, E., Chapman, R.G., Holmlin, R.E., Takayama, S. & Whitesides, G.M. A Survey of Structure−Property Relationships of Surfaces that Resist the Adsorption of Protein. *Langmuir* **17**, 5605-5620 (2001).

155. Ma, H., Hyun, J., Stiller, P. & Chilkoti, A. "Non-Fouling" Oligo(ethylene glycol)- Functionalized Polymer Brushes Synthesized by Surface-Initiated Atom Transfer Radical Polymerization. *Adv. Mater.* **16**, 338-341 (2004).

156. Ma, H., Li, D., Sheng, X., Zhao, B. & Chilkoti, A. Protein-Resistant Polymer Coatings on Silicon Oxide by Surface-Initiated Atom Transfer Radical Polymerization. *Langmuir* **22**, 3751-3756 (2006).

157. Glinel, K. et al. Antibacterial and Antifouling Polymer Brushes Incorporating Antimicrobial Peptide. *Bioconjugate Chem.* **20**, 71-77 (2008).

158. Matyjaszewski, K. & Tsarevsky, N.V. Nanostructured functional materials prepared by atom transfer radical polymerization. *Nat. Chem.* **1**, 276-288 (2009).

159. Savin, D.A., Pyun, J., Patterson, G.D., Kowalewski, T. & Matyjaszewski, K. Synthesis and characterization of silica-graft-polystyrene hybrid nanoparticles: Effect of constraint on the glass-transition temperature of spherical polymer brushes. *J. Phys. Chem. Sci. Part B Polym. Phys.* **40**, 2667-2676 (2002).

160. Ohno, K., Morinaga, T., Takeno, S., Tsujii, Y. & Fukuda, T. Suspensions of Silica Particles Grafted with Concentrated Polymer Brush: Effects of Graft Chain Length on Brush Layer Thickness and Colloidal Crystallization. *Macromolecules* **40**, 9143-9150 (2007).

161. Ohno, K., Morinaga, T., Koh, K., Tsujii, Y. & Fukuda, T. Synthesis of Monodisperse Silica Particles Coated with Well-Defined, High-Density Polymer Brushes by Surface-Initiated Atom Transfer Radical Polymerization. *Macromolecules* **38**, 2137-2142 (2005).

162. Wunder, S., Polzer, F., Lu, Y., Mei, Y. & Ballauff, M. Kinetic Analysis of Catalytic Reduction of 4-Nitrophenol by Metallic Nanoparticles Immobilized in Spherical Polyelectrolyte Brushes. *J. Phys. Chem. C* **114**, 8814-8820 (2010).

163. Sharma, G. & Ballauff, M. Cationic Spherical Polyelectrolyte Brushes as Nanoreactors for the Generation of Gold Particles. *Macromol.Rapid Commun.* **25**, 547-552 (2004).

164. Schrinner, M. et al. Stable Bimetallic Gold–Platinum Nanoparticles Immobilized on Spherical Polyelectrolyte Brushes: Synthesis, Characterization, and Application for the Oxidation of Alcohols. *Adv. Mater.* **20**, 1928-1933 (2008).

165. Guo, X., Weiss, A. & Ballauff, M. Synthesis of Spherical Polyelectrolyte Brushes by Photoemulsion Polymerization. *Macromolecules* **32**, 6043-6046 (1999).

166. Kizhakkedathu, J.N. & Brooks, D.E. Synthesis of Poly(N,N-dimethylacrylamide) Brushes from Charged Polymeric

Surfaces by Aqueous ATRP: Effect of Surface Initiator Concentration. *Macromolecules* **36**, 591-598 (2003).

167. Wittemann, A., Drechsler, M., Talmon, Y. & Ballauff, M. High Elongation of Polyelectrolyte Chains in the Osmotic Limit of Spherical Polyelectrolyte Brushes: A Study by Cryogenic Transmission Electron Microscopy. *J. Am. Chem. Soc.* **127**, 9688-9689 (2005).

168. Zelikin, A.N. Drug Releasing Polymer Thin Films: New Era of Surface-Mediated Drug Delivery. *ACS Nano* **4**, 2494-2509 (2010).

3 Temperature Dependence of the Surface and Volume Hydrophilicity of Hydrophilic Polymer Brushes

*Pengyu Zhuang, Ali Dirani, Karine Glinel and Alain M. Jonas**

Bio & Soft Matter, Institute of Condensed Matter and Nanosciences, Université catholique de Louvain, Croix du Sud 1/L7.04.02, 1348 Louvain-la-Neuve, Belgium

(*Langmuir* **2016**, *32*, 3433-3444)

3.1 Abstract

The temperature-dependence of the volume and surface hydrophilicity of a series of water-swollen dense polymer brushes is measured by contact angle measurements in the captive bubble configuration, ellipsometry and quartz crystal microbalance with dissipation monitoring (QCM-D). Thermo-responsive poly(*N*-isopropylacrylamide) (PNIPAM) and poly(di(methoxyethoxy) ethylmethacrylate) ($PMEO_2MA$), strongly hydrophilic poly(*N*,*N*-dimethylacrylamide) (PDMA) and poly(oligo(ethylene glycol) methacrylate) (POEGMA), and weakly hydrophilic poly(2-hydroxyethyl methacrylate) (PHEMA) brushes were synthesized by surface-initiated atom-transfer radical polymerization (SI-ATRP). Conditions leading to reproducible measurements of the contact angle

are first provided, giving access to the surface hydrophilicity. Volume hydrophilicity is quantified by measuring the swelling of the brushes, either by QCM-D or ellipsometry. A model-free methodology is proposed to analyze the QCM-D data. Comparison between the acoustic and optical swelling coefficients shows that QCM-D is sensitive to the maximal thickness of swollen brushes, while ellipsometry provides an integral thickness. Diagrams of surface versus volume hydrophilicity of the brushes finally lead to identify two types of behavior: strongly water-swollen brushes exhibit a progressive decrease of volume hydrophilicity with temperature, while surface hydrophilicity changes moderately; weakly water-swollen brushes have a close-to-constant volume hydrophilicity, while surface hydrophilicity decreases with temperature. Thermo-responsive brushes abruptly switch from one behavior to the other, and do not exhibit an abrupt change of surface hydrophilicity across their collapse transition contrarily to a common erroneous belief. In general, there is no direct correlation between surface and volume hydrophilicity, because surface properties are dependent on the details of conformation and composition at the surface, whereas volume properties are averaged over a finite region within the brush.

Chapter 3: Temperature Dependence of the Surface and Volume Hydrophilicity of Hydrophilic Polymer Brushes

3.2 Introduction

Stimuli-responsive polymer brushes are made of macromolecules densely grafted on a substrate, with chain conformation and layer properties dramatically altered when exposed to an external stimulus such as temperature, pH, ionic strength or light.[1-4] Among these stimuli-responsive brushes, the popular thermo-responsive hydrophilic polymer brushes are based on polymers exhibiting a lower critical solution temperature (LCST) in water. When grafted in a brush, the chains experience in water a broad collapse transition close to the LCST of the free chains, resulting in a large variation of the degree of swelling of the brush layer; hence, the volume of the brush switches abruptly from a more to a less hydrophilic state upon increasing temperature. Such brushes therefore play a critical role in various fields as sensors and actuators,[5] anti-fouling and anti-bacterial surfaces,[6, 7] systems for drug and cell delivery,[8] and smart substrates for cell culture.[9, 10]

In the literature, it is often stated that the collapse transition is also accompanied with a change of wettability, *i.e.*, a change of surface hydrophilicity. Such claims essentially rest on measurements performed in out-of-equilibrium conditions, *e.g.*, by measuring the contact angle of a droplet of water on a brush in air, which casts doubts on their relevance. Indeed, preliminary experiments performed in conditions closer to equilibrium indicate that an abrupt change of surface hydrophilicity is unlikely.[10-12] Since the above-mentioned applications are certainly dependent on surface and not only on volume properties, we found interesting and useful to critically compare the hydrophilicity of the volume and of the surface of water-swollen brushes, thermo-responsive or not, as a function of temperature. Here,

we demonstrate that the surface and volume hydrophilicity of water-swollen brushes are two distinct notions which do not evolve identically with temperature and do not directly correlate with each other; as a particular example, we also confirm that the surface of thermo-responsive polymer brushes does not switch from hydrophilic to hydrophobic across the collapse transition.

Different dense polymer brushes were grown from silicon substrates by surface-initiated atom transfer radical polymerization (Si-ATRP) (Scheme 1): thermo-responsive poly(*N*-isopropylacrylamide) (PNIPAM) and poly(di(methoxyethoxy)ethylmethacrylate) ($PMEO_2MA$), strongly hydrophilic poly(*N*,*N*-dimethylacrylamide) (PDMA) and poly(oligo(ethylene glycol) methacrylate) (POEGMA), and weakly hydrophilic poly(2-hydroxyethyl methacrylate) (PHEMA) brushes. With its LCST of 32°C, PNIPAM is probably the most popular thermo-responsive polymer studied so far;[13] $PMEO_2MA$ is a more recent challenger with a close LCST of 26°C.[13-15] PDMA and POEGMA do not exhibit a LCST in water in the accessible temperature range. As for PHEMA, whose hydrogels are used for intraocular lenses,[16] and whose dense brushes resist protein adsorption,[17] it is generally considered as a water-swellable rather than water-soluble polymer, even though its low molar mass chains may exhibit a complex behavior.[18]

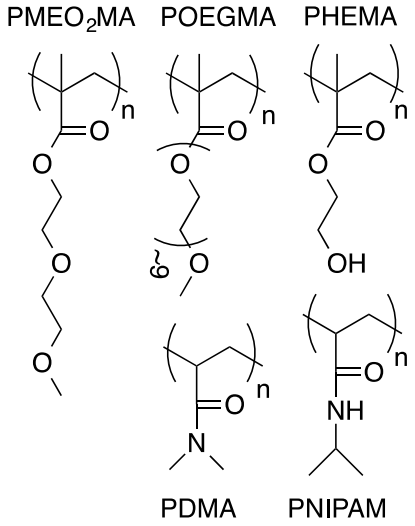

Scheme 1. Chemical structure of the five hydrophilic polymers investigated in this study.

We study the average swelling of the volume of the brushes by two complementary techniques, Quartz Crystal Microbalance with Dissipation monitoring (QCM-D) and ellipsometry. The QCM-D data is analyzed by a new, "model-free" simple methodology, which allows to extract the swelling coefficients without requiring to fit the equations. Both QCM(-D)[7, 16-23] and ellipsometry[24-28] have been used before to monitor the swelling of polymer brushes; these techniques were also combined for that purpose.[19, 29-31] Because our aim is only to obtain an average degree of swelling, we will not take into account the fine details of the brush segment density profiles; nevertheless, since QCM-D and ellipsometry are not sensitive to the same parameters,[19] the comparison of the results from these two techniques provides indirect pieces of information on these profiles. The surface wettability is characterized by contact angle measurements performed in the captive

bubble configuration, which allow us to reach if not an equilibrium at least a stationary state.[12] We thoroughly investigate the experimental conditions leading to reproducible and reversible contact angle values in this configuration, and finally correlate surface and volume hydrophilicity for the five selected brushes.

3.3 Experimental section

3.3.1 Materials

N,*N*-dimethylacrylamide (DMA), 2(2-methoxyethxy)ethyl-methacrylate (MEO_2MA), 2-hydroxyethyl methacrylate (HEMA), oligo(ethyleneglycol)methylether-methacrylate (OEGMA) with 475 g/mol average molar mass by number were purchased from Sigma-Aldrich. DMA was purified by distillation under vacuum at about 70°C before use. MEO_2MA, HEMA, and OEGMA were run three times through an aluminum oxide column. *N*-isopropylacrylamide (PNIPAM) was obtained from TCI Chemicals and used as received. Copper(I) chloride (99.995+%) (CuCl), copper(II) chloride (99.999+%) ($CuCl_2$), and copper(II) bromide (99+%) ($CuBr_2$), 1,1,4,7,10,10-hexamethyltriethylenetetramine (HMTETA), 2,2'-bipyridyl (99+%) (bipy), were purchased from Sigma-Aldrich. Tris(2-dimethylaminoethyl)amine (99+%) (Me_6TREN) was supplied by Alpha Aesar. Milli-Q water (resistivity: 18.2 MΩ.cm) was obtained from a Millipore system. When needed, water was degassed by heating under argon. Single-side polished wafers (<100> orientation) were obtained from ACM (France). Quartz crystal sensors covered with a layer of SiO_2 (QSX 303) were purchased from Q-Sense (Sweden) and rinsed with ethanol before use. The ATRP silane initiator (3-

(chlorodimethylsilyl)propyl 2-bromo-2-methylpropanoate) was synthesized as described previously.[11]

3.3.2 Brush synthesis.

A monolayer of ATRP silane was grafted on Si wafers or quartz sensors by gas phase silanation as described in Supplementary Information. Dense polymer brushes were then grown by ATRP from the substrates, using various conditions (ligand and solvent nature) to obtain in a few hours brushes with a dry thickness ranging from *ca.* 50 to 120 nm. The detailed experimental conditions used for each specific system are described in the Supporting Information. The grafting density of similarly synthesized $PMEO_2MA$ brushes was estimated to be in the range of 0.3 nm^{-2}.[32] The molar mass distribution of the chains could not be measured because the amount of material collected after degrafting the chains from the substrate (about 0.1 $\mu g/cm^2$) is too small for analysis; furthermore, the standard methodology which consists of growing free chains in parallel with the surface-initiated polymerization is generally not valid.[33, 34] Instead, kinetic growth curves are presented in the Supporting Information (Figure S1).

3.3.3 QCM-D

A brush-covered crystal sensor was placed in the flow module of a commercial apparatus (Q-Sense E4, Biolin Scientific, Sweden). The temperature was initially kept at 20°C without water running in the cell chamber. When the frequency and dissipation shifts were stable, a measurement was performed for 5 min in air to acquire a reference value for the dry brush. The temperature was then decreased to 15°C in

one min, and stabilized for about 15 min. Degassed Milli-Q water was then introduced with a peristatic pump in the cell chamber at a flow rate of 0.2 mL/min and the machine was stabilized for about 45 min at 15°C. The temperature was subsequently increased at 0.2°C/min to *ca.* 50°C then decreased to 15°C while recording the frequency and dissipation shifts for all harmonics.

3.3.4 Ellipsometry

The dry thickness of a brush grown on Si wafer was first measured with a spectroscopic ellipsometer (Uvisel, Horiba-Jobin-Yvon, France). The refractive index of the brush was in particular obtained at $\lambda = 632.8$ nm wavelength. The brush grafted on a Si wafer was then placed in an ellipsometric liquid cell (nanofilm-sl65, Accurion, Germany) mounted on a rotating compensator single wavelength laser ellipsometer (Jobin-Yvon Digisel, France) working at $\lambda = 632.8$ nm and at an incidence angle of *ca.* 65° previously calibrated with a reference SiO_2/Si wafer (in the absence of cell windows). The ellipsometric angles (ψ and Δ) of the brush sample were then measured in air in the absence of cell windows, and the dry brush thickness and index of refraction were computed again. These generally agreed with values previously determined by spectroscopic ellipsometry. The cell windows were then placed, and the dry brush was again measured in air to investigate the influence of the windows on the ellipsometry data. In case the ellipsometric angles obtained in the presence of the cell windows differed significantly from their values without windows, the whole sample placement was repeated until a good agreement between both measurements was obtained. The cell was then filled with

degassed Milli-Q water, taking care to avoid the formation of bubbles. The temperature was decreased to 5°C, and then increased by 5°C steps up to 75°C with a Peltier heater/cooler. Temperature was stabilized for 10 min at each temperature; prior tests performed with a tiny thermocouple immersed in water showed minimal difference with the set point of the Peltier element and very rapid thermal equilibration times. To study the reversible behavior of the brush, measurements were also performed upon cooling. The brush thickness and index of refraction were obtained from the two ellipsometric angles by a standard fitting routine, using the published indices of refraction of water and Si as a function of temperature;[35, 36] the small imaginary part of the complex refractive index of Si, which is due to absorption, was kept constant at 0.019.

3.3.5 Equilibrium contact angle measurement

Contact angle measurements were performed as a function of temperature in the captive air bubble configuration with a contact angle goniometer (OCA, DataPhysics, Germany) equipped with a home-made water-filled copper cell with two quartz glass windows placed on a Peltier heater/cooler (see picture in Supplementary Information). Different protocols were tested; however, in this section, we describe only the finally-selected protocol. The sample was fixed on the sample holder and immersed face-down in non-degassed Milli-Q water. A thermocouple was fixed on the other side of the sample to obtain a direct reading of the actual water temperature close to the sample. The temperature was changed in steps. At each pre-set temperature (except for 5°C), the sample was kept for 15 min (30 min at 5°C) to reach

thermal equilibrium, as checked by the thermocouple; then an air bubble of *ca.* 6 μL volume was gently deposited on the surface of the sample with a U-shaped needle connected to an electronic syringe. After 5 min bubble equilibration, an image of the bubble was recorded with a digital camera. The air bubble was removed after each measurement and a new bubble was placed at almost the same place. The bubble shape was fitted near the triple line by arcs of a circle, and the left and right contact angles were averaged to obtain the final contact angle.

3.4 Results and discussion

3.4.1 Brush surface hydrophilicity by equilibrium contact angle measurements

Brush surface hydrophilicity can be estimated by recording the contact angle of water on the brush. However, such measurements are well-known to be prone to artifacts; therefore, we first thoroughly studied the reproducibility of contact angles as a function of temperature for reference brushes exhibiting or not a collapse transition in the accessible temperature range. As already reported elsewhere,[11] measuring the contact angle of a water droplet placed over the heated brush in air is not an option, because the fast evaporation of the droplet with the associated recess of the triple line prevents obtaining a stable recording. In contrast, the captive bubble configuration, which consists of placing an air bubble below the flipped surface immersed in water, allowed us to perform measurements over extremely long times until an equilibrium or at least stationary state was reached.

We tested many different experimental conditions, using bubbles of varying sizes, placed in degassed or non-degassed water in containers of different sizes and component materials, progressively heated and equilibrated for different times, before taking a record of contact angle, bubble volume and bubble contact area with the brush. A complete account of these experiments is in Supplementary Information. The results of a typical improper measurement are shown in Figure 1; in this experiment, an air bubble of 6 μL was placed in contact with a $PMEO_2MA$ brush sample immersed face down in degassed water at 20°C, stabilized for 2 h, then cooled to 5°C. The bubble volume, contact area with the sample, and contact angle were then measured for 15 h at 5°C; then the sample was heated and cooled by *ca.* 4.5°C steps, and the same parameters were measured after 30 min equilibration time at each temperature. The results of many similar experiments are provided in Supplementary Information.

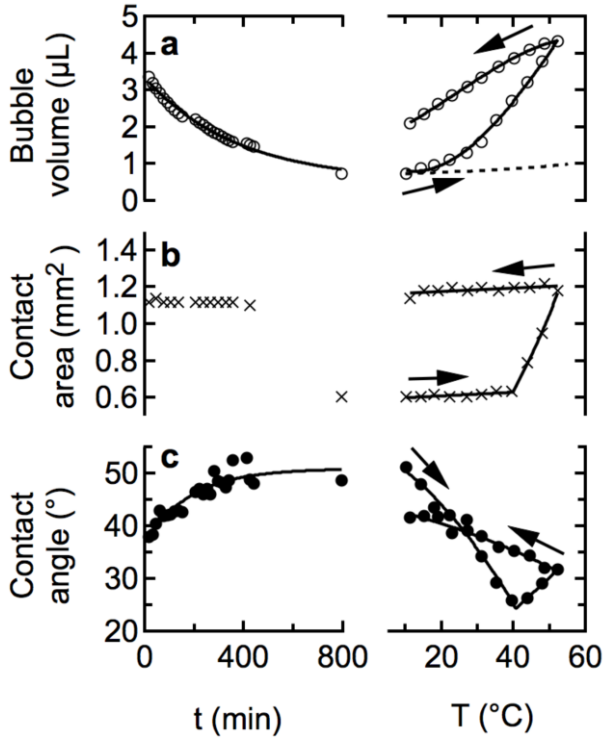

Figure 1. Example of an improper measurement of water contact angle versus temperature in the captive bubble configuration, affected by air transfer between bubble and water, bubble pinning and irreversible thermal behavior. The sample is a $PMEO_2MA$ brush; the water used for this experiment was initially degassed; a container of large volume (16 cm^3) was used. The initial air bubble of 6 µL was placed on the sample at room temperature, held for 2 h then cooled to 5°C. The left part of the graphs presents the evolution of the bubble volume (a), bubble contact area (b) and water contact angle (c) versus equilibration time at 5°C. The right part of the graphs shows these parameters when the sample was subsequently heated and cooled by *ca.* 4.5°C steps with 30 min equilibration time at each step. The arrows indicate the direction of the thermal cycle. The continuous lines are drawn to guide the eye; the dashed line in (a) gives the variation of volume of the bubble when the exchange of air between the bubble and water is ignored (equation (1)).

When the air bubble is placed in contact with the surface at low temperature (*i.e.*, 5°C), its volume decreases slowly with time by a factor that can be as large as 10 over 15 h (the factor is *ca.* 5 in Figure 1a). When heated progressively, its volume increases dramatically with temperature, and vice-versa; again, the variation factor can be as large as 10 over a 40°C temperature range. These variations of bubble volume result from (1) the thermal expansion of air according to the law of ideal gases; (2) the exchange of water molecules between the liquid and bubble to reach the equilibrium vapor pressure of water in the bubble; (3) the exchange of air between water and bubble, due to the finite solubility of air in water, which decreases at higher temperatures.[37] Whereas the first two phenomena are relatively rapid (a few minutes), the third one is slower and takes many hours because it requires diffusion of air from a small bubble into a large volume of water (which is not stirred for obvious reasons). This third equilibrium is a very important component of the variation of bubble volume and cannot be ignored. It is possible to compute the volume at any temperature, $V(T)$, of an initially-equilibrated bubble of volume V_0 at T_0, at constant total pressure $p°$, if variations were only due to thermal dilatation and changes of water vapor pressure:

$$V(T) = V_0 \frac{RT}{RT_0} \frac{p^\circ - p_{\mathrm{vap}}(T_0)}{p^\circ - p_{\mathrm{vap}}(T)} \qquad (1),$$

where $p_{\mathrm{vap}}(T)$ is the vapor pressure of water at T; this relationship is shown by the dashed line in Figure 1a. Clearly, the main part of the experimental variation of the bubble volume does not arise from thermal expansion nor changes of water vapor pressure with temperature; it is therefore due to the slow equilibration of dissolved air

in water. Because this equilibrium operates through two interfaces, the captive bubble surface and the air/water interface at the top of the container, we found that the time- and temperature-dependence of the bubble volume depends on the size of the water container.

The variation of bubble volume has strong consequences on the validity of the contact angle measurements. Indeed, depending on whether the volume increases or decreases with time or temperature, the experiments are actually advancing- or receding-contact angle measurements. Unfortunately, the bubble is often pinned on the surface of the brush. Figure 1b presents the contact area of the bubble with the sample; during heating, the contact area on the brush remains constant despite the increase of bubble volume, resulting in a deformation of the bubble and a decrease of contact angle (Figure 1c). Pinning most probably results from conformational differences at the surface of the brush, below the water vapor-saturated bubble and below liquid water. The degree of swelling of the brush are identical at these two locations, because the chemical potentials of water vapor and liquid water are identical at equilibrium; however, local conformational rearrangements and water interfacial adsorption are still possible at the very brush surface, resulting in the presence of a free energy barrier opposing the motion of the triple line.

At some point during heating (at 40°C for the specific case of Figure 1), the excess of surface tension at the triple line overcomes the free energy barrier, and depinning occurs. A similar pinning/depinning mechanism (albeit for a fully different system) was proposed before,[38] involving two different liquid/solid surface tensions associated to different chain conformations at a surface. After depinning, the contact

area and the contact angle of the droplet increase with temperature. Depinning therefore results in the apparition of a kink in the contact angle curve. It is easy to check that this kink does not signal a thermodynamic transition of the brush: the kink is not reversible upon cooling the system, as shown in Figure 1c, illustrating its essentially kinetic nature.

In the case of thermo-responsive $PMEO_2MA$ brushes, a real thermodynamic surface transition actually exists at *ca.* 32°C,[12] and depinning should somehow be triggered by this transition. Therefore, unsurprisingly, a kink is always observed on $PMEO_2MA$ contact angle heating curves; however, its location varies from 32 to 50°C depending on experimental conditions. Most annoyingly, depinning kinks are also sometimes observed on samples which do not have a thermodynamic transition in the probed thermal range, like POEGMA brushes.

It is possible to minimize the occurrence of pinning and the associated depinning transition by using conditions which reduce bubble inflation and deflation during temperature scanning: reducing thermal equilibration times by using smaller containers with walls of higher thermal conductance, heating and cooling faster, or using non-degassed water are favorable factors. Nevertheless, to completely get rid of these issues, it is easier to use a new bubble for each measurement temperature, and shorten the equilibration times. While this certainly results in larger random errors and more scattered data, the use of a new bubble for each measurement leads to reproducible results, provided the bubble be kept long enough to equilibrate thermally, but short enough for the air dissolution equilibrium not to interfere with the measurements.

For our finally-selected copper cell of limited water content (cell III in Figure S2, Supplementary Information), thermal equilibrium is reached in less than 10 min, as was checked by a tiny thermocouple placed at the sample position. Therefore, a 15 min thermal equilibration time was selected, after which the bubble is placed on the sample. In addition, time-resolved ellipsometry measurements show that the equilibration time for the swelling of brushes by water is shorter than 5 min. Consistently measurements of the contact angle after 0, 5 and 10 min bubble deposition showed that identical values are obtained after 5 and 10 min, indicating that the equilibrium of the bubble, excluding air intake, is rapidly reached. Hence, measurements were invariably performed 5 min after droplet deposition.

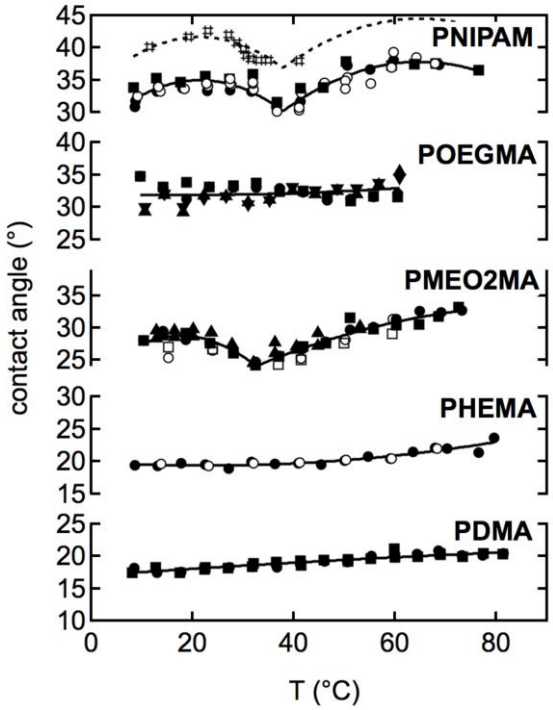

Figure 2. Equilibrium water contact angle versus temperature measured with the proper final protocol for the brushes of this study. Closed symbols indicate data acquired on heating; open symbols are for cooling. The different symbols used for PNIPAM, POEGMA and $PMEO_2MA$ correspond to measurements performed separately on the same sample. The continuous lines are polynomial fits to the data. The dry brush thickness are: PDMA 125 nm, PNIPAM 77 nm, $PMEO_2MA$ 77 nm, POEGMA 77 nm, PHEMA 90 nm. The hashtags are measurements performed on a dense PNIPAM brush of 62 nm thickness by Suzuki *et al*;[39] the dashed line is the vertically-translated polynomial fit of the PNIPAM data of this study.

With these conditions, although the contact angles of samples such as POEGMA, PNIPAM and $PMEO_2MA$ brushes which are independently measured more than once by heating and cooling are

scattered a bit, they are very close and kinks in the contact angle curves appeared reproducibly and reversibly only in heating and cooling curves of thermo-responsive samples (*i.e.*, PNIPAM and $PMEO_2MA$, Figure 2), whereas the other polymer brushes exhibited only a rather weak temperature dependence, as expected (Figure 2). Kinks in the equilibrium contact angle curves were discussed previously;[11, 12, 40] they originate from a discontinuity in the excess configurational surface entropy of the brush at the collapse transition, and mark the collapse of the very outer part of the brush (which occurs at a higher temperature than the collapse of innermost parts of the brush). The collapse of the brush surface occurs at 32.5°C for $PMEO_2MA$, in good agreement with our previous report from measurements made with another setup,[11] and at 38.1°C for PNIPAM. A previous measurement performed by Suzuki *et al*. [39] on a similar dense PNIPAM brush is also compared in Figure 2 (hashtags): although the absolute values of contact angle differ due to systematic errors, the temperature dependence is preserved, as testified by the fact that polynomial fits to our data can simply be translated to fit Suzuki's data (dashed line in Figure 2). Unfortunately, the much smaller thermal range of this previous report led to the incorrect conclusion that the contact angle reaches a plateau above 32°C, which is clearly not the case. Similar measurements performed over an unfortunately similarly limited temperature range were also reported by Jalili *et al*.[41] Importantly, the final data collected in Figure 2 show that, although the surface of all brushes are hydrophilic, their specific values of contact angles may differ by as much as 20° at a given temperature, which is well above the experimental error.

3.4.2 Determination of brush swelling by ellipsometry

Evaluating the degree of swelling of a brush allows us to estimate the average hydrophilicity of the brush, *i.e.*, the hydrophilicity of the volume of the brush. The ellipsometric angles ψ and Δ measured during heating and cooling a $PMEO_2MA$ brush grafted on Si and immersed in water are shown in Figure 3. Each point is an average of 5 to 10 measurements. Heating and cooling curves (closed and open symbols, respectively) fully superimpose, showing the reversibility of the swelling when a 10 min thermal equilibration time is used.

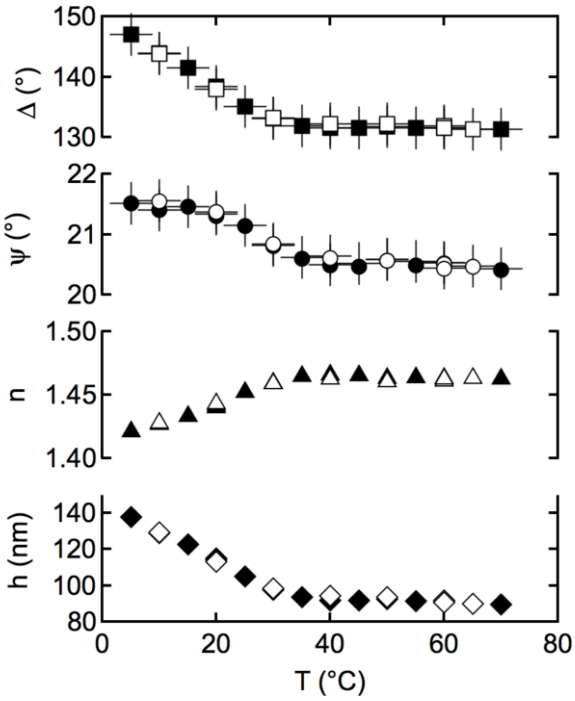

Figure 3. Ellipsometry data obtained on a $PMEO_2MA$ brush of 78 nm dry thickness, heated (closed symbols) then cooled (open symbols) in water. The ellipsometric angles ψ and Δ are shown at the top; the fit of a single-layer optical model with the thickness h and refractive index n of the wet brush as parameters give the values indicated by the crosses.

The variations of Δ and ψ contain information on the variation with temperature of the swollen brush thickness and of the complex refractive indices of Si, water and swollen brush. Because the refractive indices of Si and water are known for all temperatures at the wavelength of the experiments (632.8 nm),[35, 36] the average index of refraction of the brush *n* and its average swollen thickness *h* can be obtained by standard fitting methods.[42] However, this is only possible when the ellipsometric trajectory lies in a (Δ,ψ) region for which the sensitivity to *n* and *h* is high, which for swollen layers of refractive index in the 1.37-1.45 range corresponds to (swollen) thicknesses in the 80-340 nm range (Figure 7b), as for the brushes of this study.

The values of Δ and ψ computed from an optical model of homogenous film of index of refraction *n* and thickness *h* are in very good agreement with the experimental data (crosses in Figure 3). The temperature dependence of *n* and *h* indicates the presence of a broad collapse transition, as expected for $PMEO_2MA$ brush layers:[43, 44] whereas the thickness decreases dramatically from 5°C to 35°C, the index of refraction increases, due to the expulsion of water from the layer. Above 35°C, in the fully collapsed state, the thickness and index of refraction are constant. As previously observed,[12] the end of the collapse coincides very well with the temperature of the kink in the curve of contact angle (Figure 2).

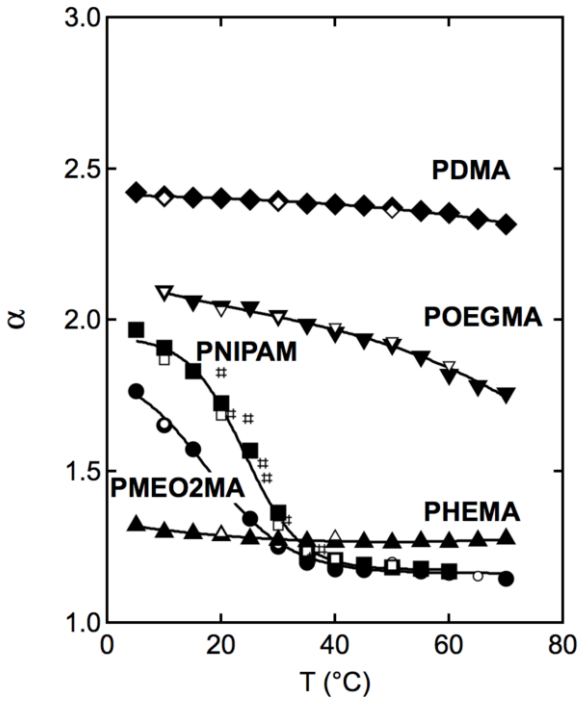

Figure 4. Ellipsometry-determined swelling coefficients of the brushes versus temperature. Closed symbols are for heating, open symbols for cooling. The dry thicknesses of the brushes are: PNIPAM 118 nm, $PMEO_2MA$ 78 nm, POEGMA 58 nm, PDMA 91 nm and PHEMA 96 nm. The hashtags are AFM measurements performed on a similar dense PNIPAM brush of 121 nm thickness, taken from Suzuki *et al*.[39]

A similar analysis was performed for the other brush layers, from which the swelling coefficient α was obtained by division of the swollen thickness by the dry thickness. Experiments repeated on identical samples indicate that the absolute values of the swelling coefficient have a precision of not better than 0.2, most probably due to errors in the calibration of the incidence angle of the laser. However, the relative precision is much better, as testified by the coincidence of

heating and cooling curves on a same sample. The ellipsometric swelling coefficients of the different brushes are shown in Figure 4. The measurements of Suzuki et al.[39] performed by scanning an AFM tip across a scratch made in a dense 121 nm-thick PNIPAM brush are also shown for comparison (hashtags): the present ellipsometric results agree quite well with this previous, independent measurement. However, one should be aware that the degree of swelling depends on the grafting density[28, 45] and force applied during the measurement; [4546, 47] therefore, the quantitative agreement in Figure 4 is essentially coincidental.

3.4.3 Determination of the brush swelling by QCM-D

The optical model we used for ellipsometry assumes a homogeneously swollen brush layer, which is not the case; hence, using another technique with a different sensitivity to the monomer density of the brush is certainly useful. Therefore, QCM-D was used in this work, based on the Voigt model of a single homogeneous layer grafted on a quartz sensor immersed in a fluid. This model describes the frequency and dissipation shifts of each odd harmonic ($2n+1$) compared to the bare quartz crystal, Δf_n and ΔD_n: [48, 49]

$$\Delta f_n \approx -\frac{1}{2\pi\rho_q t_q}\left(\frac{\eta_L}{\delta_L}+h\rho\omega_n-2h(\frac{\eta_L}{\delta_L})^2\frac{\eta\omega_n^2}{\mu^2+\omega_n^2\eta^2}\right)+a_f(\omega_n)$$
$$\Delta D_n \approx \frac{1}{\omega_n\rho_q t_q}\left(\frac{\eta_L}{\delta_L}+2h(\frac{\eta_L}{\delta_L})^2\frac{\mu\omega_n^2}{\mu^2+\omega_n^2\eta^2}\right)+a_D(\omega_n) \quad (2);$$

in these equations, $\omega_n = 2\pi(2n+1)f_0$ is the angular frequency of the $(2n+1)^{th}$ harmonic (with f_0 the fundamental frequency of the quartz crystal, 5 MHz in our case); $\rho_q = 2650$ kg/m^3 and $t_q = 3$ mm are the

density and thickness of the quartz crystal, respectively; $\eta_L \approx 1.68\ 10^{-3} - 0.024\ 10^{-3}\ T$ Pa.s is the shear viscosity of water at temperature T (in °C), and $\delta_L = (2\ \eta_L\ \rho_L^{-1}\ \omega_n^{-1})^{1/2}$ is the viscous penetration depth with $\rho_L \approx 1004 - (9/30)\ T$ kg/m^3 (T in °C) being the density of water;[11] h and ρ are the temperature-dependent thickness and density of the swollen brush, respectively; and μ and η are the temperature and frequency-dependent shear modulus and viscosity of the swollen film, respectively. In addition, two frequency-dependent systematic shifts, a_f and a_D, have been added to the equations. These shifts arise from imperfections associated to the mounting of the crystal in the cell, and change when the crystal is removed then mounted again. If the brush could be grown *in situ* in the QCM-D cell, it would be possible to measure precisely the characteristics of the as mounted crystal before polymerization, thereby effectively obtaining a_f and a_D. Unfortunately, this procedure is not possible due to the requirements of ATRP polymerization; therefore the systematic shifts are unknown.

These unknown systematic shifts considerably complicate the analysis of the experimental data, and effectively prevent a fully quantitative analysis to be performed. We and others have fitted equation (2) to experimental QCM-D data,[12] in order to obtain the collapse transition temperatures of polymer brushes. However, here we need to obtain the swelling ratio, *i.e.*, extract quantitatively $h(T)$ from equation (2); this is unfortunately not possible unless supplementary knowledge is available, such as the knowledge of the shear modulus, shear viscosity, or systematic shifts. Indeed, suppose (h, μ, η, a_D, a_f) is a solution of equation (2). Then, (ch, $c\mu$, $c\eta$, a_D, $a_f + (c-1)\ h\rho\omega_n / (2\pi\rho_q t_q)$) is also a solution, in which c is any positive real

number. Accordingly, Supplementary Information shows two equally valid fits of the QCM-D data measured for $PMEO_2MA$ and POEGMA brushes from 15 to 45 °C and for different harmonics, obtained with values of $h(T)$, and therefore $\alpha(T)$, differing by a factor of almost 2.

One way to solve the issue is by subtracting from equation (2) the values $\Delta f°$ and $\Delta D°$ measured on a reference sample having the same systematic shifts as the sample of interest. In practice, since the systematic shifts vary upon mounting the crystal, the reference sample must be the same as the sample of interest, measured in reference conditions. If the reference conditions are in water, then only a differential swelling coefficient will result. However, if the reference conditions are in air before injecting water in the system, then:

$$\begin{aligned} \Delta f_n^{\circ} &\approx -\frac{h_{\mathrm{d}}\rho_{\mathrm{d}}\omega_n}{2\pi\rho_q t_q} + a_f(\omega_n) \\ \Delta D_n^{\circ} &\approx a_D(\omega_n) \end{aligned} \qquad (3),$$

with ρ_{d} and h_{d} the thickness and density of the dry layer, respectively. Therefore, assuming that the systematic shifts do not vary upon introduction of water and are not dependent on temperature,

$$\begin{aligned} \Delta^{\circ} f_n \triangleq \Delta f_n - \Delta f_n^{\circ} &\approx -\frac{1}{2\pi\rho_q t_q}\left(\frac{\eta_L}{\delta_L} + (h\rho - h_{\mathrm{d}}\rho_{\mathrm{d}})\omega_n - 2h(\right. \\ \Delta^{\circ} D_n \triangleq \Delta D_n - \Delta D_n^{\circ} &\approx \frac{1}{\omega_n\rho_q t_q}\left(\frac{\eta_L}{\delta_L} + 2h(\frac{\eta_L}{\delta_L})^2 \frac{\mu\omega_n^2}{\mu^2 + \omega_n^2\eta^2}\right. \end{aligned} \qquad (4)$$

The first equation can be transformed in:

$$-\frac{2\pi\rho_q t_q \Delta^{\circ} f_n + \frac{\eta_L}{\delta_L}}{\omega_n} = (h\rho - h_{\mathrm{d}}\rho_{\mathrm{d}}) - 2h(\frac{\eta_L}{\delta_L})^2 \frac{\eta\omega_n}{\mu^2 + \omega_n^2\eta^2} \qquad (5);$$

furthermore, since $h\rho = h_d\rho_d + (h - h_d)\,\rho_L$ and $\alpha = h / h_d$, we can define a generalized acoustic swelling coefficient $\alpha^*(T,\omega)$:

$$\alpha^*(T,\omega_n) \triangleq 1 - \frac{2\pi\rho_q t_q \Delta^\circ f_n + \frac{\eta_L}{\delta_L}}{\omega_n h_d \rho_L} = \alpha\left(1 - \frac{2}{\rho_L}\left(\frac{\eta_L}{\delta_L}\right)^2 \frac{\eta\omega_n}{\mu^2 + \omega_n^2\eta^2}\right) \quad (6).$$

This function can be easily computed from the experimental QCM-D data using the first equality, provided the dry thickness is known. On the other hand, the second equality shows that:

$$\lim_{\omega\to 0} \alpha^*(T,\omega) = \alpha(T) \quad (7).$$

Therefore, if at each temperature the generalized acoustic swelling coefficient $\alpha^*(T,\omega)$ computed from the data obtained at different harmonics is extrapolated to zero angular frequency, the acoustic swelling coefficient should be obtained as a function of temperature. For this extrapolation, the fundamental mode (n=0) was never taken, as it was clearly affected by large systematic errors. The generalized acoustic swelling coefficients of all brushes are displayed in Supplementary Information.

For the less strongly hydrated $PMEO_2MA$, PNIPAM and PHEMA brushes, the generalized acoustic swelling coefficient $\alpha^*(T,\omega)$ was practically not dependent on angular frequency (an example is shown in Figure 5 left), meaning that the shear modulus was too large and/or the shear viscosity too low to affect significantly the QCM-D data. In these cases, the extrapolation can simply be replaced by an averaging (Figure 5 left). In general, a better agreement between the harmonics was found on cooling curves, whereas the first heating curve was more

noisy probably due to the perturbation when switching from air to water; for this reason, only cooling curves were retained. Measurements performed on different PNIPAM brushes suggest that the absolute precision on the swelling coefficient is in the range of *ca.* 0.2 for collapsed brushes, and 0.5 when swollen (Figure 6 right); however, the relative precision is much better. These repeated experiments also suggest that the effect of thickness on the swelling is not significant in the thickness range of our study.

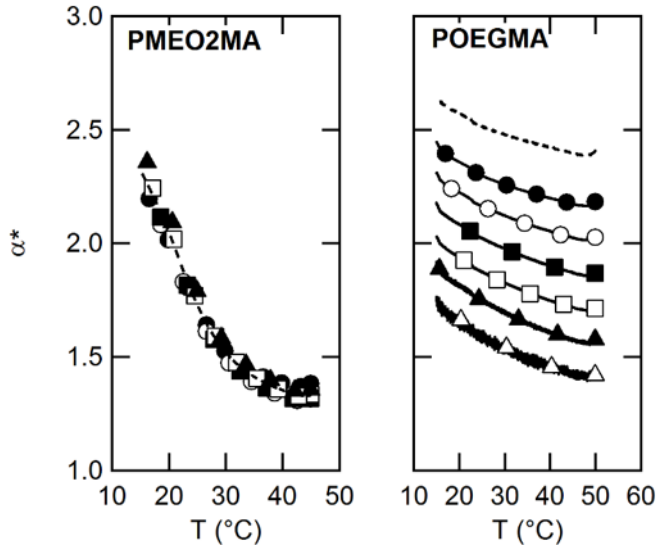

Figure 5. Generalized acoustic swelling coefficient $\alpha^*(T, \omega)$ (equation (6)) versus temperature for two brushes measured in cooling ramps, showing two possible frequency behaviors. The symbols indicate each $(2n+1)^{th}$ harmonic (closed circles: n=1; open circles: n=2; closed squares: n=3; open squares: n=4; closed triangles: n=5; open triangles: n=6); not all data points are shown for clarity. The dashed lines show the frequency-independent acoustic swelling coefficients $\alpha(T)$, obtained either by averaging α^* ($PMEO_2MA$, left) or by extrapolating it to zero frequency (POEGMA, right) (equation (7)).

However, the more strongly hydrated POEGMA and PDMA brushes behave differently, with $\alpha^*(T,\omega_n) < \alpha^*(T,\omega_{n-1})$ (Figure 5 right for an example), due to a low shear modulus and/or high shear viscosity of these brushes. In these cases, the data had to be extrapolated to zero frequency by either a linear (POEGMA) or a second order polynomial fit (PDMA). We also found that a significant number of samples provided clearly erroneous measurements, with different harmonics not showing any regular relation to each other. Repeating experiments led in most cases to more consistent variations, indicating how sensitive the QCM-D is on the positioning (and possibly aging) of the quartz sensor. Generally speaking, obtaining reproducible values with our QCM-D apparatus was much more difficult than with ellipsometry, and the reliability of the acoustic swelling coefficients is clearly lower.

3.4.4 Comparison between ellipsometric and acoustic swelling coefficients

The acoustic swelling coefficients are collected in Figure 6. Comparison with the ellipsometric swelling coefficients of Figure 4 indicates that the acoustic coefficient is larger than the ellipsometric one, except for PHEMA and the collapsed state of PNIPAM for which they are almost equal. For other samples, the acoustic coefficient is larger by 10 to 50% depending on sample and temperature.

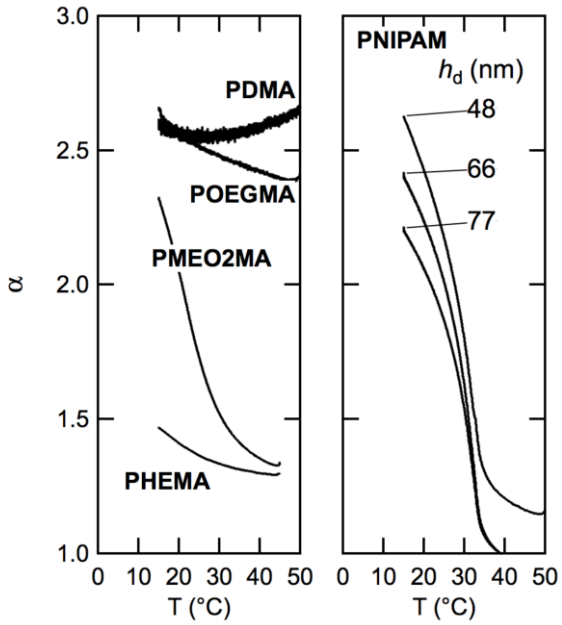

Figure 6. Acoustic swelling coefficient α of the brushes versus temperature. For PNIPAM, the results from three different experiments performed on brushes of different starting dry thickness (as indicated) provide an estimation for the accuracy of the determination of α. The dry thickness of the brushes shown in the left panel are: $PMEO_2MA$ 77 nm, POEGMA 77 nm, PDMA 118 nm and PHEMA 96 nm.

A comparison of the swelling of a polystyrene brush in cyclohexane as measured by ellipsometry and QCM-D was published some time ago.[19] It was shown that ellipsometry and QCM-D are not sensitive in the same way to the details of the vertical profile of solvent content of the brush. Optical reflection is sensitive to the normalized gradient of index of refraction, whereas the QCM-D frequency shift is sensitive to the gradient of the logarithm of acoustic impedance, $Z = (\rho G)^{1/2}$ with G the shear modulus of the swollen film. Because these

parameters do not depend in the same way on solvent content, the type of averaging performed by ellipsometry or QCM-D for a film having a non-homogeneous water content will differ significantly. More precisely, it was shown that the acoustic thickness is much larger than the ellipsometric thickness when the solvent content increases from the bottom to the top of the brush. The brush thicknesses that can be detected by ellipsometry and QCM-D are drawn in scheme 2. The authors used sigmoidal profiles of varying width, and demonstrated numerically that, if a sharp homogeneous layer is used to represent measurements performed on a real layer with a graded solvent content, ellipsometry provides an average thickness which is significantly smaller than the acoustic, QCM-derived one. For the specific case of polystyrene in cyclohexane, the ratio between acoustic and ellipsometric thickness could be as high as 2.5.

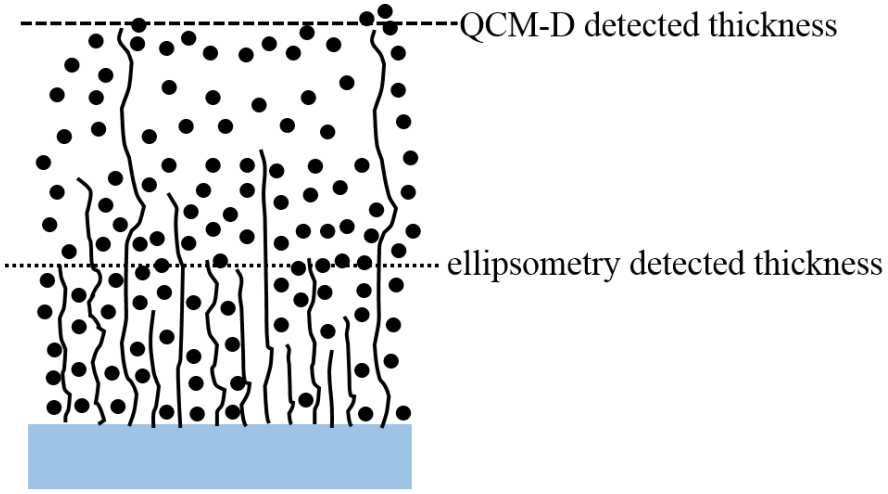

Scheme 2. Schematic of brush thickness detected by ellipsometry and QCM-D. Black lines represent polymer chains grafted and black dots represent water molecules.

To provide a more quantitative comparison between ellipsometry and QCM-D for our case of hydrophilic brushes in water, one can compute the signals expected for a swollen brush displaying a graded density profile, and find out to which equivalent homogeneous layer these signals would correspond. For simplicity, we use the brush segment density profile provided by the strong-stretching approximation,[50] for which the volume fraction in monomer units can be written as:

$$\phi(z) = \phi_0(1 - \frac{z^2}{h_{\max}^2}) \qquad (8).$$

where $h_{\max}$ is the maximal thickness of the brush, ϕ_0 is the volume fraction in monomer units close to the grafting plane, and z is the vertical distance measured from the grafting plane. Other, more accurate descriptions certainly exist, but are not required for our purposes. To be more specific, we model a virtual brush grafted on Si with $\phi_0 = 0.5$ and $h_{\max} = 300$ nm. The corresponding density profile of the swollen brush is given in Figure 7a. The dry thickness of the brush is $h_d = \int_0^{h_{\max}} \phi(z) \cdot dz \approx 100$ nm, whereas the integral average thickness of the wet brush is $< h >= \phi_0^{-1} \int_0^{h_{\max}} \phi(z) \cdot dz \approx 200$ nm, which are well in the thickness range of the brushes probed in this work.

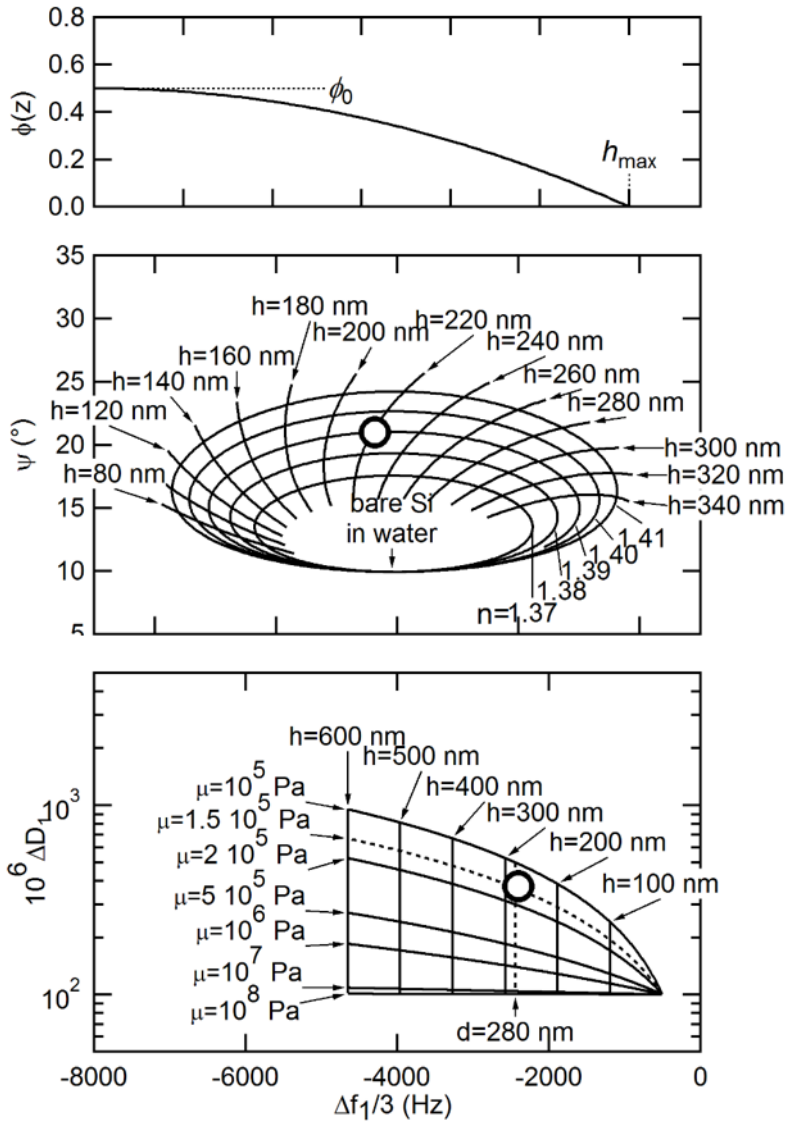

Figure 7. Simulation of ellipsometry (b) and QCM-D (third harmonic) (c) for swollen brushes in water. The lines are trajectories for brushes of constant density profile, of thickness h, index of refraction n and shear modulus μ as indicated. The big open circles are computed for a brush having a parabolic segment density profile (shown in a).

The ellipsometric angles of the graded brush can be obtained by dividing the profile of the brush in thin virtual layers, taken here of 2 nm thickness, and by using a matrix description of optical reflection by multilayered structures.[42] This requires to know the index of refraction of each virtual layer, $n(z)$. Here, we assume that $n(z)$ varies with solvent content according to the Bruggeman's effective medium approximation:[51]

$$\phi(z)\frac{n_{\mathrm{d}}^2 - n^2(z)}{n_{\mathrm{d}}^2 + 2n^2(z)} + (1-\phi(z))\frac{n_L^2 - n^2(z)}{n_L^2 + 2n^2(z)} = 0 \qquad (9),$$

where n_L and n_{d} are the indices of refraction of water and dry brush, respectively. The ellipsometric angles are computed for an incident wavelength of 632.8 nm and an incident angle of 65° corresponding to the parameters of our experimental setup, using $n_{\mathrm{Si}} = 3.882$, $n_L = 1.3321$ (which is the value of the index of refraction of water at 20°C), and $n_{\mathrm{d}} = 1.48$. Absorption is ignored for simplicity.

Figure 7b presents the predicted ellipsometric angular coordinates of the parabolic brush (open circle); also shown are the ellipsometric trajectories for a homogeneous film in water, drawn for different thicknesses at a constant index of refraction (elliptic curves), and at constant thickness for an increasing index of refraction (arcs of curves). The ellipsometric angles of the parabolic film coincide with the ones of a homogeneous film of *ca.* 220 nm thickness and 1.39 index of refraction. These are the values which would be obtained by ellipsometry when the details of the profile of the brush are ignored. Thus, the ellipsometric thickness tends to be slightly larger than the integral thickness of the wet parabolic film (200 nm), by *ca.* 10%; this

results from the faster decrease of the segment density profile of the brush close to the outer interface, resulting in a larger gradient of index of refraction at this location, and therefore a slightly larger weight being placed on the more external layers. As a rule of thumb, it is nevertheless valid to state that ellipsometry provides a value of thickness close to the integral thickness of the brush.

For QCM-D, it is also possible to compute Δf and ΔD by a recursive matrix formalism applied to a multilayer of thin virtual layers of 2 nm thickness, similar to the optical case;[49] the program written for this computation is in Supplementary Information. The computation however requires a larger number of parameters since the vertical profiles of shear viscosity, shear modulus, and density are now required. The density profile is written as:

$$\rho(z) = \phi(z)\rho_d + (1-\phi(z))\rho_L \qquad (10) \quad ,$$

with ρ_d = 1100 kg/m^3 for the dry polymer and ρ_L = 998 kg/m^3 for the fluid (water at 20°C). For the shear modulus and viscosity, the following approximations were taken:

$$\mu(z) \approx \frac{\phi(z)}{\phi_0}\mu_0$$
$$\eta(z) \approx \frac{\phi(z)}{\phi_0}\eta_0 + (1-\frac{\phi(z)}{\phi_0})\eta_L \qquad (11) \quad ,$$

where μ_0 and η_0 are the shear modulus and viscosity of the swollen polymer at volume fraction ϕ_0, and η_L = 0.0012 Pa.s is the shear viscosity of water at 20°C. The unknown parameters μ_0 and η_0 were roughly estimated to be 3.10^6 Pa and 0.004 Pa.s, respectively, based on the values found for the $PMEO_2MA$ brush in its collapsed state when

fitting the QCM-D data while requesting that the swelling coefficient be close to the one measured by ellipsometry.

The resulting values of $\Delta f_n/(2n+1)$ and ΔD_n for the third harmonic ($n = 1$; $f_1 = 3f_0$) are shown in Figure 7c (open circle). Also drawn in Figure 7c are curves corresponding to increasing thickness or increasing shear modulus, for homogeneous films of 1100 kg/m^3 dry density and zero shear viscosity, computed by using equations (2) with zero systematic shift. The assumption of negligible shear viscosity for the films was taken to simplify the drawing; we found that introducing a small component of shear viscosity did anyway not change considerably the curves. The point computed for the graded brush lies in the diagram at shifts corresponding to an equivalent homogeneous film of *ca.* 280 nm thickness and 150 kPa shear modulus. This confirms that the acoustic thickness of hydrophilic brushes is close to the maximal extension of the brush ($h_{max} = 300$ nm), and significantly larger than the optical thickness (220 nm).

This analysis explains why the experimental swelling coefficients determined by the two techniques are close for the slightly swollen PHEMA brush or for the collapsed thermo-responsive brushes. Brushes of lower degree of swelling tend to form films with sharper interfaces, and thus having less difference between the integral and maximal film thickness which are probed by ellipsometry and QCM-D, respectively. In contrast, highly-swollen brushes such as POEGMA, PDMA or thermo-responsive brushes below their collapse transition exhibit a much higher swelling coefficient by QCM-D than by ellipsometry. This is because highly-swollen brushes display a monomer-density profile

which varies strongly with distance from the substrate, resulting in a different averaging by QCM-D and ellipsometry.

Ellipsometry and QCM-D thus appear to be complementary techniques, providing emphasis on either the average or the maximal thickness of a swollen polymer brush. Both parameters may be of interest for specific applications; however, in the sequel, we will concentrate on average 'volume' properties of the brushes, and will therefore set aside the QCM-D results. This is also justified by the narrower temperature range probed by our QCM-D setup compared to our ellipsometric setup, to which we add the larger number of unknown parameters needed for QCM-D data interpretation, as well as the higher experimental difficulties to obtain absolute values of swelling by QCM-D.

3.4.5 Brush volume hydrophilicity from swelling measurements

According to mean-field theory,[43, 5036,43] the thickness of a polymer brush in good solvent is:

$$h = \left(\frac{8}{\pi^2}\right)^{1/3} \nu^{1/3} (a^2\sigma)^{1/3} Na \qquad (12) \quad ,$$

where h is the swollen layer thickness, N is the number of repeat units of volume a^3, σ is the number of chains grafted per unit surface, and v is the adimensional second virial coefficient, *i.e.*, the excluded volume of the Kuhn segment normalized by its volume. For the brushes of this study, grown in the presence of a very dense initiator layer, the grafting density is limited by the size of the monomer units. Therefore, we assume here for simplicity that $a^2\sigma$ is a constant for all brushes, which means that the average area per chain is proportional to the

monomer cross-section. In addition, since the thickness of the dry brush is $h_d = Na^3\sigma$, the swelling coefficient of the brush is:

$$\alpha \triangleq \frac{h}{h_d} \propto \nu^{1/3} \qquad (13)$$

This equation shows that the swelling coefficient of densely-grafted brushes provides information on the dimensionless second virial coefficient, which evaluates solvent quality. The degree of swelling of brushes in a good solvent, grafted to the maximal possible density, thus provides a direct image of water affinity for the volume of the brush.

3.4.6 Surface versus volume hydrophilicity of a brush

From the ellipsometry data (Figure 4), the brushes can thus be sorted by order of increasing volume hydrophilicity: collapsed PNIPAM = collapsed $PMEO_2MA$ < PHEMA < swollen $PMEO_2MA$ ≈ swollen PNIPAM < POEGMA < PDMA. This order is different from the surface hydrophilicity of the brushes, which from Figure 2 is: PNIPAM ≈ POEGMA < $PMEO_2MA$ < PHEMA ≈ PDMA. The behavior of PHEMA and POEGMA are quite contrasted: whereas the swelling of a PHEMA brush is very small, its surface proves to be very hydrophilic. In contrast, POEGMA brushes swell strongly in water but their water contact angle is 15° higher than PHEMA brushes. The slighly lower contact angle of PHEMA compared to PDMA might be due to the accumulation of hydroxyl groups on the surface due to its limited swellability which allows surface reorganization. Likewise, contrarily to a common belief, the surface of thermo-responsive brushes is not more hydrophobic just above the collapse transition temperature than below, which actually would contradict the principles of

thermodynamics;[11] however, their swelling and volume hydrophilicity varies dramatically across the collapse temperature.

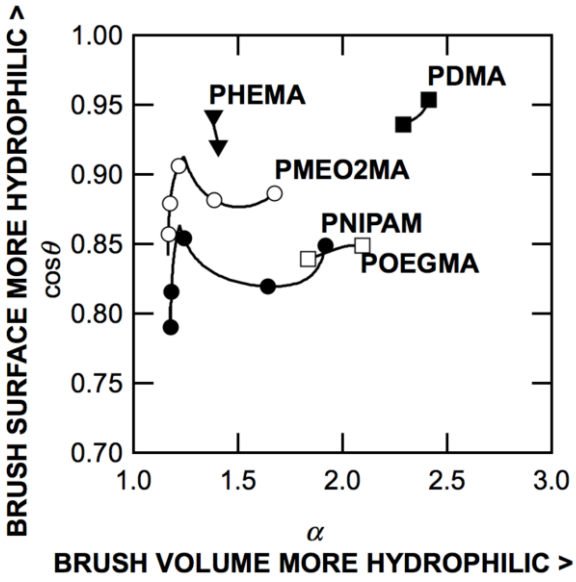

Figure 8. Combined graph of the hydrophilicity of the surface and volume of the brushes, plotted with T as implicit parameter. Lower temperatures correspond to the symbol located close to the name tag of the curve. Only a few symbols are plotted for clarity.

Figure 8 summarizes the final results of this study, by plotting the brush trajectories in a diagram in which the x-axis is the ellipsometric swelling ratio, hence volume hydrophilicity according to equation (13), and the y-axis is the cosine of the water contact angle, which is the surface hydrophilicity according to the Young-Dupré's equation. In this representation, the trajectories of the two thermo-responsive brushes are similar, consisting below the collapse transition of a strong variation of volume hydrophilicity with a moderate decrease and increase of surface hydrophilicity, followed above the collapse transition by a

regularly decreasing surface hydrophilicity at almost constant volume hydrophilicity. The three other brushes exhibit only very modest variations of surface and volume hydrophilicity; nevertheless, the two highly swollen brushes, PDMA and POEGMA, have combined variations of surface and volume hydrophilicity, similar to the thermo-responsive brushes above their collapse temperature, whereas the weakly-swollen PHEMA brush essentially experiences a decrease of surface hydrophilicity at close to constant volume hydrophilicity, which is reminiscent of the behavior of collapsed thermo-responsive brushes. The behavior of these brushes is thus consistent with the existence of a collapse temperature at an unreachable temperature lower than 0°C for PHEMA, and at a (possibly unreachable) temperature higher than 80°C for POEGMA and PDMA.

The lack of correlation between volume and surface properties of a brush arises from the fact that surface properties are dependent on the specific details of the conformations and atomic composition at the outmost surface of the brush, whereas the volume properties are average values. A PHEMA brush, for instance, probably tends to accumulate hydroxyl end groups at the interface, with the required mobility to fit ideally within the water network of H-bonds, resulting in a low contact angle despite the low volume hydrophilicity of PHEMA. The methoxy-ended oligo(ethylene oxide) side chains of POEGMA are in this respect less favorable, despite the much higher average hydrophilicity of the chains. These subtle differences may be of considerable practical importance when considering surface-sensitive phenomena such as protein adsorption. For instance, densely grafted brushes of PHEMA have been demonstrated to be protein-resistant, whereas loosely grafted

ones and cast PHEMA films absorb significant amounts of the same proteins.[52] Protein absorption within loose brushes and cast films confirms the rather hydrophobic character of PHEMA, as found here. The anti-fouling properties of dense PHEMA brushes indicate that steric repulsion prevents proteins to penetrate and absorb within the brushes, and in addition that the surface of PHEMA brushes prevents protein adsorption, which results from its high surface hydrophilicity. These observations are thus fully consistent with the location of dense PHEMA brushes in the diagram of Figure 8.

Given our observation that the equilibrium water contact angle does not change abruptly from a low to a higher value when crossing the collapse transition of a thermo-responsive brush, why do some articles report that advancing or static water contact angles do (interestingly, this is not the case for receding contact angles as was shown for PNIPAM brushes by Plunkett *et al*.?[53] This is because, when placing a droplet of water on a volume-hydrophilic brush in air, impregnation readily occurs, resulting in a low apparent contact angle. In contrast, above the collapse temperature, impregnation is much more limited, with a consequentially higher water contact angle. Hence, standard contact angle measurements are most probably sensitive to volume hydrophilicity, which controls impregnation. It is thus possible to qualitatively estimate the volume hydrophobicity by such measurements, although an accurate quantification is probably impossible. However, it is not correct to conclude from such measurements about a change of surface hydrophilicity across the collapse temperature. More generally, standard measurements do not provide information on surface hydrophilicity, only on the volume

hydrophobicity of the water-swollen brush, a conclusion further supported by the work of Pelton on PNIPAM gels.[54] A same reasoning applies to AFM friction measurements, which in some range of temperatures do not only involve sliding at the surface of the brush, but also partial deformation of the layer, resulting in a sensitivity to volume properties.[47] In contrast, it is likely that the continuous increase of adhesion forces between surfaces covered by PNIPAM brushes above their collapse transition[45] reflects the continuous evolution of the brush surface evidenced here by equilibrium contact angle measurements.

3.5 Conclusions

We have quantified the volume and surface hydrophilicity of a range of water-swollen dense polymer brushes as a function of temperature. The conditions leading to reproducible measurements of the equilibrium water contact angle by the captive bubble method were first thoroughly investigated, giving access to the surface hydrophilicity. Volume hydrophilicity was quantified by measuring the swelling of the brushes, either by QCM-D or ellipsometry. A new methodology was developed to analyze the QCM-D data, providing a model-free access to the swelling. Comparison between the acoustic and optical swelling coefficients shows that QCM-D is sensitive to the maximal thickness of swollen brushes, while ellipsometry provides an integral thickness.

Diagrams of surface versus volume hydrophilicity of the brushes allow to identify two types of behavior: strongly-swollen brushes exhibit a progressive decrease of volume hydrophilicity with temperature, while surface hydrophilicity changes moderately; weakly-swollen brushes have a close-to-constant volume hydrophilicity, while surface hydrophilicity decreases with temperature. Thermo-responsive brushes abruptly switch from one behavior to the other. In general, there is no direct correlation between surface and volume hydrophilicity, because surface properties are dependent on the details of conformation and composition at the surface, whereas volume properties are averaged over some region of the brush.

These observations allow us to explain the antifouling properties of dense PHEMA brushes, and explain why standard contact angle measurements provide a qualitative information on the volume, not the

surface hydrophilicity of water-swollen brushes. We hope that our analysis will contribute to delineate better the role of volume and surface properties for water-swollen polymer brushes. It is probable that the findings of this work also apply to hydrogels, although complementary work is needed to confirm this point.

3.6 Supporting information

3.6.1 Detailed synthesis protocols of the brushes

Gas phase silanization with the ATRP initiator

Deposition of the ATRP initiator was performed in gas phase on silicon wafers or quartz sensors. Silicon wafers were cut in 1×1 or 1×2 cm^2 pieces, washed thoroughly with water and methanol, and then treated by an air plasma for 10 min. Quartz sensors were cleaned by UV/ozone for 20 min. A large Schlenk tube was cleaned by immersion in a freshly-prepared piranha solution (H_2O_2:H_2SO_4 3:1 v:v) for 30 min and then extensively washed with Milli-Q water and dried in an oven (Caution! Piranha solution is a strong oxidant which reacts violently with organic compounds). The substrates were placed on a Teflon holder which was introduced in the Schlenk tube. After sealing with a rubber septum, the Schlenk was placed in an oil bath at 80°C. Three cycles of vacuum/argon (15/5 min, respectively) were performed before injection of the ATRP silane initiator. After 2 h reaction time, the substrates covered by a monolayer of initiator were washed by toluene and methanol for several times then dried with argon. The thickness of the ATRP silane monolayer was 0.7 ± 0.2 nm as determined by X-ray reflectometry.

Growth of PHEMA and PMEO$_2$MA brushes

8 mL of monomer (HEMA: 8.58 g, 66.0 mmol; MEO$_2$MA: 8.16 g, 43.4 mmol) was dissolved in 8 mL of Milli-Q water at room temperature. This solution was stirred and degassed with argon for 15 min to remove dissolved oxygen. Then 72 mg $CuBr_2$ (0.32 mmol), 110 mg CuCl (1.1 mmol) and 488 mg bipyridine (3.1 mmol) were rapidly added. The mixed solution was further stirred and degassed for 30 min. Meanwhile, Schlenk tubes containing initiator-silanized substrates were degassed three times with vacuum and argon (10 and~~n~~5 min, respectively). 3 or 6 mL (depending on substrate size) of the prepared solution was syringed into each Schlenk tubes. At a pre-determined time, the samples were taken out and washed thoroughly with water and methanol, then dried with argon.

Growth of POEGMA brush

9.7 mL of OEGMA (21 mmol) was dissolved in 11 mL of Milli-Q water at room temperature and the solution was stirred and degassed with argon for 15 min. 160 mg bipyridine (1.0 mmol), 41 mg CuCl (420 μmol) and 9 mg $CuBr_2$ (42 μmol) were added into the above solution. The mixture was then further stirred and degassed with argon for 30 min. The initiator-silanized substrates were sealed in Schlenk tubes, degassed with three cycles of vacuum/argon (10/5 min, respectively). 3 or 6 mL (depending on the substrate size) of the polymerization solution was then syringed into each Schlenk tube. At a pre-determined time, the sample was taken out and washed thoroughly with water and methanol, then dried with argon.

Growth of PDMA and PNIPAM brushes

At room temperature, 8 mL water/methanol (6/4, v:v) mixed solvent was introduced in a flask capped with a rubber septum, and was stirred and degassed with argon for 15 min to remove dissolved oxygen. Then 7.4 mg CuCl ($7.4.10^{-2}$ mmol) was added and degassed for 5 min. After that, 20.2 µL HMTETA ligand ($7.4.10^{-2}$ mmol) was added and degassed for another 5 min. Later on, 3.85 mL of DMA monomer (37 mmol) was added and degassed for 20 min. At the same time, Schlenk tubes containing initiator-silanized substrates were degassed three times with vacuum and argon (10/5 min). 3 mL of the above prepared solution was added into each Schlenk tube. At a pre-determined time, the samples were taken out and washed thoroughly with water and methanol, then dried with argon. For PNIPAM, the same procedure was used, just changing the 20.2 µL HMTETA by 20.6 µL Me_6TREN ($7.4.10^{-2}$ mmol), and 3.85 mL DMA by 1.675 g NIPAM (14.8 mmol).

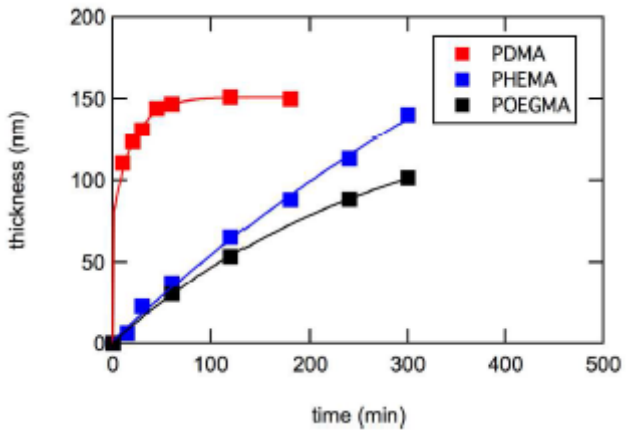

Figure S1. Kinetic growth curves for brushes grown with the three conditions selected in this study.

3.6.2 Effect of measurement conditions on the water contact angle measured in the captive bubble configuration

Different conditions of acquisition of the water contact angle on $PMEO_2MA$ or POEGMA brushes were tested, using degassed or non-degassed water, with different thermal equilibration times and different bubble equilibration times. The different testing conditions are collected in Table S1; in most cases, the bubble was left to equilibrate for some time at 5°C, before the water and sample were heated and cooled by *ca.* 4.5°C steps of varying duration.

Table S1. Experimental conditions used for testing the measurement of contact angles in the captive bubble configuration.

Sample	type of scan[a]	cell[b]	initial bubble volume (µL)	water degassing	polymer	t_1 (min) [c]	t_2 (min) [d]	t_3 (min) [e]	t_4 (min) [f]	t_5 (min) [g]
1	single	I	6	yes	$PMEO_2MA$	120	-	800	-	30
2	single	I	6	yes	$PMEO_2MA$	-	-	800	-	30
3	single	I	3	yes	$PMEO_2MA$	120	-	800	-	30
4	single	I	3	yes	$PMEO_2MA$	-	-	800	-	30
5	single	I	6	no	$PMEO_2MA$	120	-	800	-	30
6	single	II	6	no	$PMEO_2MA$	120	-	800	-	30
7	single	II	3	no	$PMEO_2MA$	-	-	800	-	30
8	single	II	4	no	$PMEO_2MA$	-	-	800	-	5
9	single	II	5	no	$PMEO_2MA$	-	30	5	-	5
10	single	II	4	yes	$PMEO_2MA$	-	30	5	-	5
11	single	I	4	no	$PMEO_2MA$	-	-	30	-	30
12	mult	I	6	no	$PMEO_2MA$	-	60	5	60	5

13	single	I	5	no	$PMEO_2MA$	-	-	120	-	60
14a	mult	I	6	no	$PMEO_2MA$	-	120	0	60	0
14b	mult	I	6	no	$PMEO_2MA$	-	120	5	60	5
14c	mult	I	6	no	$PMEO_2MA$	-	120	10	60	10
16	single	I	5	no	POEGMA	-	-	120	-	60
17a	mult	I	6	no	POEGMA	-	120	0	60	0
17b	mult	I	6	no	POEGMA	-	120	5	60	5
17c	mult	I	6	no	POEGMA	-	120	10	60	10
19a	mult	III	6	no	$PMEO_2MA$	-	15	5	15	5
19b	mult	III	6	no	$PMEO_2MA$	-	30	5	30	5

(a) single: one single bubble is initially placed on the sample, and the same bubble is imaged through all thermal treatments; mult: a new bubble is placed for each measurement, then removed. (b) I: large glass cell of 16 cm^3 volume; II: small copper cell with glass windows, of 1 cm^3 volume; III: intermediate copper cell with glass windows, of 8 cm^3 volume. (c) t_1, bubble equilibration time at room temperature. (d) t_2, thermal equilibration time at 5°C before placing bubble, if not already placed. (e) t_3, bubble equilibration time at 5°C. (f) t_4, thermal equilibration time at each subsequent temperature step, before placing the bubble if not already placed. (g) t_5, bubble equilibration time at each subsequent temperature step, after t_4.

Three different cells were used (Figure S2), differing in their volume (an important aspect when considering the air dissolution equilibrium) and material (which controls thermal equilibration times). Cell I was in glass and had a volume of 16 cm^3, resulting in long thermal equilibration times (1 h to be within 0.1°C of the plateau); cell II was in copper and had a volume of 1 cm^3, resulting in short thermal equilibration times (smaller than 5 min.); cell III was in copper and had

a volume of 8 cm^3, resulting in reasonably short thermal equilibration times (*ca.* 10 min.). This is the cell which was retained at the end, because the small size of cell II resulted in problems due to water evaporation.

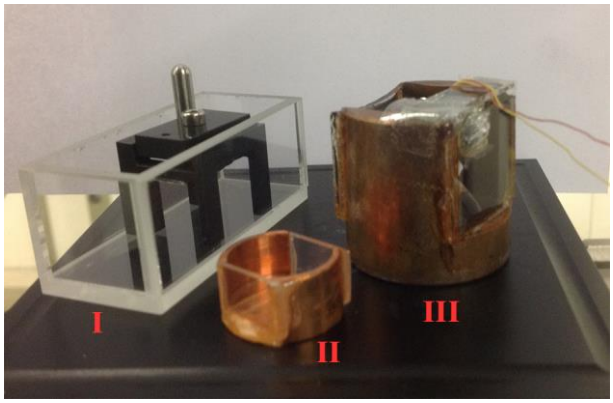

Figure S2. Picture of the three cells tested for contact angle measurements. Cell III shows the thermocouple used to measure temperature, as well as a sample placed face-down on a glass support.

The results of the measurements performed on the samples of Table S1 are collected in Figure S3.

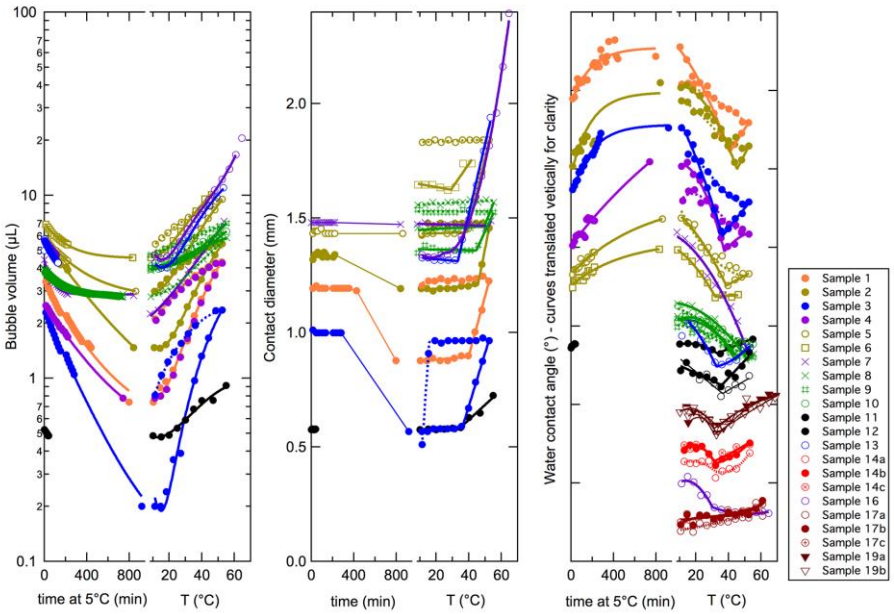

Figure S3. Bubble volume (left), diameter of contact of the bubble with the sample (center) and water contact angle (right) for the different samples of Table S1. The contact angles are displaced vertically for clarity.

Figure S3 left shows that a single bubble of gas initially at 20°C, placed on the brush surface and cooled to 5°C, shrinks with time at 5°C; be it in degassed or non-degassed water; the shrinking can be extremely important. When heated, the bubble strongly expands; when cooled it shrinks again. However, expansion and shrinking are not reversible over the time scale of the experiments. As explained in the companion article, this phenomenon results from exchange of air between the bubble and water, according to the solubility constant of air in water, which varies strongly with temperature. Because this process is slow, experiments conducted rapidly have bubbles which vary less in volume

than experiments performed while waiting hours before taking a measurement. Minimizing volume changes can be obtained by using smaller cells, reducing equilibration times, and using non-degassed water.

Figure S3 (center) shows that the contact diameter (and thus contact area) of the bubble remains constant while the bubble varies in size, during the initial equilibration at 5°C (except for very long times), in the first heating run, and in most of the subsequent cooling run, indicating pinning of the droplet with as a consequence a variation of contact angle. Figure 2 (right) indicates that kinks appear in the curves of contact angle versus temperature for all samples, irrespective of whether they have or not a real collapse transition, when the sample is probed with a single bubble which is progressively heated. A comparison between the contact diameter diagram shows that the kink always coincide with the temperature at which the triple line of the bubble begins to move on the surface (*i.e.*, the temperature at which the contact diameter increases). This leads to the conclusion that the kink seen on heating marks the onset of bubble depinning. Depinning occurs for all samples, whether they have or not a real collapse transition (e.g., Sample 16 which is POEGMA). When a single bubble is cooled down, pinning also occurs; in most cases, the depinning transition is not seen upon cooling, resulting in a continuously increasing contact angle when temperature decreases. The heating and cooling contact angle curves are thus not reversible.

However, when a new bubble is created for each measurement temperature, kinks in the contact angle only appear for $PMEO_2MA$, at the expected collapse transition temperature. POEGMA brushes do not show a kink, as expected. Furthermore, the contact angle curve is now fully reversible on heating and cooling. Finally, the contact angles measured after 5 and 10 min are almost identical, although they differ from the measurement performed at 0 min. Based on these observations, a recommended measurement protocol was devised; it is provided in the Experimental Section of the companion article.

3.6.3 Different possible fits of the QCM-D data of a $PMEO_2MA$ and a POEGMA brush

Due to systematic errors resulting from the mounting of QCM-D crystals in the flow cell, the frequency and dissipation shifts are only known up to a constant possibly different for each harmonic. Therefore, when these constants are not known, they must be included in the fit parameters, resulting in different possible solutions. Equations (2) of the companion article were fitted to the QCM-D data on POEGMA and $PMEO_2MA$ brushes using a methodology similar to what we reported previously.[12] Figure S4 shows two possible solutions for each sample, having rather different values of the swelling coefficient α. When only relative variations of the swelling are desired, as when measuring the collapse transition temperature of a thermoresponsive polymer brush, the uncertainty on the systematic shifts is not a real concern. However, for absolute determinations, it is a serious issue.

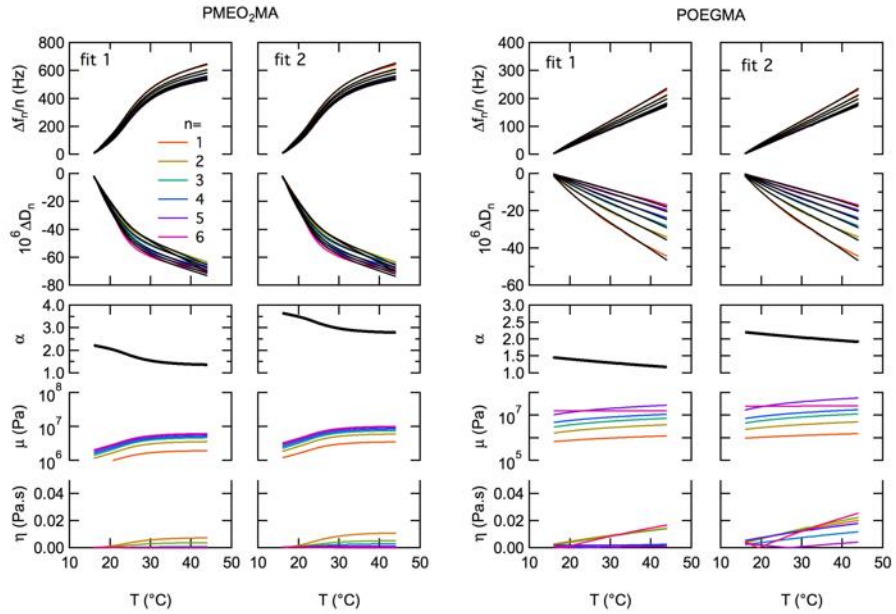

Figure S4. QCM-D data obtained on a PMEO2MA brush (left) and on a POEGMA brush (right), with for each brush two possible fits of equation (2) of the companion article. In the top panels, the fits are given by the continuous black lines. The color code used to identify the harmonics is explained in the top- and left-most panel. The fundamental mode (n=0) is not represented, because it is much more affected by systematic errors and was not used for the fits.

3.6.4 Generalized acoustic swelling coefficients of all brushes

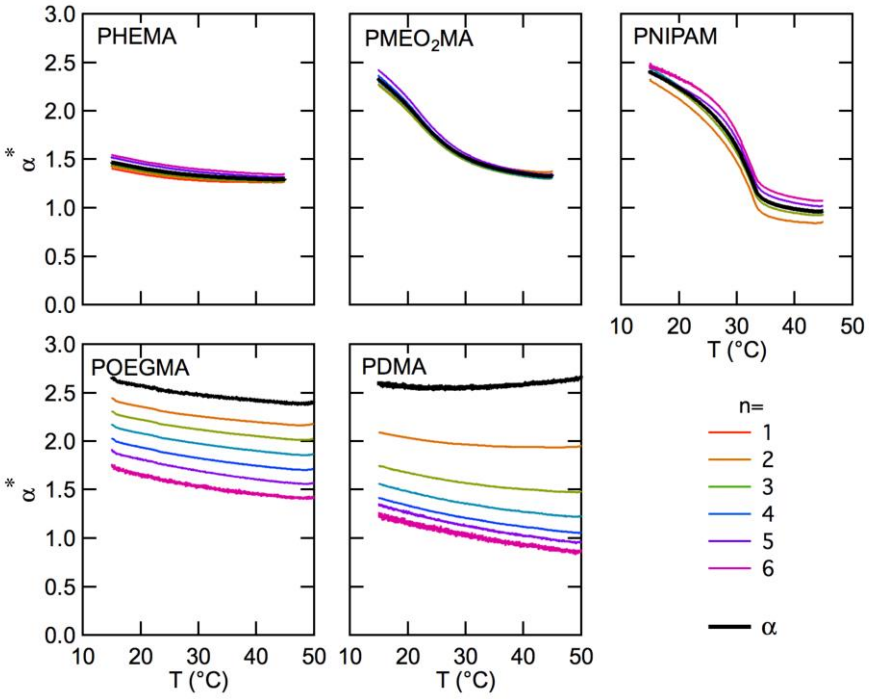

Figure S5. Generalized acoustic swelling coefficients for the five types of brushes of this study. The references for the frequency and dissipation shifts are the dry brushes measured in air. Each color corresponds to a different harmonic of index 2n+1 (the fundamental, n=0, is not plotted since it is error-prone). The thick dark lines are the results of the extrapolation of the harmonic data to zero frequency, and give the swelling coefficient α.

QCM-D data were measured taking as reference the signal of the dry brush in air. Then, the generalized acoustic swelling coefficient α* was computed for all harmonics (equation (6) of the companion article), except for the fundamental frequency (which is affected by strong systematic errors). After elimination of possible spurious harmonics,

the α*'s of each harmonic were either averaged (PHEMA, PMEO2MA, PNIPAM) or extrapolated to zero frequency (POEGMA, PDMA) as per equation (7) of the companion article.

3.7 Acknowledgments

P.Z. thanks the Chinese Scholarship Council (CSC) for a research fellowship. K.G. is a Research Associate of the F.R.S.-FNRS. The work was supported by the F.R.S.-FNRS and the Belgian Federal Science Policy (IAP/PAI P7/05). The authors thank C. Dupont-Gillain for access to the QCM-D.

References

1. Li, L., Xing, X. & Liu, Z. Triply-responsive (thermo/light/pH) copolymeric hydrogel of N-isopropylacrylamide with an azobenzene-containing monomer. *J. Appl. Polym. Sci.* **124**, 1128-1136 (2012).
2. Minko, S. Responsive Polymer Brushes. *Journal of Macromolecular Science, Part C* **46**, 397-420 (2006).
3. Barbey, R. et al. Polymer Brushes via Surface-Initiated Controlled Radical Polymerization Synthesis, Characterization, Properties, and Applications. *Chem. Rev.* **109**, 5437-5527 (2009).
4. Chen, T., Ferris, R., Zhang, J., Ducker, R. & Zauscher, S. Stimulus-responsive polymer brushes on surfaces: Transduction mechanisms and applications. *Prog. Polym. Sci.* **35**, 94-112 (2010).
5. Li, B., Du, T., Yu, B., van der Gucht, J. & Zhou, F. Caterpillar-Inspired Design and Fabrication of A Self-Walking Actuator with Anisotropy, Gradient, and Instant Response. *Small* **11**, 3494-3501 (2015).
6. Glinel, K. et al. Antibacterial and Antifouling Polymer Brushes Incorporating Antimicrobial Peptide. *Bioconjugate Chem.* **20**, 71-77 (2008).
7. Laloyaux, X. et al. Temperature-Responsive Polymer Brushes Switching from Bactericidal to Cell-Repellent. *Adv. Mater.* **22**, 5024-5028 (2010).
8. Liu, H. et al. Dual-Responsive Surfaces Modified with Phenylboronic Acid-Containing Polymer Brush To Reversibly

Capture and Release Cancer Cells. *J. Am. Chem. Soc.* **135**, 7603-7609 (2013).

9. Takahashi, H., Nakayama, M., Yamato, M. & Okano, T. Controlled Chain Length and Graft Density of Thermoresponsive Polymer Brushes for Optimizing Cell Sheet Harvest. *Biomacromolecules* **11**, 1991-1999 (2010).
10. Krishnamoorthy, M., Hakobyan, S., Ramstedt, M. & Gautrot, J.E. Surface-initiated polymer brushes in the biomedical field: applications in membrane science, biosensing, cell culture, regenerative medicine and antibacterial coatings. *Chem. Rev.* **114**, 10976-11026 (2014).
11. Jonas, A.M., Glinel, K., Oren, R., Nysten, B. & Huck, W.T.S. Thermo-Responsive Polymer Brushes with Tunable Collapse Temperatures in the Physiological Range. *Macromolecules* **40**, 4403-4405 (2007).
12. Laloyaux, X., Mathy, B., Nysten, B. & Jonas, A.M. Surface and Bulk Collapse Transitions of Thermoresponsive Polymer Brushes. *Langmuir* **26**, 838-847 (2009).
13. Schild, H.G. Poly(N-isopropylacrylamide): experiment, theory and application. *Prog. Polym. Sci.* **17**, 163-249 (1992).
14. Lutz, J.-F., Akdemir, Ö. & Hoth, A. Point by Point Comparison of Two Thermosensitive Polymers Exhibiting a Similar LCST: Is the Age of Poly(NIPAM) Over? *J. Am. Chem. Soc.* **128**, 13046-13047 (2006).
15. Lutz, J.-F. & Hoth, A. Preparation of Ideal PEG Analogues with a Tunable Thermosensitivity by Controlled Radical Copolymerization of 2-(2-Methoxyethoxy)ethyl Methacrylate

and Oligo(ethylene glycol) Methacrylate. *Macromolecules* **39**, 893-896 (2005).

16. M. Cunanan, C., M. Tarbaux, N. & M. Knight, P. Surface properties of intraocular lens materials and their influence on in vitro cell adhesion. *J. Cataract. Refract. Surg.***17**, 767-773 (1991).
17. Ibanescu, S.-A., Nowakowska, J., Khanna, N., Landmann, R. & Klok, H.-A. Effects of Grafting Density and Film Thickness on the Adhesion of Staphylococcus epidermidis to Poly(2-hydroxy ethyl methacrylate) and Poly(poly(ethylene glycol)methacrylate) Brushes. *Macromol. Biosci.* **16**, 676-685 (2016).
18. Longenecker, R., Mu, T., Hanna, M., Burke, N.A.D. & Stöver, H.D.H. Thermally Responsive 2-Hydroxyethyl Methacrylate Polymers: Soluble–Insoluble and Soluble–Insoluble–Soluble Transitions. *Macromolecules* **44**, 8962-8971 (2011).
19. Domack, A., Prucker, O., Rühe, J. & Johannsmann, D. Swelling of a polymer brush probed with a quartz crystal resonator. *Phys. Rev. E* **56**, 680-689 (1997).
20. Kaufmann, M. et al. Tuneable swelling of thermo- and pH-responsive copolymer films. *Soft Matter* **6**, 937 (2010).
21. Cheng, H., Liu, G., Wang, C., Zhang, G. & Wu, C. Collapse and swelling of poly(N-isopropylacrylamide-co-sodium acrylate) copolymer brushes grafted on a flat SiO2 surface. *J. Phys. Chem. Sci. Part B Polym. Phys.* **44**, 770-778 (2006).
22. Laloyaux, X., Mathy, B., Nysten, B. & Jonas, A.M. Bidimensional Response Maps of Adaptive Thermo- and pH-

Responsive Polymer Brushes. *Macromolecules* **43**, 7744-7751 (2010).

23. Chen, W.-L., Shull, K.R., Papatheodorou, T., Styrkas, D.A. & Keddie, J.L. Equilibrium Swelling of Hydrophilic Polyacrylates in Humid Environments. *Macromolecules* **32**, 136-144 (1999).
24. Xue, C. et al. Protein adsorption on poly(N-isopropylacrylamide) brushes: dependence on grafting density and chain collapse. *Langmuir* **27**, 8810-8818 (2011).
25. Habicht, J., Schmidt, M., Rühe, J. & Johannsmann, D. Swelling of Thick Polymer Brushes Investigated with Ellipsometry. *Langmuir* **15**, 2460-2465 (1999).
26. Kooij, E.S., Sui, X., Hempenius, M.A., Zandvliet, H.J.W. & Vancso, G.J. Probing the Thermal Collapse of Poly(N-isopropylacrylamide) Grafts by Quantitative in Situ Ellipsometry. *J. Phys. Chem. B* **116**, 9261-9268 (2012).
27. Edmondson, S., Nguyen, N.T., Lewis, A.L. & Armes, S.P. Co-Nonsolvency Effects for Surface-Initiated Poly(2-(methacryloyloxy)ethyl phosphorylcholine) Brushes in Alcohol/Water Mixtures. *Langmuir* **26**, 7216-7226 (2010).
28. Bittrich, E. et al. Temperature-sensitive swelling of poly(N-isopropylacrylamide) brushes with low molecular weight and grafting density. *Langmuir* **28**, 3439-3448 (2012).
29. Bittrich, E. et al. Protein adsorption on and swelling of polyelectrolyte brushes: A simultaneous ellipsometry-quartz crystal microbalance study. *Biointerphases* **5**, 159 (2010).

30. Wiener, C.G., Weiss, R.A. & Vogt, B.D. Overcoming confinement limited swelling in hydrogel thin films using supramolecular interactions. *Soft Matter* **10**, 6705 (2014).
31. Cheesman, B.T. et al. Polyelectrolyte brush pH-response at the silica-aqueous solution interface: a kinetic and equilibrium investigation. *Phys. Chem. Chem. Phys.* **15**, 14502-14510 (2013).
32. Jonas, A.M., Hu, Z., Glinel, K. & Huck, W.T.S. Chain Entropy and Wetting Energy Control the Shape of Nanopatterned Polymer Brushes. *Macromolecules* **41**, 6859-6863 (2008).
33. Turgman-Cohen, S. & Genzer, J. Simultaneous bulk- and surface-initiated controlled radical polymerization from planar substrates. *J. Am. Chem. Soc.* **133**, 17567-17569 (2011).
34. Turgman-Cohen, S. & Genzer, J. Computer Simulation of Controlled Radical Polymerization: Effect of Chain Confinement Due to Initiator Grafting Density and Solvent Quality in "Grafting From" Method. *Macromolecules* **43**, 9567-9577 (2010).
35. Jellison, G.E. & Burke, H.H. The temperature dependence of the refractive index of silicon at elevated temperatures at several laser wavelengths. *J. Appl. Phys.* **60**, 841-843 (1986).
36. Bashkatov, A.N. & Genina, E.A., Vol. 5068 393-395 (2003).
37. Battino, R., Rettich, T.R. & Tominaga, T. The Solubility of Nitrogen and Air in Liquids. *J. Phys. Chem. Ref. Data* **13**, 563-600 (1984).

38. Hong, S.-J. et al. Anomalous Contact Angle Hysteresis of a Captive Bubble: Advancing Contact Line Pinning. *Langmuir* **27**, 6890-6896 (2011).
39. Suzuki, H. et al. Precise Synthesis and Physicochemical Properties of High-Density Polymer Brushes designed with Poly(N-isopropylacrylamide). *Macromolecules* **43**, 9945-9956 (2010).
40. Neumann, A.W. Contact angles and their temperature dependence: thermodynamic status, measurement, interpretation and application. *Adv. Colloid Interface Sci.* **4**, 105-191 (1974).
41. Jalili, K., Abbasi, F. & Milchev, A. Surface Microdynamics Phase Transition and Internal Structure of High-Density, Ultrathin PHEMA-b-PNIPAM Diblock Copolymer Brushes on Silicone Rubber. *Macromolecules* **46**, 5260-5278 (2013).
42. Azzam, R.M.A., Bashara, N.M. & Thorburn Burns, D. Ellipsometry and polarized light. *Anal. Chim. Acta* **199**, 283-284 (1987).
43. Zhulina, E.B., Borisov, O.V., Pryamitsyn, V.A. & Birshtein, T.M. Coil-globule type transitions in polymers. 1. Collapse of layers of grafted polymer chains. *Macromolecules* **24**, 140-149 (1991).
44. Balamurugan, S., Mendez, S., Balamurugan, S.S., O'Brie, M.J. & López, G.P. Thermal Response of Poly(N-isopropylacrylamide) Brushes Probed by Surface Plasmon Resonance. *Langmuir* **19**, 2545-2549 (2003).

45. Malham, I.B. & Bureau, L. Density Effects on Collapse, Compression, and Adhesion of Thermoresponsive Polymer Brushes. *Langmuir* **26**, 4762-4768 (2010).
46. Ishida, N. & Biggs, S. Direct Observation of the Phase Transition for a Poly(N-isopropylacryamide) Layer Grafted onto a Solid Surface by AFM and QCM-D. *Langmuir* **23**, 11083-11088 (2007).
47. Yu, Y. et al. Stretching of collapsed polymers causes an enhanced dissipative response of PNIPAM brushes near their LCST. *Soft Matter* **11**, 8508-8516 (2015).
48. Voinova, M.V., Rodahl, M., Jonson, M. & Kasemo, B. Viscoelastic Acoustic Response of Layered Polymer Films at Fluid-Solid Interfaces: Continuum Mechanics Approach. *Phys. Scripta* **59**, 391 (1999).
49. Johannsmann, D. in Piezoelectric Sensors. (eds. C. Steinem & A. Janshoff) 49-109 (Springer Berlin Heidelberg, Berlin, Heidelberg; 2007).
50. Milner, S.T. Polymer Brushes. *Science* **251**, 905 (1991).
51. Riegler, H. A user's guide to ellipsometry. By Harland G. Tompkins, Academic Press, New York 1993, 260 pp. hardback, ISBN 0-12-603050-0. *Adv. Mater.* **5**, 778-778 (1993).
52. Yoshikawa, C. et al. Protein Repellency of Well-Defined, Concentrated Poly(2-hydroxyethyl methacrylate) Brushes by the Size-Exclusion Effect. *Macromolecules* **39**, 2284-2290 (2006).

53. Plunkett, K.N., Zhu, X., Moore, J.S. & Leckband, D.E. PNIPAM Chain Collapse Depends on the Molecular Weight and Grafting Density. *Langmuir* **22**, 4259-4266 (2006).

54. Pelton, R. Poly(N-isopropylacrylamide) (PNIPAM) is never hydrophobic. *J. Colloid Interface Sci.* **348**, 673-674 (2010).

Chapter 3: Temperature Dependence of the Surface and Volume Hydrophilicity of Hydrophilic Polymer Brushes

4 Temperature-Dependence of the Swelling and Surface Wettability of Dense Polymer Brushes

Pengyu Zhuang, Ali Dirani, Karine Glinel, Alain M. Jonas

Université catholique de Louvain, Institute of Condensed Matter and Nanosciences, Bio & Soft Matter, Croix du Sud 1 L7.04.02, 1348 Louvain-la-Neuve, Belgium

(Submitted as a book chapter in *Polymer and Biopolymer Brushes: Fundamentals and Applications in Materials Science and Biotechnology*, O. Azzaroni & Igal Szleifer, Eds, Wiley)

4.1 Abstract

We review the variation with temperature of the volume and surface hydrophilicity of dense polymer brushes, including thermo-responsive systems. First, methods for the measurement of the degree of swelling and wettability of hydrophilic polymer brushes in water are discussed based on the case example of poly(*N*-isopropylacrylamide) (PNIPAM) thermo-responsive brushes. Consistent swelling results can be obtained with different techniques such as scanning probe microscopy (AFM), ellipsometry, or quartz crystal microbalance with dissipation monitoring (QCM-D); reproducible contact angles of water-equilibrated surfaces can be also measured in the captive bubble configuration. During the collapse transition, the volume of PNIPAM brushes switches from more to less hydrophilic; however, the surface

of the brush equilibrated in water does not change significantly its hydrophilicity, due to the continuous rearrangement of segments at the brush/water interface. Second, we concentrate on the design of the temperature-dependence of the swelling and surface properties of dense hydrophilic brushes by copolymerization of methacrylate units substituted by oligo(ethylene oxide) side chains of varying length, which provides access to a wide variety of brushes of varying volume hydrophilicity and close-to-constant surface hydrophilicity. Inclusion of hydroxyl-substituted side chains provides a supplementary handle for tuning the properties of the brushes, as exemplified by the synthesis of brushes comprising photochromic azobenzene units. We also discuss brushes of poly(diethylene glycol methyl ether methacrylate) ($PMEO_2MA$) and its copolymers with oligo(ethylene oxide) methacrylate (OEGMA), which afford systems of which the collapse transition can be easily tuned, providing suitable alternatives to PNIPAM.

Chapter 4: Temperature Dependence of the Swelling and Surface Wettability of Dense Polymer Brushes

4.2 Introduction

Hydrophilic polymer brushes are important systems for biology-related applications, since they may provide antifouling, stealth or lubrication properties to a surface, or may serve as platforms for anchoring biomacromolecules and cell culturing.[1] A central property of such brushes is their degree of swelling in water, which controls their mechanical properties (*e.g.*, Young's modulus, compressibility, and friction), their penetrability and osmotic pressure, and their entropic repulsion. Therefore, the capability to design their swelling in water, as well as their response to changes in environmental conditions, is highly desirable.

Whereas the volume of a brush controls most of its properties, there are specific instances for which the outer surface of the brush is the controlling parameter; this is the case of protein adsorption,[2] which mediates the interactions between a surface and biological cells. Hence, it is also important to develop designing methodologies of the surface properties of brushes in water-equilibrated conditions, and to understand finely the link between the hydrophilicity of the volume and of the surface of a brush.

Therefore, in this chapter we first discuss methods allowing us to measure the degree of swelling and surface properties of hydrophilic polymer brushes immersed in water, using as case example the archetypical thermo-responsive poly(*N*-isopropylacrylamide), PNIPAM (Scheme 1). PNIPAM chains exhibit a lower critical solution temperature (LCST) in water close to 32°C, making this polymer especially interesting for biological applications.[3] When grafted in a

brush, the chains experience a collapse transition in water in the LCST range, whereby the brush switches from a highly- to a poorly-swollen (or collapsed) state; this transition thus offers interesting opportunities to critically test a range of characterization methodologies.

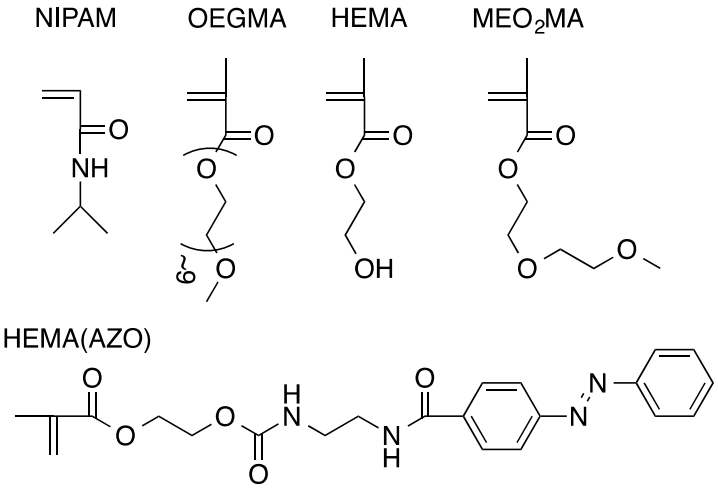

Scheme 1. Chemical structure of the monomer units of the brushes discussed in this chapter.

Next, we concentrate on the design of the temperature-dependence of the swelling and surface properties of a series of hydrophilic copolymer brushes based on chains having a poly(methacrylate) backbone grafted with oligo(ethylene oxide) side chains of varying length (Scheme 1), which are ideal candidates for applications in biology. Poly(hydroxyethyl methacrylate) (PHEMA) is a moderately hydrophilic polymer whose hydrogels are used for intraocular lenses,[4] and of which dense brushes were recently demonstrated to resist bacterial adhesion;[5] as will be shown here, its copolymers with oligo(ethylene oxide) methacrylate (OEGMA) (Scheme 1) also provide access to a wide variety of brushes of varying volume hydrophilicity

and close-to-constant surface hydrophilicity. In addition, brushes containing HEMA or hydroxyl-ended OEGMA can be easily derivatized after polymerization, providing a supplementary handle to tune their volume and surface hydrophilicities, or to display new functions such as catalytic [6, 7] or biological activity.[8, 9]

We also report on poly(diethylene glycol methyl ether methacrylate) ($PMEO_2MA$) and its copolymers with oligo(ethylene oxide) methacrylate (OEGMA), which offer a particularly interesting thermo-responsive alternative to PNIPAM [10-12] and have been used before for temperature-controlled cell culture and detachment.[13, 14] When copolymerized with either HEMA or OH-bearing OEGMA comonomer units, they also offer an elegant platform for grafting biological cues which can be shown and hidden depending on temperature,[15, 16] or for grafting functional groups such as photochromes for the reversible photomodulation of their degree of swelling.[17] In this chapter, the methods used to synthesize polymer brushes by ATRP, and measure the swelling coefficients and the equilibrium water contact angles of polymer brushes, are identical to the relative methods described in **chapter 3**.

4.3 Surface and volume hydrophilicity of dense polymer brushes

The surface and volume hydrophilicity of polymer brushes can be determined by measuring the equilibrium water contact angles and the swelling coefficients as elaborated in **chapter 2**.

4.3.1 Temperature-dependent surface hydrophilicity of dense PNIPAM brushes

The main issue to calculate the difference of excess surface free enthalpy Δg_s by equation 8 in chapter 2 and the difference of excess surface entropy Δs_s by equation 9 in chapter 2 of the brush below water vapor and liquid water is the need to reach equilibrium conditions of the brush with both liquid water and water vapor, while varying temperature. This can be conveniently obtained by using a captive bubble configuration, wherein a small bubble of air is placed in contact with the brush immersed in water of controlled temperature.[18] The bubble is rapidly saturated by water vapor, and controlling the temperature of water is straightforward, leading to consistent results between independent studies on PNIPAM.[19-21]

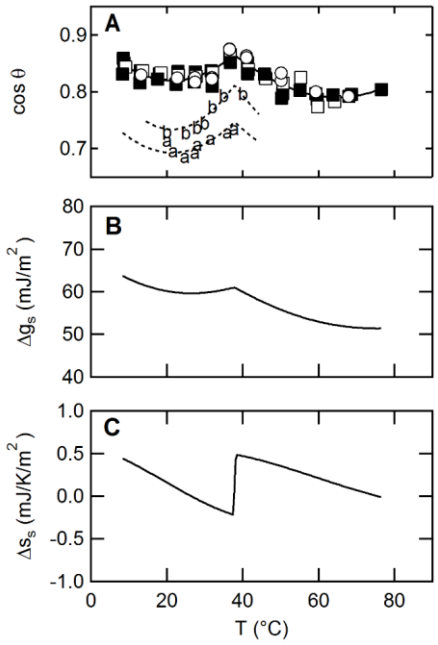

Figure 1. Surface properties of dense PNIPAM brushes grown by SI-ATRP. **(A)** Cosine of the water contact angle of the brushes measured in the captive bubble configuration. Full and hollow symbols correspond to heating and cooling ramps, respectively, performed on a dense brush of 77 nm thickness; the results from two independent measurements are shown (squares and circles).[24] The continuous line is the fit of two polynomials to the average data. Lettered curves are adapted from literature data obtained on PNIPAM brushes of 62 nm thickness and 0.47 chain/nm^2 grafting density (sample a [25]), and 35.8 nm thickness and 0.53 chain/nm^2 grafting density (sample b [23,]); they are shifted downwards by 0.05 for clarity. The dashed lines are fits to the same functional shape as used for the more complete data set (*i.e.*, shown with symbols). **(B)** Difference of excess surface free enthalpy for the 77 nm-thick brush in water vapor and in liquid water, equation.[8] **(C)** Difference of excess surface configurational entropy for the 77 nm-thick brush in water vapor and in liquid water, equation.[9]

Figure 1 collects the data obtained over a wide temperature range for a dense PNIPAM brush grown from silicon by surface-initiated atom transfer radical polymerization (SI-ATRP),[20] as well as data obtained over narrower thermal ranges for a dense PNIPAM brush of similar thickness grown from gold by SI-ATRP [21] and a half thinner PNIPAM brush grown by SI-ATRP from a PHEMA brush grafted on silicone rubber.[19] The absolute values of contact angle differ somewhat, up to *ca.* 5°, which is to be expected considering the differences between sample preparation; however, the relative variations with temperature are essentially identical.

Figure 1A shows that a proper view of the effect of the collapse transition on the contact angle requires to perform measurements over a wide thermal range (*e.g.*, from 10 to 80°C). The surface collapse transition temperature of the brush in Figure 1 is signaled at *ca.* 37°C by an abrupt change of slope in the temperature-dependence of the contact angle. Because free enthalpy is necessarily a continuous function of temperature, equation (8) indicates that the contact angle cannot experience a jump at a first order transition (at constant pressure and sample area);[10] this is indeed what is observed in Figure 1A-B. However, its first temperature derivative, and therefore the excess surface entropy of the brush (Figure 1C), are discontinuous when the surface experiences the collapse transition. Jumps in the contact angle have been reported before for PNIPAM close to its collapse transition temperature (*e.g.*, [19, 22-24]), but only for measurements performed in non-equilibrium conditions, using droplets placed on the sample in air; such measurements should not be recommended as they are extremely sensitive to the dynamic reorganization of the chain segments at the

interface depending on whether air or water is present, and probably reflect more the impregnation of the brush by water rather than true surface properties.[24, 25]

Figure 1 also shows that the surface hydrophilicity of a water-equilibrated PNIPAM dense brush, as defined by the cosine of the contact angle, does not vary strongly between 10 and 80°C, which certainly does not support the notion that the surface of a PNIPAM brush would switch in water from a hydrophilic to a hydrophobic state when going across its collapse transition. A similar conclusion was obtained by Leckband *et al.* [26] from measurements of receding (hence, closer to water-equilibrated) contact angles, which were also not found to vary across the collapse transition, and by Pelton [25] for crosslinked PNIPAM gels immersed in water and measured by the captive bubble method. On a molecular scale, the chain segments simply arrange at the brush external interface in order to expose their most hydrophilic groups to water, be it above or below the collapse transition. However, the collapse of the volume of the brush layer requires rearrangements of the chain conformations at the interface, resulting in changes of the excess surface entropy which are detected in the derivative of the contact angle, as shown in Figure 1C.

4.3.2 Temperature-dependent swelling and volume hydrophilicity of dense PNIPAM brushes

Different ways to measure quantitatively the swelling of polymer brushes in water have been reported; they essentially belong to three categories : scanning probe microscopy-based methods, reflection-based methods (ellipsometry and reflectometry), and acoustic methods.

When these methods provide a single value of swelling, they perform by necessity some averaging over a brush whose content in water varies continuously from the brush/substrate interface to the brush/water interface. Profiles of chain segment density have been measured by neutron reflectometry [26-29] and spectroscopic ellipsometry [30] on PNIPAM brushes immersed in water, showing that, below the collapse transition, the segment density profile of the brush exhibits a long tailing. In addition, because of the dependence on chain concentration of the χ_{12} of PNIPAM, [31] it has been theoretically predicted,[32, 33] and experimentally verified by neutron reflectometry [31,34] and spectroscopic ellipsometry,[30] that the collapse occurs over a broad temperature range, with the lower part of the brush (close to the substrate) collapsing at lower temperatures than its upper portion, resulting in a two-compartment profile for the segment density in the collapse transition region.

Consequently, a single-number representation of such complex segment density profiles can only provide a very simplified view of the brush, and one should not be surprised by having different values for the average swelling coefficient of a brush depending on the measurement method. For instance, it was shown that ellipsometry and quartz-crystal microbalance measurements with dissipation monitoring (QCM-D) provide average thicknesses close to the integral and maximal thickness of the segment density profile, respectively.[20, 35] Furthermore, the swelling of a brush depends on its grafting density (equations 4 and 6); in addition, the concentration dependence of the water/PNIPAM interaction parameter further complicates the issue, resulting in a cumbersome dependence of the swelling coefficient on

both grafting density and molar mass. [28, 32, 36] For these reasons, we only concentrate in the sequel on dense brushes grafted from surfaces. With these *caveats* in mind, it is then possible to compare qualitatively the results from different techniques.

Scanning probe methods such as atomic force microscopy (AFM) have been used to measure the thickness of PNIPAM brushes as a function of water temperature by scanning the tip across a scratch, or a pattern, made in the brush. [21, 34, 37] Obviously, the force applied by the AFM cantilever on the brush is an important parameter to control, as it directly affects the degree of indentation of the tip in the soft brush;[41, 38] this necessarily introduces some arbitrariness in the absolute values of swelling. Figure 2A shows the AFM-derived swelling coefficient for PNIPAM brushes of similarly high grafting density; values of 2-3 are obtained in the swollen temperature range, going down to 1-1.2 in the collapsed range, with the transition ending at *ca.* 36°C (except for sample c measured in D_2O, conditions which are known to offset the PNIPAM LCST by *ca.* 2°C compared to H_2O).[39] Other AFM modes have been used to monitor the collapse transition,[41,40-42] but since they do not lead to an absolute determination of sample thickness, they are not discussed here.

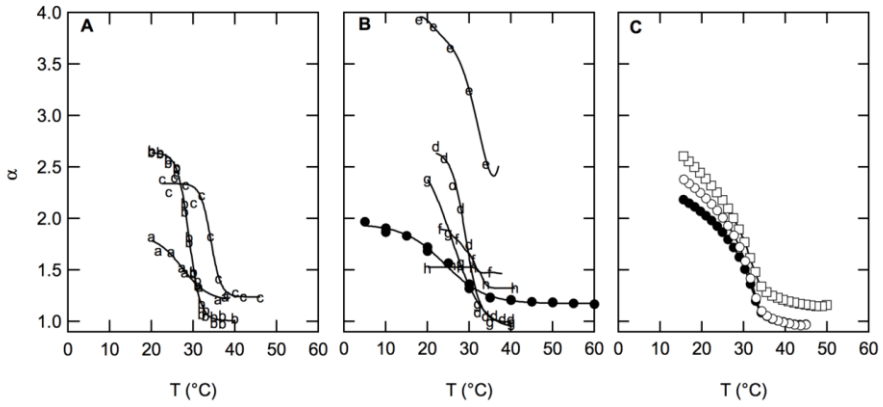

Figure 2. Comparison of literature data on the swelling coefficient of dense PNIPAM brushes in water (except samples c and h acquired in D_2O). The different methods used are : **(A)** AFM; **(B)** ellipsometry (samples d-f and full circles), x-ray reflectometry (sample g) or neutron reflectometry (sample h); **(C)** QCM-D. The brushes were grown by SI-ATRP, except sample d which was grown by surface-initiated photopolymerization. Full circles, hollow circles and hollow squares correspond to our own measurements on brushes of 77, 66 and 48 nm thickness, respectively. Lettered curves are data adapted from the literature, with the following values of thickness in nm and grafting density in nm^{-2}: a (121;0.48);[21] b (-;0.45);[41] c (35.2 nm; -);[38] d (132.2;-);[43] e (21;-);[44] f (35.2;0.21);[28] g (9.45;0.55);[23] h (21.5; > 0.25).[30] For sample h (neutron reflectometry), the integral thickness of the published volume fraction profiles was used to obtain the brush thickness.

More reports have been published on the determination of the thickness of dense PNIPAM brushes by *in situ* reflection-based methods, with a logical dominance of ellipsometry [28, 43, 44] over the more complex neutron[30] or x-ray reflectometry.[23] Generally, the swelling coefficient in the collapsed state is comprised between 1 and 1.3, similarly to the AFM-derived values, except for thinner brushes (*e.g.*,

samples e and f in Figure 2B) for which the error on ellipsometric measurements is expected to be higher (see below). In contrast, the swelling coefficients of all brushes differ substantially in the swollen regime, most probably due to differences of openness (equations 4 and 6). Overall, the ellipsometry and reflectometry results agree reasonably well with the AFM measurements.

The reason why ellipsometry has larger errors on thinner brushes can be understood by considering Figure 3, which shows the predicted ellipsometric angles Ψ and Δ depending on the average thickness h and average index of refraction n of the swollen brush, for standard measurement conditions.

Since h and n are computed by inversion from Ψ and Δ, a good precision on these values can only be obtained when the sample falls in a region where both Ψ and Δ vary rapidly with both n and h. This is not the case when the sample is very thin or has an average swollen thickness close to a multiple of the ellipsometric period (which is the repetition period along the h-axis in Figure 3), in which case the dependence on n of both Ψ and Δ is quite weak; this is also not the case when the film is so swollen that its average index of refraction is very close to the one of water (1.3321 at 20°C [45]), in which case there is no sensitivity to h. In all other cases, the precision should be reasonable : repeated ellipsometry measurements performed on the same sample led us to estimate the accuracy on the swelling coefficient to *ca.* 0.2, consistent with the range of swelling coefficients found for *collapsed* brushes in Figure 2B.

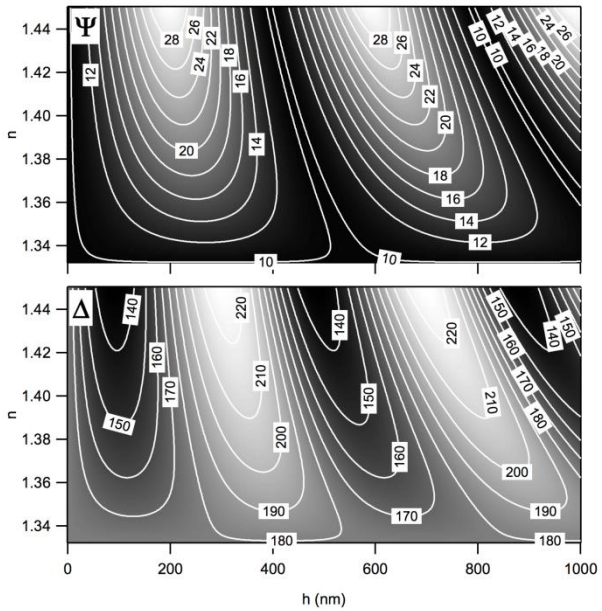

Figure 3. Map with contour lines of ellipsometric angles simulated for a swollen brush grafted on a silicon wafer, in water at 20°C, for an incidence angle of 65° and a wavelength of 632.8 nm, depending on the average index of refraction *n* and average thickness *h* of the swollen brush.

The swollen thickness of PNIPAM brushes can also be obtained from an extrapolation procedure performed on QCM-D measurements acquired at different overtones;[24] the results are shown in Figure 2C, which comprises one sample also measured by ellipsometry in Figure 2B (closed circles). The general behavior agrees well with AFM and ellipsometry results, even though the absolute values differ somewhat for the reasons explained before. The typical precision on the swelling coefficients obtained by QCM-D is *ca.* 0.2 for brushes in the collapsed state, and *ca.* 0.5 in their highly-swollen state.[24]

Interestingly, all techniques provide within experimental precision identical values for the end of the collapse transition (between 33.5 and

36.5°C), slightly lower than the *ca.* 37°C found for the surface collapse transition (Figure 1), confirming that the surface of the brush undertakes its transition at the very end of the collapse process. The previous analysis thus shows that a range of reliable techniques is available to monitor quantitatively the swelling of polymer brushes in water, and therefore their volume hydrophilicity. From our experience, single wavelength ellipsometry is especially convenient and easy to use, provided the brushes are not too thin. In addition, a consistent picture of the collapse transition of PNIPAM brushes can be formed when considering the ensemble of results presented here. The collapse progresses from the bottom to the top of the brush as temperature increases, until the surface finally changes its configuration and excess surface entropy. The collapse induces a significant reduction of hydrophilicity of the volume of the brush, whereas the surface hydrophilicity in water is essentially unchanged.

4.3.3 Thermo-responsive poly(oligo(ethylene oxide)methacrylate) copolymer brushes – versatile functional alternatives to PNIPAM

Dense thermo-responsive P(MEO_2MA-*co*-OEGMA) brushes (Scheme 1) of varying composition were prepared by SI-ATRP using standard protocols starting from the same commercial monomers as in the reference [24] (the OEGMA was methoxy-ended and of 475 g/mol average molar mass). Since both monomers are similarly-substituted methacrylates, we surmise that the composition of the copolymer brushes is close to the molar composition of the synthesis solutions and thus random P(MEO_2MA-*co*-OEGMA) brushes are most likely formed.

Chapter 4: Temperature Dependence of the Swelling and Surface Wettability of Dense Polymer Brushes

The temperature dependences of the swelling coefficient and of the cosine of the water-equilibrated contact angle of the brushes are shown in Figures 4A and B, respectively, with PNIPAM also shown for comparison.

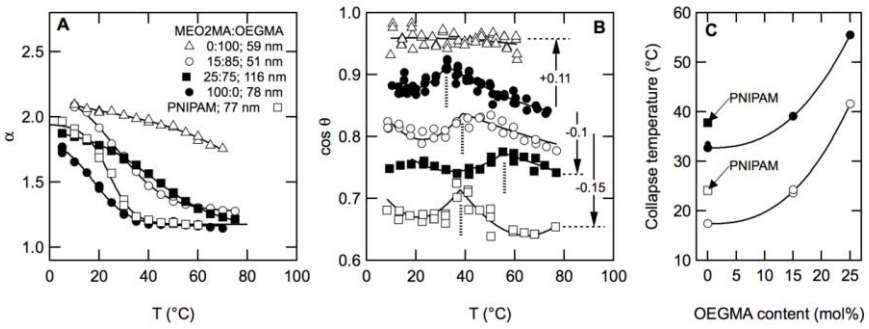

Figure 4. Swelling and surface hydrophilicity of thermo-responsive P(MEO_2MA-*co*-OEGMA) copolymer brushes, with PNIPAM also shown for reference. **(A)** Ellipsometric swelling coefficient; **(B)** cosine of the water contact angle. **(C)** Collapse transition temperatures of the brush volume (open symbol) and surface (closed symbols), as a function of OEGMA content in the synthesis solution. The molar composition of the synthesis solutions, and the dry brush thickness in nm, are given in panel A. In B, some curves are displaced vertically for clarity as shown by the vertical arrows; the thick vertical dashed lines indicate the location of the surface collapse transition.

All brushes have similar values of surface hydrophilicity, although PNIPAM and the 15% OEGMA copolymer appear to be slightly less hydrophilic. In addition, all of them except the POEGMA homopolymer show the presence of a collapse transition in both their surface (kink in the contact angle) and volume properties; the collapse of POEGMA, if any, might occur at a temperature higher than 80°C.

All thermo-responsive brushes including PNIPAM have a surface transition temperature (closed symbols in Figure 4C) from 13 to 15°C higher than the volume transition temperature (open symbols), the volume transition being here defined as the temperature corresponding to the steepest slope of the ellipsometry-determined $\alpha(T)$. Similar results are obtained when using the QCM-D-determined swelling coefficient, although the difference between volume and surface is then only of *ca.* 8°C. [11] This confirms the generality of the temperature-progressiveness of the brush collapse already discussed in our case study of PNIPAM, even though neutron reflectometry performed on similar P(MEO_2MA-*co*-OEGMA) brushes did not report two-compartment profiles for the brush segment density in the collapse transition region,[46] contrarily to PNIPAM.[31]

Nevertheless, the widths of the volume collapse of the brushes are different (Figure 4A), being narrower for PNIPAM and progressively broadening for the $PMEO_2MA$-based copolymers with increasing amounts of OEGMA. This effect most probably results from the larger average size of the monomer units (NIPAM being the smallest, OEGMA the largest), which reduces the brush grafting density for steric reasons and apparently broadens the collapse transition. Except for this effect, the copolymer containing 15% OEGMA displays surface and volume transition temperatures almost identical to PNIPAM, as well as the same surface hydrophilicity.

In addition, as Figure 4C demonstrates, tuning the collapse transition can be easily achieved by random copolymerization, demonstrating the interest of OEGMA-based polymer brushes for practical applications. This is even truer when considering the

demonstrated possibility to copolymerize MEO_2MA with methacrylic acid, which provides a supplementary handle for actuation through pH, [47] or with OH-ended OEGMA or HEMA units for grafting functional units within the brush leading to, *e.g.*, temperature-responsive antibacterial surfaces,[47] temperature-tunable cell-adhesive surfaces,[16] or brushes displaying photomodulated swelling properties in water.[17]

4.3.4 Surface and volume hydrophilicity of non-thermo-responsive poly(oligo(ethylene oxide)methacrylate) copolymer brushes

PHEMA is a moderately water-swellable polymer, whereas POEGMA is fully soluble in water; therefore, copolymerization provides access to a wide range of polymers of varying hydrophilicity, equipped with –OH side groups for the installation of functional moieties. The swelling and surface properties of pristine P(OEGMA-*co*-HEMA) brushes are displayed in Figure 5A and B. Brushes comprising up to 40 mol% HEMA display an essentially identical swelling coefficient (Figure 5A). This results from the volume of the OEGMA repeat unit which is a factor of *ca.* 4 larger than the one of HEMA; consequently, a 40% molar composition in HEMA only corresponds to a *ca.* 15% volume fraction in HEMA. However, starting from 60 mol% in HEMA (*ca.* 27 vol%), the swelling coefficient decreases regularly for increasing HEMA contents, affording a range of brushes of easily-tunable volume hydrophilicity. The temperature dependence remains however similar to the one of POEGMA brushes, namely a broad decrease of hydrophilicity with temperature with no indication for the presence of a sharp collapse transition.

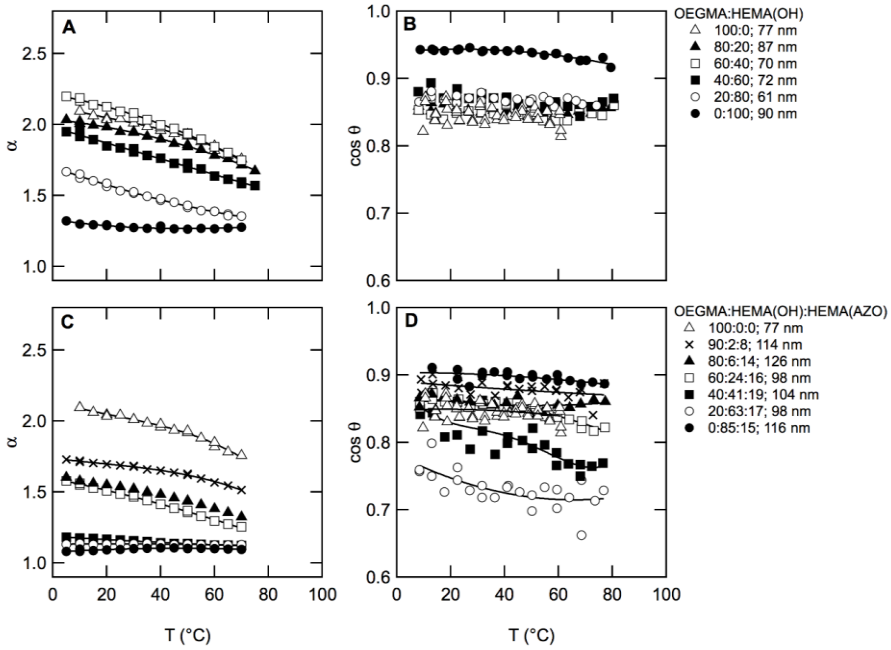

Figure 5. Swelling and surface hydrophilicity of non-thermo-responsive P(OEGMA-*co*-HEMA) copolymer brushes. **(A,C)** Ellipsometric swelling coefficient; **(B,D)** cosine of the water contact angle. The top panels show the results for pristine brushes, with the molar composition and dry brush thickness given in the legend; the bottom panels are for brushes post-modified with a hydrophobic azobenzene photochromic group.

The absence of collapse transition is confirmed by the contact angle data (Figure 5B), with the surface hydrophilicity remaining constant over the whole temperature range. In addition, all brushes have the same surface hydrophilicity identical to POEGMA's, which is significantly lower than the surface hydrophilicity of PHEMA. This might look surprising from a thermodynamical point of view, since one would be tempted to think that the brush would accumulate the groups of lower surface tension – hence the hydroxyl groups of HEMA – at the water interface. However, the HEMA repeat units are short and considerably constrained by the chain backbone, contrarily to the long methoxy-

ended OEGMA side chains which can freely explore a wide range of conformations. Hence, OEGMA segments accumulate at the surface for entropic reasons, resulting in a quasi-independence of surface hydrophilicity with composition. Taken together, Figures 5A and B thus confirm the lack of correlation between surface and volume hydrophilicity, a point which we discussed previously elsewhere.[20] In the present context, this leads to a collection of brushes of tunable volume hydrophilicity and degree of swelling, displaying an identical surface hydrophilicity (except for pure PHEMA).

As mentioned before, a very nice feature of HEMA-containing brushes is the possibility to install functional groups on the hydroxyl side chains by standard conjugation strategies,[6, 7, 9, 17] which broadens considerably their application range, even though grafting might be vertically non-homogeneous depending on brush grafting density and size of grafted units as was shown by neutron reflectometry.[9] Here, we grafted photochromic amine-substituted hydrophobic azobenzene moieties on the hydroxyl groups of dense P(OEGMA-*co*-HEMA) brushes (Scheme 1) : after activation by *N,N′*-disuccinimidyl carbonate, *N*-(2-Aminoethyl)-4-(2-phenyldiazenyl)benzamide[48] was grafted on the hydroxyl groups of the brush following a published protocol,[17] and its content determined by UV/visible spectroscopy. For most brushes, the content in azobenzene-substituted HEMA saturates to about 15-19 mol%, well below the initial content in HEMA, due to steric limitations to the amount of azobenzene which can be inserted in the brushes. The brushes are thus made of terpolymer chains composed of OEGMA, unreacted HEMA and azobenzene-grafted HEMA units; the precise composition of the brushes is shown in the legend of Figure 5D.

Figure 5C shows that the introduction of a relatively small amount of azobenzene group substantially decreases the volume hydrophilicity of the brushes, with brushes initially containing more than 60 mol% of HEMA being strongly collapsed over the complete temperature range after azobenzene grafting. For smaller initial contents in HEMA, the swelling scales inversely with initial HEMA content, again providing access to a complete range of hydrophilic brushes with a slowing decreasing hydrophilicity as temperature increases.

We checked by UV/visible spectroscopy that the azobenzene groups in the brushes immersed in water are able to switch from their trans to their cis configuration upon UV irradiation. The configurational switch results in an increase of the dipole moment of azobenzene by 2-3 D,[49, 50] expected to change the hydrophilic balance of the polymer chains. However, the ellipsometric swelling coefficient of the brushes in water varied negligibly upon continuous UV irradiation, with on average only 0.6% of increase, and no significant difference between the different compositions in HEMA. This is consistent with results previously obtained on MEO_2MA-based dense terpolymer brushes grafted with the same azobenzene group, of which the QCM-D-measured degree of swelling varied by less than *ca.* 0.5% upon irradiation;[17] larger variations of the swelling coefficient could be attained by strongly decreasing the brush grafting density, but remained lower than 2%. This confirms that the change of polarity depending on the configuration of the azobenzene is a minor disturbance of the hydrophilic balance of the volume of OEGMA-based brushes.

Turning to the surface hydrophilicity of the azobenzene-grafted brushes (Figure 5D), it does not deviate substantially from the one of

pure POEGMA when the swelling of the brush is significant, *i.e.*, for HEMA initial contents of 40 mol% or less. This is similar to the case of azobenzene-free brushes : when the brush is swollen, the long OEGMA side chains accumulate at the water interface and almost fully screen the other groups, be them hydroxyl-ended HEMA side chains or hydrophobic azobenzene-substituted HEMA units. However, for more hydrophobic brushes which do not swell in water, the HEMA units are now partially present at the surface : then, the surface hydrophilicity becomes slightly decreased by the azobenzene content (Figure 5D). This is because the decrease of interfacial segmental mobility in unswollen brushes results in a partial trapping of azobenzene units at the water interface, leading to an average surface composition closer to the volume composition.

Nevertheless, even on a fully collapsed brush having azobenzene partly expressed at the brush/water interface (the brush with 17 mol% azobenzene-grafted HEMA units and 63 mol% unmodified HEMA units shown as open circles in Figure 5D), the contact angles measured in water by the captive bubble method do not vary significantly upon UV or visible irradiation (less than 0.6° on average, which is within the error bar). This results from the low concentration of azobenzene groups at the brush/water interface, and by the residual segmental mobility at the surface, which conspire to strongly decrease the effect of the switching of the polarity of the azobenzene groups upon UV irradiation. Again, we conclude that water-equilibrated brushes, even in a collapsed state and even including substantial amount of hydrophobic groups, manage to present a mostly hydrophilic dynamic surface to water.

4.4 Conclusions

We have reviewed the swelling and surface hydrophilicity of dense polymer brushes, including thermo-responsive systems. Consistent swelling results can be obtained with different techniques such as AFM, ellipsometry, or QCM-D; reproducible contact angles of water-equilibrated surfaces can be measured in the captive bubble configuration. From this large ensemble of results, the following conclusions can be derived:

1. dense thermo-responsive brushes collapse over a broad temperature range, with the collapse ending at the external surface, supporting models in which the brush progressively collapses from the bottom to the top as temperature increases;
2. during the collapse transition, the volume of the brush switches from more hydrophilic to more hydrophobic; however, the surface of the brush equilibrated in water does not change significantly its hydrophilicity, due to the continuous rearrangement of its segments at the water interface in order to expose its more hydrophilic groups whatever the state of its volume. These conformational changes are nevertheless detected in the excess surface entropy of the brush, which changes abruptly at the surface collapse transition temperature, located about 15°C higher than the ellipsometric collapse temperature of the volume of the brush;
3. responsive copolymer brushes based on oligo(ethylene oxide) methacrylate groups afford systems of which the collapse transition can be easily tuned, providing suitable alternatives to PNIPAM. Such brushes can easily be post-derivatized to provide temperature-dependent functional properties;

4. the volume and surface hydrophilicity of random copolymer brushes are not correlated, providing easy access to brushes for which the surface and volume properties can be designed independently. Inclusion of hydroxyl-ended side chains provides a supplementary handle for tuning, as shown here by the synthesis of brushes comprising photochromic groups. However, the dynamic nature of the brush surface prevents the hydrophobic photochromes to be expressed in large amount at the surface when equilibrated in water.

4.5 Acknowledgments

P.Z. thanks the Chinese Scholarship Council (CSC) for a research fellowship. K.G. is a Research Associate of the F.R.S.-FNRS. This work was supported by the F.R.S.-FNRS and the Belgian Federal Science Policy (IAP/PAI P7/05).

References

1. Barbey, R. et al. Polymer Brushes via Surface-Initiated Controlled Radical Polymerization Synthesis, Characterization, Properties, and Applications. *Chem. Rev.* **109**, 5437-5527 (2009).
2. Yoshikawa, C. et al. Protein Repellency of Well-Defined, Concentrated Poly(2-hydroxyethyl methacrylate) Brushes by the Size-Exclusion Effect. *Macromolecules* **39**, 2284-2290 (2006).
3. Schild, H.G. Poly(N-isopropylacrylamide): experiment, theory and application. *Prog. Polym. Sci.* **17**, 163-249 (1992).
4. M. Cunanan, C., M. Tarbaux, N. & M. Knight, P. Surface properties of intraocular lens materials and their influence on in vitro cell adhesion. *J. Cataract. Refract. Surg.***17**, 767-773 (1991).
5. Ibanescu, S.-A., Nowakowska, J., Khanna, N., Landmann, R. & Klok, H.-A. Effects of Grafting Density and Film Thickness on the Adhesion of Staphylococcus epidermidis to Poly(2-hydroxy ethyl methacrylate) and Poly(poly(ethylene glycol)methacrylate) Brushes. *Macromol. Biosci.* **16**, 676-685 (2016).
6. Fernandes, A.E. et al. Thicker is Better? Synthesis and Evaluation of Well-Defined Polymer Brushes with Controllable Catalytic Loadings. *Chem. Eur. J.* **18**, 16226-16233 (2012).
7. Fernandes, A.E. et al. Effects of Thickness and Grafting Density on the Activity of Polymer-Brush-Immobilized Tris(triazolyl) Copper(I) Catalysts. *ChemCatChem* **7**, 856-864 (2015).

8. Glinel, K. et al. Antibacterial and Antifouling Polymer Brushes Incorporating Antimicrobial Peptide. *Bioconjugate Chem.* **20**, 71-77 (2008).
9. Schüwer, N., Geue, T., Hinestrosa, J.P. & Klok, H.-A. Neutron Reflectivity Study on the Postpolymerization Modification of Poly(2-hydroxyethyl methacrylate) Brushes. *Macromolecules* **44**, 6868-6874 (2011).
10. Jonas, A.M., Glinel, K., Oren, R., Nysten, B. & Huck, W.T.S. Thermo-Responsive Polymer Brushes with Tunable Collapse Temperatures in the Physiological Range. *Macromolecules* **40**, 4403-4405 (2007).
11. Laloyaux, X., Mathy, B., Nysten, B. & Jonas, A.M. Surface and Bulk Collapse Transitions of Thermo-responsive Polymer Brushes. *Langmuir* **26**, 838-847 (2009).
12. Krishnamoorthy, M., Hakobyan, S., Ramstedt, M. & Gautrot, J.E. Surface-initiated polymer brushes in the biomedical field: applications in membrane science, biosensing, cell culture, regenerative medicine and antibacterial coatings. *Chem. Rev.* **114**, 10976-11026 (2014).
13. Wischerhoff, E. et al. Controlled cell adhesion on PEG-based switchable surfaces. *Angew. Chem.* **47**, 5666-5668 (2008).
14. Sefcik, L.S. et al. Effects of PEG-Based Thermo-responsive Polymer Brushes on Fibroblast Spreading and Gene Expression. *Cell. Mol. Bioeng.* **6**, 287-298 (2013).
15. Laloyaux, X. et al. Temperature-Responsive Polymer Brushes Switching from Bactericidal to Cell-Repellent. *Adv. Mater.* **22**, 5024-5028 (2010).

16. Desseaux, S. & Klok, H.-A. Temperature-Controlled Masking/Unmasking of Cell-Adhesive Cues with Poly(ethylene glycol) Methacrylate Based Brushes. *Biomacromolecules* **15**, 3859-3865 (2014).
17. Dirani, A. et al. Reversible Photomodulation of the Swelling of Poly(oligo(ethylene glycol) methacrylate) Thermo-responsive Polymer Brushes. *Macromolecules* **45**, 9400-9408 (2012).
18. Yuan, Y. & Lee, T.R. Contact Angle and Wetting Properties. *Springer Series in Surface Sciences* **51**, 3-34 (2013).
19. Jalili, K., Abbasi, F. & Milchev, A. Surface Microdynamics Phase Transition and Internal Structure of High-Density, Ultrathin PHEMA-b-PNIPAM Diblock Copolymer Brushes on Silicone Rubber. *Macromolecules* **46**, 5260-5278 (2013).
20. Zhuang, P., Dirani, A., Glinel, K. & Jonas, A.M. Temperature Dependence of the Surface and Volume Hydrophilicity of Hydrophilic Polymer Brushes. *Langmuir* **32**, 3433–3444 (2016).
21. Suzuki, H. et al. Precise Synthesis and Physicochemical Properties of High-Density Polymer Brushes designed with Poly(N-isopropylacrylamide). *Macromolecules* **43**, 9945-9956 (2010).
22. Plunkett, K.N., Zhu, X., Moore, J.S. & Leckband, D.E. PNIPAM Chain Collapse Depends on the Molecular Weight and Grafting Density. *Langmuir* **22**, 4259-4266 (2006).
23. Burdukova, E., Li, H., Ishida, N., O'Shea, J.-P. & Franks, G.V. Temperature controlled surface hydrophobicity and interaction forces induced by poly (N-isopropylacrylamide). *J. Colloid Interface Sci.* **342**, 586-592 (2010).

24. Xue, C. et al. Protein adsorption on poly(N-isopropylacrylamide) brushes: dependence on grafting density and chain collapse. *Langmuir* **27**, 8810-8818 (2011).
25. Pelton, R. Poly(N-isopropylacrylamide) (PNIPAM) is never hydrophobic. *J. Colloid Interface Sci.* **348**, 673-674 (2010).
26. Yim, H. et al. Temperature-Dependent Conformational Change of PNIPAM Grafted Chains at High Surface Density in Water. *Macromolecules* **37**, 1994-1997 (2004).
27. Yim, H. et al. Evidence for vertical phase separation in densely grafted, high-molecular-weight poly(N-isopropylacrylamide) brushes in water. *Phys. Rev. E* **72**, 051801 (2005).
28. Yim, H. et al. Effects of Grafting Density and Molecular Weight on the Temperature-Dependent Conformational Change of Poly(N-isopropylacrylamide) Grafted Chains in Water. *Macromolecules* **39**, 3420-3426 (2006).
29. Yim, H. et al. Conformation of End-Tethered PNIPAM Chains in Water and in Acetone by Neutron Reflectivity. *Macromolecules* **36**, 5244-5251 (2003).
30. Kooij, E.S., Sui, X., Hempenius, M.A., Zandvliet, H.J.W. & Vancso, G.J. Probing the Thermal Collapse of Poly(N-isopropylacrylamide) Grafts by Quantitative in Situ Ellipsometry. *J. Phys. Chem. B* **116**, 9261-9268 (2012).
31. Afroze, F., Nies, E. & Berghmans, H. Phase transitions in the system poly(N-isopropylacrylamide)/water and swelling behaviour of the corresponding networks. *J. Mol. Struct.* **554**, 55-68 (2000).

32. Baulin, V.A., Zhulina, E.B. & Halperin, A. Self-consistent field theory of brushes of neutral water-soluble polymers. *J. Chem. Phys.* **119**, 10977-10988 (2003).
33. Baulin, V.A. & Halperin, A. Signatures of a Concentration-Dependent Flory χ Parameter: Swelling and Collapse of Coils and Brushes. *Macromol. Theory Simul.* **12**, 549-559 (2003).
34. Elliott, L.C.C. et al. Loading and Distribution of a Model Small Molecule Drug in Poly(N-isopropylacrylamide) Brushes: a Neutron Reflectometry and AFM Study. *Langmuir* **29**, 3259-3268 (2013).
35. Domack, A., Prucker, O., Rühe, J. & Johannsmann, D. Swelling of a polymer brush probed with a quartz crystal resonator. *Phys. Rev.* **56**, 680-689 (1997).
36. Yim, H. et al. Study of the conformational change of poly(N-isopropylacrylamide)-grafted chains in water with neutron reflection: Molecular weight dependence at high grafting density. *J. Phys. Chem. Sci. Part B Polym. Phys.* **42**, 3302-3310 (2004).
37. Yu, Y. et al. Stretching of collapsed polymers causes an enhanced dissipative response of PNIPAM brushes near their LCST. *Soft Matter* **11**, 8508-8516 (2015).
38. Kidoaki, S., Ohya, S., Nakayama, Y. & Matsuda, T. Thermo-responsive Structural Change of a Poly(N-isopropylacrylamide) Graft Layer Measured with an Atomic Force Microscope. *Langmuir* **17**, 2402-2407 (2001).
39. Kujawa, P. & Winnik, F.M. Volumetric Studies of Aqueous Polymer Solutions Using Pressure Perturbation Calorimetry: A

New Look at the Temperature-Induced Phase Transition of Poly(N-isopropylacrylamide) in Water and D2O. *Macromolecules* **34**, 4130-4135 (2001).

40. Jones, D.M., Smith, J.R., Huck, W.T.S. & Alexander, C. Variable Adhesion of Micropatterned Thermo-responsive Polymer Brushes: AFM Investigations of Poly(N-isopropylacrylamide) Brushes Prepared by Surface-Initiated Polymerizations. *Adv. Mater.* **14**, 1130-1134 (2002).
41. Ishida, N. & Biggs, S. Direct Observation of the Phase Transition for a Poly(N-isopropylacryamide) Layer Grafted onto a Solid Surface by AFM and QCM-D. *Langmuir* **23**, 11083-11088 (2007).
42. Cole, M.A., Voelcker, N.H., Thissen, H., Horn, R.G. & Griesser, H.J. Colloid probe AFM study of thermal collapse and protein interactions of poly(N-isopropylacrylamide) coatings. *Soft Matter* **6**, 2657-2667 (2010).
43. Rahane, S.B., Floyd, J.A., Metters, A.T. & Kilbey, S.M. Swelling Behavior of Multiresponsive Poly(methacrylic acid)-block--poly(N-isopropylacrylamide) Brushes Synthesized Using Surface-Initiated Photoiniferter-Mediated Photopolymerization. *Adv. Funct. Mater.* **18**, 1232-1240 (2008).
44. Tu, H., Heitzman, C.E. & Braun, P.V. Patterned Poly(N-isopropylacrylamide) Brushes on Silica Surfaces by Microcontact Printing Followed by Surface-Initiated Polymerization. *Langmuir* **20**, 8313-8320 (2004).
45. Bashkatov, A.N. & Genina, E.A., Vol. 5068 393-395 (2003).

46. Gao, X. et al. Chain conformation of a new class of PEG-based thermo-responsive polymer brushes grafted on silicon as determined by neutron reflectometry. *Langmuir* **25**, 10271-10278 (2009).
47. Laloyaux, X., Mathy, B., Nysten, B. & Jonas, A.M. Bidimensional Response Maps of Adaptive Thermo- and pH-Responsive Polymer Brushes. *Macromolecules* **43**, 7744-7751 (2010).
48. Jochum, F.D. & Theato, P. Temperature and light sensitive copolymers containing azobenzene moieties prepared via a polymer analogous reaction. *Polymer* **50**, 3079-3085 (2009).
49. Akiyama, H., Tamada, K., Nagasawa, J.i., Abe, K. & Tamaki, T. Photoreactivity in Self-Assembled Monolayers Formed from Asymmetric Disulfides Having para-Substituted Azobenzenes. *J. Phys. Chem. B* **107**, 130-135 (2003).
50. Yang, D. et al. Photon Control of Liquid Motion on Reversibly Photoresponsive Surfaces. *Langmuir* **23**, 10864-10872 (2007).

Chapter 4: Temperature Dependence of the Swelling and Surface Wettability of Dense Polymer Brushes

5 Synthesis of Hydrophilic P(DMA-*co*-HEMA) Copolymer Brushes by Surface-initiated ATRP

5.1 Abstract

Homopolymer brushes of PDMA and PHEMA and P(DMA-*co*-HEMA) brushes were synthesized by SI-ATRP in aqueous solution. The kinetics of the synthesis of the polymer brushes were studied by varying different parameters such as monomer concentration, ligands, and H_2O/CH_3OH ratios. The reaction conditions were finally optimized to control the synthesis of homopolymer and copolymer brushes in at least 60 min, with a resultant brush thickness reaching at least 100 nm. The HEMA content in copolymer brushes was measured by FTIR, from which the reactivity ratios of DMA and HEMA were determined to be r(DMA) = 0.17 and r(HEMA) = 3.40. The probable structure of P(DMA-*co*-HEMA) chains was then predicted based on these reactivity ratios, providing the sequence distributions of each monomer unit depending on the HEMA content in feed solution. For HEMA molar contents in solution lower than 2%, corresponding to 10% HEMA molar content in the brush, the chains consist on average of long PDMA blocks separated by isolated HEMA units.

Chapter 5: Synthesis of Hydrophilic P(DMA-*co*-HEMA) Copolymer Brushes by Surface-initiated ATRP

5.2 Introduction

Hydrophilic polymer brushes are of critical importance for biomedical and biological applications such as to enhance cell adhesion with hybrid peptide-polymer brushes,[1] reducing a friction coefficient by grafting hydrophilic polymers on implant surfaces,[2] providing non-specific antifouling and antibacterial properties by tethering hydrophilic polymers on surfaces, or specific antifouling and antibacterial properties by loading or conjugating bactericidal molecules on the polymer chains,[3-6] or enhancing the solubility and stability of colloidal particles in water by grafting them with hydrophilic polymers.[7] Typical are poly(*N*,*N*-dimethyl acrylamide) (PDMA) brushes, which are highly hydrophilic in water, and can be used to improve the stability of gold[8] or latex[9, 10] particles in water, or to prevent fouling from proteins and bacteria and even to kill bacteria when conjugated with bactericidal peptides[3]. In this chapter, we study the formation of PDMA-based brushes, incorporating limited amounts of hydroxyl-substituted comonomer units for further derivatization into brushes of higher functionality as will be demonstrated in the next chapter.

With the increasing development of controlled/"living" radical polymerization techniques, such as RAFT, NMR and ATRP for the control molar masses, polydispersities, compositions and structures of polymers, these methods have become excellent tools to synthesize polymer brushes.[11-16] Among them, ATRP is most popular for the synthesis of polymer brushes of high grafting densities, which is usually performed by first introducing a suitable initiator on the substrate

surface, then grafting macromolecules from this surface, a process called surface-initiated ATRP (SI-ATRP).

Although SI-ATRP is the most common technique used to synthesize polymer brushes, it is still a challenge to synthesize in a controlled way by ATRP acrylamide-based polymers or polymer brushes including PDMA.[17-19] In order to polymerize acrylamides in a controlled way, different conditions were tested, including changing initiators, ligands, solvents, activators and deactivators. Teodorescu and Matyjaszweski[20] first tried to use CuBr as activator, and bipyridine (Bpy), *N*,*N*,*N*´,*N*´,*N*´´-pentamethylethylenetriamine (PDMETA), or 1,4,8,11-tetramethyl-1,4,8,11-tetraazacyclotetradecane (Me_4Cyclam) as various ligands to polymerize DMA in the bulk or in methanol at 90°C or 110°C. Bpy was shown to be a poor ligand which failed in the polymerization of DMA even at 110°C. The polymerization of DMA was very slow and uncontrolled as well with PMDETA. As for the Me_4Cyclam ligand, it promotes the very fast but uncontrolled polymerization of DMA, even when using methanol as solvent and $CuBr_2$ as deactivator. Soon after, Rademacher *et al.*[18] also attempted the ATRP of DMA at room temperature with various initiators, solvents, ligands, and activators. They first tried to use water as solvent and mixed solvents consisting of toluene/DMF, H_2O/DMF or butanol/DMF to tune the rate of polymerization, and compared the activity of HMTETA, Me_6TREN and Me_4Cyclam. Although the rate of polymerization could be adjusted by varying the reaction conditions, the polymerization of DMA still lost its control as proved by the resulting broad polydispersities. Teodorescu and Matyjaszweski[21] first succeeded to control the polymerization of DMA by using CuCl instead

of CuBr as activator and the less active Me_6TREN ligand (compared to Me_4Cyclam) in toluene and DMF at room temperature; however, they only reached low molar masses (M_n < 10000 g/mol). Jayachandran *et al.*[9] were the first to graft PDMA brushes from polystyrene latex surfaces by aqueous ATRP at room temperature. They used CuCl/$CuCl_2$/Cu powders or CuBr/$CuBr_2$/Cu powders and three different ligands consisting of PMDETA, HMTETA and Me_6TREN as catalytic system, and studied the molar mass, polydispersity and hydrodynamic brush thickness changes dependent on monomer concentration. Although the molar mass and hydrodynamic thickness increased with monomer concentration, their polydispersity also increased: actually, the polymerization cannot be controlled in Me_6TREN-based catalyst systems. The polydispersity can be only controlled in the range of 1.2-1.8 in PMDETA or HMTETA-based systems by varying the monomer concentration from 1.5 to 10.5 wt%. The polymerization can only be partially controlled with the PMDETA/CuCl/$CuCl_2$ or HMTETA/CuCl/$CuCl_2$ catalyst systems using a 1.5 wt% monomer concentration, leading to a polydispersity of ~1.4.

Neugebauer and Matyjaszewski[22] succeeded in controlling the polymerization of DMA by using methyl 2-chloropropionate/CuCl/Me_6TREN as the initiating/catalyst system in toluene at 25°C, and obtained high molar masses of homopolymers (M_n up to 50000 g/mol) with a narrow molar mass distribution (M_w/M_n = 1.05-1.13) by varying the monomer/CuCl/ligand ratio and the amount of solvent. However, it should be mentioned that the conversion of DMA increased linearly with time only over the first hour, with a

subsequent slowing down of the rate of polymerization. Yin and Stöver[17] used the same initiator/catalyst system with an initiator/CuCl/Me_6TREN ratio of 1/1/1 to polymerize DMA in different solvents. It was mentioned that the polymerization proceeded initially very rapidly in ethyl acetate, THF and DMF but quickly stopped within 5-10 min at room temperature with a polydispersity lower than 1.1 in each solvent. In more details, they tried to polymerize DMA with a monomer/initiator ratio from 100 to 400 in methanol. The monomer conversion increased rapidly over the first 10 min, then increased almost linearly in the later 30 min, but quickly stopped after that. Increasing the monomer/initiator ratio helps increase molar mass (only up to 10000 g/mol) without loss of control (PDI < 1.1). Besides, they also randomly copolymerized DMA with N-Phenylacrylamide (PhAm) in methanol or in a methanol/H_2O mixed solvent in a finely controlled way, but the catalyst quickly lost its activity in 10 min.

In order to better control the polymerization of DMA, the reaction conditions required to polymerize N-isopropylacrylamide (NIPAM) by ATRP in a controlled way can also be referred to, considering the similar structures of NIPAM and DMA. Masci *et al.*[23] controlled the polymerization of NIPAM by using ethyl 2-chloropropionate (ECP) as initiator together with CuCl and Me_6TREN in a 50/50 DMF/water mixed solvent at room temperature, but the highest molar mass was only 22000 g/mol. Kapolei *et al.*[24] synthesized PNIPAM brushes by grafting from gold surfaces in a 38/1 water/methanol mixed solvent with a CuBr/PMDETA catalyst system at room temperature. The polymer brush thickness increased almost linearly with time in the first 30 min and reached ~220 nm. Using the MCP (methyl 2-

chlorophropropionate)/CuCl/Me_6TREN initiator/catalyst system, Xia *et al.*[25] carried out the ATRP of NIPAM in different alcohols including methanol, ethanol, 1-propanol (n-PrOH), 2-propanol (i-PrOH) and tert-butyl alcohol (t-BuOH) at room temperature and varied monomer/initiator and monomer/solvent ratios. All the polymers obtained had a polydispersity lower than 1.3. In 100:1:1:1 NIPAM:MCP:CuCl:Me6TREN and NIPAM:solvent (w:w) conditions, the monomer conversion increased almost linearly with time in the first 2 h for all the solvents except methanol. The conversion was highest in i-PrOH, slightly lower in t-BuOH and n-PrOH, and much lower in ethanol. Ye and Narain[26] systematically studied the ATRP of NIPAM in organic solvents including alcohols (methanol, ethanol, 1-PrOH and 2-PrOH) and water-organic mixed solvents also by using MCP/CuCl/Me_6TREN as initiator/catalyst system. At room temperature, the polymerization of NIPAM could be controlled in all organic solvents even after 15 h reaction time leading to a polydispersity close to 1.1, but a low molar mass in the range of 2000-12000 g/mol. In organic/water mixed solvents, temperature has a strong impact on the control of the polymerization of NIPAM: the degree of control is decreased but the rate of polymerization and the molar mass are strongly increased at higher temperatures. However, at 0°C, the control over the polymerization of NIPAM can be recovered. Besides, the polarity indices of the alcohols impact the rate of polymerization, which increases with polarity index due to the increasing solubility of the resulting polymer, from methanol/H_2O to i-PrOH/H_2O.[26]

In summary, in order to control the polymerization of DMA, CuCl/HMTETA and CuCl/Me_6TREN are the most popular catalyst

systems used. In aprotic organic solvents, the molar masses of PDMA or PNIPAM are usually very low, although their polymerization can be controlled. The rate and controllability of polymerization of DMA can be increased in alcohols. Adding water can accelerate the polymerization of DMA in organic solvents. So water/mixed alcohol solvents might be a good choice to control the polymerization of DMA at a high rate. Adding deactivators like $CuCl_2$ or $CuBr_2$ and sacrificial initiators can improve the control of the polymerization.

2-hydroxyethyl methacrylate (HEMA) is of importance in materials for contact lenses, drug delivery and hydrogels.[27] Besides, it is also often copolymerized with other monomers, thereby introducing functional hydroxyl groups for grafting biomolecules to provide special properties such as antibacterial activity,[28] or other molecules like photochromic groups. Robinson *et al.*[29] first synthesized well-defined PHEMA by ATRP in methanol and a water/methanol 50/50 mixed solvent without deactivator by using an oligo(ethylene glycol)-based macroinitiator, and CuBr/Bpy or CuCl/Bpy as catalyst system. Although the conversion was almost complete in 4 h, the molar masses were below 8000 g/mol. Later, Huang *et al.*[30] grafted PHEMA brushes from gold surfaces by ATRP in pure water at room temperature. They used CuBr/Bpy and CuCl/Bpy as catalyst, respectively, and studied the role of $CuBr_2$ (deactivator) in the kinetics of the polymerization. It was found that adding $CuBr_2$ helps improve the control of PHEMA brush synthesis. PHEMA brushes could only be controlled over the first 2 h and the brush thickness reached ~320 nm by adding 30 mol% of $CuBr_2$ with respect to CuBr in the CuBr/Bpy catalyst system. However, the PHEMA brush could almost be controlled over 12 h and the brush

thickness reached 700 nm by replacing CuBr with CuCl, using the CuCl/$CuBr_2$/Bpy catalyst system.

In this chapter, different reaction conditions are tried to grow PDMA, PHEMA and their copolymer brushes by SI-ATRP in a controlled way. Copolymerizing DMA with HEMA can introduce functional hydroxyl groups, which can be then modified to impart the copolymer brushes with specific properties; in chapter 6, we will attempt to reach photo-responsiveness by post-grafting azobenzene groups on the P(DMA-*co*-HEMA) copolymer brushes. Once the reaction conditions are optimized, P(DMA-*co*-HEMA) brushes are synthesized by varying the HEMA content in solution, and the composition of the copolymer brushes is then determined by FTIR measurement to obtain the reactivity ratios, from which the chain structure is computed.

5.3 Materials and methods

5.3.1 Materials

N,*N*-dimethylacrylamide (DMA) and 2-hydroxyethyl methacrylate (HEMA) were purchased from Sigma-Aldrich. DMA was purified by distillation under vacuum at ~70°C before use. HEMA was run three times through an aluminum oxide column. Copper(I) chloride (99.995+ %) (CuCl), copper(II) chloride (99.999+ %) ($CuCl_2$), and copper(II) bromide (99+ %) ($CuBr_2$), 1,1,4,7,10,10-hexamethyltriethylenetetramine (HMTETA) was purchased from Sigma-Aldrich. Tris(2-dimethylaminoethyl)amine (99+ %) (Me_6TREN) was supplied by Alpha Aesar. Methanol (99.8%) was bought from VWR. Milli-Q water (resistivity: 18.2 MΩ.cm) was obtained from a

Millipore system. When needed, water was degassed by heating under argon. Silicon wafers (<100> orientation) were obtained from ACM (France). The ATRP silane initiator (3-(chlorodimethylsilyl)propyl 2-bromo-2-methylpropanoate) was synthesized as described previously.[31]

5.3.2 Preparation of the initiator monolayer

The initiator monolayer fabrication was described in chapter 3. Here, the chemical scheme of the gas phase silanation process is simply provided (Scheme 5.1).

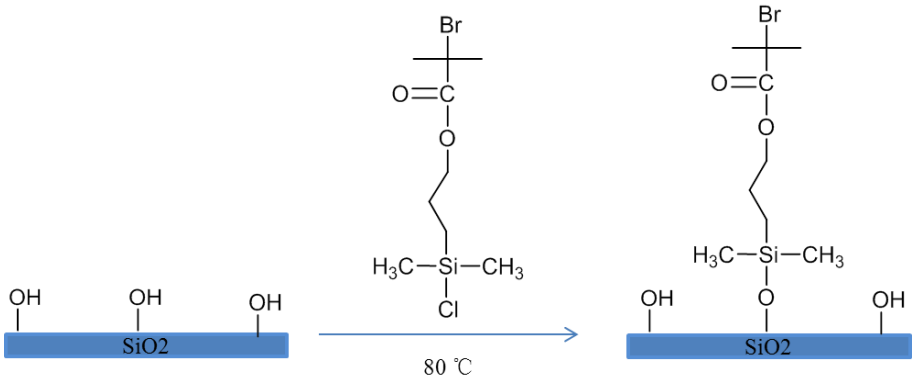

Scheme 5.1. Schematic fabrication of initiator monolayer by gas phase silanation.

5.3.3 Polymer brush synthesis

Reaction conditions 1:

At room temperature, 0.624 mL DMA (6 mmol), 0.73 mL HEMA (6 mmol), 2.19 mL HEMA (18 mmol) was dissolved in 4.5 mL Milli-Q water, respectively, contained within a flask capped with a rubber septum. 0.5 mg $CuCl_2$ (3.7×10^{-3} mmol) was added in each monomer solution. The solutions were stirred and degassed with argon for 15 min to remove dissolved oxygen. Then 3.7 mg CuCl (3.7×10^{-2} mmol) was

rapidly added under argon. After degassing for ~10 min, 22 μL HMTETA (8.1×10^{-2} mmol) was added. The mixed solution was further stirred and degassed for ~25 min. Thus the ratio of CuCl/$CuCl_2$/HMTETA was fixed to 1/0.1/2.2. Meanwhile, Schlenk tubes containing initiator-silanized silicon substrates were degassed three cycles with vacuum and argon (10 and 5 min, respectively). 3 mL of the prepared solution was syringed into each Schlenk tube. The samples were taken out at different time intervals, washed thoroughly with water and methanol, then dried with argon, and measured by ellipsometry to study the kinetics of polymerization of each brush. P(DMA-*co*-HEMA) brushes were synthesized with different DMA/HEMA ratios (1/3, 1/1, 3/1 in vol/vol) in the same condition as that used to graft homopolymer brush except adding 24 mmol monomer in total.

Reaction conditions 2:

At room temperature, 4 mL DMA was added in 8 mL different water/methanol mixed solvents (H_2O/CH_3OH 5/5 or 7/3, respectively) contained within a flask capped with a rubber septum. 0.5 mg $CuCl_2$ (3.7×10^{-3} mmol) or 0.82 $CuBr_2$ (3.7×10^{-3} mmol) deactivator was then added or not, depending on the experiment. The mixed solution was stirred and degassed with argon for ~20 min. Then 7.4 mg CuCl (7.4×10^{-2} mmol) was added and further degassed for ~5 min. After that, 20 μL HMTETA (7.4×10^{-2} mmol) was syringed into the solution and degassed for ~25 min, leading to mixed solutions with 1/1 activator/ligand or 1/0.05/1 activator/deactivator/ligand. Meanwhile, Schlenk tubes containing initiator-silanized silicon substrates were

degassed three cycles with vacuum and argon (10 and 5 min, respectively). 3 mL of the prepared solution was syringed into each Schlenk tube. The samples were taken out at different time intervals, washed thoroughly with water and methanol, then dried with argon, and measured by ellipsometry.

Reaction conditions 3:

At room temperature, 0.77 mL DMA (7.4 mmol) was added in 8 mL water/methanol 5/5 mixed solvent contained within a flask capped with a rubber septum. 0.5 mg $CuCl_2$ (3.7×10^{-3} mmol) or 0.82 mg $CuBr_2$ (3.7×10^{-3} mmol) deactivator was added or not, depending on the experiments. The mixed solution was stirred and degassed with argon for ~20 min. Then 7.4 mg CuCl (7.4×10^{-2} mmol) was added and further degassed for ~5 min. After that, 20.06 μL Me_6TREN (7.4×10^{-2} mmol) was syringed into the solution and degassed for ~25 min. In one reaction condition, the concentrations of DMA, CuCl, and Me_6TREN were only doubled without adding deactivator, leading to mixed solutions containing 100/1/1 or 200/2/2 DMA/activator/ligand, or 100/1/0.05/1 DMA/activator/deactivator/ligand. Meanwhile, Schlenck tubes containing initiator-silanized silicon substrates were degassed by three cycles with vacuum and argon (10 and 5 min, respectively). 3 mL of the prepared solution was syringed into each Schlenk tube. The samples were taken out at different time intervals, washed thoroughly with water and methanol, then dried with argon, and measured by ellipsometry. For PHEMA brush synthesis, 0.9 mL HEMA (7.4 mmol) was added instead of DMA with a 100/1/1 monomer/CuCl/Me_6TREN ratio, but without adding any deactivator or changing other conditions.

Reaction conditions 4:

At room temperature, 8 mL of water/methanol mixed solvent (5/5 or 6/4 volume ratios of water/methanol) was added into a flask capped with a rubber septum, and was stirred and degassed with argon for 10 min to remove dissolved oxygen. Then CuCl (7.4 mg, 7.4×10^{-2} mmol) was added and degassed for 10 min. After that, an equal molar amount of HMTETA (20 μL) as ligand was added and degassed for 5 min. Later on, a relative molar quantity of DMA (500 and 50 times the one of CuCl, respectively) was added and degassed for 20 min. Schlenk tubes with one substrate in each tube were degassed three times with vacuum and argon (10/5 min). 2.5 mL of the above prepared solution was added into each Schlenk tube. At different time intervals, one sample was taken out and washed with water and methanol for several times and dried with argon. The thickness of the polymer brush versus time was measured by ellipsometry to study their kinetics of growth. For the pure PHEMA brushes, a similar experimental procedure was chosen, just changing DMA monomers by an equal molar amount of HEMA monomers. For the copolymer brushes, the total quantity of monomers was kept at 37 mmol. Solutions of mixed DMA and HEMA monomers with 0.5 mol%, 1 mol%, 2 mol%, 5 mol%, 10 mol%, 20 mol% and 60 mol% of HEMA in each solution were prepared. Thus, P(DMA-*co*-HEMA) brushes with different HEMA content were synthesized (Scheme 5.2).

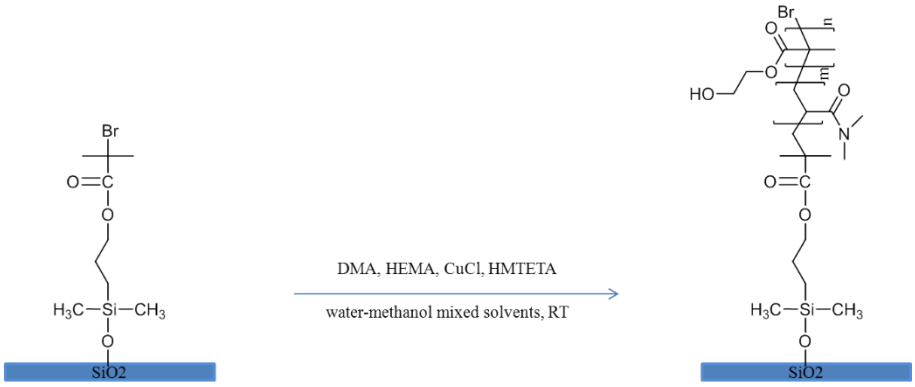

Scheme 5.2. Schematic synthesis of P(DMA-*co*-HEMA) brushes under optimized reaction conditions.

In the optimized conditions, P(DMA-*co*-HEMA) brushes were synthesized over substrates of 1 × 1 cm^2 and 1 × 2 cm^2 sizes. For the measurements of samples in the in-situ ellipsometry liquid cell and contact angle goniometer, 3 mL or 6 mL (depending on substrate size) of the prepared solution was syringed into each Schlenk tubes. At a pre-determined time, the samples were taken out and washed thoroughly with water and methanol, then dried with argon.

5.3.4 FTIR measurement

The absorbance spectra of the dry polymer brushes were recorded with a Fourier transform infrared spectrometer (FTIR) (Nicolet Nexus 870) in transmission mode. The spectra of copolymer brushes were obtained after subtraction of the atmosphere reference. 128 scans were collected and averaged for each spectrum with a resolution of 8 cm^{-1}.

The content of HEMA and DMA in P(DMA-*co*-HEMA) brushes was determined from the FTIR spectra in the dry state with pure PHEMA and PDMA brushes grafted onto two-side polished silicon

wafers as reference. According to the Lambert-Beer equation, the absorbance (A) is proportional to the thickness of the dry polymer brushes (h_{dry}):$A = \varepsilon c h_{dry}$ when c (the molar concentration in monomer units) is fixed, where ε is the extinction coefficient of the brush. In order to obtain the molar concentration of HEMA in the copolymer, the infrared spectra of PDMA and PHEMA were used to calculate the equivalent thickness in DMA and HEMA segments, h_{DMA} and h_{HEMA}, by referring to the characteristic absorbance of two reference peaks specific to DMA or HEMA moieties: the 1639 cm^{-1} peak associated with the asymmetrical stretching of the carbonyl amide I group of DMA (δ_{as}^{DMA}) and the 1722 cm^{-1} peak associated with the asymmetrical stretching of the carbonyl group of HEMA (δ_{as}^{HEMA}). For different copolymer brushes, these two peaks may shift a bit, which will influence slightly the caculated nomomer content in the copolymer brush, especially when one monomer content is low. To determine the composition of each copolymer brush, the copolymer chain can be seen as a chain consisting of two virtual sequences: one virtual sequence is composed of one monomer, the second virtual sequence is composed of the other monomer. The thickness of the virtual sequences can be calculated as follows:

$$h_{DMA} = \frac{A_{DMA}}{A_{DMA}^{ref}} * h_{DMA}^{ref} \text{ and } h_{HEMA} = \frac{A_{HEMA}}{A_{HEMA}^{ref}} * h_{HEMA}^{ref} \qquad (1),$$

with the thickness of the brush reference samples (h^{ref}) measured by ellipsometry. On the other hand, $m = \rho v = \rho h s$ and $m = n M_w$, so that $n = \rho h s / M_w$, where m is the mass of the polymer brush, ρ is the mass density of the polymer brush, v is the volume of the brush, h is its thickness, s is the area covered by the polymer brush, n is the number of monomer units in the copolymer brush, and M_w is the molar mass of

the repeat unit. The molar ratio of the two monomer units in the copolymer brush can thus be obtained from the thickness of each virtual sequence and the density of each polymer and molar mass of each repeat unit as follows:

$$\frac{n_{HEMA}}{n_{DMA}} = \frac{\rho_{PHEMA}}{\rho_{PDMA}} * \frac{M_w^{DMA}}{M_w^{HEMA}} * \frac{h_{HEMA}}{h_{DMA}} \quad (2),$$

where the density of PHEMA and PDMA is 1.27 g/cm^3[32] and 1.21 g/cm^3[33], respectively, and the molar mass of the HEMA and DMA repeat units is 130.14 and 99.13 g/mol, respectively. The molar composition in HEMA units in the copolymer brush was finally obtained as:

$$\frac{n_{HEMA}}{n_{HEMA} + n_{DMA}} = (1 + \frac{n_{DMA}}{n_{HEMA}})^{-1} = (1 + 1.25 \frac{h_{DMA}}{h_{HEMA}})^{-1} \quad (3)$$

5.4 Results and discussion

5.4.1 Polymer brush synthesis under different reaction conditions

Different reaction conditions were tested in order to grow brushes of reasonable thickness (~100 nm) in a few hours, while having some control over the reaction kinetics, and allowing to find conditions compatible with both HEMA and DMA.

Polymer brush synthesis under conditions 1:

Under these conditions, water was chosen as the solvent, which can accelerate the rate of polymerization when grafting polymer brushes. In order to improve the control of polymerization, a small amount of $CuCl_2$ was added as deactivator. When 6 mmol DMA was added, the thickness of PDMA brush increased very rapidly in the first 15 min and reached ~110 nm, but increased a little after that due to the termination of polymerization in water (Figure 5.1). When DMA was replaced with the same quantity of HEMA, the thickness of PHEMA brush increased quickly in the first 30 min, then increased very slowly after that. The final brush thickness only reached ~40 nm. The PHEMA brush thickness was almost doubled and changed in a similar trend when adding 18 mmol HEMA. P(DMA-*co*-HEMA) brushes were synthesized by varying the DMA/HEMA ratio. The kinetics of synthesis of P(DMA-*co*-HEMA) brushes behaved qualitatively similarly with that of the PDMA brush, but changed quantitatively. As the rate of polymerization of DMA was much greater than the rate of polymerization of HEMA, the rate of polymerization of DMA with HEMA was greater than that the rate of polymerization of HEMA. As a result, the thickness of P(DMA-*co*-HEMA) brush increased with higher concentration of DMA in solution. The final thickness was lower

than the thickness of the pure PDMA brush due to a much more rapid termination. Overall, we conclude that the synthesis of PDMA and PHEMA homopolymer brush and their copolymer brush is very fast and cannot be controlled in pure water, even in the presence of $CuCl_2$.

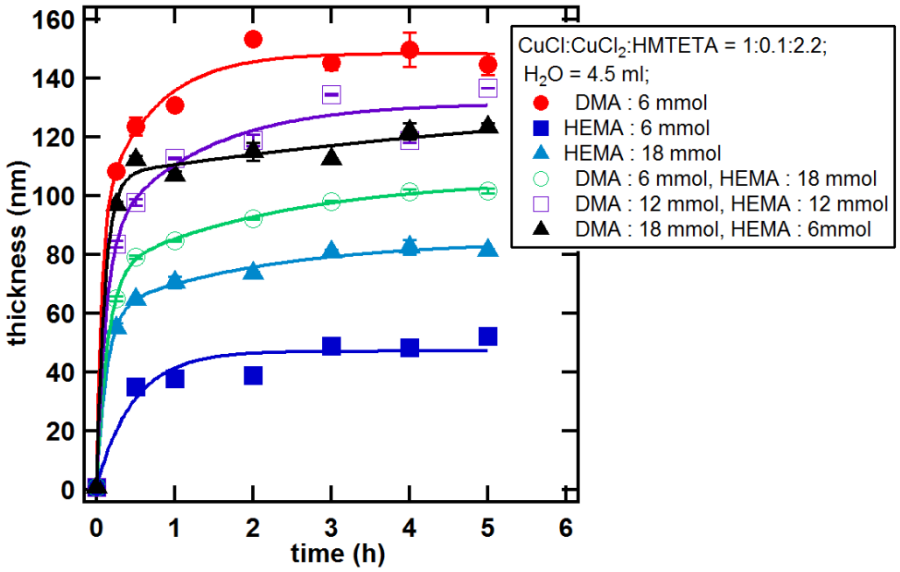

Figure 5.1. Kinetics of brush synthesis of PDMA, PHEMA and P(DMA-*co*-HEMA) determined by the evolution of the ellipsometric brush thickness with time. Reaction conditions: 20°C, CuCl (3.7 mg, 3.7×10^{-2} mmol), $CuCl_2$ (0.5 mg, 3.7×10^{-3} mmol), HMTETA (22 μL, 8.1×10^{-2} mmol). The amount of DMA and HEMA is indicated in the legend.

Polymer brush synthesis under conditions 2:

As the polymerization of PDMA and PHEMA and their copolymerization cannot be controlled in pure water, a water/methanol mixed solvent was used to reduce the termination. At the same time, $CuCl_2$ or $CuBr_2$ were added or not when synthesizing the brushes to increase the control over the polymerization process (Figure 5.2).

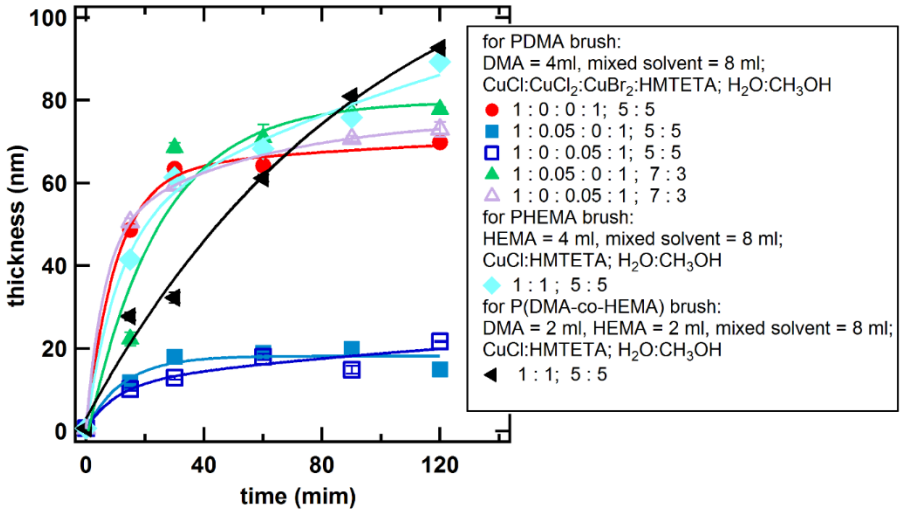

Figure 5.2. Kinetics of the synthesis of homopolymer brushes of PDMA and PHEMA, and of their copolymer brushes, determined by the evolution of the ellipsometric brush thickness with time. Reaction conditions: 20°C, CuCl (7.4 mg, 7.4×10^{-2} mmol), $CuCl_2$ (0.5 mg, 3.7×10^{-3} mmol), $CuBr_2$ (0.8 mg, 3.7×10^{-3} mmol), HMTETA (20 μL, 7.4×10^{-2} mmol), mixed solvent: 8 mL.

The thickness of PDMA brushes increased rapidly in the first 30 min, then increased very slowly when synthesized in a H_2O/CH_3OH 5/5 mixed solvent without any added deactivator. The final brush thickness only reached ~70 nm in 2 h. In the same mixed solvent, the thickness of the PDMA brush was lower but was slightly better controlled upon addition of the deactivating $CuCl_2$ or $CuBr_2$. Increasing the H_2O/CH_3OH ratio was seen to accelerate greatly the rate of polymerization in the first 30 min, without losing much control. The thickness increase of the PHEMA brush was rapid in the first 30 min, but a bit slower at a later stage in H_2O/CH_3OH 5/5 mixed solvent without any deactivator; its brush thickness can reach ~90 nm in 2 h. Interestingly, when synthesizing P(DMA-*co*-HEMA) brush in

H_2O/CH_3OH 5/5 mixed solvent without deactivator, the brush thickness almost increased linearly with time and reached 90 nm in 2 h.

Polymer brush synthesis under conditions 3:

It was found that the synthesis of PHEMA brush can be controlled by using CuCl/HMTETA catalyst system in H_2O/CH_3OH 5/5 mixed solvent without deactivator; unfortunately, the synthesis of the PDMA brush cannot be controlled in 2 h under the same conditions. Therefore, we tried Me_6TREN as alternative ligand. The kinetics of PDMA brush synthesis were studied by adding $CuCl_2$ and $CuBr_2$ or not in pure water or H_2O/CH_3OH 5/5 mixed solvent (Figure 5.3).

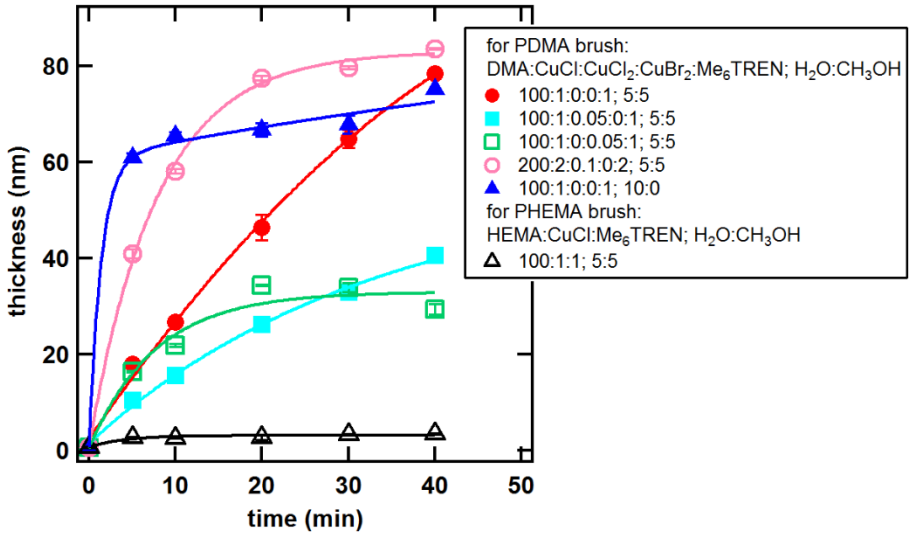

Figure 5.3. Kinetics of synthesis of PDMA and PHEMA brushes determined by the evolution of the ellipsometric brush thickness with time in H_2O/CH_3OH mixed solvents. Reaction conditions: 20°C, DMA (0.77 mL, 7.4 mmol): CuCl (7.4 mg 7.4×10^{-2} mmol): $CuCl_2$ (0.5 mg, 3.7×10^{-3} mmol): $CuBr_2$ (0.8 mg, 3.7×10^{-3} mmol): Me_6TREN (20.06 μL, 7.4×10^{-2} mmol) = 100 : 1 : 0.05 : 0.05: 1, mixed solvent: 8 mL.

In pure water, the thickness of the PDMA brush rapidly increased to ~70 nm, then increased very slowly due to termination. Adding CH_3OH can improve the control over PDMA brush synthesis, although the rate of polymerization slows down. In H_2O/CH_3OH 5/5 mixed solvent, the thickness of PDMA increased linearly with time in the absence of deactivator, corresponding to complete control. In H_2O/CH_3OH 5/5 mixed solvent, adding 5% $CuCl_2$ relative to CuCl decreases the rate of polymerization of DMA, but the thickness of PDMA increases almost linearly with time just with a lower increase rate. When $CuBr_2$ instead of $CuCl_2$ was added, the rate of polymerization of DMA was also decreased, but the brush thickness only increased linearly within 10 min, then increased very slowly. As the dissociation of the alkyl-Br bond is easier than the dissociation of alkyl-Cl bonds, the brush thickness increased faster at the beginning when $CuBr_2$ was added compared to $CuCl_2$. When the concentration of DMA/CuCl/$CuCl_2$/Me_6TREN monomer-catalyst system was doubled, the thickness of PDMA brush increased rapidly to ~80 nm in 20 min; thereafter the brush thickness only increased by a few nanometers.

Although the synthesis of a PDMA brush can be controlled very well in H_2O/CH_3OH 5/5 mixed solvent with a moderate rate of brush thickness increase without deactivator, the rate of polymerization of HEMA in these conditions is too slow, probably due to a very strong complexation between Cu^{II} and Me_6TREN causing the fast termination. The copolymerization of DMA and HEMA thus cannot be performed by using Me_6TREN as the ligand in these conditions.

Polymer brush synthesis under conditions 4:

It has been shown that although the polymerization of DMA can be controlled very well by using the CuCl/Me_6TREN catalyst system in H_2O/CH_3OH 5/5 mixed solvent, the same conditions do not allow controlled polymerization of HEMA, so that the synthesis of P(DMA-*co*-HEMA) brushes cannot be performed in these conditions. However, when CuCl/HMTETA was used as catalyst system in a H_2O/CH_3OH mixed solvent, the kinetics of PDMA, PHEMA and P(DMA-*co*-HEMA) brush synthesis could be controlled to different extents by changing the reaction conditions. Here, in order to synthesize P(DMA-*co*-HEMA) brushes in a controlled way, we tried to use CuCl/HMTETA as catalytic system and water/methanol as solvent. The concentration of DMA and HEMA and DMA/HEMA of different ratios was varied to study their influence on the polymerization. The ratio of water/methanol was also changed to study its impact on the rate of polymerization.

Figure 5.4 shows the polymerization kinetics of PDMA brushes for different DMA concentrations in two different water/methanol mixed solvents (6/4, 5/5). As can be seen, when the concentration of DMA is very low, no matter in which water/methanol mixed solvent, the polymerization of DMA quickly stops. There is no big difference in the polymerization rates of DMA depending on solvent type. The polymerization of DMA was faster by increasing the DMA concentration (DMA/CuCl 500/1), with a much greater effect in the 6/4 than in the 5/5 water/methanol mixed solvent: the polymerization rate of DMA is more than twice faster in 6/4 water/methanol. In both mixed solvents, the polymerization of DMA shows a similar kinetic reaction:

in the first 5 min, the polymerization of DMA is very fast, and then slows down progressively over the next 60 min before it stops.

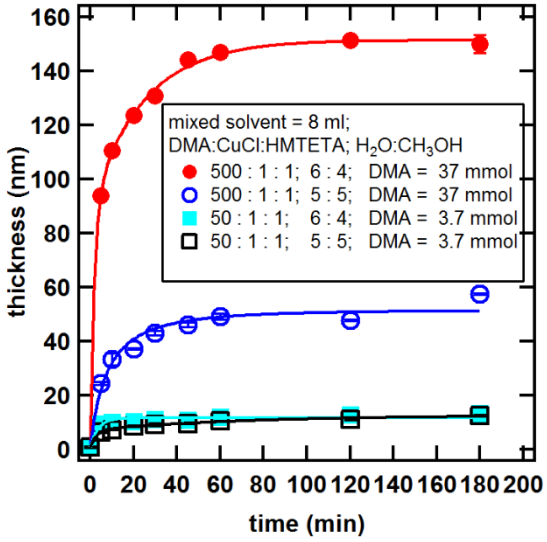

Figure 5.4. Kinetics of the PDMA brush synthesis determined by the evolution of ellipsometric brush thickness with time for different DMA concentrations and different H_2O/CH_3OH ratios. Reaction conditions: 20°C, CuCl (7.4 mg 7.4×10^{-2} mmol), HMTETA (20.06 µL, 7.4×10^{-2} mmol), mixed solvent: 8 mL.

Figure 5.5 shows the polymerization kinetics of PHEMA brushes for different HEMA concentrations in two different water/methanol mixed solvents (6/4, 5/5). The polymerization rates of HEMA in both solutions are very similar. The thickness of the PHEMA brush increases a bit faster in the first 10 min, then increases linearly in the next 40 min, before slowing down progressively, less rapidly than for PDMA. Figure 5.4 and Figure 5.5 suggest that the polymerization of DMA and HEMA exhibits similar global rates, and that they both can be controlled to a limited extent in the same conditions; therefore, they can probably be

copolymerized to prepare copolymer brushes. In addition, it is clear that the water content of the solvent has stronger effects on the polymerization of DMA than on the one of HEMA.

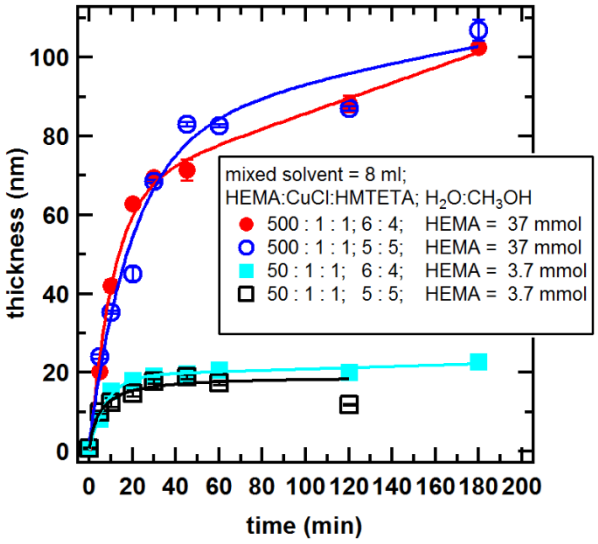

Figure 5.5. Kinetics of the PHEMA brush synthesis determined by the evolution of ellipsometric brush thickness with time for different HEMA concentrations and different H_2O/CH_3OH ratios. Reaction conditions: 20°C, CuCl (7.4 mg 7.4×10^{-2} mmol), HMTETA (20.06 µL, 7.4×10^{-2} mmol), mixed solvent: 8 mL.

Considering their somewhat similar polymerization kinetics, P(DMA-*co*-HEMA) brushes were synthesized. In order to study the effect of water on the copolymerization of DMA with HEMA, different water/methanol ratios were chosen, with 10% HEMA in solution (Figure 5.6). Water was found to accelerate the copolymerization of DMA with HEMA. In the first 5 min, the thickness of P(DMA-*co*-HEMA) brushes increases rapidly, then it progresses continuously while slowing down and saturating after *ca.* 100 min. In 60 min

polymerization time, the thickness of P(DMA-*co*-HEMA) brushes reaches 26, 53 and 130 nm in 4/6, 5/5 and 6/4 water/methanol, respectively. After 180 min, the corresponding thickness is 31, 66 and 182 nm, respectively.

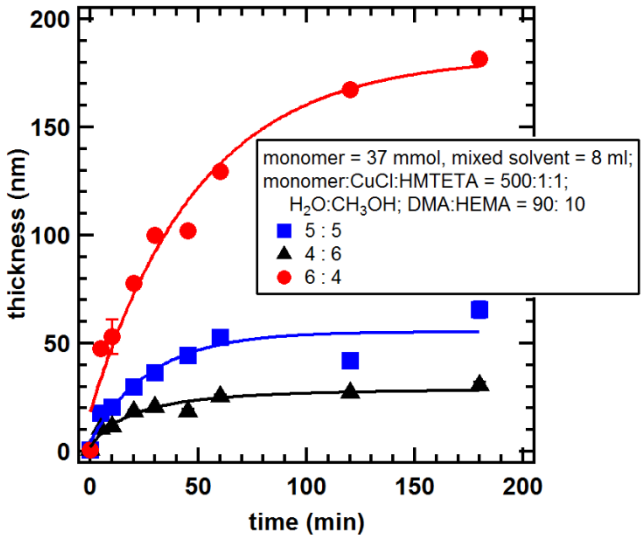

Figure 5.6. Kinetics of P(DMA-*co*-HEMA) (10% HEMA in solution) brush synthesis determined by the evolution of the ellipsometric brush thickness for different H_2O/CH_3OH ratios. Reaction conditions: 20°C, CuCl (7.4 mg 7.4×10^{-2} mmol, HMTETA (20.06 μL, 7.4×10^{-2} mmol), mixed solvent: 8 mL.

In order to synthesize P(DMA-*co*-HEMA) brushes of high thicknesses, the water/methanol 6/4 mixed solvent was chosen as final solvent. Figure 5.7 shows the kinetics of the copolymerization of DMA with HEMA with a monomer/CuCl/HMTETA ratio of 500/1/1 for different DMA/HEMA ratios. The copolymerization of DMA with HEMA behaves in a similar trend, independent on the HEMA content of the solution. In the first 5 min, the rate of the copolymerization is fast,

and then goes on continuously in the next 60 min or so. After that, the rate of the copolymerization slows down greatly. In general, in the first 30 min, the rate of the polymerization increases with decreasing HEMA content in solution. This rule is not fully respected: the rate of copolymerization with 5% HEMA in solution was lower than that with 10% HEMA after 45 min, and the rate of copolymerization with 60% HEMA in solution was greater than that with 20% HEMA.

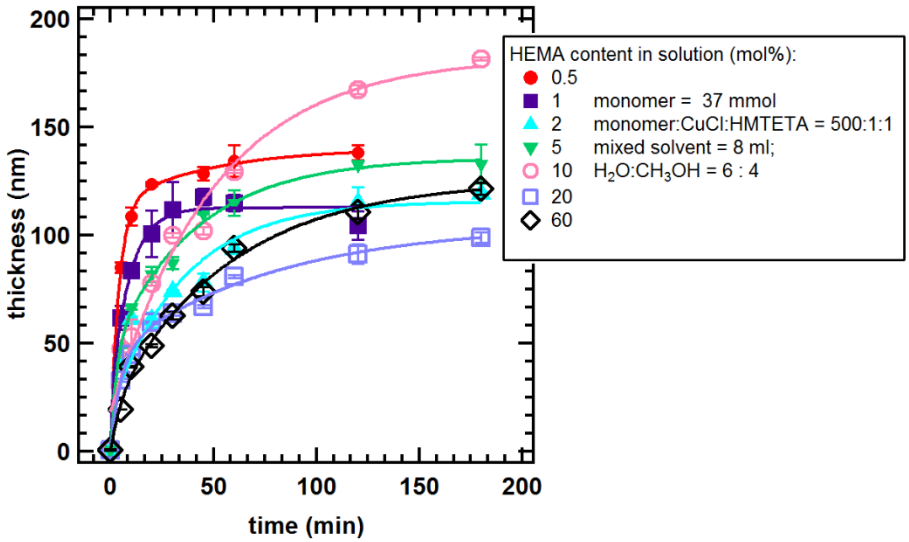

Figure 5.7. Kinetics of P(DMA-*co*-HEMA) brush synthesis determined by the evolution of the ellipsometric brush thickness with time for different DMA/HEMA ratios in 6/4 H_2O/CH_3OH mixed solvent. Reaction conditions: 20°C, CuCl (7.4 mg 7.4×10^{-2} mmol), HMTETA (20.06 µL, 7.4×10^{-2} mmol), mixed solvent: 8 mL.

5.4.2. Thickness and HEMA content of P(DMA-*co*-HEMA) brushes

During the silanization process, as silicon wafers are put onto a Teflon holder, the polished face was exposed to the silane gas, whereas the rough face was in contact with the holder surface. In addition, the rough face might have a quite different specific surface compared to the polished face. Hence, the amount of initiator grafted on both faces might be different, causing differences in brush thickness. In order to know the brush thickness on the rough face, the total thicknesses of P(DMA-*co*-HEMA) brushes were thus measured by FTIR, using homopolymer brushes of PDMA and PHEMA grown from two-face polished silicon wafers as reference samples (see Experimental Section); the total thickness was obtained from the absorbance of the sample, using a calibration relating absorbance to thickness obtained on the reference two-side polished samples. In addition, since the content in HEMA of the copolymer brush could differ from the one of the feed solution, the brush composition was also determined by FTIR. The infrared spectra of PDMA and PHEMA brushes grown from two-side polished silicon wafers and of one copolymer brush grown from a one-side polished wafer are shown in Figure 5.8. From Figure 5.8, it can be seen that there is a strong asymmetrical stretching absorption peak of carbonyl amide I group at ~1638 cm^{-1} for PDMA, while PHEMA has an absorption peak at ~1722 cm^{-1} attributed to its carbonyl group asymmetrical stretching. For the copolymer brush, these two absorption peaks appear separately and clearly at *ca.* 1638 cm^{-1} and 1722 cm^{-1}. By measuring the area of the two absorption peaks of the copolymer brushes, and rescaling by the absorbance per unit thickness measured

on the homopolymer brushes, the thicknesses of the virtual PDMA and PHEMA sequences of the copolymer brush can be determined as described in the experimental section, from which the total brush thickness and the content in HEMA of the brush are obtained. The data on the brush thickness measured by ellipsometry, virtual brush thickness for each monomer, and HEMA content are given in Table S1.

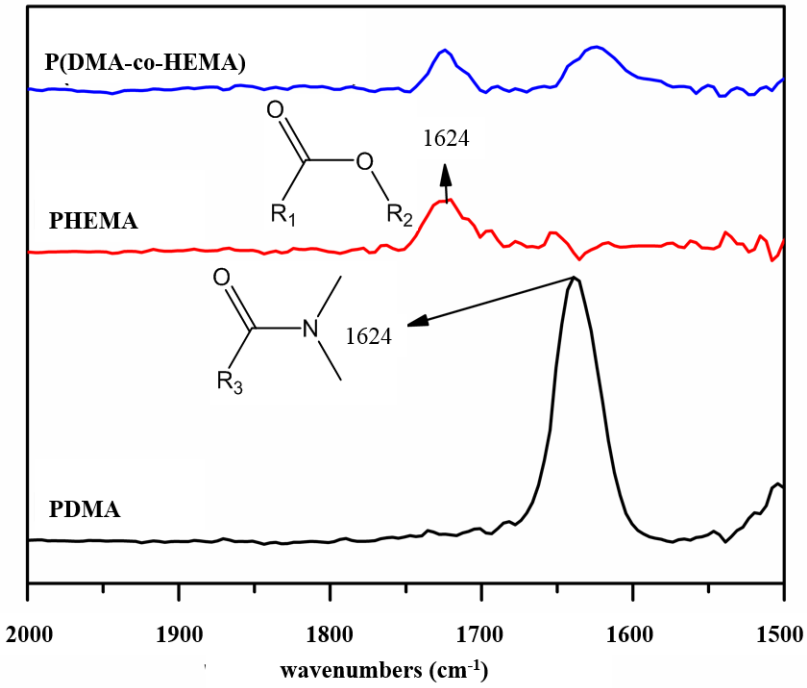

Figure 5.8. FTIR spectra of PDMA and PHEMA brushes grown from two side-polished wafers, and of one P(DMA-*co*-HEMA) brush grown from a one-side polished wafer. Total PHEMA brush thickness: 116.3 nm, total PDMA brush thickness: 384.3 nm, P(DMA-*co*-HEMA) brush thickness on polished surface: 80.8 nm.

Figure 5.9 shows the total thicknesses of copolymer brushes measured by FTIR (two sides, one rough, one polished), compared to the thicknesses of the copolymer brushes measured by ellipsometry on the smooth face only. The thickness of the brush on the rough face is only ~75% of the brush thickness on the smooth face, most probably because the rough face is in contact with the support during the silanization process, decreasing the grafting density of the initiator and therefore the thickness of the brush on the rough face.

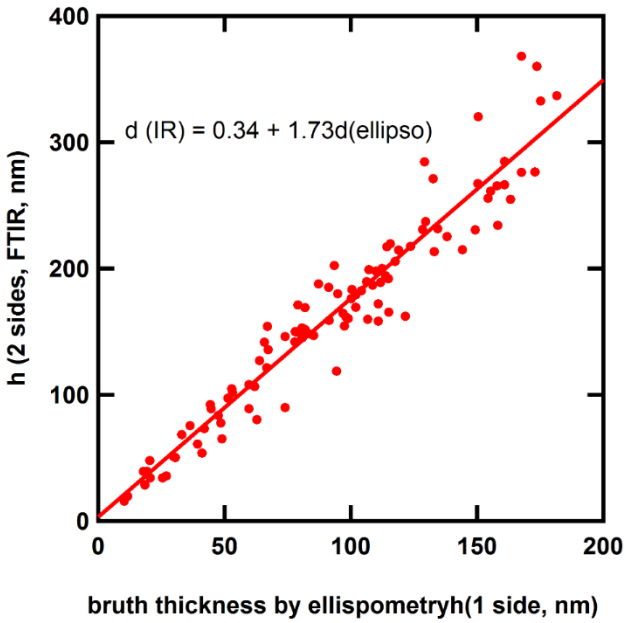

Figure 5.9. Brush thickness by FTIR (two sides) *vs* brush thickness by ellipsometry (polished side only) for all the samples measured in our work.

The generally constant relationship between ellipsometry and FTIR-derived thicknesses, as well as the closeness of the values of thickness measured by the two techniques, provide support to our methodology and therefore for the accuracy of the content in HEMA of

the copolymer brushes determined by FTIR. In addition, it suggests that the deviations from the Beer-Lambert law are not very strong for our samples. The HEMA content of the copolymer brushes is shown in Figure 5.10 as a function of the composition of the feed solutions. The copolymer brush tends to be richer in HEMA units than the feed solution, indicating preferential polymerization of HEMA compared to DMA. Infrared spectra were also acquired on samples for different polymerization times. The HEMA content of the copolymer brushes was found to be essentially time-independent, which is logical since the composition of the feed remains constant all along the process.

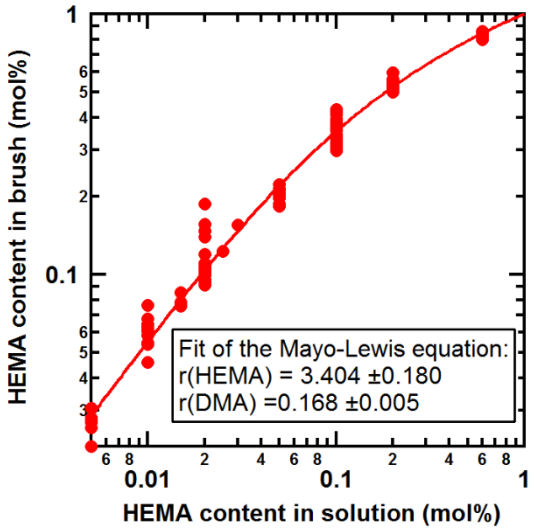

Figure 5.10. HEMA molar fraction in P(DMA-*co*-HEMA) brushes vs HEMA molar fraction in solution. The curve is a fit to the Mayo-Lewis equation.

5.4.3. Mayo-Lewis Analysis and Distribution of Sequence Lengths

The Mayo-Lewis equation relates the molar fraction of comonomer (1) in a polymer chain, f_1, to the one in the feed, F_1, by:

$f_1=(r_1F_1^2 + F_1(1- F_1)) / (r_1F_1^2 + 2F_1(1- F_1) + r_2(1- F_1)^2)$ (1).[34]

The reactivity ratios are defined as $r_i = k_{ii}/k_{ij}$, where k_{ij} are the reaction rate constants of the addition of the monomer j onto a growing chain terminated by a monomer unit i. The data of Figure 5.10 was modeled by the Mayo-Lewis equation, providing r_{DMA} = 0.168±0.005 and r_{HEMA} = 3.404±0.180. This indicates that the chain radical with HEMA as end unit favors the addition of HEMA, and that the chain radical with DMA as end unit also favors the addition of HEMA. As a result, the copolymer brush is richer in HEMA than the feed solution.

The sequence length distribution, which gives the probability to find a sequence of specific length for each monomer of the chain, provides a more complete view of the architecture of the chains. This view is important, because blocks of one monomer units may contribute to create associative structuring effects that would result in significant deviations from expectations based on a simple rule of mixture. In particular, it is especially important to understand whether the HEMA units, onto which azobenzene groups will be grafted in the sequel, are isolated randomly or make strands; this is expected to affect the way the strongly hydrophobic azobenzene units interact in the brush, and thereby the photoresponsiveness of the system.

The sequence distributions were thus computed based on the HEMA content in copolymer brush *vs* the HEMA content in feed solution using the reactivity ratios r_{DMA} and r_{HEMA} obtained from the

original equations of Mayo and Lewis, using standard equations summed up by Smith and Klier[35]:

$$(N_1)_j = (p_{11})^{(j-1)}\, p_{12} \quad (2);$$

$$p_{11} = \frac{r_1}{r1 + ([M2]/[M1])} \quad (3);$$

$$p_{12} = \frac{[M1]}{r1[M1] + [M2]} \quad (4);$$

where $(N_1)_j$ is the probability of having a sequence of monomer 1 of length j, p_{11} is the probability of monomer one connecting to itself, and p_{12} is the probability of monomer 1 being attached to monomer 2. This provides an indirect view on the architecture of the chains (Figure 5.11).

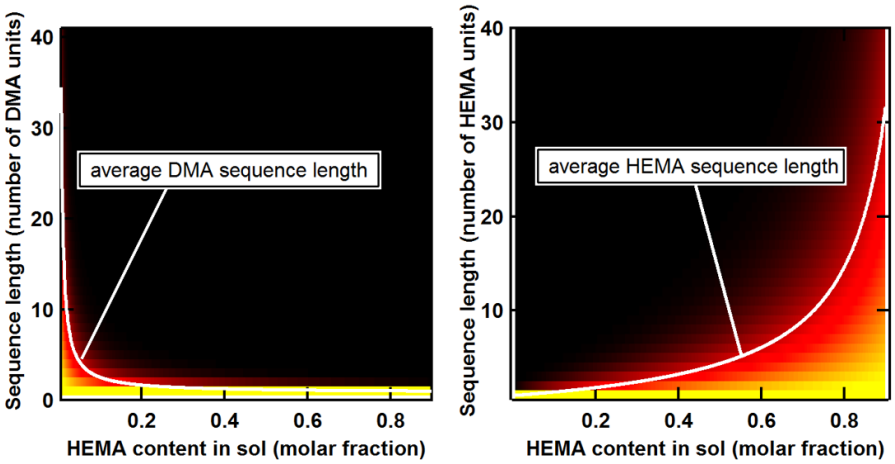

Figure 5.11. Prediction of the sequence length distribution of P(DMA-*co*-HEMA) brushes depending on the concentration of HEMA (in mol%) in the feed solution. Yellow (resp. black) corresponds to higher (resp. lower) probabilities. The maximum of the probability distributions were normalized to unit value for each HEMA content, in order to facilitate comparisons. The thick white lines report the number-average sequence length for each concentration of the feed. The left graph is for PHEMA sequences, the right one for PDMA sequences

For low HEMA contents in solution, the average PDMA sequence lengths are ~18 for brushes grown in the presence of 1% HEMA in solution, and ~9 for brushes grown with 2% HEMA in solution. In both cases, the average PHEMA sequence lengths are close to 1. This means that for a brush grown from solutions of 1% or 2% in HEMA, the chains consist of blocks of ~18 or ~9 DMA units, respectively, separated by one HEMA unit on average. For 20% HEMA in solution, the average DMA and HEMA sequence lengths are close to 1.5-2 for both units. Hence, a statistical copolymer with very short sequences of each monomer units (1-3) is formed, and the composition is close to 50/50 in the brush (52% in HEMA according to Figure. 5.11). For 60% HEMA in the solution, blocks of PHEMA ranging from 1 to 10 units are formed, with an average length of 6 units, separated by DMA sequences of close to 1 unit. It thus appears that by changing the HEMA content in the feed solution, not only is the content of the brush strongly modified, but also the distribution of monomer units.

5.5 Conclusions

The homopolymer brushes of PDMA and PHEMA, and their P(DMA-*co*-HEMA) copolymer brushes, were synthesized under different reaction conditions by SI-ARTP. We found that the system is very sensitive to changes in concentrations, nature of ligand, amount of water in mixed solvents, or presence of deactivators ($CuCl_2$ or $CuBr_2$). The kinetics of growth of PHEMA and PDMA were found to differ notably depending on conditions. After having sampled a relatively large range of conditions, we found a set of conditions allowing to grow relatively thick brushes with some control over the kinetics, for the complete range of HEMA contents. The HEMA content in P(DMA-*co*-HEMA) brushes was then determined by FTIR for these conditions, and the reactivity ratios of DMA and HEMA were determined, indicating that the addition of HEMA over growing chains is preferred. From the experimentally-determined reactivity ratios, we analyzed the structure of the copolymer brushes. For HEMA contents lower than 2% in solution, copolymer brushes consisting of long PDMA sequences separated by isolated HEMA units are most probable, covering a range of HEMA contents in the brushes up to 10% (molar). These conditions are most interesting when one desires to introduce up to 10% functional groups in a PDMA chain, without changing too much the dominant nature of the chain; they will thus be used in the next chapter in order to obtain PDMA-based photochromic brushes.

Chapter 5: Synthesis of Hydrophilic P(DMA-*co*-HEMA) Copolymer Brushes by Surface-initiated ATRP

5.6 Supporting information of brush thickness measured by ellipsometry and FTIR and P(DMA-co-HEMA) brush composition

S1. The brush thickness measured by ellipsometry, visual thickness of each monomer length and HEMA content in brush.

sample	HEMA (solution)	h (nm, ellips)	h_{HEMA} (nm, IR)	h_{DMA} (nm, IR)	C_{HEMA} (brush)
PDMA (ref)	0	384.3			0
PHEMA (ref)	1	116.3			1
P(DMA-co-HEMA)	0.6	19.4	32.7	6.6	0.799
P(DMA-co-HEMA)	0.6	39.3	52.9	8.0	0.840
P(DMA-co-HEMA)	0.6	48.9	55.4	9.8	0.819
P(DMA-co-HEMA)	0.6	62.8	68.5	12.0	0.820
P(DMA-co-HEMA)	0.6	74	76.3	13.6	0.818
P(DMA-co-HEMA)	0.6	94.3	105.2	13.6	0.861
P(DMA-co-HEMA)	0.6	110.8	139.8	18.6	0.857
P(DMA-co-HEMA)	0.6	121.6	141.3	20.8	0.844
P(DMA-co-HEMA)	0.2	33.1	41.4	267.0	0.551
P(DMA-co-HEMA)	0.2	44.7	50.2	38.9	0.508
P(DMA-co-HEMA)	0.2	59.7	60.2	47.9	0.501
P(DMA-co-HEMA)	0.2	63.9	73.8	53.4	0.525
P(DMA-co-HEMA)	0.2	66.9	93.5	60.6	0.553
P(DMA-co-HEMA)	0.2	80.8	89.4	55.9	0.561
P(DMA-co-HEMA)	0.2	91.3	95.2	63.7	0.544
P(DMA-co-HEMA)	0.2	99	104.1	56.5	0.596
P(DMA-co-HEMA)	0.1	47.5	35.9	47.7	0.376
P(DMA-co-HEMA)	0.1	53.1	44.1	57.8	0.379
P(DMA-co-HEMA)	0.1	77.9	58.3	83.6	0.358
P(DMA-co-HEMA)	0.1	100.1	68.1	108.0	0.335
P(DMA-co-HEMA)	0.1	102	66.2	103.1	0.339
P(DMA-co-HEMA)	0.1	129.6	90.9	146.2	0.332
P(DMA-co-HEMA)	0.1	167.5	138.8	229.4	0.326
P(DMA-co-HEMA)	0.1	181.6	125.9	211.0	0.323
P(DMA-co-HEMA)	0.05	48.5	20.4	57.4	0.221
P(DMA-co-HEMA)	0.05	66.7	30.4	90.9	0.211
P(DMA-co-HEMA)	0.05	81.9	41.7	127.3	0.207
P(DMA-co-HEMA)	0.05	87.2	47.4	140.4	0.213
P(DMA-co-HEMA)	0.05	110	47.1	150.8	0.200
P(DMA-co-HEMA)	0.05	114.9	46.5	145.3	0.204
P(DMA-co-HEMA)	0.05	132.6	63.3	207.7	0.196
P(DMA-co-HEMA)	0.05	133.1	47.5	165.9	0.186

References

1. Loschonsky, S. et al. Surface-Attached PDMAA−GRGDSP Hybrid Polymer Monolayers that Promote the Adhesion of Living Cells. *Biomacromolecules* **9**, 543-552 (2008).
2. Kobayashi, M. & Takahara, A. Tribological properties of hydrophilic polymer brushes under wet conditions. *Chem. Rec.* **10**, 208-216 (2010).
3. Gao, G. et al. Antibacterial surfaces based on polymer brushes: investigation on the influence of brush properties on antimicrobial peptide immobilization and antimicrobial activity. *Biomacromolecules* **12**, 3715-3727 (2011).
4. Gao, G. et al. The biocompatibility and biofilm resistance of implant coatings based on hydrophilic polymer brushes conjugated with antimicrobial peptides. *Biomaterials* **32**, 3899-3909 (2011).
5. Banerjee, I., Pangule, R.C. & Kane, R.S. Antifouling coatings: recent developments in the design of surfaces that prevent fouling by proteins, bacteria, and marine organisms. *Adv. Mater.* **23**, 690-718 (2011).
6. Krishnamoorthy, M., Hakobyan, S., Ramstedt, M. & Gautrot, J.E. Surface-initiated polymer brushes in the biomedical field: applications in membrane science, biosensing, cell culture, regenerative medicine and antibacterial coatings. *Chem. Rev.* **114**, 10976-11026 (2014).
7. Chen, X.Y., Armes, S.P., Greaves, S.J. & Watts, J.F. Synthesis of Hydrophilic Polymer-Grafted Ultrafine Inorganic Oxide Particles in Protic Media at Ambient Temperature via Atom

Transfer Radical Polymerization: Use of an Electrostatically Adsorbed Polyelectrolytic Macroinitiator. *Langmuir* **20**, 587-595 (2004).

8. Housni, A., Zhao, Y. & Zhao, Y. Using polymers to photoswitch the aggregation state of gold nanoparticles in aqueous solution. *Langmuir* **26**, 12366-12370 (2010).
9. Jayachandran, K.N., Takacs-Cox, A. & Brooks, D.E. Synthesis and Characterization of Polymer Brushes of Poly(N,N-dimethylacrylamide) from Polystyrene Latex by Aqueous Atom Transfer Radical Polymerization. *Macromolecules* **35**, 4247-4257 (2002).
10. Kizhakkedathu, J.N. & Brooks, D.E. Synthesis of Poly(N,N-dimethylacrylamide) Brushes from Charged Polymeric Surfaces by Aqueous ATRP: Effect of Surface Initiator Concentration. *Macromolecules* **36**, 591-598 (2003).
11. Matyjaszewski, K. & Tsarevsky, N.V. Nanostructured functional materials prepared by atom transfer radical polymerization. *Nat. Chem.* **1**, 276-288 (2009).
12. Chen, T., Ferris, R., Zhang, J., Ducker, R. & Zauscher, S. Stimulus-responsive polymer brushes on surfaces: Transduction mechanisms and applications. *Prog. Polym. Sci.* **35**, 94-112 (2010).
13. Barbey, R. et al. Polymer Brushes via Surface-Initiated Controlled Radical Polymerization Synthesis, Characterization, Properties, and Applications. *Chem. Rev.* **109**, 5437-5527 (2009).

14. Zhao, B. & Brittain, W.J. Polymer brushes: surface-immobilized macromolecules. *Prog. Polym. Sci.* **25**, 677-710 (2000).
15. Xu, F.J., Neoh, K.G. & Kang, E.T. Bioactive surfaces and biomaterials via atom transfer radical polymerization. *Prog. Polym. Sci.* **34**, 719-761 (2009).
16. Pyun, J., Kowalewski, T. & Matyjaszewski, K. Synthesis of Polymer Brushes Using Atom Transfer Radical Polymerization. *Macromol. Rapid Commun.* **24**, 1043-1059 (2003).
17. Yin, X. & Stöver, H.D.H. Probing the Influence of Polymer Architecture on Liquid−Liquid Phase Transitions of Aqueous Poly(N,N-dimethylacrylamide) Copolymer Solutions. *Macromolecules* **38**, 2109-2115 (2005).
18. Rademacher, J.T., Baum, M., Pallack, M.E., Brittain, W.J. & Simonsick, W.J. Atom Transfer Radical Polymerization of N,N-Dimethylacrylamide. *Macromolecules* **33**, 284-288 (2000).
19. Xiao, D. & Wirth, M.J. Kinetics of Surface-Initiated Atom Transfer Radical Polymerization of Acrylamide on Silica. *Macromolecules* **35**, 2919-2925 (2002).
20. Teodorescu, M. & Matyjaszewski, K. Atom Transfer Radical Polymerization of (Meth)acrylamides. *Macromolecules* **32**, 4826-4831 (1999).
21. Teodorescu, M. & Matyjaszewski*, K. Controlled polymerization of (meth)acrylamides by atom transfer radical polymerization. Macromol.Rapid Commun. **21**, 190-194 (2000).
22. Neugebauer, D. & Matyjaszewski, K. Copolymerization of N,N-Dimethylacrylamide with n-Butyl Acrylate via Atom

Transfer Radical Polymerization. *Macromolecules* **36**, 2598-2603 (2003).

23. Masci, G., Giacomelli, L. & Crescenzi, V. Atom Transfer Radical Polymerization of N-Isopropylacrylamide. *Macromol.Rapid Commun.* **25**, 559-564 (2004).
24. Kaholek, M. et al. Stimulus-Responsive Poly(N-isopropylacrylamide) Brushes and Nanopatterns Prepared by Surface-Initiated Polymerization. *Chem. Mater.* **16**, 3688-3696 (2004).
25. Xia, Y., Yin, X., Burke, N.A.D. & Stöver, H.D.H. thermal response of norrow-disperse poly(N-isopropylacrylamide) prepared by atom transfer radical polymerization. *Macromolecules* **38**, 5937-5943 (2005).
26. Ye, J. & Narain, R. Water-Assisted Atom Transfer Radical Polymerization of N-Isopropylacrylamide Nature of Solvent and Temperature. *J. Phys. Chem. B* **113**, 676-681 (2008).
27. Beers, K.L., Boo, S., Gaynor, S.G. & Matyjaszewski, K. Atom Transfer Radical Polymerization of 2-Hydroxyethyl Methacrylate. *Macromolecules* **32**, 5772-5776 (1999).
28. Laloyaux, X. et al. Temperature-Responsive Polymer Brushes Switching from Bactericidal to Cell-Repellent. *Adv. Mater.* **22**, 5024-5028 (2010).
29. Robinson, K.L., Khan, M.A., de Paz Báñez, M.V., Wang, X.S. & Armes, S.P. Controlled Polymerization of 2-Hydroxyethyl Methacrylate by ATRP at Ambient Temperature. *Macromolecules* **34**, 3155-3158 (2001).

30. Huang, W., Kim, J.-B., Bruening, M.L. & Baker, G.L. Functionalization of Surfaces by Water-Accelerated Atom-Transfer Radical Polymerization of Hydroxyethyl Methacrylate and Subsequent Derivatization. *Macromolecules* **35**, 1175-1179 (2002).
31. Jonas, A.M., Glinel, K., Oren, R., Nysten, B. & Huck, W.T.S. Thermo-Responsive Polymer Brushes with Tunable Collapse Temperatures in the Physiological Range. *Macromolecules* **40**, 4403-4405 (2007).
32. Peppas, N.A., Moynihan, H.J. & Lucht, L.M. The structure of highly crosslinked poly(2-hydroxyethyl methacrylate) hydrogels. *J. Biomed. Mater. Res.* **19**, 397-411 (1985).
33. Gundogan, N., Okay, O. & Oppermann, W. Swelling, Elasticity and Spatial Inhomogeneity of Poly(N,N-dimethylacrylamide) Hydrogels Formed at Various Polymer Concentrations. *Macromol. Chem. Phys.* **205**, 814-823 (2004).
34. Mayo, F.R. & Lewis, F.M. Copolymerization. I. A Basis for Comparing the Behavior of Monomers in Copolymerization; The Copolymerization of Styrene and Methyl Methacrylate. *J. Am. Chem. Soc.* **66**, 1594-1601 (1944).
35. Smith, B.L. & Klier, J. Determination of monomer reactivity ratios for copolymerizations of methacrylic acid with poly (ethylene glycol) monomethacrylate. *J. Appl. Polym. Sci.* **68**, 1019-1025 (1998).

Chapter 5: Synthesis of Hydrophilic P(DMA-*co*-HEMA) Copolymer Brushes by Surface-initiated ATRP

6 Temperature Dependence of the Surface and Volume Hydrophilicity of DMA-based Photochromic Copolymer Brushes

6.1 Abstract

A series of P(DMA-*co*-HEMA) brushes are synthesized by SI-ATRP, and azobenzene (AZO) groups are grafted onto the HEMA units via either esterification or amination reactions. The composition of the terpolymer is determined by FTIR and UV spectroscopic measurements. The grafting yield of AZO groups decreases with HEMA content increasing, from about 80% at low HEMA contents to *ca.* 30% at high HEMA contents. The reversible photo-isomerization of the AZO groups grafted on polymer brushes upon photo-irradiation is proved by UV spectroscopy and in-situ ellipsometry. The volume and surface hydrophilicities of PDMA-based copolymer brushes grafted or not with AZO groups are studied by in-situ ellipsometry and equilibrium contact angle measurements in water. The volume hydrophilicity of the copolymer brushes can be continuously tuned by changing the HEMA content or by grafting AZO groups. In contrast, the surface of P(DMA-*co*-HEMA) of low to high HEMA content is always hydrophilic and changes little with temperature, as well as the AZO-grafted P(DMA-*co*-HEMA) brushes containing less then 20% HEMA. Only when the HEMA content is higher, the surface hydrophilicity of P(DMA-*co*-HEMA) decreases by addition of AZO groups. Although the AZO groups change their configurations upon irradiation, this change of configuration does not affect significantly the volume and surface hydrophilicities.

Chapter 6: Temperature Dependence of the Surface and Volume Hydrophilicity of DMA-based Photochromic Copolymer Brushes

6.2 Introduction

In chapter 5, it has been mentioned that hydrophilic polymer brushes are critically important in biomedical and biological applications such as cell culturing,[1] lubrication,[2] non-fouling and antibacterial surfaces[3-6] and drug delivery.[7, 8] Depending on the specific application, the extent of attention paid to the volume properties such as volume swelling and surface properties like surface wettability is different. For instance, when hydrophilic polymer brushes are used for drug or biomolecule releasing systems, their volume swelling should be considered due to its great influence on the loading capacity, whereas the surface hydrophilicity becomes a very critical parameter in lubrication[9] and non-fouling[10] applications. In addition to plain hydrophilic polymer brushes, stimuli-responsive polymer brushes are interesting because their volume properties (and to a lesser extent surface properties – as was shown earlier in this thesis) can be dramatically altered by external stimuli such as temperature or pH.[11, 12] Light is another stimulus used to tune reversibly the volume and surface properties of polymer brushes thanks to its neat application, which allows for remote operation without damaging the materials.[13] Here, we restrict ourselves to reversible photo-switching, thereby excluding the numerous works which have been done on systems that can be photo-activated only once.

For photo-responsive polymer brushes bearing photochromic spiropyran groups, the surface wettability was reported to be tunable upon photo-irradiation with different wavelengths of light;[14] however, this was performed in out-of-equilibrium conditions (as defined in previous chapters); in addition, no thickness change was reported in

water, and slight morphological effects were observed in organic solvents. For azobenzene-substituted brushes, small effects were also reported in chapter 4 and in the reference published by Dirani *et al*[15]for OEGMA-based polymer brushes in water. In addition, a recent review[16] highlights the complexity of azobenzene-modified polymer surfaces, for which the dominant factors playing a role in the change of surface wettability are not yet fully elucidated. This might in part be due to inappropriate, out-of-equilibrium measurements, sometimes combined with simplistic views derived from 'cartoon chemistry'. In this chapter, we will attempt to investigate more deeply the behavior of azobenzene-modified hydrophilic polymer brushes with the tools we have developed before.

There has been considerable work done on the behavior in water of water-soluble polymers substituted by azobenzene. As the azobenzene changes configuration and polarity upon irradiation, the interaction parameter of the polymer with water is expected to change and results in a modification of excluded volume and critical temperature (LCST). A summarized information is provided in Table 6.1. A significant amount of work was performed on thermo-responsive polymers such as PNIPAM.[17-26] $PMEO_2MA$ and related polymers,[15, 27-29] or PDMAEMA,[30] with different grafting methodologies used to connect the azobenzene groups. The reported change of LCST upon irradiation was most of the time modest, below 5 °C, except for two reports by Irie et al.[23] and Kroeger et al.[31] in which slightly larger shifts of LCST of 6.6 and 7.6 °C were measured upon irradiation, and a more recent work by Akiyama et al.[24] in which a shift of 12°C was obtained using short PNIPAM chains with an azobenzene end-group. In our group,[15] we also

observed small variations of swelling of azobenzene-substituted $PMEO_2MA$-based brushes upon UV irradiation and no change of the brush collapse transition temperature. Taken together, these previous studies suggests that the substitution of thermo-responsive polymers by azobenzene groups is not likely to lead to a strong control of brush properties by light.

Chapter 6: Temperature Dependence of the Surface and Volume Hydrophilicity of DMA-based Photochromic Copolymer Brushes

Table 6.1. Literature data showing the chemical composition (*i.e.* polymer backbone (column 2) and number of polymer after incorporating AZO groups (column 3)) of polymers bearing AZO groups, the technique used to synthesize polymers before and after incorporating AZO groups (column 4), the state in which the responsive behavior of the polymers was investigated (column 5), the AZO content in these polymers (column 6), the LCST of the polymer backbone (column 7) and the AZO-modified polymers before (column 8) and after UV irradiation (column 9) and the variation of LCST of AZO-modified polymers resulting from UV irradiation (column 10). The chemical structures of the polymers before and after incorporating AZO groups are shown in Figure 6.1 and Figure 6.2, respectively and the structure of AZO groups and linkers can be seen in Figure 6.2.

1	2	3	4	5	6	7	8	9	10	11
sample number	polymer without AZO	polymer with AZO	technique of synthesis of polymer	polymer state	Azo content/ mol%	LCST of polymer/°C	LCST of polymer-AZO/°C,dark	LCST of polymer-AZO /°C,UV	ΔLCST/ °C,UV	Ref.
0	PDMA	P10	RAFT	solution and brush	10	111	42	27	-15	44
1	PDMA	P10	RAFT	solution	12,5	111	33,5	21,5	-12	28
2	PDMA	P11	RAFT	solution	8,1	111	28	17	-11	28
3	PDMA	P10	free radical polymerization	solution	6	111	46	37	-9	40
4	PDMA	P10	free radical polymerization	solution	9,6	111	42	37	-5	39
3	PDMA	P10	free radical polymerization	solution	1	-	33,7	33	-0,7	43
4	PDMA	P12	free radical polymerization	brush	8	111	34	38	4	47
5	PDMA	P13	post-polymerization	solution	12	111	37,9	45,2	7,3	21
6	PDMA	P12	free radical polymerization	solution	5,9	111	39	47	8	40
7	PDMA	P12	free radical polymerization	solution	-	111	-	-	20,4	39
8	P1	P14	free radical polymerization + post-modification	solution	1	-	33,7	33	-0,7	17
9	P1	P15	free radical polymerization + post-modification	solution	4	-	27,3	27,6	0,3	17
10	P2	p16	free radical polymerization + post-modification	solution	5	-	17	18,8	1,8	17
11	PNIPAM	P17	RAFT	solution	2,6	31	21	23,5	2,5	28
12	PNIPAM	P18	free radical polymerization	solution	1,9	31,9	21	23,5	2,5	19
13	PNIPAM	P19	free radical polymerization	solution	1,8	31,9	21,5	24,5	3	19
14	PNIPAM	P20	free radical polymerization	gel	3,1	27	18	21	3	20
15	PNIPAM	P21	free radical polymerization	solution	3	31	20,5	23,7	3,2	21
16	PNIPAM	P22	free radical polymerization	solution	1,9	31,9	13,8	17,3	3,5	19
17	PNIPAM	P23	free radical polymerization	solution	2,1	31,9	24,4	27,9	3,5	19
18	PNIPAM	P24	free radical polymerization	gel	1,9	35,6	32,3	36	3,7	25
19	PNIPAM	P25	ATRP	solution	7	31	-	-	12	24
20	P3-co- P4	P26	ATRP + click chemisty	solution	1,4	31	23,6	27,7	4,1	26
21	P5	P27	free radical polymerization + post-modification	solution	1,7	50	23,3	27,7	4,4	31
22	P5	P28	free radical polymerization + post-modification	solution	3,1	50	20	27,6	7,6	31
23	P6	P29	free radical polymerization + post-modification	solution	-	-	-	-	0	32
24	P6	P30	free radical polymerization + post-modification	solution	-	-	-	-	0	32
25	P7	P31	RAFT	solution	2,8	27	18	21	3	28
26	P8	P32	ATRP	solution	5	44	-	3	-	30
27	P9	P33	RAFT+ post-modification	solution	12	43,4	-	4,3	-	29

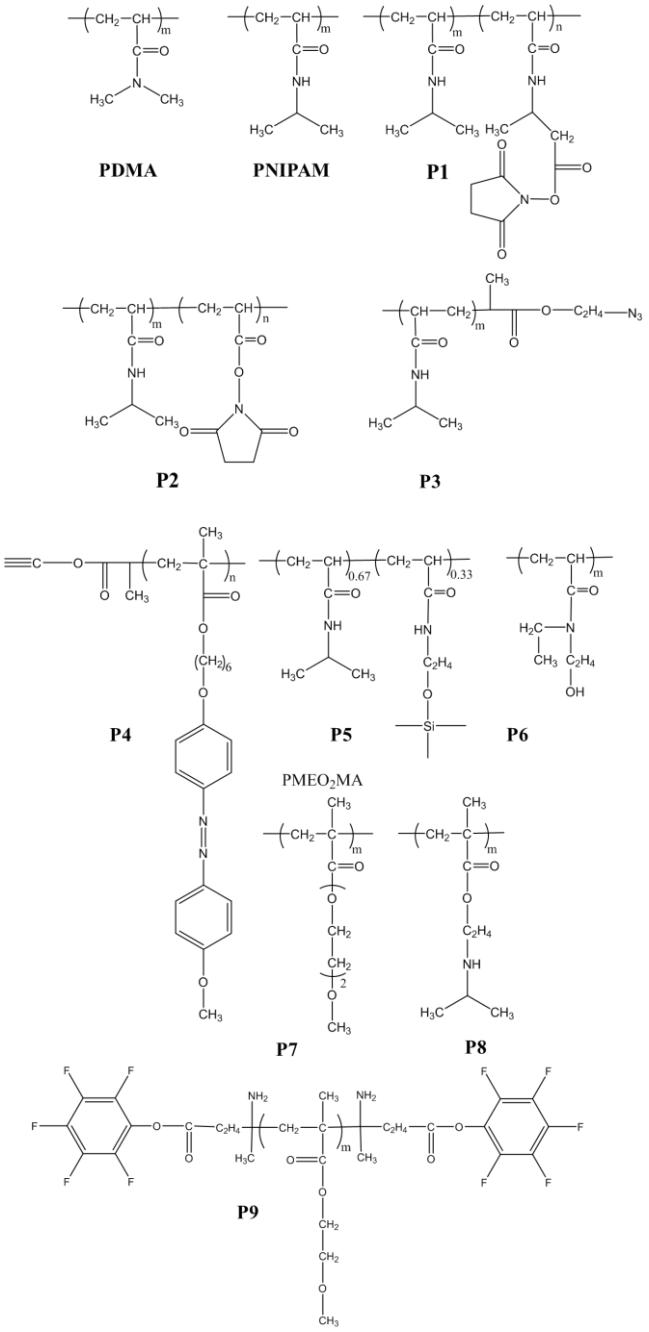

Scheme 6.1. Chemical structures of polymers used in table 6.1 to synthesize photo-responsive polymers.

Chapter 6: Temperature Dependence of the Surface and Volume Hydrophilicity of DMA-based Photochromic Copolymer Brushes

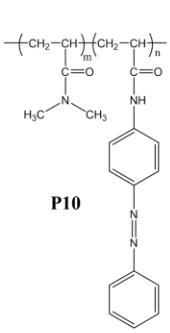

P10

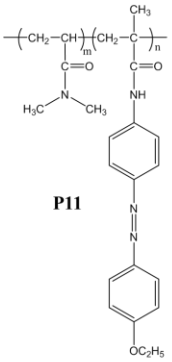

P11

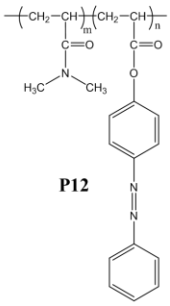

P12

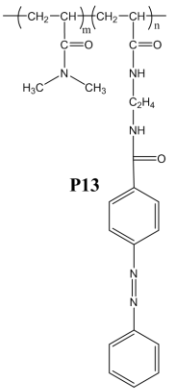

P13

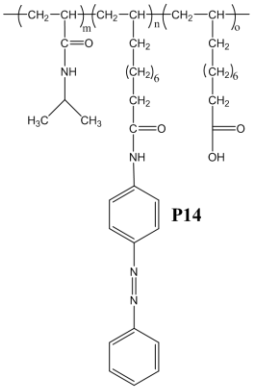

P14

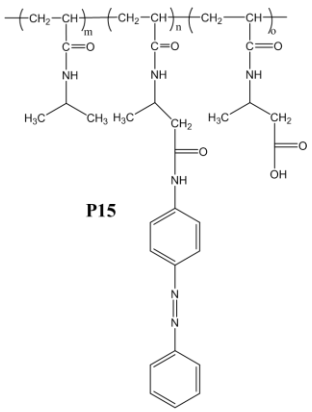

P15

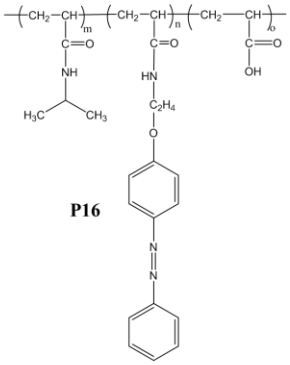

P16

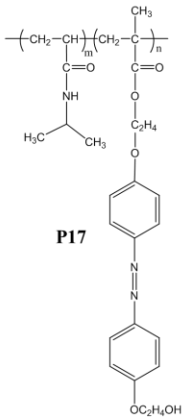

P17

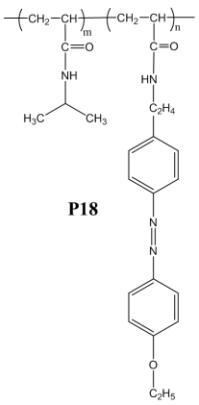

P18

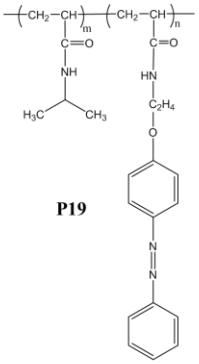

P19

Chapter 6: Temperature Dependence of the Surface and Volume Hydrophilicity of DMA-based Photochromic Copolymer Brushes

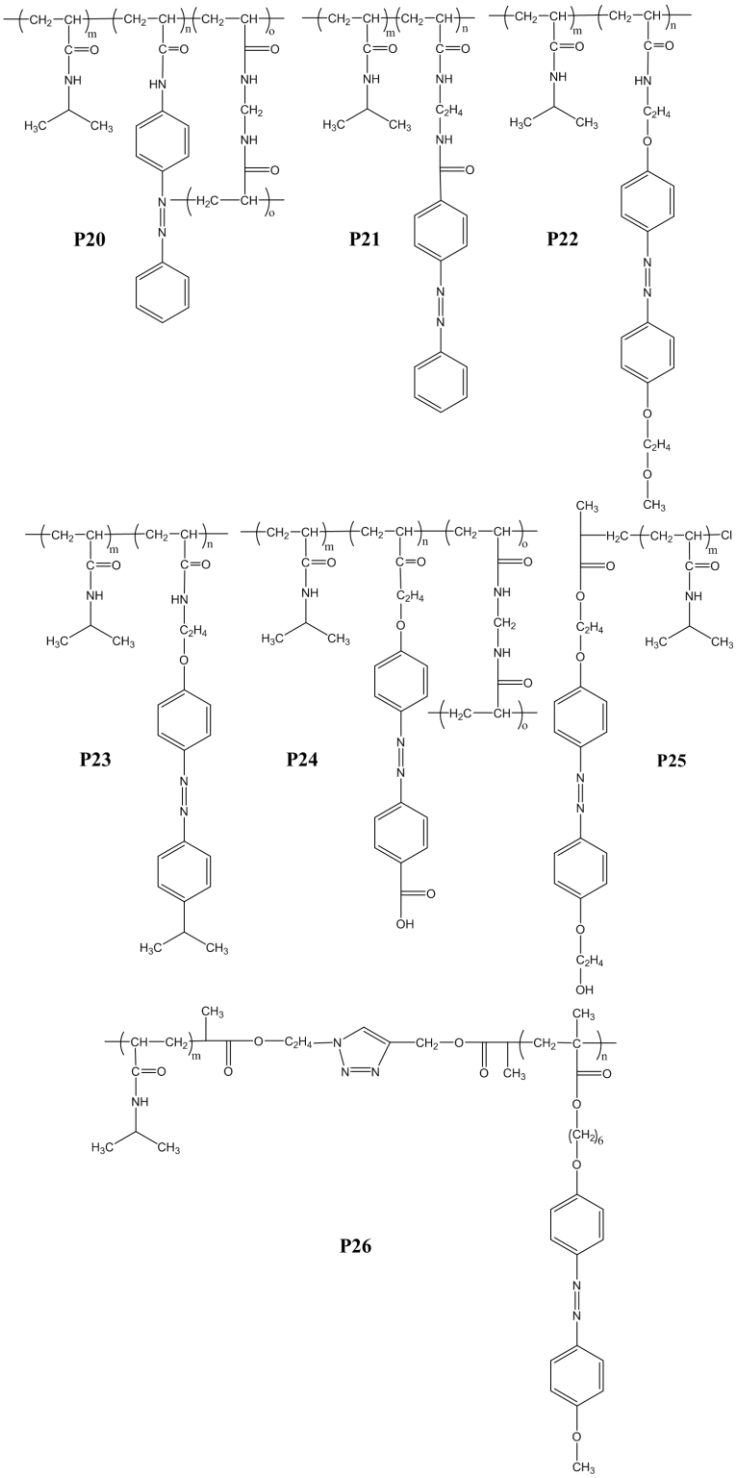

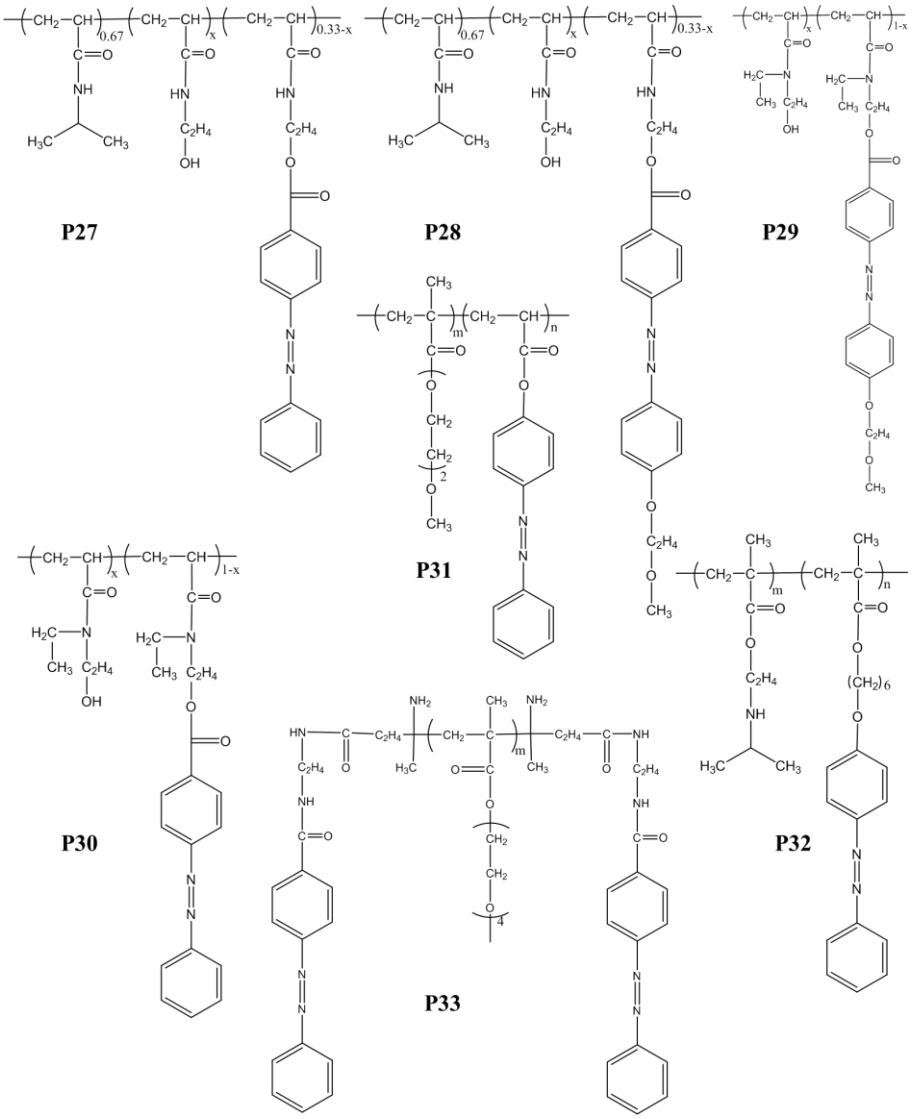

Scheme 6.2. Chemical structures of the photo-responsive polymers synthesized in table 6.1.

More intriguing are reports dealing with non-thermo-responsive water-soluble polymers substituted by azobenzene moieties. Menzel et al.[32] studied the behavior in solution of azobenzene-substituted poly(*N*-ethyl-*N*-(2 hydroxyethyl)acrylamide); the addition of azobenzene

resulted in the appearance of a cloud point which shifted towards lower temperatures for increasing azobenzene content, reaching 30°C for 8 mol% of azobenzene. This cloud point was however found not to be affected by UV irradiation. Likewise, our own work on POEGMA-based brushes (chapter 4) indicated only modest variations of swelling upon irradiation. However, a fully different situation emerges when considering PDMA. The addition of azobenzene-substituted units also results in the apparition of a cloud point; this cloud point was reported to vary upon UV irradiation. The variation varies strongly depending on the report, being as large as -15°C or +20°C, and sometimes close to zero (Table 6.1). It is difficult to understand the source of this variability, which does not seem to originate from the mode of grafting of the azobenzene (Table 6.1), nor on molar mass. In all cases, the degree of substitution remains modest, below 12 mol%; this is logical, since larger degrees of substitution are likely to make the polymer insoluble in water. As the reasons for this wide and even antagonist distribution of responses are not clear yet, further investigation about PDMA and its copolymers needs to be conducted before they can be used for biomedical applications as photo-responsive polymer brushes.

PDMA is a very important hydrophilic polymer, which has a very high LCST estimated to be above 100 °C in pure water.[33, 34] Therefore, its thermo-sensitiveness is usually unobvious. However, it can also be copolymerized with more hydrophobic comonomers to tune its LCST into a proper value as wanted.[33-35] In chapter 5, P(DMA-*co*-HEMA) brushes of different HEMA contents have been synthesized by SI-ATRP in a controlled way. In this chapter, the temperature dependence of volume and surface hydrophilicity of these copolymer brushes are

studied by in-situ ellipsometric measurement and equilibrium contact angle measurement in water. Besides, the copolymer brushes are grafted with azobenzene (AZO) groups connected by different linkages via DSC-activated esterification or amination to impart them with photo-responsiveness. The HEMA content of the copolymer brush is then determined by FTIR as described in chapter 5, and the yield of grafting of the azobenzene is calculated by UV spectroscopy. The volume swelling and surface wettability of the photo-responsive copolymer brushes are then measured in water as already detailed before. Additionally, the volume swelling property dependent on photo-irradiation is also studied in water. Although the photo-reversible photochromism of AZO in the brushes was confirmed by UV spectroscopy, our results indicate that the photo-response of the brushes with respect to swelling or surface properties is again very small, casting serious doubt on the possibility to use azobenzene units to control the behavior of polymer brushes in water.

6.3 Materials and Experiments

6.3.1 Materials

N,*N*-dimethylacrylamide (DMA) and 2-hydroxyethyl methacrylate (HEMA) were purchased from Sigma-Aldrich. DMA was purified by distillation under vacuum at ~70°C before use. HEMA was run three times through an aluminum oxide column. Copper (I) chloride (99.995+%) (CuCl), 1,1,4,7,10,10-hexamethyltriethylenetetramine (HMTETA, 97%), pentafluorophenyl trifluoroacetate (98%), *N*-hydroxysuccinimide (NHS, 98%) and ethylenediamine (99.5%) were purchased from Sigma-Aldrich. *N*,*N*'-disuccinimidyl carbonate (DSC,

98%), 4-(dimethylamino)pyridine (DMAP, 99%), and *N*,*N*'-dicyclohexylcarbodiimide (DCC, 99%) were from Acros. 4-(phenylazo)benzoic acid (98%) was purchased from TCI. Methanol (99.8%) and ethanol (99.8%) were from VWR. Milli-Q water (resistivity: 18.2 MΩ.cm) was obtained from a Millipore system. When needed, water was degassed by heating under argon. Silicon wafers (<100> orientation) were obtained from ACM (France). The ATRP silane initiator (3-(chlorodimethylsilyl)propyl 2-bromo-2-methylpropanoate) was synthesized as described previously.[36]

6.3.2 Azobenzene synthesis

Two azobenzene derivatives with different structures were grafted on the P(DMA-*co*-HEMA) polymer chains), since the photo-irradiation of different structural azobenzene groups might influence differently the volume and surface properties of photo-responsive polymers or brushes. One is the commercial product 4-(phenylazo)benzoic acid (**AZO-COOH**) (shown in Scheme 6.3) and the other is *N*-(2-aminoethyl)-4-(2-phenyldiazenyl)benzamide (**AZO-NH$_2$**) synthesized according to the literature (Scheme 6.3).[21] Briefly, 4-(2-phenyldiazenyl)benzoic acid was reacted with pentafluorophenyl trifluroacetate to form an active pentafluorophenyl 4-(2-phenyldiazenyl)benzoate molecule. A large excess of ethyelnediamine was slowly added into pentafluorophenyl 4-(2-phenyldiazenyl)benzoate in THF to obtain **AZO-NH$_2$**. The ^{1}H-NMR spectra are similar to those obtained in the reference.[21]

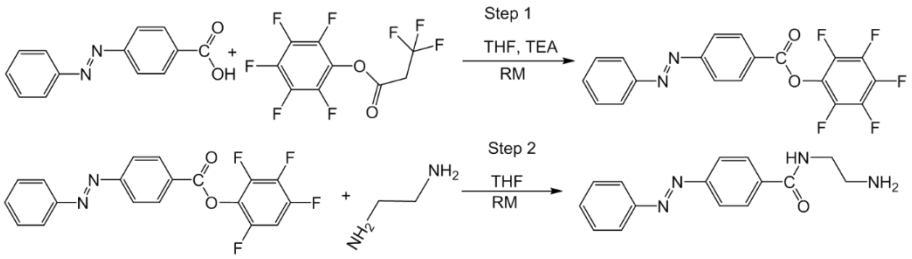

Scheme 6.3. Description of the synthesis of *N* -(2-aminoethyl)-4-(2-phenyldiazenyl)benzamide.

6.3.3 Determination of the extinction coefficient by Ultraviolet-visible (UV) spectroscopy

The UV absorbance spectra of free AZO chromophores were measured for a series of concentrations in methanol and ethanol by UV/visible spectrometry on a Varian Cary 50 in the wavelength range 200-800 nm, with a scan rate of 4 nm/s. According to the Beer-Lambert Law: $A = \varepsilon \times c \times l$, where A is the absorbance of the light, c is the concentration of the substance, l is the length of the pathway of light (here l = 1 cm), and ε is the extinction coefficient. From the slope of the curve of absorbance versus concentration, the extinction coefficient can be determined in methanol and ethanol.

6.3.4 Grafting azobenzene groups onto P(DMA-*co*-HEMA) brushes

The copolymer brushes were first activated with *N*,*N*′-disuccinimidyl carbonate (DSC) prior to coupling with the AZO-NH_2 compound. Each sample was immersed in a solution composed of DSC (0.20 mmol per sample) and 4-dimethylaminopyridine (DMAP, 0.20 mmol per sample) in DMF (2 mL per sample) for 1 h. The samples were removed, washed with DMF and directly immersed into a solution

containing AZO-HN_2 (0.15 mmol per sample) in DMF (2 mL per sample). After 24 h reaction, the samples were taken out and washed several times with DMF and methanol, and finally washed under ultrasonic vibration for ~ 1 min in methanol to completely remove the AZO-NH_2 physically adsorbed on surfaces. The resultant terpolymer brush is called **P(DMA-*co*-HEMA)-CONH-AZO** (Scheme 6.4).

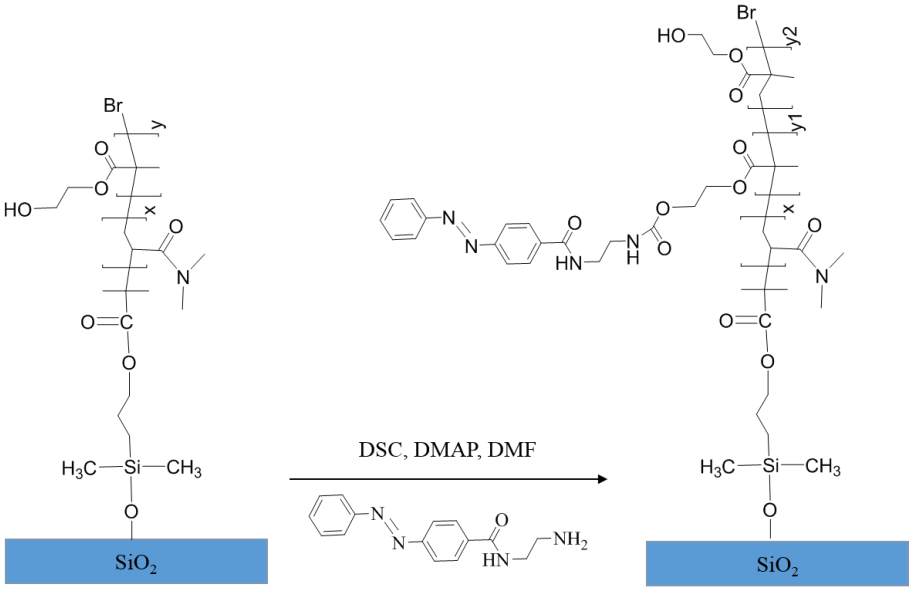

Scheme 6.4. Description of grafting of AZO-NH_2 groups onto a P(DMA-*co*-HEMA) brush.

The P(DMA-*co*-HEMA) brushes grown from quartz and silicon substrates were put in a Schlenk tube, which was sealed with a septum and degassed by several cycles of vacuum/argon (5/5min). 144.6 mg of *N*,*N*'-dicyclohexylcarbodiimide (DCC, 0.7 mmol) and 16.8 mg of DMAP (0.14 mmol) were added into 3.5 mL DMF in a small flask. The mixed solution was stirred for 20 min under argon atmosphere. Then the mixed solution was added into the Schlenk tube in an ice bath. After 10 min, a solution consisting of 3.5 mL DMF and 158.4 mg AZO-

COOH (0.7 mmol) was added slowly into the Schlenk tube. Then, the Schlenk tube was taken out from the ice bath. The samples were taken out at different times and washed with DMF and methanol for several times, and then washed for ~ 1 min in methanol under ultrasonic vibration. The resultant terpolymer brush is called **P(DMA-*co*-HEMA)-OOC-AZO** (Scheme 6.5).

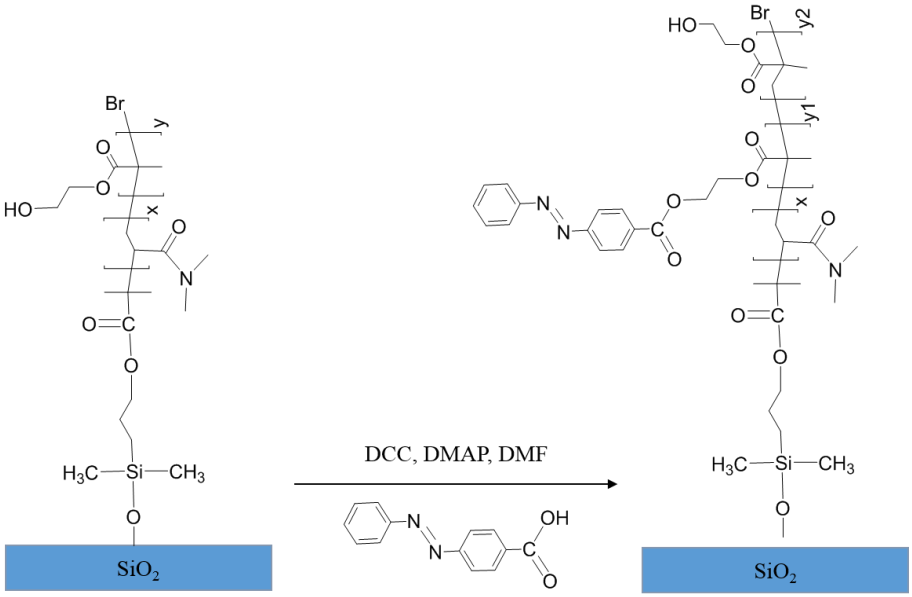

Scheme 6.5. Description of grafting of AZO-COOH groups onto a P(DMA-*co*-HEMA) brush.

6.3.5 Yields of AZO grafted onto P(DMA-*co*-HEMA) brushes

The AZO-specific absorbance of the UV spectra of the copolymer brushes containing pendent AZO groups can be obtained in methanol or ethanol after subtraction of the absorbance spectra of pure polymer brushes in methanol or ethanol. For the measurement of copolymer brushes, the substrate (a quartz slide) was immersed vertically in a UV cuvette filled with methanol or ethanol. The yield of AZO coupling can

be extracted as follows: the AZO surface concentration in a dry polymer brush is:

$$C_{AZO} = ch = A_{br}/\varepsilon \text{ (mol/cm}^2\text{)} \quad (1),$$

where h is the polymer brush thickness, c is the volume concentration of azobenzene, and A_{br} is the absorbance of the AZO-grafted dry polymer brush, integrated from 265 to 400 nm (which is the spectral region of the main absorbance peak of the *trans*-azobenzene). C_{AZO} is the number of moles of AZO groups per unit area of the dry polymer brush. On the other hand, the molar fraction of HEMA units in the copolymer brushes is:

$$f_{HEMA} \approx \rho_{PHEMA} \times h_{PHEMA} / M_{w,HEMA} / (\rho_{PHEMA} \times h_{HEMA} / M_{w,PHEMA} + \rho_{PDMA} \times h_{PDMA} / M_{w,DMA}) \quad (2),$$

where h_{PHEMA} is the thickness of the HEMA virtual sequence in the copolymer brush, $M_{w,HEMA}$ (130.14 g/mol) is the molar mass of HEMA repeat units, and ρ_{PHEMA} (1.274 g/cm^3)[37] is the mass density of the dry PHEMA brush; h_{PDMA} is the thickness of the DMA virtual sequence in the copolymer brush, $M_{w,DMA}$ (99.13 g/mol) is the molar mass of DMA repeat units, and ρ_{PDMA} (1.21 g/cm^3)[38] is the mass density of the dry PDMA brush. The surface concentration of hydroxyl groups in the copolymer brush is:

$$C_{HEMA} = \rho_{PHEMA} \times h_{PHEMA} \times 10^{-7} / M_{w,HEMA} \text{ (mol/cm}^2\text{)} \quad (3),$$

The yield of the AZO coupling in the copolymer brush is then defined as

$$Y_{AZO} = C_{AZO}/C_{HEMA} \quad (4),$$

which was obtained by averaging the yield of AZO measured in methanol and ethanol. Thus the composition of the terpolymer brush in

molar fraction can be defined by two molar fractions, the one of azobenzene-substituted HEMA units:

$f_{HEMA(AZO)} = Y_{AZO} \times f_{HEMA}$ (5),

and the one of non-substituted HEMA units:

$f_{HEMA(OH)} = (1-Y_{AZO}) \times f_{HEMA}$ (6),

the molar fraction in DMA units is obviously:

$f_{DMA} = 1 - f_{HEMA}$ (7).

6.3.6 Photo-isomerization

Photo-isomerization experiments were conducted using a Lightningcure UV Spot light source LC5 from Hamamatsu equipped with a 150 W xenon bulb (L8253) of wavelength ranging from 240 to 2000 nm, and assorted optical fibers. A colored glass filter (Lot Oriel) with a pass band from 290 to 400 nm was used for the *trans*-to-*cis* isomerization, while a filter with a pass band from 400 to 500 nm was used for the *cis*-to-*trans* isomerization. The light intensity is *ca.* 300 mW/cm^2 at the end of the optical fiber.

6.3.7 Volume swelling measurement by ellipsometry

The volume swelling measurements of the copolymer brushes by ellipsometry are described in Chapter 3. Before measuring the P(DMA-*co*-HEMA)-AZO brush under UV light, the sample was first irradiated by UV for 1 h, then the measurements were performed under UV.

6.3.8 Equilibrium contact angle measurement

The equilibrium contact angle measurements are described in Chapter 3.

6.4 Results and discussion

6.4.1 Extinction coefficient determination

Different quantities of AZO groups were dissolved either in methanol or ethanol, thereby making a series of AZO solutions with different AZO concentrations. The absorbance of AZO groups in *trans*-form in each solution was measured at λ = 325 nm by UV spectroscopy. The extinction coefficient was calculated from the slope of the curve of absorbance versus AZO concentration. The extinction coefficient ε of the AZO moieties in methanol and ethanol, integrated over the 265−400 nm spectral range, was determined to be 2.30 × 10^4 $L \cdot mol^{-1} \cdot cm^{-1}$ and 2.04 × 10^4 $L \cdot mol^{-1} \cdot cm^{1}$, respectively, that is 2.30 × 10^7 $cm^2\ mol^{-1}$ and 2.04 × 10^7 $cm^2\ mol^{-1}$, respectively, which are used here.

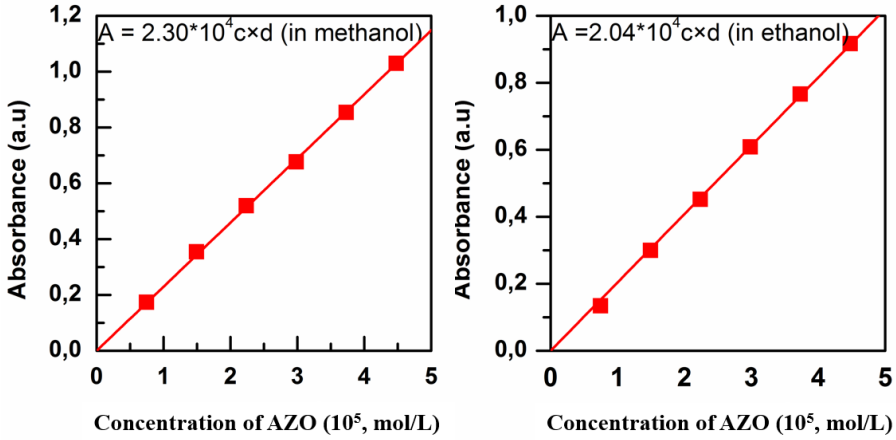

Figure 6.1. Ultraviolet-visible light absorption of AZO groups at λ = 325 nm (at which the maximum absorbance is measured) in methanol and ethanol for different concentrations of AZO.

6.4.2 Yield of AZO grafted onto P(DMA-*co*-HEMA) brushes

The AZO-NH_2 groups were grafted onto P(DMA-*co*-HEMA) brushes of different HEMA content using 24 h reaction time. The grafting yield of AZO-NH_2 in each copolymer brush was measured separately in methanol and ethanol, and averaged to obtain the final value (both values were very close). The grafting yield of AZO-NH_2 decreases when larger amounts of HEMA are present in the brush (Figure 6.2). This variation of the grafting yield results from the steric difficulty to incorporate increasing amounts of azobenzene units in the brushes, which requires chain stretching and therefore decreases entropy. In addition, the sequence length distribution might be another factor to consider, since the average PHEMA sequence length increases with HEMA content: it is easier to graft azobenzene side groups on HEMA groups that are more distant along the chain.

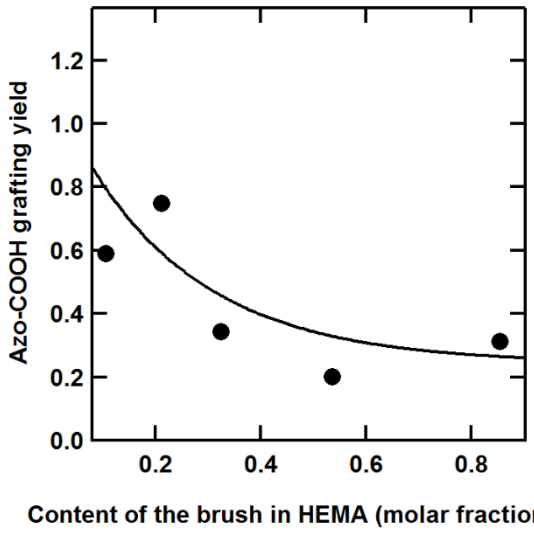

Figure 6.2. Grafting yield of AZO-NH_2 in P(DMA-*co*-HEMA) brushes of different HEMA content (24 h reaction time).

For grafting AZO-COOH onto P(DMA-*co*-HEMA) brushes, only the P(DMA-*co*-HEMA) brushes of low HEMA content were studied, as the grafting yield and HEMA content are already high enough in the copolymer brush to reach the range of azobenzene concentration in the brushes most likely to be of interest. In Figure 6.3 a, the grafting yield of AZO-COOH is displayed versus grafting time for a series of P(DMA-*co*-HEMA) brushes containing ~ 10% HEMA, corresponding to 2% HEMA in solution. The grafting yield of AZO-COOH increases with time and reaches a constant value of *ca.* 80% after 10 h. The grafting yield of AZO-COOH onto P(DMA-*co*-HEMA) with different HEMA contents (below 20%) also reaches ~ 80 % after at least 12 h reaction time (Figure 6.5 b); this is very close to the grafting yield of AZO-NH_2 onto P(DMA-*co*-HEMA) with less than 20% HEMA in the brush. Some fluctuations are observed about 80%, most likely due to variations of monomer content, brush thickness, and brush density.

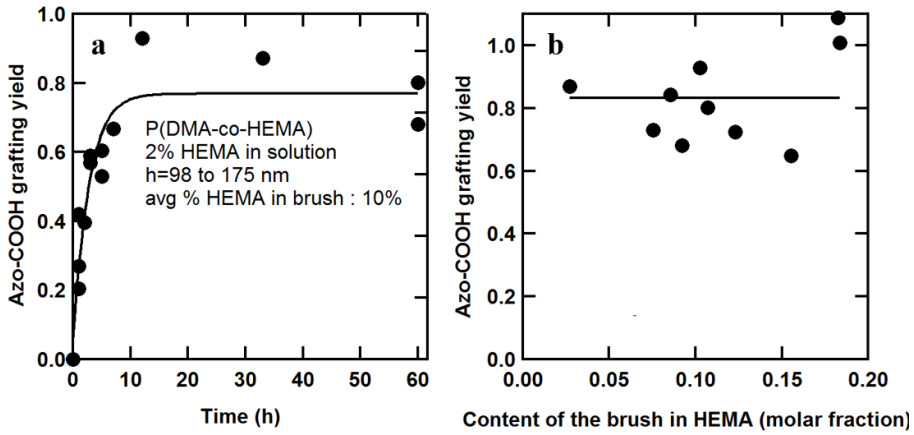

Figure 6.3. Grafting yield of AZO-COOH in P(DMA-*co*-HEMA) brushes: (a) grafting onto brushes of 10% HEMA for different reaction times; (b) grafting onto the brushes of different HEMA contents after more than 12 h reaction.

6.4.3 Photo-isomerization of AZO groups in P(DMA-*co*-HEMA)-CONH-AZO brush

To evaluate the photo-response of the anchored pendent AZO groups and their reversibility, the AZO-grafted P(DMA-*co*-HEMA) brush with ~ 7 mol% HEMA-OH and ~3.3% HEMA-AZO was successively irradiated by light of proper wavelength and its ultraviolet/visible absorption spectra in ethanol were recorded (Figure 6.6). Initially, there is a strong absorbance of *trans*-AZO chromophores at *ca.* 325 nm originating from the AZO π−π* transition (Figure 6.4 a); upon UV irradiation, the intensity of this band decreases and the absorption peak shifts to lower wavenumbers. At the same time, the intensity of the n−π* transition band at *ca.* 440 nm gradually increases due to the isomerization of more AZO chromophores from *trans* to *cis* form (Figure 6.6 b). Irradiation with visible light isomerizes the *cis*-AZO form back to the *trans*-AZO configuration, as evidenced by the spectra gradually reverting to the original curve. This indicates that the AZO-modified P(DMA-*co*-HEMA) brush is not only photo-responsive, but that its photo-responsiveness is also reversible. The reversible isomerization of AZO groups between their *trans* and *cis* form is completed in ~30 min.

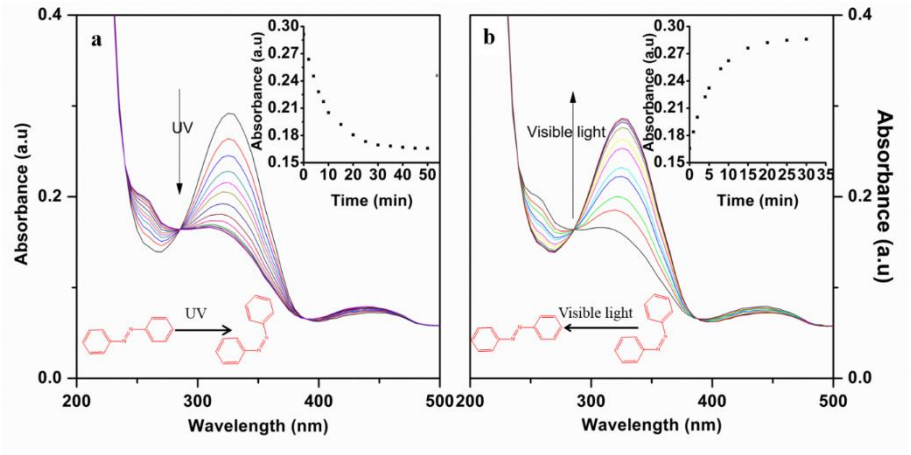

Figure 6.4. Photoisomerization of AZO groups in a P(DMA-*co*-HEMA) brush of ~ 7 mol% HEMA-OH and ~ 3.3% HEMA-AZO measured by UV/visible spectroscopy in ethanol

6.4.4 Swelling coefficients of P(DMA-*co*-HEMA) brushes

The swelling coefficients of P(DMA-*co*-HEMA) brushes with different HEMA contents are shown in Figure 6.5. As PHEMA is poorly water-soluble, the swelling coefficient of a PHEMA brush is low and constant with temperature. In contrast, PDMA is highly water soluble, and the swelling degree of its brush changes gradually but very slowly with temperature. P(DMA-*co*-HEMA) brushes shows a qualitatively similar swelling behavior versus temperature; however, quantitatively, the swelling degree of the copolymer brush decreases strongly with the HEMA content of the brush. Below 20% HEMA in the brush, the swelling degree is close to the one of a pure PDMA brush, indicating high hydrophilicity. Then, the volume hydrophilicity decreases regularly, although not in direct proportion to the HEMA content. For a copolymer brush containing as much as 85% HEMA, the

swelling degree is still much higher than the swelling degree of a pure PHEMA brush.

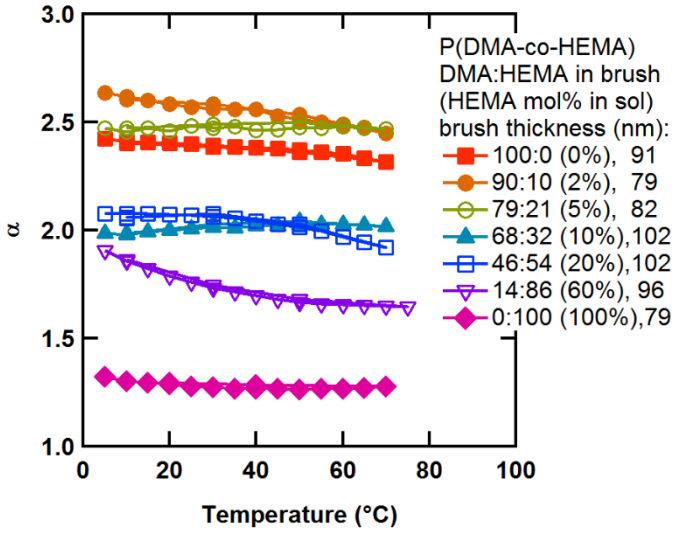

Figure 6.5. Temperature-dependence of the ellipsometry-determined swelling coefficients of P(DMA-*co*-HEMA) brushes with different HEMA contents.

6.4.5 Swelling coefficients of P(DMA-*co*-HEMA)-CONH-AZO brushes

The variation with temperature of the swelling coefficient of P(DMA-*co*-HEMA) brushes grafted with AZO-NH_2 groups is displayed in Figure 6.6. For the sample containing 10% HEMA before AZO grafting (brown trace), the ellipsometric angles were in a region of the ellipsometric diagram in which the brush thickness and index of refraction depend critically on the angle of incidence. Slight errors in the incidence angle, due to refraction at the window/water interface, result in significantly different thickness and indices of refraction, resulting in physically impossible solutions such as an increase of the thickness (which signals water uptake) with a parallel increase of index of refraction (which signals water loss). To get rid of this problem, the

angle of incidence of this sample was corrected by a few degrees until the variation of the index of refraction and of brush thickness agreed. Nevertheless, the precision on this sample is certainly lower.

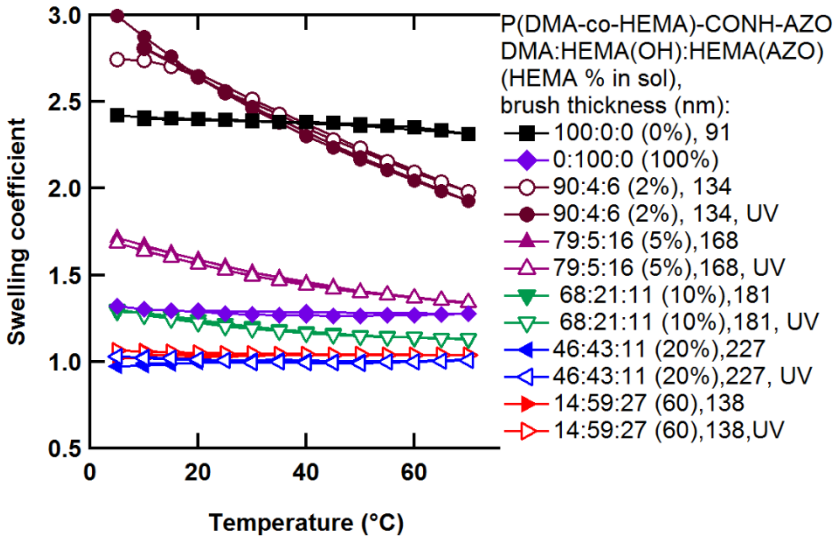

Figure 6.6. Ellipsometry-determined swelling coefficients of P(DMA-*co*-HEMA)-CONH-AZO brushes of different AZO-NH_2 and HEMA contents. The solid symbols are the data measured in the dark; the open symbols are the data measured under continuous UV light irradiation.

Small amounts of AZO groups result in the apparition of a strong temperature dependence, with a more hydrophobic character observed at higher temperatures. This is not sharp enough to qualify as a real collapse transition but is compatible with the observation of a cloud point for azobenzene-substituted PDMA in solution.[39-41] When the content in azobenzene increases, the brushes are increasingly hydrophobic; for large contents in azobenzene and HEMA-OH, the swelling ratio of the terpolymer brush is even lower than the swelling ratio of pure PHEMA, and close to 1. UV light was also used to irradiate

the samples to study the photo-isomerization of AZO groups on the change of the volume swelling (the solid symbols in Figure 6.6 are the data measured in the dark, the open symbols are the data measured under UV light). The swelling coefficients of P(DMA-*co*-HEMA)-CONH-AZO brushes change very modestly upon UV irradiation regardless of the number of AZO groups grafted, suggesting that the change of the polarity due to the configurational change is not large enough to change the volume swelling.

6.4.6 Swelling coefficients of P(DMA-*co*-HEMA)-OOC-AZO brushes

As minor amounts of azobenzene already lead to strong variations of the swelling coefficients of P(DMA-*co*-HEMA) brush, we concentrated on the P(DMA-*co*-HEMA) brushes synthesized in the presence of only 1 to 5% of HEMA in solution, giving rise after grafting to 1 to 10% of azobenzene-substituted monomer units. This degree of substitution in AZO is also in the range of the values for which a UV-induced shift of the cloud point was reported for PDMA-based polymers in solution.[28, 39-44] As the sequence of AZO groups might influence the interaction between polymer chains and water,[41] we focused on AZO-COOH groups grafted for increasing reaction times on P(DMA-*co*-HEMA) brushes synthesized in the presence of 2% HEMA in solution, thereby tuning the grafting yield of AZO at constant chain structure, and on brushes grown in solutions of different HEMA contents grafted with AZO for a reaction time of 60 h. In addition, two brushes were also grown from an initiator layer of reduced density, obtained by silanizing the wafers in the presence of a mixture of

initiator silane and benzyldimethylchlorosilane, with 20 and 30 mol% of initiator silane (samples S11 and S12).

Table 6.2. Nomenclature, conditions of synthesis (grafting density = % of initiator in the silane mixture used to silanize the wafers; mol % of HEMA in solution; reaction time for the grafting of the AZO), fraction of HEMA units with OH groups, fraction of DMA units, fraction of HEMA units substituted by AZO-COOH groups, relative fraction of grafted HEMA units, and brush thickness before and after grafting AZO, for the P(DMA-*co*-HEMA)-OOC-AZO brushes of this study.

sample number	grafting density (%)	HEMA_sol (%)	t_grafting (h)	f_HEMA (OH)	f_DMA	f_HEMA (AZO)	grafting yield_AZO	h_noAZO (nm)	h_AZO (nm)
S0	100	2	1	0.081	0.898	0.021	0.206	104.1	105.7
S1	100	2	2	0.066	0.891	0.043	0.394	110.8	115.8
S2	100	2	3	0.041	0.899	0.059	0.59	97.5	105.3
S3	100	2	7	0.035	0.895	0.07	0.667	113.7	126.7
S4	100	2	12	0.007	0.898	0.095	0.931	149.3	184.4
S5	100	2	60	0.021	0.893	0.086	0.804	158.2	195.1
S6	100	2	1	0.062	0.892	0.045	0.421	114.3	121.1
S7	100	2	3	0.046	0.892	0.061	0.57	115.6	125.1
S8	100	2	5	0.043	0.892	0.065	0.602	175.1	189.2
S9	100	2	1	0.077	0.895	0.028	0.267	155.4	166.4
S10	100	2	33	0.012	0.909	0.079	0.868	96.9	105.2
S11	20	2	60	0.011	0.892	0.096	0.897	94.8	102.6
S12	30	2	60	0.057	0.892	0.051	0.472	78.9	92.7
S13	100	1	60	0.057	0.935	0.0075	0.116	173.6	176.6
S14	100	1.5	60	0.02	0.924	0.055	0.733	150.3	161.4
S15	100	2.5	60	0.034	0.877	0.089	0.724	91.2	108.8
S16	100	3	60	0.055	0.845	0.1	0.645	157.9	185.4
S17	100	5	60	0	0.816	0.184	1	144.2	206.3

The "ψ vs Δ" ellipsometric trajectories of these P(DMA-*co*-HEMA)-OOC-AZO brushes are plotted in Figure 6.7, corresponding to the heating and cooling of the measured samples in the absence of UV irradiation. The variation of ψ and Δ with temperature reflects the change of volume swelling of the brushes with temperature. Significant variations of ψ and Δ with temperature correspond to a large change of volume swelling of the brush versus temperature. It can be seen that significant change of the volume swelling of P(DMA-*co*-HEMA)-

OOC-AZO brush versus temperature happens after grafting, compared to pure PHEMA and PDMA (dark brown and black symbols, respectively). In addition, the reversibility of the swelling is demonstrated for all samples, except S11.

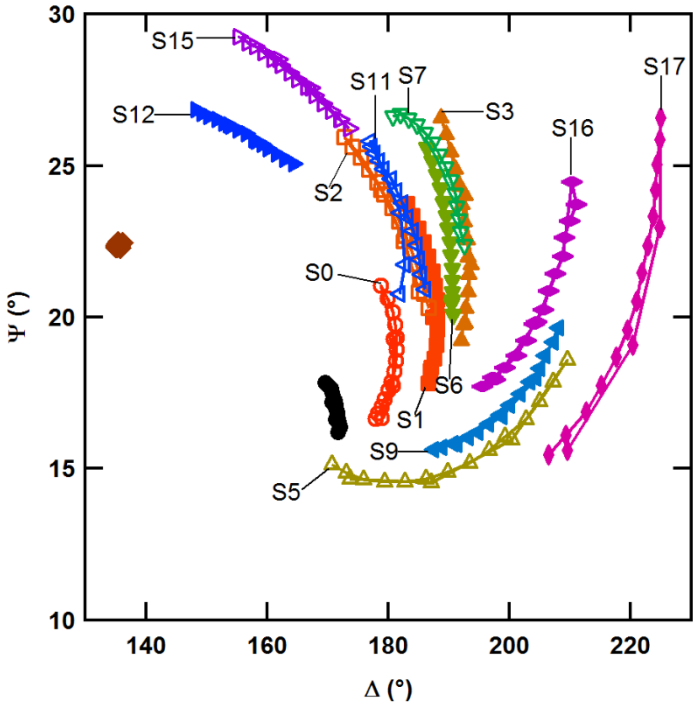

Figure 6.7. Ellipsometric trajectories for P(DMA-*co*-HEMA)-OOC-AZO brushes of different grafting yields of AZO-COOH and HEMA contents in the absence of UV irradiation, drawn as a function of temperature (hidden parameter; heating and cooling ramps are plotted together). The ψ value generally increases with temperature. The numbering of the sample refers to Table 6.2. The dark brown and black points are for pristine PHEMA and PDMA brushes, respectively.

The brush thickness and index of refraction were obtained by fitting the ellipsometric angles (ψ,Δ) as detailed before. However, for some

highly swollen samples, the ellipsometric angles were in a region of the ellipsometric diagram in which an independent determination of the thickness and index of refraction of the brush is not possible. For these samples, the values of thickness and index of refraction were thus not computed for the temperatures corresponding to these regions of the ellipsometric trajectories. This is the case, for instance, of the low temperature points of S0, S9 and S16.

The swelling coefficients of the brushes calculated from the obtained brush thicknesses are shown in Figure 6.8. Each sample is given a color symbol identical to the one of Figure 6.7, and is numbered same as in Table 6.2, in which all the relevant information on the samples is provided.

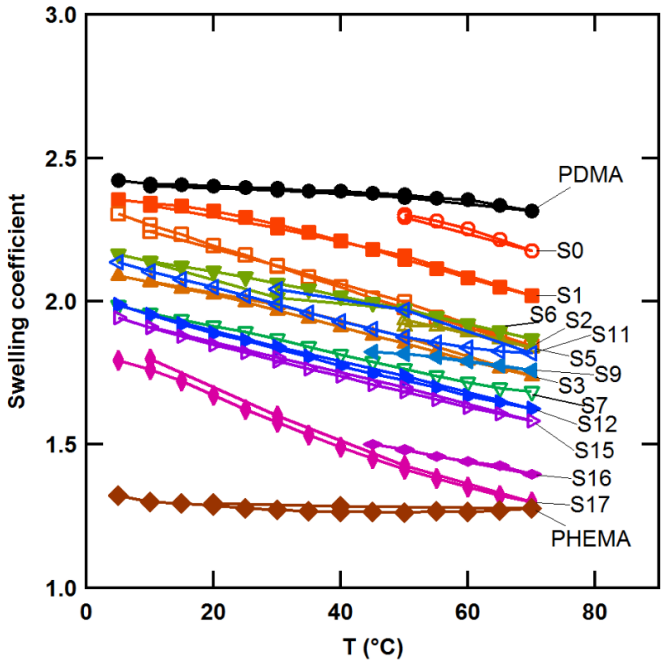

Figure 6.8. Ellipsometry-determined swelling coefficients of P(DMA-*co*-HEMA)-OOC-AZO brushes of different grafting yields of AZO-COOH and HEMA contents, without UV irradiation.

Samples with less DMA units, or with more azobenzene-substituted units at the same DMA content, display lower swelling coefficients, as already seen in Figure 6.6. There are however some variations to this rule, most probably due to the influence of thickness on swelling (compare S0 with S6, for instance, which have similar compositions but rather different thicknesses and give quite different swelling coefficients). Clearly, the brushes displayed in Figure 6.8 cover a very wide range of possible swelling coefficients, showing that the range of explored parameters is wide enough for our purposes.

The variation of the ellipsometric angles upon irradiation at room temperature are shown in Figure 6.9. The solid symbols are the data measured without UV irradiation; the open symbols are the data acquired during UV irradiation. The changes are in all cases quite small, and correspond to absolute variations of the swelling ratio varying between 0 and 0.06, which remains marginal. However, the changes were reversible upon cyclic irradiation. Changing the temperature from 20 to 55°C did not change significantly the variations of the swelling resulting from irradiation. We may thus conclude that the phototunable solubility reported in the literature for azobenzene-substituted PDMA-based copolymers is not reproduced in azobenzene-substituted P(DMA-*co*-HEMA) brushes, made using two different coupling reactions, for a range of azobenzene concentrations (1 to 10 mol%), brush thickness (from 90 to 230 nm) and brush "grafting densities" of 20%, 30% and 100%.

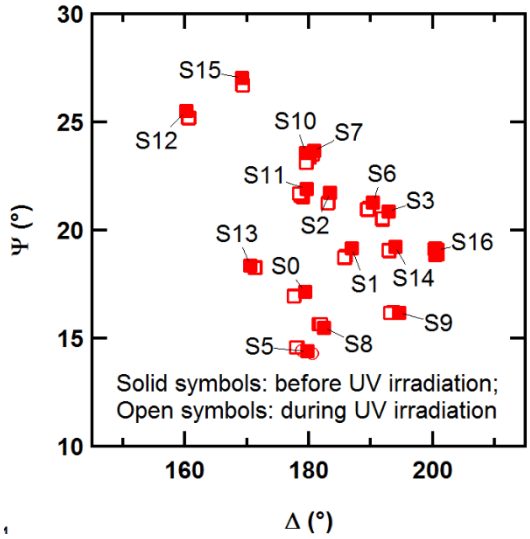

Figure 6.9. The room temperature ellipsometric angles of Psy and Delta for P(DMA-*co*-HEMA)-OOC-AZO brushes of Table 6.2, measured without and with UV irradiation.

As mentioned in the introduction, it is known that the AZO group will switch from *trans*- to *cis*-configuration upon UV irradiation of ~450 nm wavelength, resulting in a dipole moment change from 0 to 3 D,[45] and with the AZO group becoming less hydrophobic. Using the small change of polarity of AZO groups upon photo-irradiation, people synthesized dual thermo- and photo-responsive polymers[28, 30, 39-43, 46] or polymer brushes[15, 47] to tune the phase separation temperature or collapse transition temperature. However, the published results are not consistent. The extent of tuning of the phase separation upon irradiation is not only closely related with the content in AZO and the degree of isomerization of AZO,[21, 39] it is also related to the sequence of AZO moieties[21] and the structure of polymer chains.[28, 40] It is also dependent on the whether the material is a free polymer[39] or in a polymer brush.[47]

For instance, Kröger. *et al*.[39] synthesized the free copolymers of *N*,*N*-dimethylacrylamide and 4-phenylazophenyl acrylate by radical polymerization, while Yuan. *et al*.[47] synthesized a polymer brush composed of the same monomers by radical polymerization. Although the copolymer and copolymer brush both have ~7% AZO, the photo-irradiation on tuning the phase separation temperature or collapse transition temperature is quite different. The phase separation temperature of the free polymer is increased by 22°C after 85% isomerization of AZO groups from their *trans*- to *cis*-form upon UV irradiation. However, the collapse transition temperature of the polymer brush is only shifted by 5°C towards higher temperatures after UV irradiation; unfortunately, the measurements of Yuan *et al.* rely on the measurement of water contact angles as a function of temperature in the standard 'droplet on substrate' configuration, which might not be the best method to obtain valid results as we showed before. Luo. *et al*.[43] also synthesized by radical polymerization the same free copolymers with different contents in AZO. However, the phase separation temperature was reported to decrease slightly after UV irradiation,[43] in stark contrast with the increase of phase separation temperature after UV irradiation reported by Kröger *et al*. Shimoboji *et al*.[40] synthesized PDMA-based copolymers with two photo-responsive monomers, *N*-4-phenylazophenyl acrylamide (AZAAm) and 4-phenylazophenyl acrylate (AZAA), which have amide or ester bonds, respectively, as linking groups between the azobenzenes and the main chain. The copolymers of P(DMA-*co*-AZAAm) with 5.5 mol% of AZAAm, and P(DMA-*co*-AZAA) with 6 mol% AZAA, both of similar molar mass, showed a LCST of ~37.5 and ~47°C, respectively, under visible light

irradiation. After UV irradiation, the LCST of P(DMA-*co*-AZAAm) was increased to ~47°C, while the LCST of P(DMA-*co*-AZAA) decreased to ~40°C. The authors suggest that the different photo-tunable solubility of the polymers may come from the different hydrophobic interactions of the pendant AZO groups: the interactions of hydrophobic AZO groups will be predominantly intramolecular if the AZO groups are linked via amide bonds; the interactions of AZO groups will predominantly be intermolecular if the AZO groups are linked via ester bonds.[40] It is however hard to understand why that would be the case; it is more likely that the water structure close to the ester or amide is different, resulting in a change of excluded volume interactions which translates in subtle variations of the cloud point. At any rate, this shows that the photo-tunable phase separation of the thermo-responsive polymers is very sensitive to subtle changes in the structure of the polymer, and is certainly related to the perturbation of the structure of water close to the whole polymer chains. Similar effects are also the reason why cloud points of PNIPAM are dependent on the concentration of the chains in water.

In our studied brushes, the situation is very different from the one existing in a dilute solution of free chains, since the local polymer segment density is very high and the chains are highly stretched with a significant entropy decrease. Apparently, this results in a very modest effect of the configuration of the azobenzene on the swelling, independently on whether the AZO groups are linked via amide/urethane bonds or ester bonds. As limited effects were also found in other brushes based on thermo-responsive polymers[15, 44, 47] or other hydrophilic polymers such as the terpolymers of P(OEGMA-*co*-

HEMA)-CONH-AZO presented in chapter 4 of this thesis, it becomes obvious that the perturbation of the interaction parameter resulting from the change of configuration of the AZO groups is not large enough to affect polymer brushes, and that this line of research should be fully reconsidered to lead to practically interesting systems.

6.4.7 Surface hydrophilicity of P(DMA-*co*-HEMA) brushes

We just described that the volume properties of the AZO-grafted brushes were hardly affected by the change of configuration of the azobenzene groups. However, it might be possible that surface properties behave differently. This is not very likely, since our previous work clearly showed that the surfaces organize in water in order to shield hydrophobic groups, in which case the effect of azobenzene is expected to be much reduced. Nevertheless, the study was performed in order to have a complete understanding of these systems.

The equilibrium water contact angles of P(DMA-*co*-HEMA) brushes of different HEMA contents were thus measured at different temperatures (Figure 6.10). Generally, the surfaces of all the copolymer brushes are highly hydrophilic. The surface hydrophilicity is largely similar for all the systems, the slight differences being essentially within experimental error. This confirms that the surface hydrophilicity is not related to the composition of the copolymer brush. The surface hydrophilicity of P(DMA-*co*-HEMA) brushes thus shows a behavior with temperature similar to P(OEGMA-*co*-HEMA) brushes.

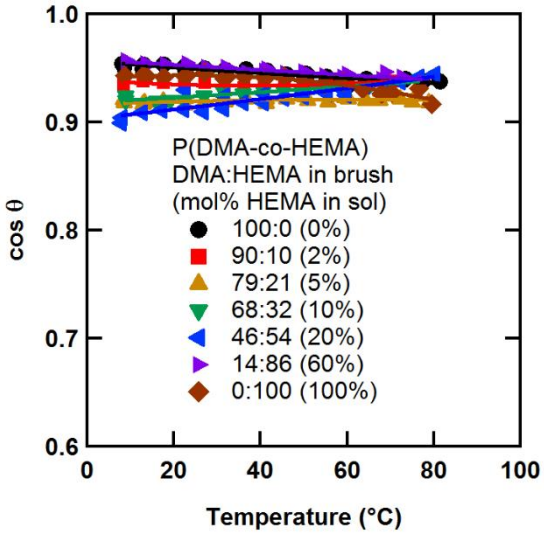

Figure 6.10. Equilibrium contact angles of P(DMA-*co*-HEMA) brushes of different HEMA content versus temperature.

6.4.8 Surface hydrophilicity of P(DMA-*co*-HEMA)-CONH-AZO brushes

Figure 6.11 shows the equilibrium contact angles versus temperature of P(DMA-*co*-HEMA)-CONH-AZO brushes with different AZO and HEMA contents in the polymer brush. When the HEMA content in the brush is lower than 21% and the AZO content is lower than 16%, the surface hydrophilicity of the brush is close to the surface hydrophilicity of PDMA. When increasing the HEMA content to 33%, resulting in an AZO content of 11%, the surface hydrophilicity of the brush decreases a bit and changes little with temperature. Increasing the HEMA content further, the surface hydrophilicity of the brush decreases a lot, even though the AZO content in the brush is also about 11%. Besides, the surface hydrophilicity decreases a bit with temperature due to the surface dehydration. The surface hydrophilicity

of the brush with 86% HEMA and 27% AZO decreases significantly compared to the brush of 54% HEMA and 11% AZO, and its surface hydrophilicity generally increases with temperature but with large surface hydrophilicity fluctuations.

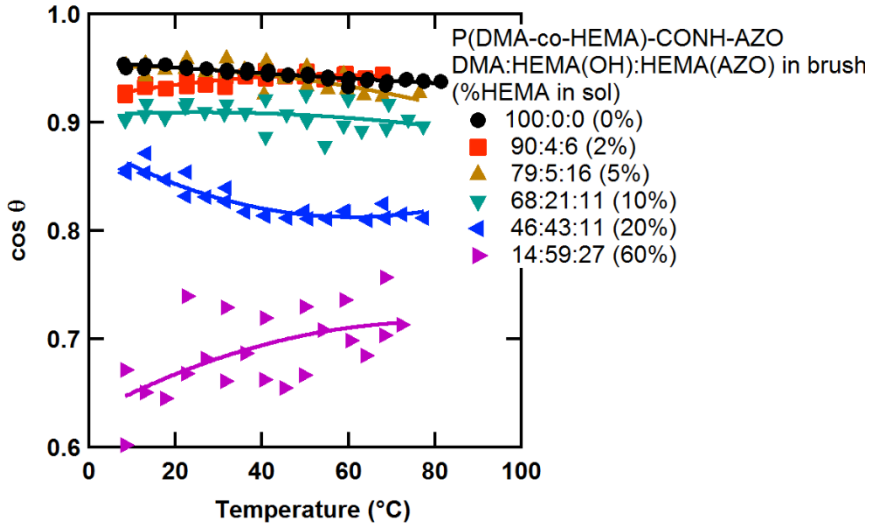

Figure 6.11. Equilibrium contact angles of P(DMA-*co*-HEMA)-CONH-AZO brushes of different -CONH-AZO grafting yields and HEMA contents, versus temperature in the dark.

These results suggest that the structure of the chains, and their substitution pattern, affect the expression of azobenzene at the surface in water. Systems which are more blocky in PHEMA sequences (grown in the presence of larger amounts of HEMA in solution) are likely to present strings of neighboring azobenzene groups, which cannot be fully hidden from the surface, contrarily to single azobenzene groups dispersed along the chain. In general, this is thus similar to what we observed for azobenzene-substituted P(OEGMA-*co*-HEMA) brushes in chapter 4.

6.4.9 Surface hydrophilicity of P(DMA-*co*-HEMA)-OOC-AZO brushes

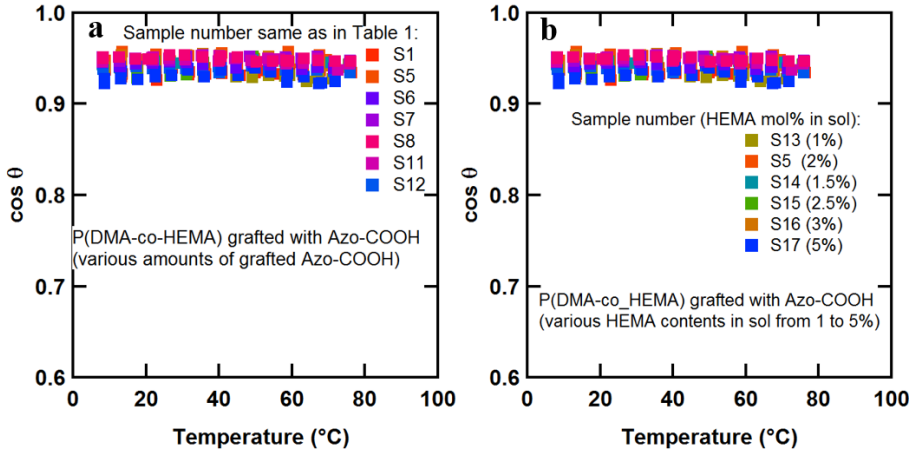

Figure 6.12. Equilibrium contact angles of P(DMA-*co*-HEMA)-OOC-AZO brushes of different AZO grafting yields and HEMA contents versus temperature in the dark: (a) 2% HEMA in solution for different grafting times; (b) different HEMA contents in solution for 60 h grafting time.

Figure 6.12 a shows the equilibrium contact angles of P(DMA-*co*-HEMA)-OOC-AZO brushes containing ~10% HEMA in the brush after grafting the azobenzene for different times, resulting in different grafting yields of AZO groups, and Figure 6.14 b shows the equilibrium contact angles of P(DMA-*co*-HEMA)-OOC-AZO brushes with different HEMA contents and AZO-COOH groups having been grafted for 60 h. All the surfaces of the copolymer brushes display a high surface hydrophilicity, close to the surface hydrophilicity of non-AZO grafted copolymer brushes, which does not change significantly with temperature, no matter how many AZO-COOH groups are grafted and the HEMA content in the copolymer brushes. This is compatible with

our previous conclusion, since these brushes have a structure of isolated azobenzene units interspersed in long hydrophilic sequences, which rearrange at the surface in order to bury the hydrophobic azobenzene below the surface. As reported P(OEGMA-co-HEMA) brushes grafted with AZO groups in chapter 4, there is little effect of UV irradiation on the surface hydrophilicity of P(DMA-co-HEMA)-OOC-AZO brush.

6.5. Conclusions

Two differently-substituted azobenzene groups were grafted onto hydrophilic P(DMA-*co*-HEMA) brushes of different HEMA content via esterification and amination reactions, and the composition of the terpolymer brushes was determined by UV spectroscopy and FTIR. The reversible photo-isomerization of AZO groups was proved by UV spectroscopy and ellipsometry. The volume hydrophilicity and surface hydrophilicity of PDMA-based copolymer brushes were studied by in-situ ellipsometry and equilibrium water contact angle measurements, respectively. The volume hydrophilicity of PDMA-based copolymer brushes can be tuned by changing the HEMA content or by grafting hydrophobic AZO groups and changing its content. However, the effect of photo-irradiation on the volume swelling of AZO-grafted P(DMA-*co*-HEMA) brushes was rather limited. The surface hydrophilicity of P(DMA-*co*-HEMA) brushes is always hydrophilic, and the surface of the AZO-grafted P(DMA-co-HEMA) brush of low HEMA content has a high hydrophilicity. These results show that brushes are dynamic systems, which reorganize at the surface or induce a modification of water structure upon irradiation, resulting in a compensation of the change of polarity of the azobenzene upon irradiation. Therefore, it is unlikely that further research in this direction will lead to useful systems, and exploring alternative routes bringing larger changes in the brushes upon irradiation, is probably a better route to follow. One possible route would be to use reversible charge generation upon irradiation, since the electrostatic interaction is known to modulate strongly the swelling of polymer brushes, as shown by brushes of weak polyelectrolytes which swell differently depending on pH.

References

1. Loschonsky, S. et al. Surface-Attached PDMAA−GRGDSP Hybrid Polymer Monolayers that Promote the Adhesion of Living Cells. *Biomacromolecules* 9, 543-552 (2008).
2. Kobayashi, M. & Takahara, A. Tribological properties of hydrophilic polymer brushes under wet conditions. *Chem. Rec.* 10, 208-216 (2010).
3. Gao, G. et al. Antibacterial surfaces based on polymer brushes: investigation on the influence of brush properties on antimicrobial peptide immobilization and antimicrobial activity. *Biomacromolecules* 12, 3715-3727 (2011).
4. Gao, G. et al. The biocompatibility and biofilm resistance of implant coatings based on hydrophilic polymer brushes conjugated with antimicrobial peptides. *Biomaterials* 32, 3899-3909 (2011).
5. Banerjee, I., Pangule, R.C. & Kane, R.S. Antifouling coatings: recent developments in the design of surfaces that prevent fouling by proteins, bacteria, and marine organisms. *Adv. Mater.* 23, 690-718 (2011).
6. Krishnamoorthy, M., Hakobyan, S., Ramstedt, M. & Gautrot, J.E. Surface-initiated polymer brushes in the biomedical field: applications in membrane science, biosensing, cell culture, regenerative medicine and antibacterial coatings. *Chem. Rev.* 114, 10976-11026 (2014).
7. Wu, L., Glebe, U. & Böker, A. Surface-initiated controlled radical polymerizations from silica nanoparticles, gold

nanocrystals, and bionanoparticles. *Polym. Chem.* 6, 5143-5184 (2015).

8. Stuart, M.A. et al. Emerging applications of stimuli-responsive polymer materials. *Nat. Mater.* 9, 101-113 (2010).
9. Zappone, B., Ruths, M., Greene, G.W., Jay, G.D. & Israelachvili, J.N. Adsorption, Lubrication, and Wear of Lubricin on Model Surfaces: Polymer Brush-Like Behavior of a Glycoprotein. *Biophys. J.* 92, 1693-1708 (2007).
10. Fan, X. et al. Fabrication of polyvinyl chloride ultrafiltration membranes with stable antifouling property by exploring the pore formation and surface modification capabilities of polyvinyl formal. *J. Membr. Sci.* 464, 100-109 (2014).
11. Minko, S. Responsive Polymer Brushes. *J. Macromol. Sci., Polymer. Rev.* 46, 397-420 (2006).
12. Chen, T., Ferris, R., Zhang, J., Ducker, R. & Zauscher, S. Stimulus-responsive polymer brushes on surfaces: Transduction mechanisms and applications. *Prog. Polym. Sci.* 35, 94-112 (2010).
13. Mura, S., Nicolas, J. & Couvreur, P. Stimuli-responsive nanocarriers for drug delivery. *Nat. Mater.* 12, 991-1003 (2013).
14. Samanta, S. & Locklin, J. Formation of Photochromic Spiropyran Polymer Brushes via Surface-Initiated, Ring-Opening Metathesis Polymerization: Reversible Photocontrol of Wetting Behavior and Solvent Dependent Morphology Changes. *Langmuir* 24, 9558-9565 (2008).

15. Dirani, A. et al. Reversible Photomodulation of the Swelling of Poly(oligo(ethylene glycol) methacrylate) Thermoresponsive Polymer Brushes. *Macromolecules* 45, 9400-9408 (2012).
16. Wagner, N. & Theato, P. Light-induced wettability changes on polymer surfaces. *Polymer* 55, 3436–3453 (2014).
17. Desponds, A. & Freitag, R. Synthesis and Characterization of Photoresponsive N-Isopropylacrylamide Cotelomers. *Langmuir* 19, 6261-6270 (2003).
18. Irie, M. & Mohri, M. Thermally irreversible photochromic systems. Reversible photocyclization of diarylethene derivatives. *J. Org. Chem.* 53, 803-808 (1988).
19. Akiyama, H. & Tamaoki, N. Polymers derived from N-isopropylacrylamide and azobenzene-containing acrylamides: Photoresponsive affinity to water. *J. Polym. Sci. A Polym. Chem.* 42, 5200-5214 (2004).
20. Matsubara, K., Watanabe, M. & Takeoka, Y. A Thermally Adjustable Multicolor Photochromic Hydrogel. *Angew. Chem. Int. Ed.* 46, 1688-1692 (2007).
21. Jochum, F.D. & Theato, P. Temperature and light sensitive copolymers containing azobenzene moieties prepared via a polymer analogous reaction. *Polymer* 50, 3079-3085 (2009).
22. Kungwatchakun, D. & Irie, M. Photoresponsive polymers. Photocontrol of the phase separation temperature of aqueous solutions of poly-[N-isopropylacrylamide-co-N-(4-phenylazophenyl)acrylamide]. *Die Makromolekulare Chem. Rapid Commun.* 9, 243-246 (1988).

23. Irie, M. & Kungwatchakun, D. Stimuli-responsive Polymers. Photostimulated Reversible Phase Separation of Aqueous Solutions of Poly(N-isopropylacrylamide) with Pendant Azobenzene Groups. *Proceedings of the Japan Academy, Series B* 68, 127-132 (1992).
24. Akiyama, H. & Tamaoki, N. Synthesis and Photoinduced Phase Transitions of Poly(N-isopropylacrylamide) Derivative Functionalized with Terminal Azobenzene Units. *Macromolecules* 40, 5129-5132 (2007).
25. Li, L., Xing, X. & Liu, Z. Triply-responsive (thermo/light/pH) copolymeric hydrogel of N-isopropylacrylamide with an azobenzene-containing monomer. *J. Appl. Polym. Sci.* 124, 1128-1136 (2012).
26. Tao, X. et al. Synthesis and characterization of well-defined thermo- and light-responsive diblock copolymers by atom transfer radical polymerization and click chemistry. *Polym. Chem.* 2, 2068 (2011).
27. Roth, P.J., Jochum, F.D., Forst, F.R., Zentel, R. & Theato, P. Influence of End Groups on the Stimulus-Responsive Behavior of Poly[oligo(ethylene glycol) methacrylate] in Water. *Macromolecules* 43, 4638-4645 (2010).
28. Zhao, Y., Tremblay, L. & Zhao, Y. Doubly photoresponsive and water-soluble block copolymers: Synthesis and thermosensitivity. *J. Polym. Sci. A Polym. Chem.* 48, 4055-4066 (2010).
29. Jochum, F.D., zur Borg, L., Roth, P.J. & Theato, P. Thermo- and Light-Responsive Polymers Containing Photoswitchable

Azobenzene End Groups. *Macromolecules* 42, 7854-7862 (2009).

30. Ravi, P. et al. New water soluble azobenzene-containing diblock copolymers: synthesis and aggregation behavior. *Polymer* 46, 137-146 (2005).
31. Menzel, H., Kröger, R. & Hallensleben, M.L. Polymers with Light Controlled Water Solubility. *J. Macromol. Sci. A* 32, 779-787 (1995).
32. Menzel, H., Kröger, R. & Hallensleben, M.L. polymers with light controlled water solubility. *conference preprint* (1995).
33. Pietrasik, J., Sumerlin, B.S., Lee, R.Y. & Matyjaszewski, K. Solution Behavior of Temperature-Responsive Molecular Brushes Prepared by ATRP. *Macromol. Chem. Phys.* 208, 30-36 (2007).
34. Eggenhuisen, T.M. et al. Libraries of Statistical Hydroxypropyl Acrylate Containing Copolymers with LCST Properties Prepared by NMP. *Macromolecules* 41, 5132-5140 (2008).
35. Yin, X. & Stöver, H.D.H. Probing the Influence of Polymer Architecture on Liquid−Liquid Phase Transitions of Aqueous Poly(N,N-dimethylacrylamide) Copolymer Solutions. *Macromolecules* 38, 2109-2115 (2005).
36. Jonas, A.M., Glinel, K., Oren, R., Nysten, B. & Huck, W.T.S. Thermo-Responsive Polymer Brushes with Tunable Collapse Temperatures in the Physiological Range. *Macromolecules* 40, 4403-4405 (2007).

37. Peppas, N.A., Moynihan, H.J. & Lucht, L.M. The structure of highly crosslinked poly(2-hydroxyethyl methacrylate) hydrogels. *J. Biomed. Mater. Res.* 19, 397-411 (1985).

38. Gundogan, N., Okay, O. & Oppermann, W. Swelling, Elasticity and Spatial Inhomogeneity of Poly(N,N-dimethylacrylamide) Hydrogels Formed at Various Polymer Concentrations. *Macromol. Chem. Phys.* 205, 814-823 (2004).

39. Kröger, R., Menzel, H. & Hallensleben, M.L. Light controlled solubility change of polymers: Copolymers of N,N-dimethylacrylamide and 4-phenylazophenyl acrylate. *Macromol. Chem. Phys.* 195, 2291-2298 (1994).

40. Shimoboji, T. et al. Photoresponsive polymer-enzyme switches. *Proc. Natl. Acad. Sci. U.S.A.* 99, 16592-16596 (2002).

41. Shimoboji, T., Ding, Z.L., Stayton, P.S. & Hoffman, A.S. Photoswitching of Ligand Association with a Photoresponsive Polymer−Protein Conjugate. *Bioconjugate Chem.* 13, 915-919 (2002).

42. Shimoboji, T., Larenas, E., Fowler, T., Hoffman, A.S. & Stayton, P.S. Temperature-Induced Switching of Enzyme Activity with Smart Polymer−Enzyme Conjugates. *Bioconjugate Chem.* 14, 517-525 (2003).

43. Luo, C. et al. Light-triggered reversible solubility of α-cyclodextrin and azobenzene moiety complexes in PDMAA-co-PAPA via molecular recognition. *J. Appl. Polym. Sci.* 107, 2118-2125 (2008).

44. Housni, A., Zhao, Y. & Zhao, Y. Using polymers to photoswitch the aggregation state of gold nanoparticles in aqueous solution. *Langmuir* 26, 12366-12370 (2010).

45. Hartley, G.S. & Le Fevre, R.J.W. The dipole moments of cis- and trans-azobenzenes and of some related compounds. *J. Chem.Soc. (Resumed)*, 531-535 (1939).

46. Jochum, F.D. & Theato, P. Temperature- and light-responsive smart polymer materials. *Chem. Soc. Rev.* 42, 7468-7483 (2013).

47. Yuan, W. et al. Temperature/Light Dual-Responsive Surface with Tunable Wettability Created by Modification with an Azobenzene-Containing Copolymer. *Macromolecules* 39, 1300-1303 (2006).

Chapter 6: Temperature Dependence of the Surface and Volume Hydrophilicity of DMA-based Photochromic Copolymer Brushes

7 Conclusions and Perspectives

Hydrophilic polymer brushes, especially, trigger-responsive polymer brushes whose volume and surface hydrophilicity can be tuned by external stimuli such as temperature, light or pH are critically important in biological and biomedical fields. For instance, such layers are developed to produce surfaces with antifouling or lubrication properties or with switchable bioactivity to control cell attachment/detachment or drug release. Moreover, multi-responsive brushes that respond to several stimuli are of a great interest to develop multi-purpose surfaces. For instance dual stimuli-responsive polymer brushes that respond to both temperature and light offer the possibility to tune the collapse temperature of the polymer chains, and consequently the volume and surface properties of the brush, upon photo-irradiation.

The preparation of such sophisticated smart layers requires robust polymerization techniques such as control/“living” radical polymerization techniques recently developed, especially the atom transfer radical polymerization (ATRP), which allow to control the thickness, composition and architecture of the brush.

The elaboration of these smart layers also requires the development of reliable characterization methods to measure the volume and surface properties of brushes. However, the correlation between volume properties and surface properties of polymer brushes still needs to be clarified. The understanding of these properties is critical to design new layers whose behavior meets the requirements related to a given application.

Chapter 7 Conclusions and Perspectives

This thesis aimed at generally synthesizing hydrophilic polymer brushes including trigger-responsive polymer brushes such as temperature- or photo-responsive polymer brushes and understanding better the temperature dependent behaviors of the these brushes in water. Characterizing and studying the volume and surface properties of polymer brushes depending on temperature by using appropriate techniques or establishing new protocol of measurement are also critically important. Thus, the correlations between the volume and surface properties of these polymer brushes can be established.

In this context, my thesis centered on understanding better the in-situ behavior of responsive brushes, and on the development of a series of brushes with the purpose of reaching photo-responsiveness. Whereas the first objective was certainly reached, with new insights given on the swelling and surface properties of hydrophilic polymer brushes, the second objective remained illusive.

First, several representative hydrophilic thermo-responsive polymer brushes that are already known and include the non-thermo-responsive PHEMA, POEGMA and PDMA polymers, the first one being slightly and the later highly hydrophilic, as well as the thermo-responsive $PMEO_2MA$ and PNIPAM polymers, both exhibiting a broad brush collapse transition in the physiological range, were synthesized by SI-ATRP as described in Chapter 3. A reliable protocol of equilibrium water contact angle measurement was developed to study the surface hydrophilicity of these polymer brushes as a function of the temperature. Moreover the volume hydrophilicity of these polymer brushes was studied in water as a function of the temperature, by two

methodologies: in-situ ellipsometry and quartz crystal microbalance with dissipation monitoring (QCM-D).

We notably showed that the surface hydrophilicity of the polymer brushes in the equilibrated state changes marginally with temperature no matter whether they are thermo-responsive or not. Moreover the degree of swelling of highly hydrophilic polymer brushes measured by in-situ ellipsometry decreases very slowly with temperature, while the thermo-responsive polymer brushes with a moderate LCST show a broad but strong collapse transition and its degree of swelling changes gradually but greatly with distance from the surface. The acoustic swelling coefficients of the homopolymer brushes measured by QCM-D are higher than the optical ones measured by ellipsometry due to the difference of sensitivity of both techniques. The non-direct correlation between volume and surface hydrophilicity suggests that the volume and surface hydrophilicity can be independently designed. Although of basic rather than applied nature, this research provides a view differing with the sometimes cartoon-like views developed in the field.

In chapter 4, the results obtained on PNIPAM brushes were compared to literature data. AFM, ellipsometry, neutron reflectometry and QCM-D were demonstrated to give rise to consistent results, supporting the notion of a collapse transition occurring from the bottom to the top of the brush. The copolymerization between highly hydrophilic monomers of OEGMA, and the monomer of MEO_2MA, afforded polymer brushes of adjustable collapse transition temperature. Their surface and volume properties were qualitatively identical to PNIPAM and pure $PMEO_2MA$, confirming the generality of our previous findings.

We then turned to the fabrication of brushes including azobenzene photochromes, in view of obtaining photo-responsive brushes. Our first attempt (in chapter 4) involved the copolymerization of OEGMA and HEMA, leading to brushes with hydroxyl-bearing side chains onto which we successfully grafted azobenzene moieties. The volume properties were strongly affected by the incorporation of the hydrophobic azobenzene, whereas the surface properties were basically not or moderately affected, showing the capacity of such brushes to reorganize dynamically their surface in water and to bury hydrophobic groups inside the brush. Logically, as the azobenzene groups are buried in the brush, the surface hydrophilicity of the photo-responsive polymer brushes changes little upon photo-irradiation. More surprising was the observation that the brush swelling was not sensitive to the change of configuration of the azobenzene.

Intrigued by these results, we elicited to study another hydrophilic polymer brush comprising azobenzene groups. Based on a literature survey of free polymer chains in solution, PDMA was selected as most likely to exhibit interesting effects, although conflicting results were published in the literature. We then entered in a very complete study of the copolymerization of DMA and HEMA in chapter 5. In chapter 6, we produced azobenzene-substituted P(DMA-*co*-HEMA) brushes and investigated their properties. The study of the surface and volume properties of these brushes in water provided results compatible with our previous work, and indicated a very moderate response to UV irradiation. We ascribed this to the reorganization of water structure around the azobenzene groups, which finally shields the changes of polarity resulting from the switching of the azobenzene configuration.

We concluded that other strategies are required to obtain photoresponsive brushes, suggesting that photo-induced charge generation might be a better option based on the important role of the degree of ionization on the swelling of brushes of weak polyelectrolytes.

Temperature has a little effect on the volume and surface hydrophilicities of polymer brushes without LCST. Keeping the stability of volume and surface properties for hydrophilic polymer brushes is also very important when they are used to prepare antifouling surfaces. This requires long time study on the volume and surface properties of these hydrophilic polymer brushes and testing their antifouling properties at the same time. Thus, how to enhance the durability of the volume and surface properties of hydrophilic polymer brushes is a critically important aspect for practical applications.

Besides the antifouling properties, the antibacterial properties of a hydrophilic polymer brushes is also usually desired in some biomedical fields. Anchoring bactericidal molecules on the macromolecular chains of the brushes is a good option. To do this, copolymerization between different monomers, one of which bearing functional groups, can be performed. Then, the bactericidal moities can be grafted onto the macromolecular chains of the brushes. The factors such as brush thickness, grafting density should also be considered when studying the volume and surface properties and their applications.

Sophisticated systems consisting of trigger-responsive polymer brushes such as thermo-, photo- or dual thermo- and photo-responsive polymer brushes are extremely intriguing, since their volume and surface properties can be altered by external stimuli without changing the composition. However, it is very difficult to synthesize the stimuli-

responsive polymer brushes exhibiting the needed properties because it involves many aspects of studies before putting them into practical applications. Based on our research, several valuable suggestions can be made.

Thermo-responsive polymer brushes containing highly hydrophilic monomers such as OEGMA or DMA, can be fabricated by copolymerizing these monomers with the monomers such as NIPAM or MEO_2MA, whose homopolymer has a moderate LCST. Functional monomer units can be introduced into the thermo-responsive polymer brushes making terpolymer brushes to provide them with extra properties by post-modification.

Photochromic moieties are mostly incorporated into thermo-responsive polymer brushes, making thermo- and photo-responsive polymer brushes. Thus, the LCSTs of thermo-responsive polymer brushes can be dynamically changed by photo-irradiation of different wavelengths, thus tuning the swelling or collapse of the macromolecular chains without changing temperature. It is very limited to photo-tune the volume and surface hydrophilicities of hydrophilic polymer brushes without LCSTs, and the real reason is still not clear. As these hydrophilic polymer brushes are not sensitive to temperature, it is difficult to study the photo-tuning volume and surface properties. More sophisticated techniques such as FTIR connected with in-situ ellipsometry might help to study the photo-tuning volume swelling of hydrophilic photo-responsive brushes by detecting the change of interactions such as hydrogen bondings between the macromolecular chains and water molecules. Another research aspect involves synthesizing dual thermo- and photo-responsive polymer brushes

bearing azobenzene groups and studying the change of hydrogen bondings formed between polymer chains and water as a function of temperature by photo-irradiation of visible or UV light. Thus the mechanism for the photo-tuning volume and surface properties might become clearer. As photo-irradiation has a little effect on the volume and surface hydrophilicities of AZO-grafted polymer brushes grafted by different linkers, AZO groups of different structures, especially the AZO substituted by –OH or –COOH groups can be tried.

Spiropyran is another important photochromic moiety, which also undergoes reversible isomerization like AZO upon photo-irradiation. Spiropyran and its derivatives instead of azobenzene derivatives can be incorporated into hydrophilic polymer brushes including the thermo-responsive polymer brushes to improve the effect of photo-tuning the volume and surface properties of polymer brushes. Because, larger polarities of spiropyran groups compared to AZO occur when they isomerize between different forms upon photo-irradiation, which might cause larger change of the volume and surface properties. In addition, the ionization of spiropyran also happens, which usually allows changing the volume and surface properties greatly by changing pH.

Chapter 7 Conclusions and Perspectives

Dissemination

Publications

1. Pengyu Zhuang, Ali Dirani, Karine Glinel, Alain M. Jonas. "Temperature Dependence of the Surface and Volume Hydrophilicity of Hydrophilic Polymer Brushes". Langmuir 32 (2016), 3433-3444.
2. Pengyu Zhuang, Ali Dirani, Karine Glinel, Alain M. Jonas. "Temperature Dependence of the Swelling and Surface Wettability of Dense Polymer Brushes". (Submitted as a book chapter in *Polymer and Biopolymer Brushes: Fundamentals and Applications in Materials Science and Biotechnology*, O. Azzaroni & Igal Szleifer, Eds, Wiley)
3. Pengyu Zhuang, Ali Dirani, Karine Glinel, Alain M. Jonas. "Temperature-dependence properties of hydrophilic P(DMA-co-HEMA) brushes and their photo-responsiveness by post-grafting azobenzene". (in preparation).

Conferences and communications

1. "Temperature dependence of the swelling and wettability of hydrophilic polymer Brushes".

Pengyu Zhuang, Ali Dirani, Karine Glinel, Alain M. Jonas. Warwick 2016 International Conference on Polymer Chemistry. July, 2016, University of Warwick, UK. (Oral Presentation)

2. "The volume and surface properties versus temperature of hydrophilic polymer brushes".

Pengyu Zhuang, Ali Dirani, Karine Glinel, Alain M. Jonas. Ph.D Students' Day, May, 2016, UCL, Belgium. (Oral Presentation)

3. "Volume and surface properties versus temperature of hydrophilic polymer brushes". Pengyu Zhuang, Ali Dirani, Karine Glinel, Alain M. Jonas. 13th Nanowal scientific Meeting-Main Ph.D Student Day "STM and AFM: What's new 30 years later", 2016, UCL， Belgium. (Poster presentation)
4. “Synthesis and characterization of reversibly switchable thermo- and photo-responsive copolymer brushes”. Pengyu Zhuang, Ali Dirani, Karine Glinel, Alain M. Jonas. Interuniversity Attraction Poles (IAP) “Functional Supramolecular Systems” Annual Meeting. September, 2015, Hasselt, Belgium. (Poster presentation)
5. “First steps towards thermoresponsive copolymer brushes exhibiting a large and reversible photoresponse”. Pengyu Zhuang, Ali Dirani, Karine Glinel, Alain M. Jonas. Interuniversity Attraction Poles (IAP) “Functional Supramolecular Systems” Annual Meeting. September, 2014, UCL, Belgium. (Poster presentation)
6. “Synthesis by ATRP of poly(N,N-dimethylacrylamide) brushes and of their copolymer brushes with 2-hydroxyethyl methacrylate”. Pengyu Zhuang, Ali Dirani, Karine Glinel, Alain M. Jonas. Annual Meeting of the Belgian Polymer Group, May, 2014, Ghent, Belgium. (Poster presentation)
7. “Photo- and thermo-responsive polymer brushes by surface-initiated atom transfer radical polymerization”. Pengyu Zhuang, Ali Dirani, Karine Glinel, Alain M. Jonas. IAP “Functional Supramolecular Systems” Annual Meeting, September, 2013, Ghent, Belgium. (Poster presentation)